Characterization of the Role of Copper Transporting ATPase, ATP7B (Wilsons Disease Protein), in Copper Homeostasis

by

Mee Y. Bartee

A Doctoral Thesis

Presented to the Department of Biochemistry & Molecular Biology

at the Oregon Health & Science University

School of Medicine

in partial fulfillment of

the requirements for the degree of

Doctor of Philosophy

September 15, 2008

School of Medicine
Oregon Health & Science University

CERTIFICATE OF APPROVAL

This is certify that the:

(●) PhD DISSERTATION

( ) MASTER's THESIS

of

Mee Yong Bartee

Student Name

has been approved

Peter Rotwein	
Committee Chair	Signature
Svetlana Lutsenko	
Mentor/Advisor	Signature
David Farrens	
Member	Signature
Caroline Enns	
Member	Signature
David Koeller	
Member	Signature
Member	Signature
Member	Signature
Member	Signature

After all signatures are obtained, take this original form to the LIBRARY with the dissertation/thesis to be bound. The Office of Graduate Studies does not require this form.

Revised 10/3/2008

Table of Contents

List of Figures

I

II

III

IV

V

AI

AII

AIII

VI

Acknowledgements

I would like to thank my family and friends for their support and friendship during the years spent on my graduate studies. Without them, the entire experience would not have been as enjoyable. In particular, I can't express enough my gratitude towards my husband, Eric, whose patience and encouragement helped me through my most trying moments.

I would also like to thank Ruslan for generating the baculovirus constructs and showing me how to use the insect cell system. I thank Joel for helping me in the lab, and being there for me during all my lab disasters. I would like to thank Natalie for training me to do immunofluorescence, and for doing the experiments on primary mice cells, siRNA, and cell staining for chapter 2. I would also like to thank Vladimir Ustiyan for performing the copper uptake studies. I thank Larry David and Martina for help with the mass spectroscopy experiments, and Jin from the Lu lab for showing me how to use the FPLC. I would like to thank Eric for helping me with flow cytometry, and Jason for making the CBD-N-ATP7B deletion constructs. I also thank the Adelman lab for the protocols and reagents for the yeast two hybrid system. I also thank Matt for help with insect cells and the Kaplan lab for reagents. I also thank the members of my committee and the Biochemistry department, because at some point, I've borrowed reagents, equipment, or gotten help from everyone. Finally, I would like to thank my thesis advisor, Sveta, for allowing me to do research in her lab and making the thesis happen.

Abstract

All organisms must implement a method of copper regulation in order to utilize yet protect the cell from cytotoxic effects. ATP7B, a P-type ATPase, is a copper transporter expressed in human cells that regulates the delivery of copper to proteins in the biosynthetic pathway and maintains the intracellular concentration of copper. Copper homeostasis is preserved through several mechanisms. The expression of a smaller protein product in the kidney, as opposed to full length ATP7B in the liver, leads to the different trafficking responses to elevated copper, no trafficking in the former and vesicular localization in the latter. Spatial control of ATP7B localization at the TGN, vesicles, or canalicular membrane is dependent on the copper status of the cell, controlling the ratio of intracellular copper to that destined for export. Phosphorylation of ATP7B in the serine rich region between MBD3 and 4 is also important in the regulation of ATP7B intracellular localization. The many mechanisms utilized by ATP7B for regulation of copper suggest there is a delicate balance between copper necessity and excess. In addition to direct regulation of copper homeostasis through ATP7B, other interacting proteins such as ceruloplasmin may play a role in copper maintenance.

Statement of Purpose

In humans, ATP7B is a copper transporter important for the maintenance of copper homeostasis and delivery of copper into the biosynthetic pathway. To better understand the role of ATP7B, my thesis work focuses on studying the regulation of ATP7B trafficking. My hypothesis is that the localization of ATP7B is central to its export function. At the beginning of my thesis work, it was known ATP7B traffics from the TGN to a vesicular compartment when cells, endogenous ATP7B in HepG2 cells or recombinant ATP7B in fibroblasts, were treated with copper. Based on this finding, I wanted to address the following questions: (1) In cells that express both ATP7B and its homologue ATP7A, are there differences in the copper response compared to cells that express only ATP7B? (2) Is the model of recombinant ATP7B recycling from copper laden vesicles in fibroblasts valid in a polarized hepatocyte model looking at endogenously expressed ATP7B? (3) Does copper dependent phosphorylation play a role in the regulation of ATP7B trafficking? (4) What is the kinase that phosphorylates ATP7B? (5) Is there an effect of copper dependent phosphorylation on ATP7B structure? (6) Can ceruloplasmin play a role in ATP7B mediated copper export? (7) What proteins regulate ATP7B phosphorylation and trafficking?

Chapter II overview:

In the liver, ATP7B is the only known copper transporter expressed. ATP7B serves two major roles in the liver, copper delivery to ceruloplasmin, a copper dependent ferroxidase, and export of excess copper into the bile. In tissues where both ATP7B and ATP7A, a homologous copper transporter with overlapping function, are expressed it is not clear what role ATP7B may have in the cell separate from ATP7A. To address this question, the copper dependent localization of ATP7B was investigated in Hek293 cells, where both ATP7B and ATP7A are expressed. By indirect immunofluorescent confocal microscopy, ATP7A was shown to relocalize from the TGN in a wide range of copper concentrations whereas ATP7B remained at the TGN. Several different approaches were taken to discover the cause of ATP7B unresponsiveness to copper in Hek293 cells. ATP7A is known to be a more efficient transporter, with a turnover rate 6 times faster than ATP7B. To test whether the lack of ATP7B relocalization is due to ATP7A transporting activity, siRNA knockdown experiments were done to down regulate the expression of ATP7A. Under these conditions, ATP7B still does not traffic in response to copper.

Trafficking of ATP7B was investigated by indirect immunofluorescence in COS7, BeWo, MDCK, OK, Huh7, and HepG2 cells to test if this lack of trafficking is exclusive to Hek293 cells. ATP7B trafficked only in the hepatocyte derived cells, suggesting perhaps tissue dependent regulation of ATP7B trafficking. This phenomenon was confirmed in mouse primary kidney and liver cells, where ATP7B trafficked only in mouse hepatocytes. Another possibility for the lack of

trafficking could be differences in copper uptake in kidney derived Hek293 cells as opposed to liver derived HepG2 cells. Copper accumulation was monitored with ^{64}Cu, but both cell lines had similar rates of copper uptake.

ATP7B was known to undergo copper dependent phosphorylation, which could be visualized by a mobility change on a gel. Protein mobility of ATP7B containing membranes from Hek293 and HepG2 were compared by western blot analysis to test for post-translational modification. ATP7B from Hek293 membranes migrated faster on 7.5% Laemmli gel than ATP7B from HepG2 membranes. This result suggested a role for phosphorylation, however comparison of in vivo metabolically labeled ATP7B from Hek293 and HepG2 cells were similarly phosphorylated.

An alternative possibility for the protein size difference is proteolysis. Full length ATP7B cDNA was transfected into Hek293 cells, and then protein mobilities compared with endogenous ATP7B from Hek293 and HepG2 cells. The recombinant protein migrated slower than endogenous ATP7B from Hek293 cells and was similar in size to ATP7B from HepG2 cells suggesting the difference in mobility is not due to proteolysis.

From these results, transcriptional regulation of the ATP7B transcript seemed to be a good candidate for the difference in protein size. Of the 21 exons that encode ATP7B, exons 1, 6, and 21 were potential targets for alternative splicing because splicing of these exons would result in the appropriate size protein without greatly impacting the structure or catalytic activity of the protein. RT-PCR of these regions showed exon 6 and 21 are present in

Hek293 cells but under the conditions used, exon1 is not. To test whether the presence of exon1 would restore trafficking, full length ATP7B cDNA was stably expressed in a tetracycline inducible trafficking system. In this system, recombinant ATP7B trafficked to a vesicular compartment in response to copper, suggesting exon 1is needed for trafficking. Although alternative splicing of exon 1 was not demonstrated, the importance of the presence of the sequence encoded in exon 1 was shown. From the work presented in chapter 2, it was established ATP7B may have tissue specific transcriptional regulation in cells where both ATP7A and ATP7B are expressed. The lack of trafficking in Hek293 cells suggests ATP7B performs primarily a biosynthetic role whereas ATP7A maintains intracellular copper homeostasis when the two transporters are co-expressed.

Chapter III overview:

The model proposed in the literature suggested ATP7B traffics to a vesicular compartment when copper is elevated and then is retrieved back to the TGN, separating from the copper laden vesicles which are eventually released to the plasma membrane. In contrast to this model, we proposed that in a more relevant polarized hepatocyte model, ATP7B traffics to the apical membrane, consistent with its role in the liver to export copper, and is recycled/ retrieved to the TGN. To answer this question, conditions were optimized to polarize HepG2 membranes and study the trafficking of endogenous ATP7B by indirect immunofluorescence. These studies showed that HepG2 cells can be polarized, establishing a basolateral and apical membrane that can be stained with markers,

and the localization of these markers are not affected by copper. ATP7B localized to structures reminiscent of the bile canalicular membrane, suggesting ATP7B traffics to the apical membrane. Co-localization with the canalicular membrane marker, MRP2, shows that a small fraction of ATP7B stains at the canalicular membrane under copper limiting conditions, perhaps as a result of constitutive trafficking. More importantly, ATP7B re-localizes to the apical membrane when cells are treated with copper, supporting the hypothesis that in the liver, ATP7B may recycle/ be retrieved from the canalicular membrane rather than vesicles, contrary to the accepted model of ATP7B trafficking.

Chapter IV overview:

Along with copper dependent trafficking, it was observed that ATP7B also undergoes copper dependent phosphorylation. To determine whether these two events are connected, I identified the site(s) of phosphorylation and analyzed the effects of mutagenizing the phosphorylation site(s). First, an assay was developed to in vitro phosphorylate full length ATP7B from baculovirus mediated infected Sf9 cells. In this system, there were two major bands, full length ATP7B and a N-terminal degradation band. The degradation was shown to be more efficiently phosphorylated than full length protein. Also catalytically active ATP7B was better phosphorylated than the catalytic inactive D^{1027}>A mutant. For further identification of the phosphorylation site(s), the target of phosphorylation was narrowed from full length protein to a domain, a region, then to several residues. The N-terminal domain was determined to be a good candidate for phosphorylation, and was shown to be phosphorylated both in vitro and in vivo.

To further narrow the region of phosphorylation, a combination of 2-D electrophoresis of trypsinized phosphorylated N-ATP7B as well as phosphorylation of N-ATP7B deletion constructs pointed to loop3 between MBD 3 and MBD 4 as the target for phosphorylation. Phosphorylation of the serine to alanine N-ATP7B mutant constructs pointed to $S^{340}S^{341}$>AA as the primary target for phosphorylation. Trafficking of the full length $S^{340}S^{341}$>AA mutant in the tetracycline inducible system showed a vesicular localization of this mutant, under both BCS and copper treated conditions. This finding suggested phosphorylation could be important for the retrieval or recycling of ATP7B.

Chapter V overview:

Phosphorylation of ATP7B affects its trafficking behavior. Regulation of this phosphorylation event occurs when copper is elevated. A series of experiments were conducted using different buffer conditions to try to characterize the kinase that phosphorylates ATP7B. Originally, HepG2 cell lysate was used to phosphorylate ATP7B containing Sf9 membranes. However, it was shown that the kinase activity could be seen in Sf9 membranes without the addition of lysate. This ATP7B kinase is tightly associated with ATP7B in the membranes because treatment of membranes with high salt does not significantly alter the kinase activity. ATP7B was found to require $MgCl_2$ or $MnCl_2$ for this kinase activity. The apparent Km of kinase mediated phosphorylation was determined to be 50μM for ATP, which suggests this observed phosphorylation is not due to catalytic phosphorylation, but kinase mediated because the Km for ATP in catalytic phosphorylation is 1μM of ATP.

Some kinases can utilize both ATP and GTP, but the ATP7B kinase only uses ATP. Phosphorylation of sucrose fractionated ATP7B containing Sf9 membranes result in ATP7B phosphorylation in all three enriched membrane fractions, ER, Golgi, and plasma membrane. This may imply the ATP7B kinase is either ubiquitous in the three membranes, or that it could be intimately associated with ATP7B. Although the in vitro phosphorylation experiments of ATP7B containing membranes show that membranes are sufficient for the phosphorylation of ATP7B, HepG2 and Hek293 lysates can also be used for the phosphorylation of N-ATP7B. This hints the ATP7B kinase is perhaps a peripheral membrane protein, existing as both a soluble protein and associating to membranes. Gel filtration and anion exchange chromatography was used to isolate fractions containing kinase activity, phosphorylating His-N-ATP7B bound to Ni-NTA plates.

Phosphorylation of MBP-N-ATP7B showed that copper bound protein was better phosphorylated than apo-protein. Whether cells that were made into lysate were pre-treated with copper made no difference to the phosphorylation of MBP-N-ATP7B. ABD interaction to N-ATP7B was previously shown to be copper dependent [1]. As copper binds to MBP-N-ATP7B, the interaction with ABD weakens. Phosphorylation of MBP-N-ATP7B in the presence of ABD for both copper bound and apo protein decreased the level of phosphorylation to that of apo protein.

Appendix I overview:

Copper binding to the MBDs was shown to elicit structural changes in N-ATP7B, with reorganization of the linker regions between the domains. The

change in protein mobility of ATP7B upon copper dependent phosphorylation on Laemmli gels also hinted at the possibility of structural changes. Solubility of ATP7B is altered when it is phosphorylated. Binding of ATP7B-His on Ni-NTA is inhibited after the protein is phosphorylated, suggesting the epitope has become obscured, perhaps due to conformational changes that obscure the C-terminal tail or by the formation of aggregates or oligomers.

Appendix II overview:

In patients with Wilsons disease, low serum ceruloplasmin, a copper dependent ferroxidase secreted from the liver, is one of the features of the disease. It has been shown in a yeast complementation assay, expression of ATP7B in Δccc2 (the yeast homologue of ATP7B) yeast, copper delivery to Fet3, the yeast homologue of ceruloplasmin, is restored, suggesting the importance of ATP7B in ceruloplasmin activity. Reciprocally, ceruloplasmin may play a role in ATP7B copper export, by acting as a copper oxidase, facilitating efficient export of copper. To test whether this could be a possibility, co-localization of ATP7B and ceruloplasmin in either copper laden vesicles or at the apical membrane needed to be established. Indirect immunofluorescence for ATP7B and ceruloplasmin in HepG2 cells showed that when copper is elevated, ATP7B and ceruloplasmin could not be co-localized to the vesicles. Interestingly, ceruloplasmin was localized at the plasma membrane. Cell surface immuno-staining, biotinylation of the plasma membrane, and flow cytometry independently confirmed the plasma membrane localization. Polarization of HepG2 cells revealed canalicular membrane staining of ceruloplasmin. ATP7B is

also localized to the canalicular membrane. It would be important to test whether these two proteins co-localize at the apical membrane in polarized cells.

Appendix III overview:

In order to identify proteins that interact with ATP7B, constructs were generated for a yeast two hybrid. Methods for growing and transforming yeast were optimized.

Function and regulation of human copper-transporting ATPases

S. Lutsenko[1], N.L. Barnes, M.Y. Bartee, and O.Y. Dmitriev

Key words: Adenosine Triphosphatases/genetics/*metabolism, Cation Transport Proteins/genetics/*metabolism, Gene Expression Regulation, Enzymologic, Genomics, Humans, Protein Structure, Tertiary

1 - The correspondence should be addressed to:

Svetlana Lutsenko, Oregon Health & Science University, Department of Biochemistry and Molecular Biology, 3181 SW Sam Jackson Park Rd., Portland, OR 97239-3098, U.S.A.; Tel.: 503-494-6953; E-mail: lutsenko@ohsu.edu

-Published in Physiological Reviews 2007; 87(3): 1011-46.

-The Introductory chapter was taken from a near final version of the review which is not the final printed version; and I made only minor changes (addition/subtraction of sentences). I wrote sections 1.7.4-1.10, 1.18-1.23, and part of 1.7.2. I assisted in the proofreading and revision of the review. I also generated Figure 1.

-Natalie Barnes wrote section 1.4-1.5

-Svetlana Lutsenko wrote the rest of the review and reorganized/ proofread/ and edited the review and generated Figure 2.

-Oleg Dmitriev provided figures of the NMR solution structure he solved of the N-domain that is not included in this thesis.

I. Introduction[2]

1.1 The role of copper transporting ATPases, ATP7A and ATP7B, in human physiology

Copper transporting ATPases (Cu-ATPases) are evolutionarily conserved transport proteins with essential roles in cellular survival in both eukaryotes and prokaryotes. In humans, these intrinsic membrane proteins function to transport copper from the cytosol to other compartments, thus reducing the intracellular copper concentration. In addition, the Cu-ATPases perform an important biosynthetic function by delivering copper into the secretory pathway, where the metal ion is incorporated into copper dependent enzymes, such as dopamine-β-hydroxylase[3], tyrosinase[4], lysyl oxidase, peptidyl-α-monooxygenase[5], and ceruloplasmin[6]. The physiological importance of Cu-ATPases in humans is demonstrated by the deleterious consequences resulting from the loss of the Cu-ATPase function. Mutations or deletions in a gene encoding the Cu-ATPase ATP7A are associated with a severe childhood disorder, Menkes disease. Patients with Menkes disease display dramatic developmental and neurological impairment due to disrupted delivery of copper to the brain [7]. In addition, patients have a variety of other symptoms resulting from decreased function of copper dependent enzymes, including connective tissue abnormalities, lack of pigmentation, and tortuosity of blood vessels [7-11]. The majority of Menkes disease patients die in early childhood.

Mutations in the gene encoding the Cu-ATPase ATP7B also result in severe pathologies, although the phenotypic manifestations of this disease are

very different. ATP7B inactivation is associated with copper accumulation in several tissues, particularly in liver and brain, and a spectrum of severe hepatic and neurological abnormalities. These may include liver dysfunction or failure, movement disorders, and psychiatric manifestations [12-14]. Although copper chelation therapy using D-penicilamine is available for treatment of Wilson disease, this therapy is not always successful if diagnosis is delayed and may have severe side effects [15-17]. Genetic screening at birth, similar to that of phenylketonuria [18], has been suggested, to forestall the progression of the disease by administration of copper chelating agents, however, the effectiveness of such a treatment plan has yet to be proven.

These two diseases illustrate a fundamental need for precise homeostatic control of intracellular copper as either copper deficiency (Menkes disease) or copper accumulation (Wilson disease) are extremely deleterious to cell function. Such control is mediated through the coordinated action of several proteins, with Cu-ATPases playing a central role in copper export from the cell and copper delivery to the secretory pathway

1.2 Copper absorption and distribution in tissues

The pathway through which dietary copper is absorbed by the intestinal epithelium is not completely understood. The high affinity copper transporter hCTR1, which is selective for copper, and the low affinity divalent metal transporter DMT1 are both expressed in intestinal cells; however which of these two transporters plays a major role in copper uptake from the lumen of the intestine remains to be determined. Copper and iron metabolism have

historically been interconnected[19-25]; the current data suggests a similar relationship between iron and copper absorption, particularly in the intestine. Under conditions of iron deprivation, DMT1 expression is upregulated. Concurrently, there is increased absorption of copper at the brush border side of the intestinal epithelium in rats, which may be due to DMT1 [26]. Ctr1 has been also observed at the apical membrane of intestinal cells in agreement with a role in copper uptake from the lumen. However, in adults it had mostly an intracellular localization [27] suggesting a role in regulated rather than constitutive copper transport. Lastly, the presence at the brush border membranes of an ATP-driven, high affinity copper transport system has also been proposed [28] but the molecular nature of this putative pump remains to be determined.

Copper is exported from enterocytes into the blood by Cu-ATPase ATP7A in a process that involves trafficking of the transporter to a region that is near the basolateral membrane [26, 29]. In Menkes disease, copper export is greatly impaired and while copper accumulates in intestinal cells, less copper is delivered to the blood, resulting in a restricted copper supply to other tissues [9]. Interestingly the expression of ATP7A in the duodenum is markedly increased under conditions of iron deficiency, most likely due to the increase copper absorption by DMT1, contributing to the increased copper transport across intestinal epithelium under these conditions [26].

An important and still not completely understood question is how the oxidation state of copper is controlled during various steps of copper translocation. Current data suggests that copper enters the cell, migrates within

the cell, and then is exported from the cell in the reduced, Cu (I), form. However, in both the intestinal lumen and in the serum, copper is thought to be present in the oxidized Cu (II) state, and therefore copper must be reduced upon entry into the cell and oxidized when exiting the cell. The existence of a cytochrome b protein with copper reductase activity has been demonstrated in rabbit enterocytes [30]; such reductase activity could be an important component of the copper uptake machinery. It is not yet certain whether oxidase activity is required for copper exit and whether the transport of copper by ATP7A and ATP7B is coupled to such copper oxidase activity.

The majority of the copper that emerges from the intestinal epithelium is delivered to liver and kidney [31]. After entry into the cell, copper is distributed to various intracellular destinations by way of copper chaperones (Figure 1). In the cytosol, copper is utilized by a radical detoxifying enzyme, copper, zinc-superoxide dismutase (SOD1), which acquires copper from a specific copper chaperone, CCS (Copper Chaperone of Superoxide dismutase). Copper also enters the mitochondria, where it is incorporated into cytochrome c oxidase (COX). Several candidate proteins have been proposed to contribute to this latter process [32-34], however, the exact mechanism of copper delivery to the mitochondria is not yet understood. The third important destination of copper in the cell is the secretory pathway. The distinct compartments of the secretory pathway (most likely the *trans*-Golgi network, TGN) contain Cu-ATPases, which receive copper from the cytosolic copper chaperone Atox1 [35-37]. These Cu-

ATPases transfer copper into the lumen of the TGN to copper dependent enzymes using the energy of ATP hydrolysis.

In the liver, copper is transported into the lumen of the secretory pathway by the copper transporting ATPase, ATP7B. The primary recipient of copper from ATP7B in the liver is ceruloplasmin, a secreted ferroxidase. This protein is the major copper containing protein in the serum, however, in aceruloplasminemia mice (ceruloplasmin KO), ceruloplasmin does not play an essential role in copper metabolism [38]. Excess cytosolic copper is excreted into the bile, presumably also by Cu-ATPase ATP7B. Copper export into the bile represents the major route of copper excretion from the body. In Wilson disease patients, both copper transport to the secretory pathway and copper release into the bile are greatly impaired, resulting in marked accumulation of copper in the liver, very low levels of copper bound ceruloplasmin in the serum, and reduced levels of copper in the bile [39].

Experiments in rats using radioactive copper revealed that newly absorbed copper appears in the blood stream in two waves: the initial peak (after two hours) corresponds to copper exiting the intestine and the second peak (after ~ six hours) represent copper incorporated into ceruloplasmin, which is secreted by the liver [31]. Serum copper, bound to ceruloplasmin, albumin, and possibly low molecular weight compounds, is then delivered to other organs where it can be incorporated into copper dependent enzymes with general (cytochrome c oxidase or superoxide dismutase) and tissue specific functions (for example, dopamine-β-hydroxylase in the adrenal gland [3], peptidylglycine

alpha-amidating monooxygenase in the pituitary gland [5], or tyrosinase in melanocytes [4]). The delivery of copper to the secretory pathway and export of copper from the cell is mediated by Cu-ATPases, similarly to their role in the liver or intestine.

In certain cells or tissues, only one Cu-ATPase is expressed (for example, ATP7A in the adrenal gland [3] or ATP7B in hepatocytes [40]), performing both export and biosynthetic function. Several tissues, however, such as the brain, developing kidney, placenta, mammary gland, eye, lung and some others, express both Cu-ATPases (for details on expression profiles see NCBI database Unigene Hs.496414 (ATP7A) and UniGene Hs.492280 (ATP7B). The specific roles that each of the Cu-ATPases may play in these tissues is not yet understood. It remains whether the presence of two Cu-ATPases relate to their functional characteristics, distinct developmental regulation, or different trafficking behavior in polarized epithelia. Further understanding of whether copper transporters have complementary or overlapping functions and similar regulation have only recently begun to be addressed.

1.3 Cu-ATPases and biosynthesis of secreted copper dependent enzymes

The first evidence for ATPase mediated copper transport to the secretory pathway was obtained from *Saccharomyces cerevisiae,* which contains the ATP7A/ATP7B homologue, Ccc2p [41]. Ccc2p is located in the late Golgi compartment, where it transports copper from the cytosol to the lumen for biosynthetic incorporation into Fet3p (a copper dependent metallo-oxidase

involved in iron uptake). Genetic deletion of Ccc2 abolishes copper incorporation into Fet3p and perturbs iron uptake, as illustrated by the inability of Δ*ccc2* cells to grow under iron limiting conditions [41]. Heterologous expression of either ATP7A or ATP7B restores the copper dependent Fet3 activity and permits the growth of ccc2 mutants on iron deficient medium [42-45]. This initial evidence for the ATP7A/ATP7B mediated transport of copper to the secretory pathway was further confirmed by more recent studies, which yielded direct evidence for the role of Cu-ATPases in biosynthesis of copper dependent enzymes in mammalian cells. The described complementation of the Δ*ccc2* phenotype serves as a convenient functional assay for evaluation of ATP7A and ATP7B activity.

1.3.1 Tyrosinase

An elegant and convincing demonstration of the role of copper transporting ATPases in the delivery of copper to the secretory pathway of mammalian cells was provided by Petris and Mercer using tyrosinase as an example [4]. Tyrosinase is a copper dependent enzyme that participates in the formation of the pigment melanin by catalyzing the hydroxylation of tyrosine to L-3, 4-dihydroxyphenylalanine (DOPA) and the oxidation of DOPA to DOPA-quinone. In order to be active, tyrosinase requires the incorporation of copper into two binding sites during its passage through the secretory pathway. Petris and Mercer proposed that ATP7A was the enzyme delivering copper to tyrosinase because Menkes disease patients are known to have abnormal pigmentation [4]. The authors then showed that transfection of fibroblasts derived from the skin of Menkes patients (Menkes fibroblasts: Me32 & Me52) with a

tyrosinase expression plasmid results in the expression of apo-protein and no production holo-tyrosinase. The biosynthesis of copper bound holo-tyrosinase and the generation of pigment are restored by the transfection of the ATP7A expression plasmid into Menkes fibroblasts. These results illustrate that ATP7A is the Cu-ATPase that delivers copper to tyrosinase in the secretory pathway. ATP7B does not seem to play a role in copper delivery to tyrosinase in tissues, however in an *in vitro* system, such as cultured hepatocytes, ATP7B can mediate copper delivery to heterologously expressed tyrosinase [46]

1.3.2 Lysyl oxidase

Lysyl oxidase is a copper requiring enzyme involved in the cross-linking of collagen and elastin. Menkes disease patients display severe connective tissue defects suggesting that the lack of a functional Cu-ATPase, ATP7A, disrupts delivery of copper to lysyl oxidase in the secretory pathway. The observation of a similar temporal expression of rat lysyl oxidase and ATP7A during embryonic development using quantitative real-time PCR is supportive of this conclusion [47]. Further support for ATP7A involvement in copper incorporation into lysyl oxidase came from studies of occipital horn syndrome (OHS) patients [48]. In these patients, the levels of ATP7A are greatly reduced as a result of frame shift mutations in ATP7A mRNA. Correlating with the decreased levels of active ATP7A, the production of lysyl oxidase in OHS patients is diminished and the patients typically display connective tissue disorders [48]

1.3.3 Peptidylglycine α-Amidating Monooxygenase (PAM)

PAM is a copper dependent enzyme located in the pituitary gland, adrenal medulla, atrium of the heart, and the central nervous system. This enzyme has an important physiological role in catalyzing the conversion of over 50% of all neuropeptides into α-amidated peptides [5]. To determine whether ATP7A is responsible for copper delivery to PAM, Stevenson and co-workers used western blot analysis to demonstrate that ATP7A was highly expressed in the pituitary and adrenal gland, two regions abundant in PAM. Furthermore, immunohistochemistry of pituitary endocrine cells further revealed that ATP7A and PAM co-localize to the *trans* Golgi network, suggesting that copper may be available to PAM in this compartment [5]. To further confirm that ATP7A delivers copper to PAM, the authors investigated production and function of PAM in the mottled-brindled mutant mouse, which lack functional ATP7A. Interestingly, although the levels and the processing of PAM were normal in these mutant mice, a marked reduction in the level of amidated peptides was observed. The authors proposed that a deficiency in peptide amidation may contribute to the developmental problems associated with Menkes disease syndrome [5]

1.3.4 Ceruloplasmin

Approximately 95% of serum copper is ascribed to the copper containing ferroxidase ceruloplasmin (Cp). Unlike tyrosinase or PAM, which receive their metal from ATP7A, ATP7B is the source of biosynthetic copper for ceruloplasmin. Copper incorporation into Cp was first thought to occur in the rough endoplasmic reticulum[49] however, Terada and co-workers demonstrated that both ATP7B and holo-Cp were in the Golgi-enriched fractions of liver cells,

suggesting that ATP7B delivers copper to apo-Cp in the secretory pathway [6]. To confirm that ATP7B was directly involved in the synthesis of holo-Cp, the authors used recombinant adenovirus to introduce ATP7B cDNA into LEC rats, an animal strain that lacks functional ATP7B and only produces the apo-form of Cp. Infusion of the recombinant adenovirus restored copper incorporation into Cp in the livers of LEC rats, providing strong evidence for the role of ATP7B in ceruloplasmin biosynthesis [6].

1.4 Tissue specific expression and functions of Cu-ATPases

An accurate picture of the tissue localization of human Cu-ATPases is necessary before meaningful statements can be made about their specific roles in copper homeostasis in tissues. The cloning of each gene in 1993 and subsequent Northern blot analysis of tissues revealed that ATP7A (designated Atp7a for murine models) and ATP7B (designated Atp7b for murine models) are co-expressed in the kidney, brain, and placenta [50, 51]. Surprisingly, in more than 10 years since the discovery of human Cu-ATPases, little information is available (with the exception of a few recent studies, see below) on either the localization of these proteins to specific regions or cells in these tissues or the precise physiological functions of the Cu-ATPases. As we described above, the symptoms of Menkes disease and Wilson disease suggest some tissue specific roles for each transporter. Expression of ATP7A in gut mucosa and in the choroid plexus correlates well with the key role of ATP7A in the generalized delivery of dietary copper to the body and especially to the brain. Expression of ATP7B in the adult liver is linked to the important role of this Cu-ATPase in the

biosynthesis of ceruloplasmin and export of excess copper into the bile for eventual removal from the body. Details of the degree of overlapping function between ATP7A and ATP7B are yet unresolved, but data presented below suggests a possible distinct function in tissues.

1.4.1 Expression and localization of Atp7a and Atp7b in the kidney

The kidneys have one of the highest copper concentration among tissues (7-12 mg/g [31]). It is not clear how much copper is delivered to renal cells from the blood and how much is filtered in the glomerulus, since a large fraction of serum copper is thought to be protein bound. However, most of the filtered copper is likely to be reabsorbed, and high copper concentrations in the urine are only observed under disease conditions. Despite the involvement of kidneys in copper handling, remarkably little is known about renal copper transport. The location of Cu-ATPases along the renal tubules, their specific roles in renal copper handing, and their regulation during development remain scarcely characterized. Diamine oxidase, which is involved in the oxidative deamination of histamine and other diamines, is produced in kidneys; [52] and therefore the cells that produce this enzyme require Cu-ATPase function. It remains to be determined which Cu-ATPase, ATP7B or ATP7A, plays the key role in biosynthesis of renal copper dependent enzymes.

In mice, copper was found in the proximal and distal tubules as well as the glomeruli [53, 54]. Thus, these regions seem to represent the major sites where copper could be regulated through either uptake or export and where Cu-ATPases might be expressed. Additional information about the possible

localization of copper transporting ATPases was provided by murine models for Wilson disease (*tx* milk mouse and LEC rat [55, 56]) and Menkes disease (brindled mice and macular mice [57, 58]). In both cases, malfunction of Cu-ATPases is associated with copper accumulation in proximal tubules of the cortex, but not in the glomeruli or distal tubules [59, 60]. Similarly, in Menkes or Wilson disease patients, copper accumulation is also observed in the proximal tubules. This strongly suggests that ATP7A and ATP7B function is mainly required in proximal tubules for copper reabsorption into blood and/or excretion into the urine.

ATP7A localization in the kidney has been investigated directly using immunohistochemical staining of kidneys isolated from 10-day-old mice [61]. The authors detected ATP7A in proximal and distal tubules; very little, if any staining was seen in the glomeruli. Detailed analysis of the intracellular localization of ATP7A in proximal tubules was not carried out in this study, although staining was reported as diffuse suggesting intracellular and perhaps vesicular localization. Staining of ATP7A in distal tubules was observed at the basolateral membrane, suggesting that the role of ATP7A in this region is to transport copper into the circulation [62]. Subsequently, Murata and colleagues confirmed the presence of Atp7a mRNA in proximal tubules using *in situ* hybridization in 4-week-old mice [63]. No glomerular staining was found, consistent with previous data. In contrast to the earlier work, Murata and co-workers did not find any labeling of Atp7a in the distal tubules. This discrepancy may be due to different methods utilized, protein [62] compared to mRNA [63] detection, and the differences

in the age of the animals employed. No information is currently available on the developmental regulation of copper transporters in kidney.

Expression of ATP7B in kidney [64], as well as copper accumulation in kidneys of Wilson disease patients [65] pointed to a role of ATP7B in renal copper distribution, that appears to be distinct from the role of ATP7A. In 2002, Moore and Cox published the first report comparing the ATP7A and ATP7B mRNA expression in mouse renal tissue. ATP7B mRNA was localized to the glomeruli and correlated with the results on immunohistochemical localization of the protein [64]. Staining of both ATP7B mRNA and protein was also reported in the inner and outer zone of the medulla, which the authors suggest may be the loops of Henle. These results are quite interesting and point to region specific distribution of ATP7A and ATP7B in kidney. Surprisingly, the pattern of ATP7A distribution described in this work differed significantly from previous reports. Moore and Cox found ATP7A in glomeruli, a localization that had not been observed by two other groups, but did not discuss staining of ATP7A in any other kidney regions. Clearly, more work needs to be done to clarify discrepancies. Utilization of both mRNA and protein detection, single cell resolution of images, and developmental studies would increase confidence in the mapping results and greatly facilitate understanding of the functional roles of Cu-ATPase in renal cells.

1.4.2 Localization and possible functions of Atp7a and Atp7b in the placenta

Infants with Menkes disease exhibit many symptoms associated with copper deficiency, particularly skeletal abnormalities, hypopigmentation and

neurological problems [66]. The copper deficiency observed in these infants is thought to be caused by impaired placental copper transport to the developing fetus [7]. The placenta of both Menkes disease and Wilson disease patients accumulates copper [67, 68]. Therefore, it seems likely that ATP7A and ATP7B both have a role in the transfer of copper across the placenta during gestation. This conclusion is supported by recent studies on expression and localization of ATP7A and ATP7B in human placenta of the first trimester (7-9 weeks), second trimester (15-18 weeks) and at term (40 weeks) [69]. ATP7A and ATP7B are both expressed throughout gestation; however the localization of proteins within the placenta differs. ATP7A is expressed in the syncytiotrophoblast, the cytotrophoblast, and the fetal vascular endothelial cells [69]. In contrast, ATP7B was only detected in the syncytiotrophoblast [69].`

The observed localization of ATP7A in placenta suggests that it may transfer copper from the basolateral surface of the syncitiotrophoblast directly into the fetal circulation [69]. The ATP7B staining in the syncytiotrophoblast differed from that of ATP7A, which may reflect a different localization (and function) of ATP7B during neonatal development [69]. It was proposed that ATP7B might be present on the apical surface of the placenta and function to return copper from the placenta back toward the mother. This may represent a mechanism preventing accumulation of excess copper in the fetus [69]. Staining with single cell resolution and localization of ATP7A and ATP7B to specific plasma membranes would help to test these important hypotheses.

1.4.3 Cu-ATPases in mammary gland

The primary function of the mammary gland is to secrete nutrients into the milk during lactation. Copper is essential for neonatal growth and therefore has to be exported into the milk. Current data suggest that this is most likely accomplished by ATP7A and/or ATP7B. Several laboratories have investigated the expression of Cu-ATPases in the mammary gland of humans, mice, and rats[70-72]. Ackland and co-workers discovered that ATP7A was expressed in both lactating and non-lactating human mammary gland and that the intracellular localization of ATP7A was altered upon lactation[71]. Using immunohistochemistry on breast tissue, these authors demonstrated that in non-lactating tissue, ATP7A was confined to a perinuclear compartment in luminal epithelial cells, while myoepithelial cells were not labeled [71]. In lactating tissue, ATP7A appeared in a diffuse pattern in cells of the areola and ducts suggesting involvement of ATP7A in the cellular efflux of copper into the milk [71].

The distribution of mATP7B in the mammary gland was first investigated in control and toxic (*tx*) milk mice. *tx* mice have an inactivating mutation in mATP7B and are born copper deficient due to insufficient copper in milk produced by the mutant mothers (hence the term “toxic milk”) [73]. The *tx* pups have reduced copper levels in the stomach and often die unless nursed by non-mutant mice. These observations led to the suggestion that mATP7B (in addition to mATP7A) has an important role in delivery of copper to the milk. Localization studies revealed that in both control and *tx* non-lactating mice, mATP7B was present in the luminal epithelial cells and had a perinuclear localization [73]. This intracellular localization is consistent with a biosynthetic role for Atp7b, such as

delivery of copper to ceruloplasmin, which is produced in substantial amounts in the mammary gland [74].

With lactation, the intracellular distribution of ATP7B changes. In normal lactating mice, mATP7B was detected in a granular diffuse cytoplasmic pattern and not in the perinuclear compartment as seen in non-lactating animals [73] Interestingly, in *tx* mice the localization pattern of mutant mATP7B does not change in response to lactation [73]. The authors concluded that relocalization of mATP7B in lactating animals represents the step necessary for copper export and that "Atp7b (mATP7B) is the major copper transporter in the mammary gland" [73]. A more recent study compared the localization of both ATP7A and ATP7B in the same lactating mammary gland (in rat) using immunohistochemistry [72]. rATP7A was localized to both the luminal and serosal membrane with little intracellular staining observed for this transporter. Antibodies staining against rATP7B produced punctuate staining primarily in the luminal region of the cells. The authors proposed that the role of rATP7A at the plasma membrane is to directly export copper into the milk [72], while the high levels of ATP7B in the mammary gland could be necessary to accommodate copper incorporation into ceruloplasmin.

The change in the intracellular localization of both mATP7A and mATP7B in response to lactation is intriguing. Regulated trafficking of the Cu-ATPases has been previously described in cultured cells in response to altered concentrations of copper and also in copper perfused tissue. It is currently unknown whether the relocalization of ATP7A and ATP7B in mammary gland is

triggered by increased intracellular copper levels upon lactation, or perhaps is due to induction of signaling pathways stimulated by hormones produced during lactation. The kinase mediated phosphorylation of ATP7B that correlates with the intracellular localization of the transporter has been previously demonstrated in hepatic cells [75]. How kinase(s) sense the changing levels of copper (or other signal) to induce phosphorylation and the exact role of the kinase mediated phosphorylation in intracellular localization of Cu-ATPases in mammary glands and other tissues are important questions that remain to be addressed.

1.4.4 Expression and function of Atp7a and Atp7b in the brain

Normal function of Cu-ATPases in the brain is particularly important, as evidenced by marked neurological, developmental, and behavior abnormalities observed in patients lacking either ATP7A or ATP7B. MRI scans of patients displaying classical Menkes disease often show progressive cerebral atrophy, delayed myelination or even demyelination of the white matter and tortuosity of intracranial vessels [76, 77]. Similar studies of Wilson disease patients revealed deformities in basal ganglia, necrosis, spongiform degeneration and demyelination [78, 79]. To understand how these pathologies develop, it seems particularly important to decipher the localization and function of Cu-ATPases in the corresponding regions of the brain.

Several studies have attempted to localize ATP7A and ATP7B in murine brain; however a detailed high resolution expression map of both proteins either together or separately is yet to become available. rATP7B distribution was analyzed using *in situ* blotting of 4 week old rat brain following direct transfer of

native proteins from sectioned tissue to a blotting membrane [80]. In sagital sections, rATP7B was detected in neuronal cells of the CA1-CA4 layers of the hippocampus and this localization was confirmed by *in situ* hybridization. rATP7B was also detected in the glomerular cell layer of the olfactory bulb, and in the granular cell layer of the cerebellum [80]. More recent high resolution studies on mATP7B in adult and developing mouse brain confirmed this observation and demonstrated that Purkinje neurons are the major site of mATP7B expression in the cerebellum [81]

In 1996, Iwase and co-workers examined the expression of mATP7A in 13-day-old mouse brain using northern blot analysis and *in situ* hybridization [82]. The intense labeling in the CA1 and CA3 region of the hippocampus as well as labeling of the dentate gyrus was observed pointing to co-expression of mATP7A and mATP7B in the hippocampus. Labeling of the cell bodies in the granular, mitral and glomerular layers of the olfactory bulb was also reported. In the granular layer of the cerebellum, intense staining of mATP7A was detected however, little if any Purkinje labeling was found. The cells bodies in the molecular layer also appeared labeled but this was not commented upon. Very different results were reported by Murata and co-workers who studied expression of mATP7A in 4 weeks old mouse brain [63]. These authors found intense staining of mATP7A mRNA in the choroid plexus and dentate gyrus of the hippocampus as well as Purkinje cells in the cerebellum. The discrepancies were attributed to different ages of the mice and differences in specificity and sensitivity of the probes for *in situ* hybridization.

More recently, two independent techniques (fluorescent *in situ* hybridization and immunohistochemistry) were compared to investigate the distribution of both Cu-ATPases in the developing and adult mouse cerebellum. The experiments revealed that in the adult cerebellum (10 weeks old mice), Atp7a and Atp7b have cell specific distribution. Both experimental procedures demonstrated that Atp7a is expressed in Bergmann glia (BG) cells, while Atp7b is present in Purkinje neurons (PN) [81]. It has been previously shown that in the adult cerebellum, Bergmann glia insulate Purkinje neurons and help to maintain the structure of the neurons as well as supplying them with trophic factors [83, 84]. Therefore, the function of Atp7a in the Bergmann glia could be to regulate the copper concentration in these cells and to perhaps export copper for delivery to Purkinje neurons. In Purkinje neurons, Atp7b functions in the biosynthetic pathway, delivering copper to ceruloplasmin, which is also expressed in the Purkinje neurons [81].

The functions of these two Cu-ATPases in cerebellum appear to be tightly coordinated, as evidenced by experiments on animals lacking functional Atp7b. In genetically engineered *Atp7b*$^{-/-}$ mice, a change in cell specific expression of ceruloplasmin, a protein receiving copper from Atp7b, was observed. In control animals, Atp7b and ceruloplasmin are co-expressed in Purkinje neurons as evidenced by immunostaining of respective proteins. In the *Atp7b*$^{-/-}$ cerebellum, ceruloplasmin is co-expressed with Atp7a in Bergmann glia; this co-expression is associated with the restoration of copper delivery to ceruloplasmin. Thus, in cerebellum at least partial compensation for the loss of one of the proteins can

be achieved via utilization of the Cu-ATPase activity of the other. [81]. It is tempting to speculate that this compensation may explain at least to some degree the milder pathology in the cerebellum of Wilson disease patients compared to other regions of the brain.

1.5 Developmental changes in expression of Atp7a and Atp7b

Atp7a is widely expressed during both embryogenesis and in adult tissues, pointing to the key role of this Cu-ATPase in cellular copper homeostasis. The liver is so far the only tissue for which significant developmental regulation of Atp7a was reported [51, 85]. A detailed study of the Atp7a expression using northern blot analysis demonstrated the presence of Atp7a in the mouse liver at days E17, E19, and P2, while by P10 and P15 this expression was barely detectable. It is unclear why the liver expresses high amounts of Atp7a, which then decline shortly after birth, as opposed to Atp7b, the levels of which are increased at this time. It could be that the developmental changes in liver function require Cu-ATPases with somewhat different functional characteristics. Furthermore, ATP7A and ATP7B appear to export copper through different membranes in polarized epithelia (basolateral and apical). Thus, the switch from ATP7A to ATP7B upon liver maturation may reflect the tissue need to export excess copper via canalicular (apical) membrane into the bile.

Expression of ATP7B during development was found to be regulated in a number of tissues. Iwase and co-workers demonstrated the presence of Atp7b in the heart and liver at E9.5 and subsequent increased expression in the heart,

lung, intestine, nasal epithelia, and liver at E11.5 [82]. From E15.5 to E18, expression of Atp7b was detected in the lung, thymus, liver, intestine, and the lining of the respiratory tract [82]. In the developing intestine, both genes are expressed in the villous epithelium; the role of Atp7b in developing intestine is unclear.

Kuo and colleagues directly compared the expression patterns of the *Atp7a* and *Atp7b* genes during embryonic development [85]. In agreement with other studies, *Atp7a* was found expressed throughout the embryo during gestation whereas *Atp7b* was only expressed in a limited set of tissues, including the liver, heart, central nervous system, intestine, thymus and respiratory epithelium [85]. The authors proposed that Atp7a might be required for the maintenance of cellular copper homeostasis and the extracellular microenvironment of multiple cell types during development. The limited expression of Atp7b during gestation pointed to a more specialized function such as copper delivery to cuproenzymes. For example, while both Atp7a and Atp7b were found in the embryonic lung, Atp7a was localized to the lung parenchyma whereas Atp7b was highly expressed in the bronchial epithelium, pointing to distinct functions of the two Cu-ATPases in lung. Expression of Atp7b in the fetal lung and other respiratory organs correlates with expression of the copper dependent ferroxidase, ceruloplasmin, in these organs during gestation [85], suggesting that Atp7b plays a major role in the biosynthetic delivery of copper to this enzyme.

Interesting changes in cell specific expression of Atp7a and Atp7b are observed in maturing cerebellum during postnatal development. Expression of both Atp7a and Atp7b in the murine cerebellum is regulated, but the mode of regulation for the two Cu-ATPases is very different. At day 2 after birth (P2), both Atp7a and Atp7b are detected in the Purkinje neurons. By days P6 and P13, Atp7b expression significantly increases and is observed not only in Purkinje neurons but also in the cells of the granular layer. This expression remains constant through P18, however subsequently it decreases with Atp7b only detected in the Purkinje neurons of adult cerebellum. (In Purkinje neurons, Atp7b expression is constant from P2 through to P13). In contrast to Atp7b, expression of Atp7a appears to switch from Purkinje neurons at early stages of postnatal development (P2-P13) to Bergmann glia in adult animals. At P18, Atp7b is still found in both cell types. This coincides with a very important time for the growth and development of the cerebellum when cell-cell contacts are established between Purkinje neurons and Bergman glia [83]. How expression of Atp7a and Atp7b in the cerebellum is regulated and whether establishing of cell polarity and cell-cell communication contributes to this important physiological phenomenon are areas needing further investigation.

1.6 Genomic organization of ATP7B

The complete exon-intron structure of the Wilson disease gene, *ATP7B,* was determined in 1994[50]. Presently, the cDNA sequence and genomic information is available for several orthologs of *ATP7B* as a result of sequencing and characterization of the genome of a number of organisms. *ATP7B* is a fairly

large gene, containing 21 exons varying from 77 to 1234 bp. The ATG codon for the initiating Met is located near the 3' end of exon 1 of *ATP7B* [50] (Figure 13). The first four of the six MBDs (Metal Binding Domain) are encoded in one large exon (exon #2). The currently accepted cDNA for ATP7B encodes for a 4.5kb gene product that was derived from liver.

1.7 General components of the ATP7B protein

The ATP7B gene encodes for a 165 kDa membrane protein (Figure 2A). At the N-terminus, ATP7B contains a large domain composed of six discrete metal binding domains connected by linker regions. This domain is important for copper binding. There are eight transmembrane segments which help form a copper translocation pathway. ATP7B also has an ATP binding domain that is important for ATP driven transport of copper. The last important region of the protein is the C-terminal tail which contains trafficking signals which are necessary for the spatial regulation of ATP7B. Further detail in the function of these domains will be discussed in the following sections.

1.7.1 Cu-ATPases as members of the P-type ATPase family

ATP7B encodes a large polytopic membrane protein. In the past several years, considerable progress has been made in analyzing the biochemical properties of this protein. Recent studies have established that ATP7B belongs to the large family of P-type ATPases and identified several functional domains in its structure. It has also become apparent that ATP7B and its orthologs form a separate subgroup within the P-type ATPase family (P_{1B}-ATPases), which has distinct structural and mechanistic characteristics.

Cu-ATPases transport copper from the cytosol across cellular membranes by using the energy of ATP hydrolysis. This process involves specific recognition of copper, delivery of copper to the membrane portion of the transporter with subsequent release to the other side of the membrane, as well as binding and hydrolysis of ATP. The structure of the protein reflects the need to accommodate and couple these reactions. The copper translocation pathway is located in the transmembrane portion of Cu-ATPases, which is composed of 8 transmembrane segments (TMS). The highly conserved CPC sequence in TMS6 is one of the signature motifs characterizing Cu-ATPases and ATPases involved in transport of Zn, Cd, Ni, Ag, and Pb which together form the P_{1B}-subfamily [86]. Recently, four amino acid residues in transmembrane segments 7 and 8 of the bacterial Cu-ATPase, CopA were identified as required for copper binding[87]. These residues are conserved in the primary structure of P_{1B}-ATPases involved in the transport of Cu (I). Along with Cys residues of the CPC motif, they are likely to form copper-binding site(s) within the membrane portion. For ATP7B the corresponding residues are $Y^{1331}N^{1332}$, M^{1359} and S^{1362}. All other functional domains of Cu-ATPases are cytosolic.

1.7.2 N-terminal copper binding domain

The N-terminal portion of human Cu-ATPases encodes over 600 residues and contains 6 repetitive sequences, each harboring the sequence motif GMT/HCxxC. Each of the repeats form a sub-domain containing a single metal binding site, resulting in the stoichiometry of 1 copper ion binding to 1 metal binding site for a total of 6 metal ions per N-terminal domain [88-92]. Copper binds

in the reduced Cu(I) form and the two Cys residues in the metal binding motif CxxC are the only copper coordinating ligands [93-96]. *In vitro*, and perhaps *in vivo*, other metals such as zinc [97] or lead[98] can bind to the N-terminal domain of ATP7A; however the functional consequences and physiological significance of zinc or lead binding remains to be determined.

Structural information on individual metal binding domains (MBD) 1, 2, 4, and 5 of ATP7A has been obtained by several investigators using NMR [99-103]. These studies revealed compactly folded "ferredoxin"-like structures with a βαββαβ fold. The copper binding Cys residues of the CxxC motif are located in the βα-loop at the N-terminal portion of the first α-helix at the protein surface and, in individual MBDs, are exposed. The arrangement of the six MBDs relative to each other within the full-length protein still remains to be determined. Conserved Met, Leu, and Phe (Pro in MBD3) residues located in spatial proximity to the CxxC motif form a hydrophobic core, which is likely to stabilize the metal protein complex [101, 104]. Structural and molecular modeling studies of MBDs have predicted that the distribution of charges on the surface of MBDs differ significantly. This difference may be necessary for complementary inter-MBD interactions during assembly of the full length transporter. It has also been suggested that electrostatic interactions of oppositely charged surfaces represent an important step in copper transfer from the copper chaperone Atox1 to MBDs [104, 105].

Extensive mutational analysis and deletion studies were carried out by several laboratories to better understand the role of the multiple binding sites at

the N-terminal domain [106-111]. It now seems clear that the two sites closest to the membrane are important for the functional activity of Cu-ATPases and at least one of the two has to be present for normal transport activity. Binding of copper to these sites may affect (increase) the affinity of the intra-molecular sites for copper and thus facilitate copper transfer into the transmembrane portion of the transporter [107]. The first four metal binding sites have a regulatory function. Deletion of the region containing these four sites has no inhibitory effect on Cu-ATPases [107, 108]. In fact, deletion of metal binding domains 1-4 in ATP7B facilitates binding and hydrolysis of ATP, suggesting that the N-terminal domain, when present, may play an auto-inhibitory role, regulating copper access to the other MBDs [107]. This conclusion is supported by studies showing copper dependent interactions between the N-terminal domain and the ATP-binding domain. Specifically, binding of copper to MBDs in the N-terminal domain was shown to weaken interactions with the ATP-binding domain and increase affinity of the latter domain for ATP [1]. Thus, it seems likely that one of the roles of the N-terminal metal binding domains is to modulate enzymatic activity in response to changes in their copper occupancy. It is also possible that copper binding and consequent changes in domain-domain interactions allow Cu-ATPases to adopt specific conformations and/or interact with proteins necessary for the intracellular trafficking of these transporters.

1.7.3 ATP binding domain

The catalytic activity of Cu-ATPases (the binding and hydrolysis of ATP) is most likely mediated, as in other P-type ATPases, through coordinated action of

the A-(actuator) domain and the ATP-binding domain. The latter consists of two portions: the P (phosphorylation) -domain that includes the site of catalytic phosphorylation and the signature motifs for the P-type ATPases (DKTG, TGDN, GDGxxxD) and the N (nucleotide binding) -domain. Sequence analysis of the ATP-binding domain of Cu-ATPases shows relatively high homology with SERCA Ca^{2+}-ATPase in the P-domain; this similarity was utilized to produced a reliable structure model of the ATP7B P-domain[112]. The N-domain of ATP7B is smaller than that of Ca^{2+}-ATPase and the similarities by sequence alignment was not obvious without a high resolution structure, which has been recently solved by high resolution NMR [113]. The structure of the N-domain in the presence of ATP comprises a six-stranded β-sheet flanked by two pairs of α-helices, and a long unstructured loop. The structural motif consisting of a six-stranded antiparallel β-sheet and two flanking α-helical hairpins was proposed to represent a minimal core structure of the P-ATPase N-domain[114]. The common core is required for the essential nucleotide binding, whereas additional structural elements are responsible for other functions, which may include interactions with other domains, regulatory proteins, or modulation of the nucleotide binding properties of the enzyme. In the ATP7B N-domain, the additional element is represented by a long disordered loop comprising residues 1114-1142. This segment corresponds to a sequence insert uniquely found in all the eukaryotic copper transporting ATPases, but not in any bacterial or archaeal P_{1B}-type enzymes. The loop residues are not involved in ATP-binding, as shown by chemical shift perturbation analysis of the isolated N-domain [113]. It is possible

that the loop region may be involved in the interactions with the copper-binding domains, chaperone, or regulatory proteins. Such protein-protein interactions may induce ordering of this region into a compact structure.

Sequence alignment reveals several invariant residues in the N-domain of P_{1B}-ATPases. In ATP7B, these residues are H^{1064}, H^{1069}, G^{1101}, G^{1099} and G^{1149}. All these residues are located in the ATP-binding site. G^{1101} and G^{1099} are close to the α- and β- phosphates of ATP. Electrostatic interaction between G^{1101} and G^{1099} backbone amides and α- and perhaps β-phosphate of ATP may contribute to the tight ATP binding by the N-domain. Similar to the Ca^{2+}-ATPase structure, the ribose is located in a pocket created by G^{1149}. The adenine moiety appears to be in contact with the H^{1069} imidazole ring and is surrounded by hydrophobic side chains I^{1180} and I^{1102}. The role of E^{1064}, which is not in direct contact with ATP, is not quite clear, but its location suggests involvement in stabilization of H^{1069} interaction with adenine.

1.7.4 The A-domain and C-terminus

The A-domain is located between TMS4 and TMS5. It contains the TGE sequence motif, which is essential for enzymatic function of P-type ATPases. In Ca^{2+}-ATPases, the Glu residue in this motif is required for the phosphatase step of the catalytic cycle (dephosphorylation of the intermediate formed during ATP hydrolysis) [115]. (Although the majority of the information known about the A-domain is from ATP7A, it is assumed ATP7A and ATP7B are similar enough in overall sequence that ATP7A structural data is applicable to ATP7B). Consistent with this role, the TGE>AAA mutation in the A-domain of ATP7A leads to

hyperphosphorylated protein [116]. With the exception of the invariant TGE motif, the primary structure of the A-domain of Cu-ATPases has little similarity to other P-type ATPases. Nevertheless, structure prediction algorithms (at http://www.predictprotein.org) recognize the fold of V^{901}-K^{987} of ATP7A as very similar to that of the A-domain of SERCA, a Ca^{2+}-ATPase (the only P-type ATPase for which the high resolution structure has been determined). Thus, similar to the N-domain, the overall architecture of this key functional domain of Cu-ATPases is preserved in the absence of primary sequence conservation. More detailed modeling studies of this and other regions of ATP7A were recently performed by Moller and co-workers and provided explanations for inactivating effects of various Menkes disease mutations [117].

No structural information is available on the C-terminal region of human Cu-ATPases. The C-terminal tail is fairly long (~80 residues) and contains a conserved tri-leucine motifs in ATP7B, which are required for retrieval of the transporter from the plasma membrane [108, 118]. Mutations resulting in deletions in the C-terminal region were shown to be deleterious for protein stability [42] and associated with disease phenotype [119]. In a recent study, Hsi and co-workers demonstrated that although the C-terminus of ATP7B is necessary for protein stability, near wild-type levels of ATP7B activity can still be detected when only a third of the C-terminus is present [42].

1.8 Alternate splicing and protein variants of ATP7B

Alternative gene splicing is a common mechanism to produce protein products with distinct functional characteristics for the finely tuned regulation of

cell metabolism. Not surprisingly, many alternate spliced products of *ATP7B* mRNA have been detected, however, remarkably little is known about their functional significance. This important mechanism of increasing the diversity of the proteome remains greatly understudied in the case of copper transporters, despite the fact that it may hold important keys to a better understanding of the great phenotypic diversity observed in patients with mutations in *ATP7B*.

Petrukhin and co-workers provided the first evidence that alternate splicing of *ATP7B* occurred in the brain and liver [50]. RT-PCR experiments performed on RNA containing polyA tails isolated from these tissues demonstrated that the most abundant liver transcript contains all 21 exons of *ATP7B* found in the genomic DNA. The brain, however, appears to contain many splice variants. Curiously, the transcripts included those, which if translated, would unlikely produce functional transporter. For example, mRNA with exon 17 spliced would lack the sequence encoding the ATP binding site, whereas splicing exons 6, 7 and 8 would delete the predicted TMS 1-4. Similarly, splicing exon 13 would eliminate TMS 6, which contains the conserved copper-binding motif, CPC.

Consequently, physiological significance of these mRNA variants remains to be determined. Expression of the recombinant ATP7B variant that lacked exons 6, 7, 8 and 12 in HTB9 cells revealed that this truncated protein was dispersed throughout the cytosol [120] in contrast to the *trans*-Golgi network location of the wild-type ATP7B. It seems likely that this ATP7B variant was misfolded, however, presently one cannot exclude that either alternatively

translated *ATP7B* mRNA or the corresponding proteins may perform regulatory functions in the cell. It is important to note that Western blot analysis of cerebellum using anti-Atp7b antibody show several positive bands, which are not detected in the cerebellum of Atp7b knock-out mice (Barnes unpublished observation).

1.9 PINA

A very interesting alternative transcript of *ATP7B*, PINA, is produced in the pineal gland (hence the name –PINeal Atpase) and in retina [121]. This product is generated from an intronic promoter upstream of exon 9 in a process that results in two transcripts of 3.5kb and 4.3kb [122]. PINA expression shows a dramatic diurnal rhythm in both the pineal gland and retina, with 100-fold greater expression in the retina at night than in the day [121]. At night, expression of PINA is observed throughout the pineal gland; in the developing eye *PINA* expression is found within the retinal pigment epithelium layer, the developing ciliary body and at later stages in a subset of photoreceptor cells. In adult eyes, *PINA* is detected in the region of the outer nuclear layer where cone cells reside. The function of PINA in these cells is not clear. At the protein level, PINA is identical to ATP7B except it lacks all 6 N-terminal MBDs, the first 4 transmembrane domains, and part of the A-domain. Surprisingly, despite the lack of these important structural elements, PINA appears to compensate for the lack of ccc2, a yeast homologue of ATP7B, in Δccc2 yeast, suggesting PINA may still retain some copper transport activity [121]. The physiological role of PINA is very intriguing; unfortunately since the initial studies in 1998 and 1999, no further

reports on this Atp7b variant have been published. However, a murine model for the PINA defect has recently been reported, so perhaps more information regarding the physiological effects of this isoform will become available[123].

1.10 Transcriptional regulation/promoters

As we describe above, the expression of ATP7B is differentially regulated in several tissues during development, however the underlying mechanisms are unknown. The promoter regions of *ATP7B* have been mapped to 1.3-2.2 kb segments of genomic DNA upstream of the coding sequence and recently, the first information on promoter organization began to emerge [124-128]. Oh and colleagues identified approximately 1.3 kb of the 5'-flanking region of the ATP7B gene. When analyzed in a reporter assay, this sequence had high levels of luciferase activity in HepG2 cells [124]. The region contained four metal response elements (MREs) and six MRE-like sequences, usually found in metallothionein genes. Also, several putative regulatory elements such as Sp1, AP-1, AP-2, and E-box were identified, but no TATA box. The transcription start site was located 335 base pairs upstream of the translation initiation site [124]. Similar studies were carried out by Loudianos and co-workers [128]. It was later reported that the metal response element MREa in the promoter region of *ATP7B* plays a major role in transcriptional activation. MREa was found to bind 70 and 82 kDa proteins that were purified using avidin-biotin affinity chromatography and identified as Ku-related proteins. Subsequent functional studies produced evidence that the Ku-80 subunit is required for constitutive expression of the *ATP7B* gene [125]

To identify the regulatory elements required for expression of the pineal isoform of ATP7B (PINA, see above) Li and colleagues characterized sequences upstream of the rat PINA gene and identified a cis-acting element that was recognized by a pineal/retina-specific nuclear factor. This pineal regulatory element (PIRE) has a consensus of TAATC/T and is present in six copies in the 5' regulatory region of the PINA gene. PIRE binds a retina specific protein, cone rod homeobox (CRX), which transactivates PIRE reporter constructs [122].

1.11 Heterologous expression of Cu-ATPases and functional studies

The functional activity of ATP7B and ATP7A can be evaluated using a yeast complementation assay. The assay utilizes a strain of *S.cerevisiae* (Δ*ccc2*) in which the endogenous Cu-ATPase, Ccc2, is genetically inactivated resulting in poor delivery of copper to the secretory pathway. Insufficient supply of copper hinders formation of the holo-form of the copper dependent ferroxidase, Fet3, and since Fet3 is necessary for iron uptake, this results in poor growth of cells under iron limiting conditions [41]. Human Cu-ATPases expressed in Δ*ccc2* cells can supplement the lack of Ccc2 function and restore normal cell growth. The assay has been successfully used by a number of investigators and has yielded a wealth of information about transport activity (or the lack thereof) for various ATP7B and ATP7A mutants [41-43, 45, 111]. However, a detailed understanding of the copper transport mechanism requires more direct and quantitative measurements of Cu-ATPase function.

Recently, assays for measuring catalytic activity of ATP7B have become available. These direct functional assays are based on a characteristic property

of P-type ATPases which become transiently phosphorylated at the invariant Asp residue during ATP hydrolysis. The phosphorylated intermediate, although unstable at alkaline pH, can be trapped under acidic conditions and the phosphorylated protein is visualized by autoradiography on an acidic gel. The effects of various ligands and conditions (copper, ATP, pH) on the level and rate of formation of the phosphorylated intermediate (as well as its decay) can also be evaluated. The assay has been initially used for immunoprecipitated ATP7A overexpressed in mammalian cells [129]. The study demonstrated ATP7A forms a phosphorylated intermediate of which copper can have a stimulatory effect [129] thus confirming that ATP7A functions as a P-type ATPase.

Immunoprecipitation yields small amounts of material and requires the use of detergents, which may alter enzyme characteristics. A more recently developed heterologous expression of ATP7B in insect cells provides a more robust system for the biochemical analysis of human Cu-ATPases [81, 130]. In this method, recombinant ATP7B is produced in *Sf*9 cells following baculovirus mediated infection. The levels of expression are high for a membrane protein, approximately 1-2% of the total *Sf9* membrane protein, and permit detailed biochemical characterization of ATP7B in a native membrane environment. Using this system, ATP7B was shown to form a transient phosphorylated intermediate in a copper dependent fashion [130] and importantly, the catalytic properties of ATP7B and ATP7A have been compared directly [81].

1.12 ATP7A and ATP7B have distinct enzymatic characteristics

Experiments measuring the ATP dependence of catalytic phosphorylation (formation of phosphorylated intermediate during ATP hydrolysis) revealed that the two human Cu-ATPases have essentially identical apparent affinities for ATP, approximately 1 μM [81, 130]. At the same time, the analysis of the copper dependency illustrated that the apparent affinities of ATP7A and ATP7B for copper are not the same. (It should be noted that in the experiments analyzing the effect of copper on catalytic phosphorylation, one measures the apparent affinity of copper for the intra-membrane sites, since binding to this site(s) is required for catalysis). ATP7A has a slightly lower copper binding affinity for the intramembrane site with the apparent Km of 2.5 μM compared to 1 μM for ATP7B. This difference is small and whether or not it is physiologically significant remains to be established. It is important to emphasize that these measurements were carried out using free copper ions; while in cells, the Cu-ATPases are thought to bind copper as a result of transfer from the cytosolic copper chaperone Atox1. It seems quite likely that the interactions of ATP7A and ATP7B with the copper chaperone and the efficiency of copper transfer may differ for each Cu-ATPase and result in somewhat different responses of the two transporters to changing intracellular copper. This could be particularly significant in those cells which simultaneously express both ATP7A and ATP7B (for example Purkinje neurons during cerebellum maturation). In this case, the interactions of the Cu-ATPases with Atox1 rather than the affinity of their intramembrane sites for copper may determine to which ATPase copper is distributed.

The functional studies in insect cells also revealed significant differences between ATP7A and ATP7B in the rates of their partial reactions[81]. Measurements of the kinetics of catalytic phosphorylation and dephosphorylation demonstrate that ATP7A performs each of these steps 6-fold faster than ATP7B [81]. Thus it seems that ATP7A is a faster transporter (i.e. it has a higher turnover rate), which would allow ATP7A to remove copper from the cell more effectively than ATP7B. These functional properties along with expression of ATP7A in many tissues are consistent with the proposed housekeeping role of ATP7A in copper transport in most tissues. ATP7B, on the other hand, might have a more specialized role in copper transport that is tissue specific.

1.13 Transport activity of Cu-ATPases

While significant progress has been made in characterizing the enzymatic properties of ATP7B and ATP7A, direct measurements of copper transport activity of Cu-ATPases are yet to be optimized. The yeast complementation assay and the measurements of tyrosinase activity after co-expression of ATP7A and tyrosinase in the Menkes fibroblasts provide an effective *"in vivo"* way to evaluate the ability of protein to transport copper. However, to characterize the biochemical mechanism of copper transport, more direct quantitative approaches are needed. The stoichiometry of copper transport is still not known nor how copper is coordinated within the membrane (although recent studies on bacterial Cu-ATPases provide some clues on copper coordination [87]), and the parameters that affect copper transport efficiency. Direct measurements of copper transport activity also have an important practical value. Recent reports on the possible

role of ATP7B and ATP7A in resistance to platinum based chemotherapeutic drugs [131-135] emphasize the need to better understand how Cu-ATPases achieve transport of copper and, possibly, platinum across cell membranes.

Currently, only one group has succeeded in directly measuring copper transport by Cu-ATPases (mostly of ATP7A) using vesicles isolated from yeast or mammalian cells overexpressing the transporter [110, 136-138]. The measurements were sufficiently robust to evaluate the activity of wild-type ATP7A and a number of mutants and to illustrate that it was possible to measure the ATP dependent copper transport *in vitro*. Interestingly, some differences in the transport characteristics of the Cu-ATPase were seen, depending on whether the protein was expressed in yeast or mammalian cells. These results suggest that the protein or lipid composition of vesicles may play a role in the efficiency of copper transport by ATP7A. Only one brief report described copper transport by ATP7B *in vitro* [137] and no direct comparison of copper transport efficiency, stoichiometry, or ligand dependencies for ATP7A and ATP7B has been published. The expression of ATP7A has been achieved in Xenopus oocytes [139], however copper transport has not been described in this system.

1.14 Factors that may affect efficiency of copper transport

The available transport data and analysis of enzymatic properties of ATP7A and ATP7B expressed in insect cells suggest that copper transport by overexpressed human Cu-ATPases is very slow, relative to known P-type ATPases. In the absence of specific inhibitors of Cu-ATPases, it is difficult to obtain estimates of the endogenous copper transport in tissues and compare it

with the activities of the recombinant transporters. Thus currently, it remains uncertain whether the observed slow rate reproduces the physiological situation or reflects the absence of auxiliary proteins in the heterologous system that may be required to facilitate transport. In yeast, copper delivery to copper-dependent enzymes is pH and chloride ion-dependent [140]. Significantly, a recent study by Wang and Weinman demonstrated that ClC-4, an intracellular chloride channel, co-localizes with ATP7B and stimulates copper incorporation into ceruloplasmin, probably by improving the efficiency of ATP7B [141] although whether this effect of chloride directly affects transport to only ceruloplasmin cannot be excluded.

As we described in earlier sections, it is not yet certain whether oxidase activity is required for copper exit from cells and whether the transport of copper by ATP7B is coupled to such copper oxidase activity. Ceruloplasmin, a serum ferroxidase, has significant copper oxidizing activity [142] and genetic inactivation of ceruloplasmin in mice is associated with accumulation of copper in the liver, presumably due to entrapment of copper in vesicles [38]. It is not clear why in the absence of ceruloplasmin; copper is not exported into the bile, a step in copper distribution associated with ATP7B function. It could be that under these circumstances, ATP7B transport activity is decreased and consequently the excess copper accumulates in compartments other than secretory pathways.

1.15 Transport activity of Cu-ATPases in different cell locations

In cells, Cu-ATPases have dual functions (copper delivery to the secretory pathway and copper export), which is achieved through relocalization of the transporters from the TGN to vesicles and then eventually to the plasma

membrane. It is assumed that the Cu-ATPases transport copper effectively in these different cell locations, however comparison of Cu-ATPase function in these locations is technically difficult and so far has not been carried out. It is possible that transport rates could be different, especially considering differences in transport reported between exogenously expressed Cu-ATPases in yeast and mammalian cells. Currently, little evidence is available showing that copper export from cells is largely due to the Cu-ATPases pumping copper directly across the plasma membrane. In fact, recent data point to the possibility that the major localization, and hence function of these transporters, is in the intracellular vesicles and their presence at the plasma membrane could be a result of fusion of the copper and ATPase-containing vesicles with the plasma membrane during the exocytosis/recycling process [29].

It is worth considering that the environments of Cu-ATPases at the TGN, intracellular vesicles, and the plasma membrane are quite different, and thus the rates of transport may vary considerably. In the TGN, where copper transport was convincingly demonstrated using the tyrosinase assay [4], copper released from the ATPase is taken up by copper binding proteins, providing a “copper sink” and perhaps maintaining a driving force for overall transport. In the intracellular vesicles to which Cu-ATPases relocalize in response to elevated intracellular copper, the pH remains acidic but it is not known whether specific copper acceptor proteins are present. Thus it is not clear whether in vesicles, copper is released efficiently, if at all. At the plasma membrane, the extracellular pH and ion composition are quite different from that of vesicles and the TGN.

Thus it seems possible that at elevated copper, the role of Cu-ATPases is not only (or even not as much as) to pump copper into vesicles, but rather to target vesicles to intracellular machinery that directs the vesicles to the plasma membrane where copper can be exported via vesicle fusion and exocytosis. Determining how exactly copper is exported from the cell, through protein mediated translocation across the plasma membrane or through vesicle mediated fusion is essential for understanding of copper homeostasis.

1.16 Copper delivery to intra-membrane sites

How ions migrate from the cytosol to intramembrane sites remains an intriguing and largely unanswered question for most P-type ATPases. In Cu-ATPases, this step of the ion translocation mechanism seems particularly complex due to the presence of multiple copper binding sites within the cytosolic N-terminal portion of the molecule and the need to keep copper in a protein-bound state. Cu(I), the form of copper that binds to the N-terminal domain of ATP7B [93, 95], is thought to be extremely unstable in solution and disproportionates to Cu(0) and Cu(II) unless bound to a carrier molecule. Therefore, a protein based pathway is thought to exist that guides Cu(I) from the copper chaperone Atox1 in the cytosol to the intramembrane portion of ATP7B, presumably via the N-terminal metal binding sites.

Deletion and MBD mutation constructs used in a yeast complementation assay demonstrated that the two metal binding domains closest to the membrane portion, MBD5 and MBD6, are important for the functional activity of Cu-ATPases, while the region including MBD1-4 is likely to be regulatory. Recent

studies revealed that the truncation of MBD1-4 is associated with an increased rate of catalytic phosphorylation [107], suggesting that MBD1-4 regulates ATP7B turnover and/or access of copper to the other copper binding sites. This regulation is likely to be mediated through copper dependent protein-protein interactions between the N-terminal copper binding domain and the ATP-binding domain that have been demonstrated *in vitro* [1]. Hypothetically, copper binding to either MBD5 or MBD6 could induce conformational changes in the protein, which increase the affinity of the intramembrane copper binding sites and facilitate transfer of copper to these sites. Whether copper migrates to the membrane from MBD5 and/or MBD6 or directly from Atox1 is currently unknown.

1.17 Atox1 mediated copper transfer

The protein mediated distribution of copper from the uptake system (CTR1) to the export system (ATP7B) is a unique feature of copper transport as compared to the transport of other ions such as sodium, calcium, or protons. This distribution is performed by a small cytosolic protein Atox1, which has a striking structural homology to the individual metal binding domains of Cu-ATPases [105, 143, 144]. It has been proposed that copper bound Atox1 docks to the N-terminal MBDs, and this event initiates the copper transfer reaction, which proceeds through –SH ligand exchange [105]. This is based on the crystal structure of Atox1 which showed 1 copper atom coordinated by two Atox1 molecules [105].

Although affinities of individual MBDs for each other have not yet been tested, this mechanism of copper transfer could also serve as a potential model

for copper exchange between MBDs. The surface charge distribution of the MBDs are similar to each other, except for MBD4, which is more acidic [145], however the theoretical pI's of the MBDs are varied (Figure 28) which may suggest a possibility for interdomain interaction. Work by Achilla et al show that copper transfer can occur between isolated MBDs, specifically copper bound MBD4 to apoMBD5+6 [146].

Recent EXAFS (Extended X-ray Absorption Fine Structure) analysis of the copper coordination environment in Atox1 is consistent with the hypothesis of –SH ligand exchange [144]. The EXAFS studies demonstrated that in Atox1, copper is coordinated by two sulfurs donated by the Cys residues in the conserved metal binding site MxCxxC. Consequently, it seems likely that upon Atox1 docking to individual MBDs, a transient intermediate will be formed in which the third ligand will be donated by the Cu-ATPase MBD. This model originally proposed by Rosenzweig and colleagues [105] leads to many interesting questions.

What is the driving force for the copper transfer reaction? Does Atox1 transfer copper to any MBD in Cu-ATPases or is there a preference for certain sites? Is there a difference between the copper transfer from Atox1 to ATP7B and ATP7A? While detailed mechanistic studies are necessary to provide comprehensive answers to these questions, recent work from several laboratories shed some light on the copper transfer mechanism. It has been shown that the association constants for both the chaperone and acceptor domains are approximately 1-10 μM, suggesting that copper transfer between Atox1 and its targets are under kinetic rather than thermodynamic control [88].

This vectoral copper transfer can be explained by the fact that MBDs retain copper much better than Atox1. Specifically, experiments comparing the ability of the copper chelator, BCS, to remove copper from holo-Atox1 compared to holo-MBD2 revealed that a 100-fold excess of BCS is sufficient to remove copper from Atox1, while only 10% of the bound copper is removed from MBD2 under the same conditions [145]. Recent detailed NMR studies of MBD2-5 and Atox1 provide a structural explanation of this phenomenon. For Atox1, there are only minor structural rearrangements upon copper binding [147]. In contrast, binding of copper to a metal binding domain causes changes in the structure of the MBD, which take place in the immediate vicinity of the bound metal and leads to greater shielding of copper from the solution[104]. How copper is then released from this partially hidden state and transferred further is not clear.

Recent studies on copper transfer from Atox1 to ATP7B suggest that this process is complex and that loading of the metal binding sites in the N-terminal domain proceeds through several discrete steps [37, 145]. Although it is clear that Atox1 may interact with various individual MBDs of Cu-ATPases [99, 148, 149], this interaction appears transient [99] and in the N-terminal domain, which contains several metal-binding domains connected to by linker regions, there is a clear preference for Atox1 interaction with some sites over others [145, 149]. Copper transfer experiments using purified Atox1 and the recombinant N-terminal domain of ATP7B (N-ATP7B) revealed that in ATP7B, MBD2 is the site to which Atox1 transfers copper preferentially and that the selectivity towards this metal binding domain is observed only if Atox1 (and not ascorbate or glutathione) is

used as a copper donor. Mutations of the metal binding cysteines in MBD2 in the full-length ATP7B completely disrupts catalytic phosphorylation of the ATP7B mutant when Atox1 is used as a source of copper [145]. Significantly, the ability of "free" copper to stimulate catalytic phosphorylation of this mutant is not changed.

Thus, it appears that in ATP7B, copper transfer from Atox1 to MBD2 is the first step in the transfer of copper to the intramembrane sites of the transporter. The current evidence also suggests that this initial copper transfer event is accompanied by a conformational change in the N-terminal domain [37, 145]. It is speculated that this change allows access of Atox1 to the other metal binding sites and further transfer of copper. However, further studies are needed to test the hypothesis that copper binding to MBD2 serves as a molecular switch initiating copper delivery to the intramembrane sites.

1.18 Regulation of Cu-ATPase function through copper dependent trafficking

As was discussed in earlier sections, the transport activity of ATP7B is utilized for two major purposes, to deliver copper into the biosynthetic pathway and to regulate the intracellular copper concentration by exporting excess copper from the cell. These two functions are mediated via regulated targeting of Cu-ATPases to different cellular membranes. The original studies from Petris and colleagues [150] and subsequent studies from several laboratories provide convincing evidence that Cu-ATPases have distinct intracellular localizations depending on whether or not cells are exposed to elevated copper. The following

sections summarize the current data on the possible mechanisms underlying copper dependent trafficking of Cu-ATPases.

1.19 Localization and trafficking of ATP7B

Trafficking of endogenous ATP7B has been studied in primary liver cells, as well as in the cultured cell line HepG2 and Hep3B, where ATP7B is abundantly expressed and ATP7A is not detected. For cells grown in basal medium, ATP7B localizes to a perinuclear compartment and immunostaining of ATP7B in this location is particularly compact when HepG2 cells are treated with 40 μM BCS, a copper chelator [45, 75, 120, 151]. Addition of copper sulfate to HepG2 and Hep3b cells result in trafficking of ATP7B to vesicles [45, 75, 151].

It has been concluded that ATP7B is localized to the trans-Golgi network when the extracellular copper concentration is less than 1 μM while at higher copper levels, ATP7B redistributes to vesicular structures and to apical vacuoles reminiscent of bile canaliculi [151]. A subsequent decrease in copper is associated with the return of ATP7B to the TGN. Also, brefeldin A and nocodazole disrupt copper induced trafficking of ATP7B; following treatment the transporter accumulates in a sub-apical compartment, suggesting continuous recycling of ATP7B between vesicles and the apical membrane when copper is increased [151]. This conclusion is in good agreement with the studies on the ATP7B localization in rat liver tissue showing that copper administration *in vivo* resulted in redistribution of this protein to a vesicular compartment localized in proximity to the canalicular (apical) membrane [152]. It was proposed that in this location, ATP7B transports copper into the vesicle lumen and at some point ATP7B

returns to the TGN while the copper laden vesicles continue to the plasma membrane for fusion and copper release. This model does not explain how ATP7B and copper are separated and how ATP7B recycles from the vesicles. An alternative scenario could have ATP7B exporting copper into vesicles and then continuing to the plasma membrane with the vesicles. Following vesicle fusion with the membrane, ATP7B could interact with the endocytic machinery, rapidly retrieved from the plasma membrane and returned to the TGN. Another possibility is that ATP7B functions at the plasma membrane to export copper and the vesicular staining seen in most cells is an intermediate state in the trafficking of ATP7B. The current data discussed below favors the last two scenarios [46, 153]

1.20 Trafficking of hATP7B transfected into tissue culture cells

Trafficking studies of recombinant ATP7B have also been performed in various cell lines. Expression of hATP7B in CHO-K1 (hamster ovary cells) and fibroblasts from Menkes disease patients revealed perinuclear localization under basal conditions and vesicular staining following treatment with elevated copper [154], [155], [106]. Similarly, in human HTB9 (bladder) cells, ATP7B has a perinuclear localization just as in the 2008 (human ovarian carcinoma cells) and Huh7 (human hepatocellular carcinoma cells) cell lines [120], [156], [157]. The Harada group, however, reported co-localization of GFP-tagged ATP7B with LAMP1 (a lysosomal marker that also can localize to the late endosome), but no co-localization with the lysosomal marker, cathepsin. These authors also observed no change in the intracellular localization in response to copper. Consequently, they suggested that ATP7B is not located at the TGN, but resides in the late

endosomes, in both basal and conditions of copper excess [157-159]. Confocal images from the Howell group however clearly show a difference in localization in 2008 cells upon addition of 200μM $CuSO_4$. Thus it seems likely that this apparent difference in the trafficking behavior of ATP7B could be either due to presence of the GFP tag, which may mask appropriate targeting signals or represent a cell-specific phenomenon. An alternative explanation for the discrepancy might be found in the difference in ATP7B expression levels. Harada et al performed their immunofluorescence on transiently transfected cells (where expression is expected to be fairly high) while the Howell group used G418 selected cells that stably express ATP7B [157], [156].

An interesting observation reported by the Howell group is an induction of trafficking of ATP7B upon treatment of cells with 2μM cisplatin [156]. Cisplatin is a platinum containing compound frequently used as a chemotherapeutic agent in cancer treatment. Cisplatin resistant cells have been shown to upregulate the expression of ATP7B. It is particularly interesting that ATP7B trafficking is induced by such low levels of cisplatin. However, cisplatinum binding to the intramembrane site or transport by ATP7B have yet to be shown.

1.21 Trafficking of recombinant orthologs of ATP7B

Several mammalian orthologs of ATP7B have been cloned and characterized, providing a useful source of information for identifying sequence elements critical for ATP7B trafficking. The mouse ortholog, mATP7B, which is ~82% homologous to human ATP7B, was expressed in Me32a-T22/2L fibroblasts, cells derived from a Menkes patient, and was localized to a

perinuclear region under basal conditions. Interestingly, mATP7B did not traffic when treated with 189 μM $CuCl_2$, but did prevent copper accumulation in the cell [160]. mATP7B could have a faster rate of recycling not readily detectable or this construct may not traffic in these cells. Further studies revealed that mATP7B does traffic in response to copper in hamster CHO-K1 cells [161], suggesting that the lack of response in human Me32a cells could be due to species or cell specificity of the machinery involved in the response to elevated copper and trafficking of ATP7B. To determine which compartment mATP7B localizes in elevated copper, ultrastructural analysis was performed in transfected CHO-K1 cells following copper treatment. mATP7B was shown to be present in a multivesicular compartment that appeared to be late endosomal, but did not co-localize with the late endosomal markers lysosomal glycoprotein and lysobisphosphatidic acid [161].

Sheep are unusual in that they are highly susceptible to both copper deficiency and copper overload [162-165]. They express two forms of ATP7B, sATP7B, which is similar to the human product, and a longer version, which encodes 79 amino acids that replace the first 18 amino acids of sATP7B [166]. The role of this N-terminal substitution on ATP7B function and regulation is puzzling, since Lockhart et al demonstrated both sATP7B and the alternative splice form have perinuclear localization when transfected into Menkes fibroblasts and both efflux copper like ATP7B [167, 160]. The authors did not report if sATP7B traffics in Me32a-T22/2L in the presence of excess copper, however sATP7B was shown to traffic in the presence of copper in CHO-K1 cells [168]. It is possible that the

extra N-terminal extension provides a fine-tuning of ATP7B activity, modulating the rates of transport or sensitivity to changes in intracellular copper levels.

1.22 Molecular determinants of copper dependent trafficking of Cu-ATPases

How copper induces protein trafficking is a fascinating and important question. Several possible mechanisms have been discussed in the literature. It was suggested that the increase in intracellular copper results in saturation of the N-terminal domain of Cu-ATPases with copper, resulting in a conformational change of this domain, which in turn serves as a signal for initiation of a trafficking response [96]. Another model directly linked the catalytic activity of Cu-ATPases to its trafficking, implying increased intracellular copper raises the pool of active protein which in turn is recognized as ready for trafficking [108, 116, 138]. Lastly, elevated copper was found to increase kinase mediated phosphorylation of human Cu-ATPases, suggesting that post-translational modification and trafficking of Cu-ATPases could be linked. As we describe in following sections, supportive evidence exists for each of the proposed mechanisms, however the actual mechanism of copper dependent protein trafficking is likely to be complex and include elements of each model.

1.22.1 The role of the N-terminal domain in trafficking

The mammalian Cu-ATPases contain six metal binding domains at their N-terminus, whereas Cu-ATPases from other organisms do not have as many, 1-3. (It should be noted that rodents have six metal binding domains, but only five of them appear to be functional [169]). The extra metal binding domains in

mammalian transporters are likely to have regulatory functions, modulating the intracellular localization of the transporters and/or their activity. The role of metal binding domains in trafficking has been explored by several groups. Goodyer et al created ATP7A constructs containing various mutations in the copper binding sites in the N-terminal domain by replacing each pair of copper coordinating cysteines with serines, and tested the ability of mutants to re-localize in response to elevated copper. The Cys>Ser substitutions in all six metal binding domains produced protein that was localized to the TGN but did not traffic in response to elevated copper, as high as 600 μM $CuCl_2$ [170]. The authors then examined if one critical metal binding domain existed that could restore the copper dependent trafficking response of the mutant. The ATP7A construct with all six metal binding domains mutated was used to create five additional constructs, each with only one metal binding domain restored to cysteines, MBD1, MBD2, MBD3, MBD4, and MBD6. All five mutants trafficked in response to copper, suggesting that at least one metal binding domain needs to be functional for trafficking and that all metal binding domains are equivalent. (The authors did not show data for a wild-type MBD5 in a mutant background, but mutation of MBD5 alone results in a normal copper response, suggesting that MBD5 functions like the rest of the metal binding domains).

This initial conclusion is at odds with the subsequent results from Strausak and colleagues. These authors utilized the wild-type ATP7A for mutagenesis and deletion analysis and concluded that metal binding domains in MBD5 or MBD6 have to be functional (transport competent) for trafficking to occur, while

other sites cannot substitute for MBD5 and MBD6. In these experiments mutations of individual sites, MBD1C>S and MBD6C>S, did not affect the copper dependent trafficking [109]. Mutagenesis of MBD1-3C>S also had no effect on trafficking, but mutation of MBD4-6C>S prevented re-localization of ATP7A from the TGN under high copper. The MBD5-6C>S mutant also did not traffic [109] while ATP7A with just MBD5 inactivated did relocalize[170] [109]

Although the results of these two studies [109, 170] are difficult to reconcile, it is possible that the mutations in the metal binding domain may not only disrupt copper binding by the MBDs but also alter the interdomain interactions, further modifying the ability of the protein to respond to elevated copper. Such effects may depend on the number and location of mutations. The metal binding domains are connected to each other by linkers of variable length. It is not difficult to imagine that some metal binding domains interact and that changes in one domain may affect the overall conformation of the N-terminal domain and/or orientation of linker regions. More data is needed for a better understanding of the role of individual MBDs and how they interact with each other in the N-terminal domain structure and function. Nevertheless, it seems clear that inactivation of all N-terminal copper binding domains prevents trafficking. Importantly, the constructs MBDΔ1-4, MBDΔ1-4+5C>S, and MBDΔ1-4+6C>S, all relocalize in response to copper [109], indicating that the first four N-terminal MBDs, while playing a regulatory role, are not directly involved in trafficking event *per se.* Whether or not decreasing the number of the N-terminal metal binding domains

alters the sensitivity of Cu-ATPase to intracellular copper has not been investigated.

Similar conclusions about the role of the N-terminal domain in trafficking have been reached upon analysis of ATP7B. The Mercer group created deletions of N-ATP7B, cysteine to serine mutations of the MBDs, and chimeras of ATP7B, replacing the N-terminal domain of ATP7A with that of ATP7B [106, 108]. Five deletion constructs were tested, MBDΔ1-6, MBDΔ1-5, MBDΔ4-6, MBDΔ3-5, and MBDΔ3-6, but only one was active in a yeast complementation assay and trafficked in response to copper, MBDΔ1-5. Of various Cys>Ser mutants, MBD1-6C>S, MBD1-5C>S, MBD4-6C>S, MBD3-5C>S, MBD6C>S, and MBD1-4 + 6C>S, only MBD1-6C>S and MBD4-6C>S were not functional in a yeast complementation assay nor trafficked in response to copper [106]. Similarly to ATP7A, having MBD5 or MBD6 for ATP7B was crucial for the trafficking response with either one of these domains being sufficient.

A recent study published by Guo and colleagues [46] used polarized hepatic WIF-B cells and high resolution confocal microscopy to determine the localization of endogenous and transfected ATP7B under different copper conditions. Truncation of the N-terminus up to the fifth MBD yielded a product that was insensitive to cellular Cu levels and constitutively trafficked to the basolateral plasma membrane in contrast to the apical destination of the wild-type protein. Fusion of the N-terminal 63 amino acids of ATP7B to the truncated protein restored both correct intracellular targeting and the copper response [46]. These results are very different from the data on similar truncations of ATP7A, where

the copper response was unaffected by the large deletion of the N-terminal domain. They suggest that important targeting information is contained in this relatively short N-terminal sequence, which is absent from ATP7A.

The most convincing evidence for the involvement of the N-terminal domain of ATP7B in trafficking is the ATP7B/ ATP7A chimeras [108]. ATP7A, like ATP7B, resides in the TGN under basal copper conditions, but traffics to the plasma membrane under conditions of elevated copper. Chimeras were tested which were fusions of the ATP7B N-terminal metal binding domains and ATP7A beginning just before the first transmembrane segment. The constructs, N-ATP7B/ATP7A, N-ATP7BΔ1-2/ATP7A, and N-ATP7BΔ1-5ATP7A trafficked to a vesicular compartment when treated with copper, just as the ATP7B control [108]. This interesting finding suggests the copper dependent localization resides in the N-terminus of the protein.

1.22.2 The role of the C-terminus in endocytosis

ATP7B contains a plasma membrane retrieval signal, composed of three leucine residues, at its C-terminal tail. Mutation of the tri-leucine motif localizes ATP7B to the plasma membrane. An interesting patient mutation that results in the deletion of a portion of the C-terminal tail of ATP7B, 4193ΔC, was reported [119]. This mutation removes the tri-leucine motif and was predicted to affect ATP7B trafficking; however this hypothesis remains to be tested. Characterization of the corresponding mutant using a yeast complementation assay indicated that the protein had transport activity, suggesting that the folding of protein is not severely affected [42]. Hsi and co-workers also performed a yeast

complementation assay to assess the affect of various C-terminal deletions on ATP7B activity and found that only deletions that remove most of the C-terminus, Δ4117 and Δ4126, have a negative effect on ATP7B function. These two ATP7B constructs did not express very well and/or degraded due to protein folding problems [42].

1.22.3 Catalytic activity and trafficking

As members of the P-type ATPase family of transporters, ATP7B and ATP7A utilize the energy of ATP hydrolysis to transport copper. Current data suggest that catalytic and transport activity may be linked to the ability of Cu-ATPase to traffic. This hypothesis originated from the experiments on ATP7A constructs mutated in the CPC motif, the ATP binding domain, and TGE loop, regions conserved in the Cu-ATPases and important for their catalytic activity. The C^{1000}>R substitution in the CPC motif resulted in TGN localization under either basal or elevated copper conditions [116, 138]. Similar results were observed following mutations of invariant residues in the ATP-binding domain, H^{1086} and D^{1044}, and conserved N^{1233} in TMS7 [116]. The H^{1086} in ATP7A is equivalent to H^{1069} of ATP7B, which is the site of the most frequent Wilson disease mutation [171-173]. The H^{1086}>Q variant was targeted normally, but did not traffic out of the TGN in response to copper. Neither did the protein with a mutation at the invariant residue responsible for acyl-phosphate formation, D^{1044}>E, nor the N^{1233} mutant in which a putative copper coordinating residue was replaced.

Further study, however, revealed that the ability to adopt certain conformations could be more important for trafficking than the transport activity

per se. The ATP7A construct containing a disease mutation L^{873}>R in the A-domain was found to localize to the plasma membrane in both basal and elevated copper. A similar result, plasma membrane localization, was observed when the three conserved residues that make up the $T^{875}G^{876}E^{877}$ motif in the A-domain of ATP7A were converted to alanines [116]. The TGE motif is essential for the enzymatic activity of ATP7A and the $T^{875}G^{876}E^{877}$>AAA mutant is inactive with respect to copper transport, as confirmed by the yeast complementation assay. Interestingly, although the $T^{875}G^{876}E^{877}$>AAA mutant cannot transport copper it can undergo catalytic phosphorylation. The level of catalytic phosphorylation is higher for the $T^{875}G^{876}E^{877}$>AAA variant compared to wild-type ATP7A, suggesting that the protein is stabilized in a phosphorylated state and cannot proceed further through the catalytic cycle and transport. It is in this state that the protein relocalizes to the plasma membrane even in the absence of elevated copper [116].

This observation is very important as it offers a possible explanation of how trafficking can be triggered in response to elevated copper. Catalytic phosphorylation of Cu-ATPases requires binding of copper to the intramembrane site(s). Dephosphorylation, in turn, is associated with the release of copper from the intramembrane site into the lumen. Under basal conditions, the metal ions transported into the lumen of the secretory pathways are quickly bound by copper dependent enzymes, and it is likely that no free copper is present in the lumen under these conditions. When copper is elevated, more copper is transported into the secretory pathway, and may eventually exceed the binding

capacity of the acceptor proteins. “Free” accumulated copper in the lumen at certain concentrations would re-bind to Cu-ATPase, stabilizing the protein in a copper bound state. In this state the protein conformation is expected to be very similar, if not identical, to that of phosphorylated E_2PCu enzyme, i.e. the state in which the protein is susceptible for interaction with the trafficking machinery.

This hypothesis would predict that (1) Cu-ATPase variants with low transport activity would have delayed trafficking response or apparent lack of copper sensitivity and that (2) overexpression of the acceptor protein in the secretory pathway may slow down/prevent trafficking of the ATPase. The N-terminal disease mutation, which results in the deletion of exon 8 and consequently MBD6 [174] is likely to be such an example. The mutant has transport activity as illustrated by incorporation of copper into tyrosinase, which is overexpressed in the cells for the purpose of the assay. Nevertheless, the mutant does not traffic in response to elevated copper [174]. A less speculative example is the $H^{1086}Q$ mutant of ATP7A, which has markedly decreased transport activity and does not traffic in response to treatment with 200 μM copper, but does re-localize when cells are treated with 300 μM copper [138]. For the majority of ATP7B mutants, nonfunctional protein does not traffic.

1.22.4 Kinase mediated phosphorylation and trafficking

What signals guide Cu-ATPase trafficking from the TGN to vesicles/plasma membrane and subsequent return are not quite clear. In addition to certain structural determinants, such as specific protein conformations and characteristic sequence motifs, kinase mediated phosphorylation of Cu-

ATPases appears to play an important role. It has been shown that in hepatic cells, ATP7B is phosphorylated by a kinase and that the level of phosphorylation increases following cell treatment with elevated copper [75]. The phosphorylation of ATP7B is metal specific and reversible, i.e. following a reduction in copper concentration, ATP7B is dephosphorylated. Interestingly, the level of phosphorylation correlates with the intracellular location of the copper transporter. A basal level of phosphorylation is observed at the TGN, while upon relocalization to the vesicles, ATP7B becomes hyperphosphorylated [75] Whether phosphorylation serves as a signal for trafficking or is required for the retention of ATP7B in the vesicular compartment is yet to be determined.

ATP7B was shown to have at least two phosphorylation sites, a basal phosphorylation site and a site modified in response to increased copper concentration [75]. Comparative analyses of ATP7B, PINA, and ATP7B C-terminal truncation mutants revealed that the basal phosphorylation site is located in the C-terminal half of the protein Ser^{796}-Tyr^{1384}. The N-domain of Cu-ATPases is a part of this region; and contains a sequence insert which is absent from the structure of ATPases which do not traffic. Determining the role of this sequence insert in phosphorylation may provide insight into the link between phosphorylation and trafficking.

The copper induced phosphorylation appears to require the presence of a functional N-terminal domain. The pineal isoform of ATP7B, PINA lacks the N-terminal domain and undergoes basal phosphorylation but shows no hyperphosphorylation in response to copper [75]. Similarly, the N-terminal mutant

of ATP7B, G^{591}>D which does not interact with Atox1 and presumably has lost the ability to accept copper from the chaperone, also does not change its level of phosphorylation when copper is elevated. The intracellular localization of ATP7B variants with varying levels of phosphorylation has not so far been reported. This information is essential for a better understanding of the role of kinase mediated phosphorylation in ATP7B trafficking and function.

1.23 ATP7B and COMMD1

It has been known for some time that mutations that influence copper homeostasis must exist in genes others than just ATP7A and ATP7B. Bedlington terriers are purebred dogs that have a higher than normal frequency of copper toxicosis due to a defect in biliary copper excretion. These dogs do not have a mutation in ATP7B but display a phenotype similar to a disruption in ATP7B function. A gene was identified in these dogs, commd1 (formerly murr1), that also has a homologous counterpart in humans [175]. Immunocytochemistry experiments revealed that COMMD1 has a vesicular staining pattern and partially colocalizes with the transferrin receptor which is known to traffic to the recycling endosomes [176]. The role of COMMD1 is unclear and may involve participation in vesicle trafficking or fusion. Tao et al demonstrated *in vitro* that COMMD1 interacts with ATP7B, but not ATP7A, and also co-immunoprecipitated recombinant COMMD1 and ATP7B from cells. This interaction was shown to occur through the N-terminal MBD and not the C-terminal region [177]. More work is necessary to determine whether these two proteins co-localize and affect each other's function.

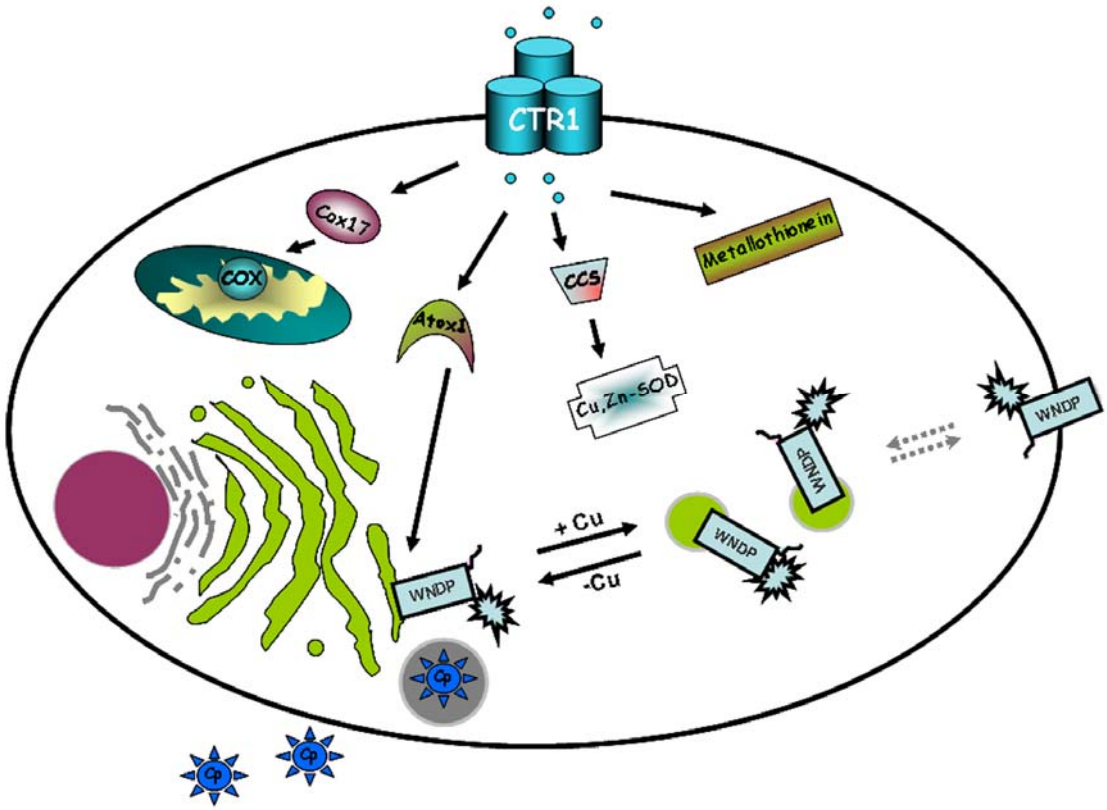

Figure 1: Cartoon of proteins involved in general cellular copper homeostasis. In the cell there are several major pathways requiring copper. CTR1 transports copper into the cell, whereby copper chaperones receive and deliver copper to various organelles. Cox17 delivers copper to COX in the mitochondria, Atox1 to ATP7B/ATP7A in the biosynthetic pathway, CCS to Cu, Zn-SOD, and Metallothionein receives copper from CTR1. In the biosynthetic pathway, ATP7B delivers copper to copper requiring enzymes, such as ceruloplasmin.

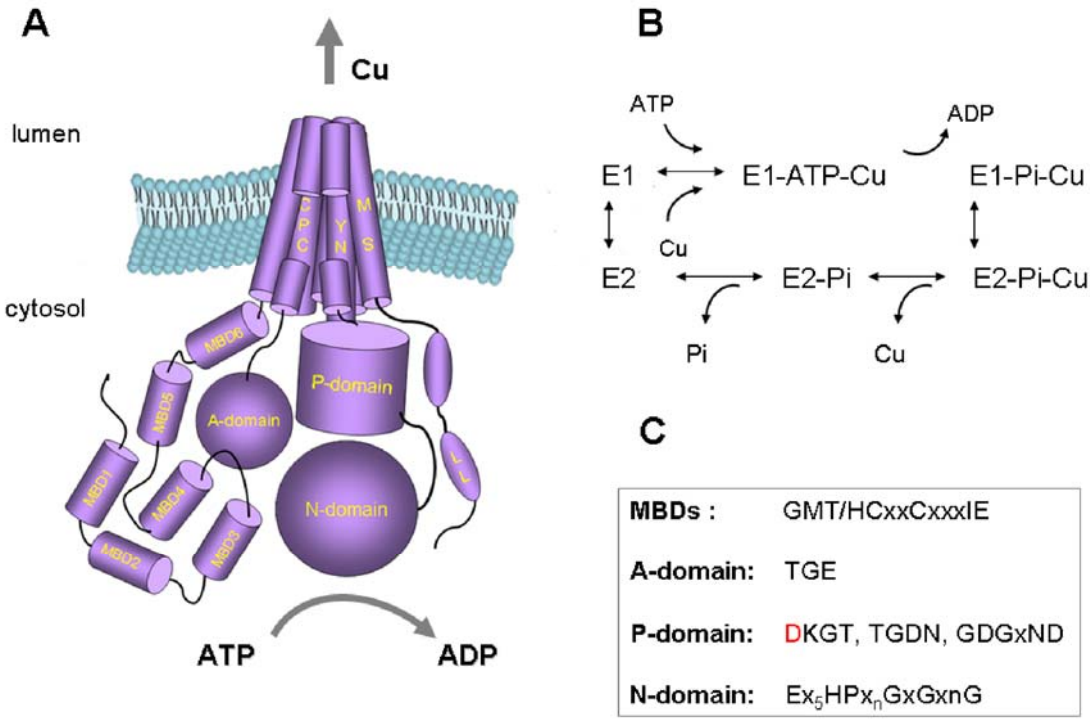

Figure 2: Cartoon of ATP7B structure and catalytic cycle. **A**) A carton illustrating the different regions of the ATP7B structure including the six metal binding domains in N-ATP7B, the eight transmembrane segments, the three domains of the ATP Binding Domain (A, N, and P domain), and the C-terminal tail. **B**) The predicted catalytic cycle of ATP7B, resulting in the hydrolysis of ATP and transport of copper. **C**) Key residues important or conserved in the different domains (Cartoon image by Svetlana Lutsenko).

CELL SPECIFIC TRAFFICKING OF ATP7B IS LINKED TO DIFFERENCES IN EXON 1

Natalie Barnes[1*], Mee Y. Bartee[1*] , Vladimir Ustiyan[2], Jack H. Kaplan[2], and Svetlana Lutsenko[1¶]

[1]Department of Biochemistry and Molecular Biology, Oregon Health and Science University, Portland, Oregon 97239-3098, [2]Department of Biochemistry and Molecular Genetics, University of Illinois in Chicago, Chicago, Illinois 60607.

Running Title: Trafficking of ATP7B in liver and kidney

* - These authors contributed equally to this work

This work was funded by the National Institute of Health Grant P01 GM 067166 to SL and JHK

¶ - To whom correspondence should be addressed:

Svetlana Lutsenko, OHSU, L224, Sam Jackson Park Road, Portland, OR 97239

Tel: 503-494-6953; Fax: 503-494-8393; E-mail: lutsenko@ohsu.edu

-This paper has been submitted to the Journal of Cell Biology and is currently under revision.

- Chapter 2 is taken from this paper.

-Figures 3B,C and 10-16 were generated by me. In the materials and methods, I did the experiments in sections 2.2.1, 2.2.5, 2.2.9 - 2.2.13. I helped write the current version of this paper, in particular 2.2.1, 2.2.9-2.2.13.

-Natalie Barnes generated Figure 3A, 4-7, and 9. She also helped write the paper, in particular section 2.2.2-2.2.8.

-Valdimir Usityan generated Figure 8 and wrote the method for section 2.2.6.

-As for the rest of the paper, it was a collaborative effort between Natalie Barnes, Svetlana Lutsenko, and me.

II. The Role of ATP7B and ATP7A in tissues

2.1 Introduction

Copper is essential for a wide variety of cellular functions. It is a co-factor for many important enzymes such as cytochrome c oxidase, tyrosinase, superoxide dismutase, ceruloplasmin, peptidylglycine α-amidating monooxygenase and others [178]. In addition, copper plays important yet poorly understood roles in embryonic development, neuronal myelination, angiogenesis, and binds with high affinity to such proteins as amyloid precursor protein and prion protein[179, 180]. The balance between copper absorption and excretion in humans is tightly regulated. Two copper-transporting ATPases (Cu-ATPases), ATP7B and ATP7A, play a key role in this process by mediating copper transport across cellular membranes in response to changing copper concentrations. Disruptions in the function of ATP7B or ATP7A result in severe metabolic disorders, Wilson disease and Menkes disease, respectively [11, 40, 181-184].

ATP7B and ATP7A are highly homologous proteins that have similar general function. They both deliver copper to the secretory pathway for incorporation into copper dependent enzymes [4] and mediate copper efflux out of the cell [150, 151]. These two functions are performed in separate cell compartments; and the targeting of Cu-ATPases to these compartments depends on copper concentration. In low copper, ATP7A is located in the *trans*-Golgi network (TGN), consistent with its role in delivering copper to copper requiring enzymes in the biosynthetic pathway. In high copper, ATP7A relocalizes to vesicles in the vicinity of the plasma membrane, where it

sequesters copper for subsequent export via vesicle mediated fusion [36, 160, 185-188].

The intracellular localization of ATP7B is also thought to be copper dependent. Studies of recombinant ATP7B in several cell lines and of endogenous ATP7B in hepatocytes demonstrated that under copper limiting and basal levels of copper, ATP7B primarily has a perinuclear TGN localization, overlapping with TGN markers [151, 154, 189, 190]. However, when copper becomes elevated, ATP7B was found to relocate to vesicles [75, 152, 154, 189, 190] and, in other reports, to both the vesicles and the apical membrane [46, 151, 191].

The similarity of ATP7A and ATP7B function is further illustrated by the ability of ATP7A to compensate, at least partially, for the lack of functional ATP7B in the cerebellum in *Atp7b*$^{-/-}$ mice, restoring copper delivery to ceruloplasmin, a copper dependent ferroxidase [81]. Reciprocally, recombinant ATP7B restores copper efflux in the fibroblasts of Menkes disease patients (where ATP7A is defective [192]). In contrast to the compensatory effect of recombinant ATP7B in fibroblasts, in tissues, such as intestine or brain, the lack of ATP7A is not compensated by ATP7B, even when co-expressed in the same cells. These observations suggest overlapping, yet distinct roles of the two Cu-ATPases and/or distinct mechanisms of regulation.

We hypothesized that the two Cu-ATPases may re-localize to their respective compartments in response to different intracellular levels of copper, thus providing fine tuned regulation in tissues, where copper is especially important. This may be the case in kidneys, which regulate their copper content

particularly well under conditions of either copper deficiency or copper overload. No information is currently available on the relative copper sensitivities of endogenous ATP7B and ATP7A in physiologically relevant cells. Consequently, characterization of the copper dependent trafficking of endogenous ATP7B and ATP7A in kidney derived cells, which express both transporters, were carried out. Marked differences in the response to elevated copper were observed for the Cu-ATPases, which points to distinct roles for ATP7B and ATP7A in intracellular renal copper balance. No trafficking of endogenous ATP7B in response to elevated copper was detected in any kidney cell line tested, nor in primary kidney cells in mice, in stark contrast to the behavior of ATP7B in hepatocytes. Tissue specific differences in the protein of ATP7B in kidney and liver cells may play an important role in the cell specific regulation of Cu-ATPases.

2.2 Materials/Methods

2.2.1 Generation of the N-ATP7B antibody

Antibody against the N-terminal metal binding domain of human ATP7B was generated in rats. Protein was first expressed from the intein construct N-ATP7B pTYB12. Transformed *Escherichia coli* (BL21(DE3) Invitrogen) were grown at 37°C to an OD_{600} of 0.6 and subsequently chilled for 30min in the cold room. Protein was induced by the addition of 1mM IPTG and grown overnight at 16°C, 250 rpm. Cells were collected and resuspended in 50 mM Tris pH 7.5, 500 mM NaCl, complete protease inhibitors (Roche), and 2mM AEBSF. Cells were then French pressed and centrifuged at 20,000 x g to separate the soluble and insoluble fraction. The soluble fraction was taken and incubated with 5 mls of

equilibrated chitin resin (New England Biolabs) batch method. After 1hr of incubation, the resin was poured onto a column and washed with 50 column volumes of the resuspension buffer. The resin was incubated at room temperature for 48 hrs in 2 column volume of resuspension buffer + 50 mM DTT to cleave N-ATP7B from the intein. Protein was eluted and dialyzed in 2 x 2 L passages of resuspension buffer using a 30 kDa cutoff dialysis tube (Pierce). Protein was concentrated using a Centricon 30 (Millipore) and protein was analyzed by Laemmli PAGE and quantitated by Bradford method. 800 ng of native N-ATP7B was sent to Strategic Biosolutions for immunization in 2 rats. Pre-bleed was first tested to confirm non-reactivity to N-ATP7B. After 2 rounds of immunizations, the animals were sanguinated and sera tested for immunoreactivity by western blot analysis. N-ATP7B#1 and N-ATP7B#2 both react specifically and with high affinity to ATP7B, N-ATP7B#2 having a slight higher affinity. The antibodies were diluted 1:2 with glycerol and stored at -20°C. A dilution of 1:10,000 can be used for western blot analysis, 1:500 for IF and IP. N-ATP7B#2 has been tested to cross react with human, mouse and dog ATP7B.

2.2.2 Mouse Strains

The generation of *Atp7b*$^{-/-}$ mice has been described previously [193]. *Atp7b*$^{-/-}$ and the background C57BLx129SV/SvEv mice were housed at the OHSU Department of Comparative Medicine according to the National Institutes of Health guidelines on the use of laboratory and experimental animals. Food and water were provided *ad libitum*. Animals were euthanized by CO_2 inhalation and

the livers and kidney were quickly removed. Two week old mice of either sex were used for the experiments.

2.2.3 Cell Lines

All cultured cell lines were purchased from American Type Culture Collection (Manassas, VA). Hek293, HepG2, Huh7, and Cos-7 cells were maintained in Dulbecco's Modified Eagle Medium (DMEM) (Gibco, Grand Island, NY) which was supplemented with 10% fetal bovine serum (Gibco, Grand Island, NY), 2 mM L-glutamine and 100U/ml penicillin and streptomycin (Invitrogen, Carlsbad, CA). BeWo cells were maintained in Hams F12 medium with 2 mM L-glutamine and 1.5 g/L of sodium bicarbonate (Gibco, Grand Island, NY), 10% bovine calf serum, 100 U/ml penicillin and streptomycin.

2.2.4 Generation of primary kidney and liver cell lines

Kidneys and liver were removed aseptically from 2 weeks-old mice and placed into cold Hibernate-A solution (BrainBits, Springfield, IL). Tissues were then chopped into 1mm pieces and digested at 37°C in 0.07 mg/ml Liberase (Blendzyme 3: Roche Applied Science, Indianapolis, IN) and DMEM with no serum for 40 minutes. 5 ml of DMEM with 15% fetal bovine serum and 100 U/ml antibiotic/antimycotic (Invitrogen, Carlsbad, CA) was then added to the digested tissue and centrifuged at 850 x g for 8 minutes. Pellets were resuspended in 3 ml culture media (as above) and plated in serial dilutions (1/10 and 1/100) for the desired density (50% to 5% confluent). The cells were maintained in DMEM and 15% fetal calf serum and 100 U/ml antibiotic/antimycotic (Invitrogen). All cells

were grown in 5% CO_2 at 37°C for 2 weeks. Primary cultures were re-plated no more than 3 times to avoid cell selection. This work was done by Natalie Barnes.

2.2.5 Immunofluorescence microscopy

The detection of ATP7B, ATP7A, and the trans-Golgi marker TGN46 in all cell lines was performed by culturing cells on glass cover slips in appropriate growth media until 80% confluent. Cells were then treated with either 200 μm bathocuproinedisulfonic acid disodium salt (BCS) to decrease copper levels or with 200 μm $CuCl_2$ for 2 hours, and then were fixed by immersion for 30 seconds in acetone at –20°C. Cells were blocked overnight in 1% gelatin/ 1% bovine serum albumin (BSA)/ 0.01% sodium azide in phosphate buffered saline (PBS) at 4°C and then incubated with appropriate antibodies in blocking solution for 1 hour at room temperature (each antibody at 1:500 dilution). After washing 4 times with PBS for one hour, cells were incubated with fluorescently labeled secondary antibodies (Alexa Fluor 488 donkey anti-rat for ATP7B, AlexaFluor 488 or 555 goat anti-rabbit for ATP7A, or Alexa Fluor 555 donkey anti-sheep for TGN46, Molecular Probes, Eugene, OR). Cells were then washed 4 more times in PBS for one hour, then cover slips were mounted onto glass slides using mounting medium containing DAPI (Vector Laboratories, Burlingame, CA). Images were analyzed using a 63x oil objective with a Zeiss Confocal Scanning microscope (Carl Zeiss, Gottingen, Germany).

2.2.6 Copper transport in Hek293 and HepG2 cells

Copper transport by mammalian cells was evaluated by measuring radioactive ^{64}Cu accumulated by cells during appropriate time periods according

to the procedure published earlier [194] with minor modifications. Specifically, cells were placed in 12-well Falcon plates (2 ml total volume per well) in standard growth media and left for 24 hours in a CO_2-incubator at 37°C to form a monolayer. The cell growth media was aspirated and cells were washed using transport buffer (25 mM Hepes, 150 mM NaCl, 2.5 mM $MgCl_2$ pH 7.4). Fresh transport buffer (0.9 ml) was then added to each well and Cu uptake was initiated by addition of 0.1 ml of 50 μM or 500 μM copper solution. At specific time points, uptake was stopped by three washes in cold stop-buffer (transport buffer supplemented by 10 mM EDTA). The wash solution was removed and the cells were resuspended in 0.1 M NaOH and 1 ml of each sample was used for radioactivity measurements in a γ-counter (Cobra Quantum, Packard Instrument Company) and for protein determination. Uptake experiments were performed at room temperature (25°C). As a control for non-specific binding of Cu, cells were pretreated with 5 μM or 50 μM copper for 15 minutes on ice, and then underwent the standard experimental procedure. Such pretreatment had no effect on the rate or amount of isotopic uptake. These experiments were performed by Vladimir Ustiyan.

2.2.7 RNA interference

siRNA of ATP7A was produced using Silencer siRNA Cocktail Kit (RNase III) (Ambion, Austin, TX). In brief, a region of 474 bp of the N-terminus of ATP7A (from residue 1256 bp) was amplified using two primer sets:

FP: 5'GAGTATGATCCTCTACTAACCTCTCC

RP: 5'GGAGGCACACGTCATTCCCC

The PCR products were cloned in both directions into the TOPO cloning vector under T7 polymerase promoters (Invitrogen, Carlsbad, CA). Anti-sense and sense strands of RNA were then synthesized using T7 polymerase and annealed generating double stranded RNA. RNA was cut into 15–20 bp fragments by RNase III and used for transfection of Hek293 cells. The RNA concentration dependence and time course were initially carried out to optimize conditions of ATP7A knock-down. For trafficking experiments, Hek293 cells in 12-well plate were transfected with approximately 800ng of siRNA per well using Lipofectamine 2000 and incubated for 48 hr in order to achieve mRNA knockdown. GAPDH siRNA was used to verify specificity of RNA interference. These experiments were done by Natalie Barnes.

2.2.8 Western blot analysis of ATP7B and ATP7A in membrane fractions

Cells grown to confluence in a 75 ml flask were harvested (by scraping) and homogenized in 500 μl of homogenization buffer: 25 mM Imidazole, pH 7.4, 0.25 M sucrose and 1 tablet of EDTA free complete protease inhibitor cocktail (Roche, Indianapolis, IN). Samples were centrifuged for 10 minutes at 500 x g to remove cell debris. The pellet was discarded and supernatant was further centrifuged for 30 minutes at 20,000 x g to collect membranes. 60 μg of membrane protein was separated on 7.5% Laemmli gel; proteins were then transferred to a PDVF membrane (Millipore, Bedford, MA) and immunostained using either anti-ATP7A (1/500) or anti-N-ATP7B (1/500) antibodies. These western blots were performed by Natalie Barnes.

2.2.9 In vivo metabolic labeling of Hek293 and HepG2 cells

Cells were grown to confluency on 10 cm plates and washed with phosphate free DMEM without serum or antibiotics, and then incubated for 30min. The buffer was then changed to phosphate free DMEM containing orthophosphate (^{32}P) at 1 mCi/mL and incubated for 2 hrs at 37°C, 5% CO_2. The cells were then incubated for 1 hr with 50 µM $CuCl_2$ or BCS. Cells were homogenized in 25 mM Imidazole pH 7.4, 0.25 M sucrose, 1 mM DTT, EDTA free complete protease inhibitor cocktail, and 2 mM AEBSF(Roche, Indianapolis, IN). Supernatants were centrifuged as described above (Section 2.2.8), and the membrane fraction was loaded onto a 7.5% Laemmli gel. Gel bands above and below the 170 kDa protein marker were excised from the Laemmli gel and crushed with a dounce. Acrylamide gel fragments were incubated overnight in immunoprecipitation buffer (20 mM Tris-HCl pH 7.5, 1 mM EDTA, 0.1% SDS, 1% Triton X-100, and 0.5% Deoxycholate, 1 M NaCl) to elute ATP7B from the gel. Gel fragments were pelleted and the supernatant was diluted by $1/4^{th}$ and transferred to a fresh tube and incubated with blocking buffer ($1/10^{th}$ of 10X PBS, 6% BSA, 1% Tween20, and 40 µl pre-immune serum) for 1 hr. Protein G resin (Pierce) was then added to the supernatant and incubated for 1 hr. Resin was pelleted and the supernatant placed in a fresh tube with 5 µl of the N-ATP7B#2 antibody for 1 hr. This supernatant was then added to Protein G resin for 1 hr and then pelleted. The supernatant was removed and the resin washed with wash buffer (PBS, 0.1% Tween) for 100 slurry volumes. Protein was eluted with sample buffer (0.17 M Tris pH 6.8, 6.8% SDS, 2.7 M Urea, 1% β-Me) and run on another 7.5% Laemmli gel. The gel was transferred onto PVDF and placed at -

80°C under film (Kodak BioMax MS Film). The exposed film was then processed and imaged.

2.2.10 Nested PCR of ATP7B cDNA

Cellular RNA was purified from Hek293 and HepG2 cells using an RNeasy kit (Qiagen) following the cellular RNA purification protocol. RNA was treated with DNase I (Invitrogen). cDNA was generated from 2 ug of cellular RNA using Superscript III Reverse Transcriptase (Invitrogen) with either poly-dT 48 mer (GeneDetect), random hexamers (Invitrogen), or random decamers (Ambion). cDNA was treated with RNase H before storing at -20°C. 2 µL of cDNA was used for PCR or nested PCR. PCR was performed using Platinum Taq DNA Polymerase (Invitrogen). The primers (Operon) used for the PCR reactions shown in Figure 12 are as follows:

CSFor: 5'CTGTGCATTGCCTGCCCCT (exon 21 round 1 nested forward primer)

RevExon21-2: 5'CATGCCTATGTGCACACTGAC (exon 21 round 1 nested reverse primer)

Scott3147For: 5'CACACTGCCCCTCAGGAAGG (exon 21 round 2 forward nested primer)

RevExon21-4: 5'CTCATACCTCTCCAGGTCAGGCTTC (exon 21 round 2 reverse nested primer)

NWNDseq5: 5'TGGCAACATTGAGCTGACA (exon 6 forward primer)

2221WndRp: 5'GCAATGCTTGTGGCCAGGACGAT (exon 6 reverse primer)

Exon1Fwd: 5'AAGGGCCTGGGGACAAAC (exon 1 round 1 nested forward primer)

EcoRI445Rev: 5’GAATTCCCAGCACTGTGGTTTCCAAGAGGG (exon 1 round 1 nested reverse primer)

274Fwd: 5’CGAAAACTGTTACAACCGATACTTCCACCAGAC (exon 1 round 2 forward nested primer)

647Exon2Rev: 5’TTGCAGTTTCCGGACCTTGCCTT (exon 1 round 2 reverse nested primer)

216WndpExon2Fwd: 5’CTTATCTAAGCTTTCTTTGCCTACCCG (exon 2 round 1 forward nested primer)

The PCR product for exon 21 was analyzed on a 1% agarose gel in TAE; the PCR products for exons 6 and exon 1 were analyzed on 8% acrylamide gels in TBE. Gels were stained with SYBR Green (Invitrogen).

2.2.11 Generation of Flag-ATP7B pcDNA 5 FRT/TO

An N-terminal FLAG tag was added to ATP7B cDNA by PCR with the following primer pair:

BamHIKozakFlag-hATP7B forward primer:

5’GGATCCACCATGGACTACAAGGATGACGATGACAAGCCTGAGCAGGAGA

G

XhoIMBS5Rev reverse primer:

5’CTCGAGGGGCTGGATGACCTCTGGG

ATP7B pcDNA 3.1(+) (based on liver cDNA) was used as the template. A BamHI restriction site was generated 5’ to the sequence for cloning purposes. The PCR fragment was TOPO TA cloned for propagation and screened by sequencing. The Flag-tagged fragment was inserted into an ATP7B pcDNA 3.1

(+) plasmid using BamHI and XhoI restriction sites. Subsequently, the full length Flag-ATP7B was subcloned into pcDNA 5 FRT/ TO (Invitrogen) using BamHI and NotI (NotI site is 3' to the stop codon of ATP7B in the pcDNA3.1 (+) construct and is unique for both vectors).

2.2.12 Generation of a stable Flag-ATP7B cell line in FlpIn TREx 293 cells

A detailed schematic for the generation of tetracycline-inducible FlpIn TREx 293 cells expressing Flag-ATP7B is given in Figure 16 and in materials method of section 4.2.15. Briefly, FlpIn T-REx cells were maintained in MEM + Penstrep + nonessential amino acids + 10% FBS + 15 µg/mL blasticidin + 100 µg/mL zeocin (Invitrogen). Once cells were co-transfected with Flag-ATP7B and recombinase containing plasmids, zeocin was removed and 200 µg/mL hygromycin was added for selection. For induction of protein expression, the FBS was replaced with tetracycline-tested FBS (Invitrogen) and after several days, tetracycline (Fisher) was added back to a concentration of 40 ng/mL. The cells were incubated with the tetracycline-tested FBS to inhibit transcription/translation of Flag-ATP7B from the high levels of tetracycline normally found in FBS. This ability to induce expression of ATP7B allows for control of the levels of expression, preventing over expression/mislocalization of Flag-ATP7B.

2.2.13 Trafficking of Flag-ATP7B pcDNA 5 FRT/TO

To induce expression of Flag-ATP7B, cells were grown in the presence of 40 ng/mL tetracycline. Cells were seeded onto coverslips in 12 well plates and allowed to grow for 48 hrs. FlpIn T-Rex 293 cells were then treated with 50µM

bathocuproine disulfonate (BCS), a copper chelator, or 50 µM copper chloride for 1 hr at 37°C in the presence of 40 ng/mL of tetracycline. Cells were then washed with cold PBS and fixed in 4% paraformaldehyde for 30 min on ice. Cells were then washed/ permeabilized with PBS + 0.02% TritonX-100. The cells were blocked overnight in blocking buffer (1% BSA + 1% gelatin + 0.02% TritonX-100 + 0.01% Sodium azide) at 4°C. Primary antibody incubation with anti-Flag (Sigma) and anti-TGN46 (GeneTex) were performed at room temperature in blocking buffer at a dilution 1:500 for 1 hour. Secondary antibody incubation was done with donkey anti-mouse AlexaFluor488 and donkey anti-sheep AlexaFluor555 (Molecular Probes) for 1 hr at room temperature in the dark. Cells were mounted in Vectashield + DAPI and sealed. Imaging of cells was done on a Zeiss LSM 5 Pascal confocal microscope.

2.3 Results

2.3.1 ATP7B and ATP7A are expressed endogenously in Hek293 cells.

In cells expressing both Cu-ATPases, the intracellular localization and/or trafficking response of ATP7B and ATP7A to elevated copper were hypothesized to be different. To test this hypothesis, Hek293 cells, which are derived from human embryonic kidney were initially utilized. Western blotting of Hek293 crude membrane fraction revealed that both ATP7B and ATP7A are endogenously expressed in these cells and easily detected (Figure 3A), providing an excellent opportunity for comparative analysis of localization and trafficking of these transporters. There is limited work investigating endogenous ATP7B and ATP7A or delineating the exact role of each transporter in cells where they are co-

expressed. Consequently, antibodies against N-ATP7B and ATP7A were utilized to first characterize the intracellular localization of each copper transporter under low copper conditions. Immunofluorescence staining of Hek293 cells following treatment with the copper chelator bathocuproine-disulfonate (BCS) demonstrated that endogenous ATP7B and ATP7A both display a characteristic perinuclear staining pattern expected for TGN staining (Figure 3B). The TGN localization was confirmed using an antibody against TGN46, a compartment specific marker, which showed overlapping staining for both ATP7B and ATP7A (Figure 3B).

2.3.2 ATP7B and ATP7A traffic differently when copper is elevated in Hek293 cells.

To compare the responses of ATP7B and ATP7A to elevated copper, the intracellular localization of ATP7B and ATP7A was analyzed by immunofluorescence following treatment with increasing copper concentrations in Hek293 cells. These experiments revealed marked differences in the trafficking behavior of ATP7B and ATP7A. ATP7A was found to re-localize from the TGN in response to elevated copper concentrations (Figure 3C, upper panel). In the physiological range of copper concentrations (5-20 μM), ATP7A trafficked to vesicles, whereas at markedly elevated copper (50-200 μM), ATP7A relocalized to both vesicles and the plasma membrane (Figure 4). The fluorescence intensity of ATP7A increases with the higher copper concentrations, and it has been shown ATP7A protein levels are elevated when cells are treated with 200 μM copper (WonJae Lee and Lawrence Gray unpublished data). However, the

ATP7A staining is due to trafficking and not synthesis as shown by the plasma membrane staining in Figure 4 as well as studies shown in the literature [150187195].

In striking contrast, no change in ATP7B localization was observed, even when cells were treated with copper as high as 200 μm (Figure 3C, lower panel). The copper induced re-distribution of ATP7A and the lack of ATP7B re-localization were verified by co-staining with anti-TGN46 (Figure 3C). The observations with ATP7B were also verified using two other antibodies, targeted to different regions of ATP7B (the ATP Binding domain and nucleotide binding domain antibody data not shown). Thus, in Hek293 cells, ATP7B does not relocalize in response to elevated copper, whereas redistribution of ATP7A occurs at a wide range of copper concentrations. It is important to note that in these experiments, basal medium complete with fetal bovine serum albumin contains an average of 5 μM copper, as measured by atomic absorption spectroscopy.

2.3.3 The copper dependent trafficking of endogenous ATP7B is cell specific.

The lack of ATP7B re-localization in response to copper was unexpected and raised concerns that this phenomenon could merely be an unusual property of Hek293 cells, considering the plethora of papers illustrating trafficking of recombinant ATP7B in response to copper. Consequently, we investigated the trafficking behavior of endogenous ATP7B in several other cell lines. In BeWo (placental cells) and Cos-7 cells (fibroblasts derived from adult green monkey kidney), endogenous ATP7B was found in a tight TGN-like compartment in low

copper, where it co-localized with TGN46 (Figure 5). In both cell lines, no trafficking of ATP7B was observed when copper was elevated. The surprising and consistent lack of ATP7B trafficking led us to examine copper induced re-localization of endogenous ATP7B in hepatocytes. HepG2 and Huh7 cells are derived from liver, and have been previously used by several groups to demonstrate trafficking of ATP7B [151, 190]. Using these cells, and the same experimental procedures as described above, we found that endogenous ATP7B is located at the TGN in the presence of the copper chelator BCS. In both HepG2 and Huh7 cells, ATP7B traffics to vesicles when copper is elevated (Figure 5) in agreement with previous reports [151, 190]. Therefore, the data suggest that copper dependent trafficking of ATP7B is a cell specific phenomenon.

2.3.4 The trafficking behavior of ATP7B and ATP7A in primary cells is consistent with the results from cultured cell lines.

To confirm the physiological relevance of cell specific trafficking of ATP7B, primary cells were generated from mouse liver and kidneys. In primary hepatocytes, ATP7B was localized in proximity to the nucleus and re-localized to vesicles when cells were treated with media containing 200 μM copper (Figure 6). To verify that the immunostaining in primary cells was specific for ATP7B, primary cells from *Atp7b*$^{-/-}$ mouse liver were generated and the experiments repeated as a negative control. Only faint background staining was observed in the *Atp7b*$^{-/-}$ hepatocytes (Figure 6). Thus, in either cultured cells or primary hepatocytes, ATP7B traffics from the TGN to a vesicular compartment in response to elevated copper.

Primary cells were generated using kidneys of 2 week old mice and demonstrated that at this stage, the kidney expresses both ATP7B and ATP7A. In these cells, ATP7A displayed a perinuclear staining at low copper and redistributed to vesicles and plasma membrane in response to elevated copper (Figure 7). ATP7B also had perinuclear location under low copper but did not re-localize when treated with copper, consistent with the observations in Hek293 cells (Figure 7). The specificity of ATP7B staining was further confirmed by utilizing kidney cells derived from the *Atp7b*$^{-/-}$ mice (Figure 7); as expected, no signal was detected in these cells. Thus, the lack of trafficking of ATP7B in cultured cells mirrors the behavior of ATP7B in primary mouse renal cells.

2.3.5 Copper uptake in HepG2 cells and Hek293 cells is similar.

Having established cell specific differences in the trafficking properties of ATP7B, the possible reason for this phenomenon was investigated. In the trafficking experiments, Hek293 and HepG2 cells were treated with the same concentration of extracellular copper. However, it seemed possible that copper uptake, and consequently the intracellular copper concentration, could differ greatly in renal and hepatic cells, resulting in the cell specific difference in trafficking of ATP7B to treatment with copper. The metabolic needs of renal cells compared to hepatic cells, which require delivery of copper to ceruloplasmin, could vary. In order to examine this possibility, the rates of ^{64}Cu uptake into Hek293 cells and HepG2 cells were compared. Figure 8 illustrates that the kinetics of copper uptake over a 2-3 hour time period (a time period corresponding to the duration of copper treatment for trafficking studies) are very

similar for Hek293 and HepG2 cells, although Hek293 cells do accumulate ~10% less copper than HepG2. These experiments were performed using two different copper concentrations, 5 μM and 50 μM, and similar results were obtained for both conditions (50 μM data not shown). Since comparable amounts of copper enter hepatic and renal cells upon copper treatment, it seems unlikely that the lack of trafficking for renal ATP7B is related to variations in copper uptake.

2.3.6 Copper efflux by ATP7A does not contribute to the lack of trafficking response by ATP7B.

Another possible reason for the different trafficking behavior of ATP7B in kidney cells compared to hepatocytes (where ATP7B is the only copper transporting ATPase) could be the expression of ATP7A in kidney cells. ATP7A proceeds faster through catalytic steps and may transport copper more rapidly than ATP7B [81]. As a result, the presence of ATP7A in kidney cells may markedly decrease the amount of copper available for ATP7B, and thus alter ATP7B trafficking. To test this hypothesis, the relative abundance of ATP7A was decreased in Hek293 cells using siRNA silencing, and further examined to whether ATP7B traffics in response to elevated copper under these conditions. GAPDH siRNA was used as a control for non-specific siRNA silencing and showed no effect on endogenous ATP7A expression (Figure 9A, left panel). In contrast, ATP7A specific siRNA markedly decreased ATP7A protein expression. The transfection efficiency in our experiments was approximately 50%, however, in transfected cells almost complete disappearance of ATP7A protein was observed (Figure 9A, right panel). Down-regulation of ATP7A in these cells had

no effect on either the intensity or distribution of ATP7B. In either low or elevated copper, ATP7B displayed a TGN-like localization (Figure 9B), which was similar to localization of endogenous ATP7B in Hek293 cells (Figure 3) and in primary kidney cells (Figure 7). From these results, it was concluded that ATP7A mediated export of copper does not contribute to the lack of ATP7B trafficking in kidney cells.

2.3.7 ATP7B from Hek293 and HepG2 cells is differentially modified in the absence of copper.

Since the copper concentration that induced trafficking of ATP7B in hepatocytes was without effect in kidney cells, ATP7B does not respond directly to extracellular changes copper in Hek293 cells, or the regulation of ATP7B in these cells are somehow altered. It seemed possible that ATP7B might be post-translationaly modified in a cell specific manner or that regulation may differ in elevated copper conditions. To examine this possibility, we isolated membrane fractions from Hek293 and HepG2 cells and analyzed ATP7B following gel electrophoresis and Western blotting. These experiments revealed a small but highly reproducible difference in electrophoretic mobility of renal and hepatic ATP7B, an apparent molecular weight change of 3kDa. ATP7B from Hek293 cells migrated faster than ATP7B from HepG2 cells (Figure 10A); this difference was independent of copper treatment. Consequently, it was concluded that ATP7B in the two cell types is differentially modified even in the absence of elevated copper.

2.3.8 ATP7B is phosphorylated in Hek293 and HepG2 cells.

The Lutsenko lab has previously shown that in hepatic cells, ATP7B is phosphorylated by a kinase in the absence of copper, and becomes hyper-phosphorylated when copper levels are increased [75]. Phosphorylation changes ATP7B mobility, causing a small upward shift in the position of ATP7B on a gel. Since the electrophoretic mobility of ATP7B from HepG2 and Hek293 cells was different (in either the presence or absence of copper), the change in ATP7B mobility from Hek293 cells was tested for a lack of phosphorylation. To examine kinase mediated phosphorylation of ATP7B, Hek293 and HepG2 cells were treated with BCS and then metabolically radiolabeled with orthophosphate, ^{32}P. ATP7B was immunoprecipitated from Hek293 and HepG2 cell lysates and incorporation of ^{32}P was evaluated by autoradiography. Figure 10B illustrates that ATP7B is phosphorylated in either Hek293 cells or HepG2 cells in the absence of copper. Therefore, phosphorylation is unlikely to be a cause of the apparent size difference.

2.3.9 Recombinant ATP7B from Hek293 cells has a similar mobility as endogenous ATP7B from HepG2 cells.

The observed faster mobility of ATP7B in renal cells corresponds to an apparent decrease in molecular weight of ATP7B by about 3 kDa and could also be a result of regulatory proteolysis or modification of corresponding mRNA. To determine whether modification of ATP7B in Hek293 cells occurs at the protein level (proteolysis), or involves changes in mRNA (alternative splicing/ translation), ATP7B cDNA was transfected into Hek293 cells, and the electrophoretic mobilities of recombinant and endogenous proteins were

compared on a Western blot. If ATP7B in Hek293 cells is proteolyzed or otherwise modified at the protein level, then the observed mobilities of the endogenous and recombinant proteins would be similar. However, if changes occur at the mRNA level, then the endogenous and cDNA encoded ATP7B will differ.

Figure 10C illustrates that the recombinant ATP7B expressed in Hek293 cells has a slower electrophoretic mobility (larger apparent molecular weight) than endogenous renal ATP7B. (Transfection of recombinant ATP7B into Hek293 results in high levels of recombinant ATP7B expression such that endogenous ATP7B is difficult to observe in these cells by western blot). Since ATP7B cDNA, which we utilized to produce recombinant protein, originates from the liver, the difference in endogenous and recombinant ATP7B in Hek293 cells is likely due to tissue specific difference between liver and kidney ATP7B mRNA, rather than proteolysis or other posttranslational modification. This conclusion is supported by the very similar mobility of recombinant ATP7B expressed in Hek293 cells and endogenous hepatic ATP7B from HepG2 cells (Figure 10C).

2.3.10 ATP7B translated product from Hek293 and HepG2 cells differ in the exon 1 region.

The cDNA derived from the liver is generally accepted as encoding full-length ATP7B. In Figure 11, ATP7B liver RNA organization is shown. The ATP7B RNA is composed of 21 exons, and the transcript is 6,638 bps. The presence of different alternatively spliced mRNA for ATP7B in tissues has been suggested based on cloning and RT-PCR results[50, 121, 196], although the existence

of corresponding protein variants have not yet been confirmed except in sheep[166]. To examine whether or not kidney and liver cells have distinct transcripts of ATP7B, cDNA was generated using cellular RNA extracted from Hek293 and HepG2 cells and three specific regions of ATP7B, exon 1, 6, and 21 (Figure 12A) were PCR amplified. Cellular RNA was used rather than total RNA to exclude unspliced mRNA products, and cDNA was generated with poly dT in parallel with random hexamers; both sets of cDNA showed the exact same results. The selected exon regions, if spliced out, would generate a shorter ATP7B gene product with a mass difference (~ 3 kDa) observed in the Western blots. However, the deletion of these regions in the ATP7B transcript is unlikely to disrupt the activity or structure of ATP7B (Figure 11).

A previous report suggested the presence of an alternate ATP7B product in a kidney library, generated by the substitution of part of exon 21 with the downstream sequence from another gene to which the authors referred to as exon 22 [196]. Nested PCR using primers specific to the putative exon 22 did not yield PCR products for either Hek293 or HepG2 derived cDNA (data not shown). In contrast, when primers designed to amplify intact exon 21 were used (Figure 12A) in both Hek293 and HepG2 derived cDNA, PCR products of expected size, ~1kb, were detected (Figure 12B). As a control, a plasmid containing full length ATP7B was used (Figure 12B, lane 5). Therefore, in both cell types, exon 21 of ATP7B transcript is intact and cannot be responsible for the observed size differences in the protein.

Exon 6, a target for alternative splicing in some WND patient mutations, which codes for the region in vicinity to transmembrane segment 1 of ATP7B, was also tested as a possible target for alternative splicing. Previously, studies with mutations in the MBDs of ATP7B suggested that perhaps in the region between MBD 6 and TMS 1, encoded by exon 6, might lay a trafficking signal. However, PCR amplification of this region showed the expected 506 bp product for both Hek293 and HepG2 cells (Figure 12C), suggesting exon 6 is not the target for alterative splicing.

In contrast, cell specific differences were detected when the 5' end of the ATP7B mRNA was analyzed. In the ATP7B RNA transcript, the codon for the first Met is located near the end of exon 1, whereas the second Met is located near the beginning of exon 2 (Figure 13). Translation of the ATP7B gene beginning at exon 2 would generate a transcript starting at the second ATG (Met) and the corresponding protein product would be smaller by ~3 kDa.

We initially attempted to perform a RACE analysis of the 5'-region but were successful only with control genes (data not shown), most likely due to an extremely GC-rich sequence in exon 1, which is predicted to form a stable hairpin loop from RNA prediction software (http://rna.tbi.univie.ac.at/cgi-bin/RNAfold.cgi) (Figure 14). Most likely, the RNA ligation step of the 5' adaptor was inhibited due to the secondary structure. A RNA ligase stable in the required temperature range to melt the hairpin loop, ~95°C, for the addition of the 5' adaptor for RACE analysis is not available, but would be interesting to do in the future to determine the complete sequence of the 5' untranslated region of the ATP7B mRNA.

Nested PCR of this region using a forward primer in exon 1 in the first round of amplification and a forward primer in exon 2 in the second round of amplification revealed a band corresponding to the expected 395 basepairs for HepG2 cells, but no equivalent band for Hek293 cells (Figure 12D, left). I was not able to do the corresponding control with ATP7B plasmid because the plasmid contains only the coding region. However, 216Exon2WndpFwd and EcoRI445Rev (first round primers) and 274Fwd and 647Exon2Rev (second round primers) were tested to see in Hek293 and HepG2 cDNA to see if they work, since three out of the four primers were used to test for the presence of exon 1. In Figure 12D, right, both Hek293 and HepG2 cells give the correct size band, 396bp, suggesting that the exon 2 primers work and the lack of an exon 1 band in Hek293 cells is due to a lack of exon 1. This data suggests cell specific difference could be due to differences in the ATP7B mRNA. The loss of exon 1 in the renal ATP7B transcript would be consistent with a 3 kDa change in protein mobility without affecting catalytic function or overall folding of the protein.

2.3.11 Hepatic form of ATP7B expressed in HEK293 cells traffics in response to copper.

To further verify that the cell specific difference in ATP7B trafficking is due to changes in the translated protein and not in cellular machinery, we characterized the localization and trafficking of the full size liver variant of ATP7B in Hek293 cells. Transient transfection experiments, as well as stably selected clones, often led to overexpression of ATP7B, which complicated trafficking studies. Cos7, HeLa, CHO-K1, Hek293, and HepG2 cells were all tested under

varying conditions with the ATP7B cDNA expressed in three different expression vectors (pcDNA3.1, pet28b, LCV) (data not shown). Overexpression resulted in what appeared to be fragmentation of the Golgi compartment into Golgi vesicles. To overcome this problem, we utilized FlpIn T-Rex 293 cells to generate a stable FlpIn Hek293 cell line expressing Flag-tagged ATP7B under the control of a tetracycline dependent promoter (schematic Figure 15). (An N-terminal Flag tag was introduced to distinguish the recombinant ATP7B from endogenous protein). Although we are testing the role of the N-terminus in trafficking, an N-terminal tag was necessary because addition of a C-terminal tag leads to an unstable construct (data not shown). Addition of epitope tags anywhere else on the protein may result in decreased protein expression, stability or affect catalytic activity [197]. In cells depleted of copper by treatment with BCS, Flag-ATP7B was found in a perinuclear compartment, where it co-localized with the TGN marker, TGN46 (Figure 16, top row), similarly to endogenous protein (Figure 3B). Unlike endogenous ATP7B which does not traffic in Hek293 cells, copper treated Flag-ATP7B was targeted to a vesicular compartment (Figure 16, bottom row). This redistribution in response to elevated copper is consistent with the trafficking pattern of hepatic ATP7B, supporting our conclusion that the cell specific trafficking behavior of ATP7B is controlled at the transcriptional level.

2.4 Discussion

2.4.1 ATP7B and ATP7A differ in their response to elevated copper.

Copper homeostasis within cells and tissues is tightly regulated. It has been suggested that the copper dependent trafficking of ATP7B and ATP7A is

the central mechanism through which these ion transporting ATPases control intracellular copper [198]. We demonstrate that cells expressing both endogenous ATP7B and ATP7A have an additional level of regulation in which the two transporters show markedly different trafficking behavior. In either cultured kidney cells or in primary cells isolated from mouse kidneys, ATP7A traffics from the TGN to vesicles and/or plasma membrane in response to a wide range of copper concentrations, whereas there is no change in the intracellular localization of ATP7B at copper concentrations as high as 200μM. This distinct trafficking behavior in response to elevated copper may reflect distinct functions of ATP7B and ATP7A in renal cells. Renal ATP7A appears to be responsible for maintaining intracellular copper concentration by exporting copper across the basolateral plasma membrane [195, 199]. Our data suggest that ATP7B regulates copper levels by transporting copper to intracellular compartments. In cells that co-express ATP7B and ATP7A, the two Cu-ATPases have distinct functions. It would be interesting to test whether total intracellular copper changes when ATP7B or ATP7A expression is knocked down to determine the degree of overlapping function and to identify the specific role of each transporter in copper regulation.

2.4.2 In kidney cells, ATP7A traffics mainly to vesicles.

Majority of previous studies on the trafficking of ATP7A used highly elevated copper (typically around 200 μM). Under these conditions, a significant fraction of ATP7A is located at/near the plasma membrane. However, our experiments using a wider range of copper concentrations (Figure 4) indicate that

at lower, and more physiological copper levels (5-10 μM copper), ATP7A still leaves the TGN, but traffics primarily to vesicles. This situation in kidney cells closely resembles the behavior of endogenous ATP7A in intestinal Caco-2 cells, where ATP7A readily redistributes from the TGN to vesicles in response to changes in copper levels but only approximately 8-10% of the ATP7A is detected at the basolateral cell surface [188]. The ATP7A containing vesicles may rapidly recycle via the plasma membrane [200] and unload their copper content. In tissues, where cells are polarized, both vesicular and basolateral staining may be seen dependent on whether ATP7A is stained in the distal or proximal tubules. In the proximal tubules where the copper concentration is lower, ATP7A may be localized primarily in vesicles. However in distal tubules where copper is concentrated for excretion into the urine, ATP7A may localize primarily at the basolateral membrane as shown in mice with acute increase in copper [199].

2.4.3 Cell specific control of ATP7B localization.

Our experiments demonstrate that cell specific differences in ATP7B trafficking is not due to different amounts of copper entering cells, since the kinetics of copper transport into Hek293 and HepG2 cells are similar. Also, ATP7A mediated copper efflux does not contribute to the lack of ATP7B response in Hek293 cells as down regulation of ATP7A by RNA silencing has no effect on ATP7B localization, which remains TGN-like in both low and high copper. One may argue that cell polarization could be necessary for the ability of ATP7B to traffic correctly, as the Hek293 cells are not polarized. However, when the localization of ATP7B was compared in polarized kidney cells (OK or MDCK

cells) in low and high copper, no effect of copper on the intracellular localization of ATP7B was observed (data not shown). This lack of trafficking in response to copper is not limited to just kidney derived cell lines. Recent reports showing the effects of hormones on ATP7B and ATP7A localization in mammary gland derived cells suggest that in non-hepatic cells, trafficking of ATP7B, if it occurs, could be modulated by stimuli other than copper [201-203].

Ceruloplasmin is the major recipient of copper from ATP7B in the biosynthetic pathway. In HepG2 cells, ceruloplasmin is expressed and secreted, as expected from a hepatocyte derived cell line. However, in Hek293 cells, full length ceruloplasmin is not detectable by western blot with two different antibodies (Figure 47 using Sigma antibody, data not shown for Bethyl Laboratories antibody). Perhaps the co-expression of ceruloplasmin in tandem with ATP7B is important for determining which ATP7B transcript is expressed. In the cerebellums of $Atp7b^{-/-}$ mice, altered ATP7B expression changes ceruloplasmin localization[204]. In ceruloplasmin KO mice, copper accumulates in the liver, where ATP7B is abundantly expressed and traffics, whereas in other organs, copper metabolism is not affected[38]. Further experiments are required to determine the effect of ceruloplasmin on ATP7B trafficking.

2.4.4 Distinct post-transcriptional modifications may play a key role in cell specific trafficking of ATP7B.

The lack of copper induced trafficking for endogenous ATP7B in all examined cell types, except hepatocytes, was initially surprising given considerable evidence showing trafficking of transiently transfected ATP7B in

CHO-K1 cells [160, 161]. However, it is now clear that transfected protein (originating from liver derived cDNA) and endogenous ATP7B in renal cells are not identical (compare Figure 3 and 10). Our data suggest that in kidney, the ATP7B mRNA translated product may be altered. Data in Figure 12D shows that under identical conditions, HepG2 derived cDNA contains exon 1 whereas in Hek293 cDNA, no exon 1 was detected by nested PCR. Transfection of ATP7B cDNA into Hek293 cells results in a protein of the same size as in the HepG2. This suggests the differences could stem from the regulation of the transcript.

The lack of exon 1 could be a result of several factors. First, the PCR reaction may not have worked, due to problems with the cDNA or the primers. However, the HepG2 cDNA resulted in a PCR product, suggesting the primers work. Also, nested PCR with three out of the four primers resulted in a signal for Hek293 cells (Figure 12D, right) suggesting the cDNA is fine.

On the other hand, the presence of exon 1 in HepG2 could be a result of the retention of exon 1 or the splicing of exon 1 in Hek293 cells. It has been shown that there are tissue specific regulations of some mRNAs. ATP7B is unique in that in the liver, it is the only copper ATP-ase expressed. Splicing of the ATP7B HepG2 mRNA could be inhibited by protein binding to the pre-mRNA, either in the 5'UTR, exon 1, or intron 1. This would physically inhibit splicing of the target site or prevent binding of the splicing complex, leading to the retention of exon 1 in the liver.

Splicing of ATP7B pre-mRNAs can also be promoted, by protein binding to the RNA and facilitating spliceosome assembly or by directly splicing the RNA,

resulting in the loss of exon 1. Splicing of introns is not always processive (from 5' to 3'), so there are many possible ways the ATP7B pre-mRNA could be spliced. However, intron 1 of ATP7B is very large, over 36 kb, compared to the rest of the ATP7B introns. During transcription of the ATP7B RNA, there could be exposure of different cryptic splicing sites that may regulate where ATP7B is spliced. Added to this complexity is that some mRNAs are exported from the nucleus and undergo further splicing in the cytoplasm by the minor splicesome [205]. So there could be differences in the transcript based on which pool of mRNA is examined, total as opposed to cellular RNA.

Examination of the 5'UTR of the ATP7B transcript shows that 12 nucleotides upstream from the 5' exon 1 boundary, there is an additional ATG codon in frame to the ATP7B transcript. Whether this exon 1 boundary is firm needs to be determined because initiation of translation at this Met in the 5' UTR would lead to an aborted transcript by a stop codon in exon 1. Another method of controlling which alternative splice site is used is by regulating the ratio of transcription. Different secondary structures in the RNA may form dependent on how fast transcription proceeds. A possibility is that in cells where ATP7B does not traffic, transcription proceeds may proceed at a specific rate, resulting in the splicing of exon 1 to eliminate the possible third translational start site. However, in cells that ATP7B does not traffic, transcription is at a different rate leading to the retention of exon 1, and requiring an additional level of control to start translation in exon 1.

A third possibility is that translation of ATP7B begins at the second methionine in Hek293 cells because of the secondary structure of exon 1 inhibits binding of the translational machinery (Figure 14). However, in HepG2 cells, there could be specific regulation of the ATP7B transcript, by the production of a protein that would bind to the 5' region of exon 1, preventing the formation of the translational inhibitory structure. Also, ATP7B could encode for an internal ribosome entry site, allowing for recruitment of the 40S ribosome to the initiation codon. This would allow for translation of ATP7B at the first methionine, when cells are undergoing nutritional stress. Since ATP7B only trafficked in response to copper in hepatocytes, this could be a simple mechanism for ATP7B control. However, in this scenario, exon 1 would be present in both Hek293 and HepG2 cells. Further experiments determining the 5'UTR of ATP7B mRNA may provide insight into the regulation of ATP7B.

This difference in the structure of the renal and hepatic ATP7B is particularly interesting in light of recent studies showing the important role of the first 63 amino acids in trafficking of ATP7B [46]. The presence of these N-terminal amino acids is necessary for the copper responsiveness of ATP7B in hepatocytes and trafficking of ATP7B towards the apical membrane [46]. Also, careful examination of some of the N-terminal deletion constructs of ATP7B used for trafficking in the literature show that the authors left this N-terminal 32 amino acid region intact, while deleting further downstream residues, suggesting the importance of this region in ATP7B trafficking. While the specific role of the first 32 residues is presently unknown, it is tempting to speculate that they may

contribute to the formation of a regulatory protein moiety containing a trafficking signal for ATP7B.

Since the region identified by Guo et al and the N-terminal 32 amino acid residues overlap, it would be interesting to compare the two constructs, to narrow the region responsible for trafficking. I would predict in polarized hepatocytes, such as HepG2 cells, deletion of exon1 would result in the mislocalization of ATP7B to the basolateral membranes, as seen for the 63 amino acid deletion constructs. However in non-polarized cells, I do not believe there would be any trafficking, as observed for endogenous ATP7B in Hek293 cells.

In conclusion, the two copper transporting ATPases, ATP7B and ATP7A, not only have distinct enzymatic properties [81], but also show markedly different trafficking behavior. In kidney cells, ATP7A traffics in response to changes in the copper concentration, while the localization of ATP7B is unaffected by copper. Our results in renal cells suggest another mode of regulation where changes in the ATP7B mRNA translation product drastically may modulate targeting of ATP7B to various compartments in the cell.

A

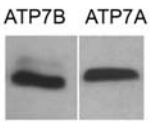
ATP7B
ATP7A

B

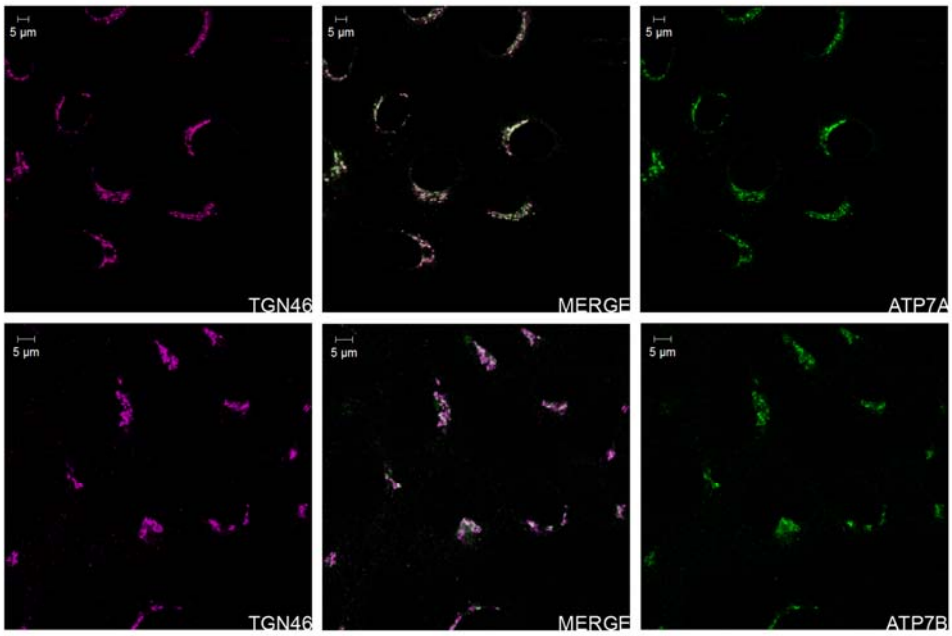
5 µm
TGN46
MERGE
ATP7A
5 µm
TGN46
MERGE
ATP7B

C

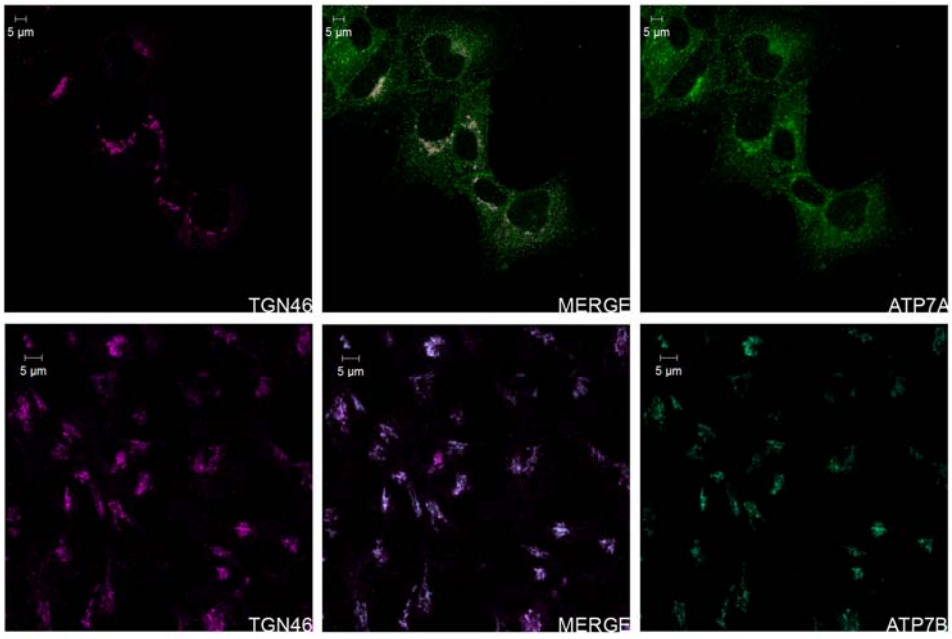
5 µm
TGN46
MERGE
ATP7A
5 µm
TGN46
MERGE
ATP7B

Figure 3: ATP7A and ATP7B are co-expressed in Hek293 cells and show different trafficking behavior. **A**) Western blots (merged) of membrane fractions Hek239 cells (60μg protein per lane) probed with anti-ATP7A or anti-N-ATP7B antibody. (Western blot by Natalie Barnes) **B**) Co-Localization of ATP7B/ATP7A (green) with TGN marker TGN46 (purple) with 50μM BCS **C**) Comparison of ATP7B and ATP7A localization following treatment with 50μM copper chloride. ATP7A (green) is localized primarily at the plasma membrane and vesicles. ATP7B (green) is co-localized with TGN46 (purple); no redistribution is detected.

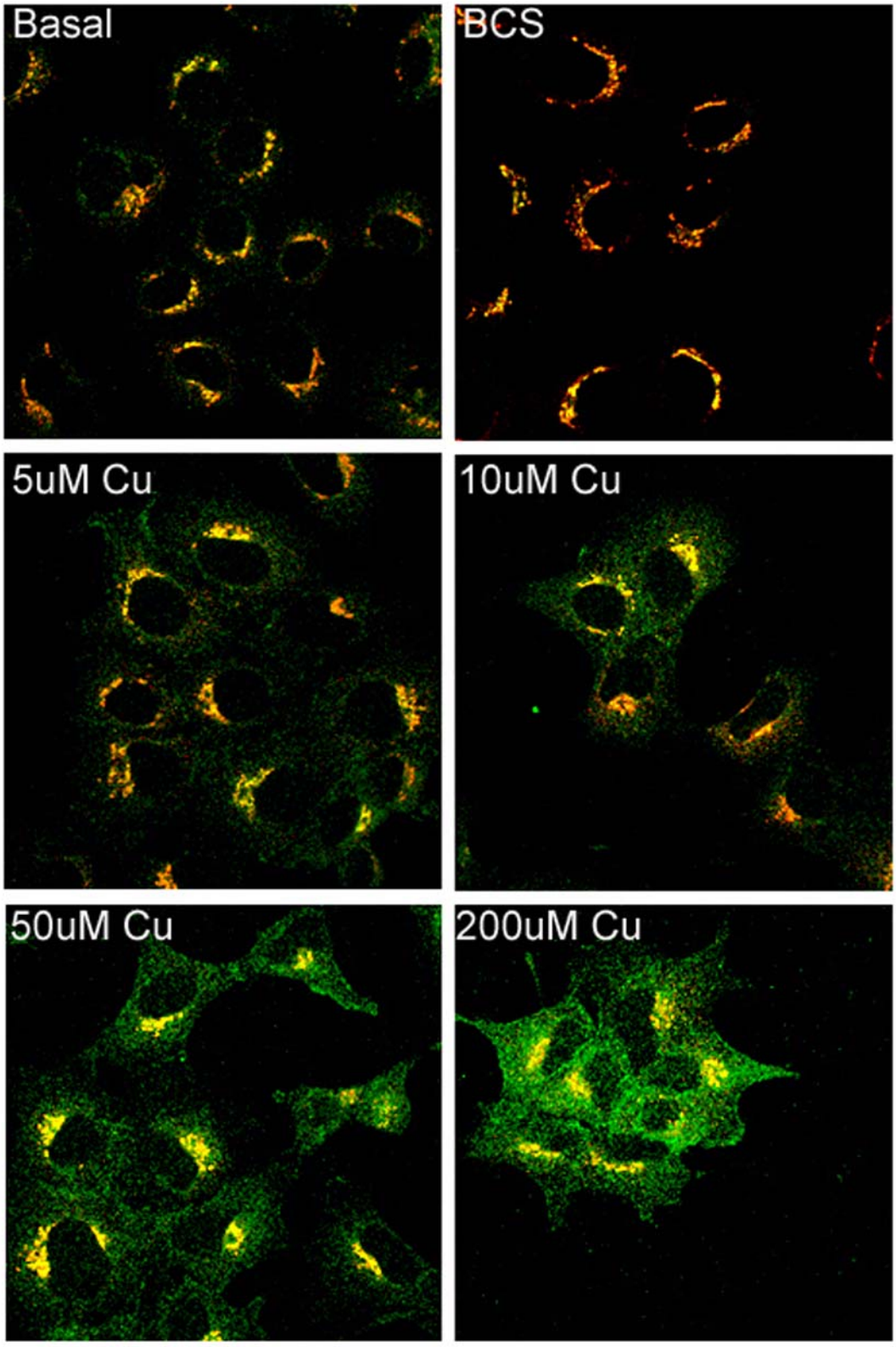
Basal
BCS
5uM Cu
10uM Cu
50uM Cu
200uM Cu

Figure 4: Trafficking of endogenous ATP7A in response to copper in Hek293 cells. Hek293 cells were treated with an increasing concentration of copper chloride. The resulting trafficking response of ATP7A was by staining for ATP7A (green) and TGN46 (red). With increasing copper, 5µM, 10µM, 50µM, and 200µM copper chloride, ATP7A localization changes from the TGN to vesicles and the plasma membrane at higher concentrations (Cell staining by Natalie Barnes). For basal and BCS treated cells, there was no change in the localization.

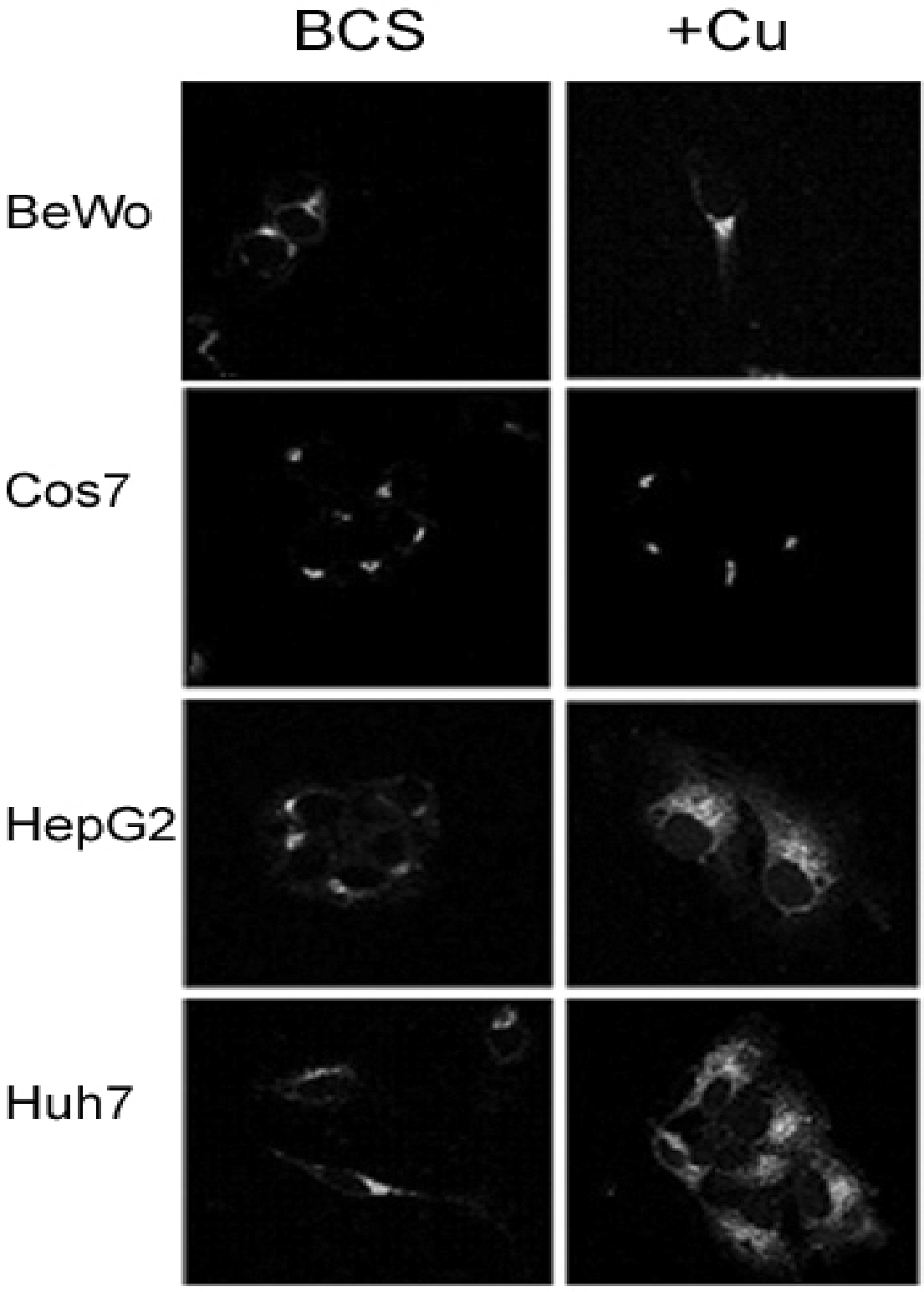
BCS
+Cu
BeWo
Cos7
HepG2
Huh7

Figure 5: Endogenous ATP7B traffics in response to copper in cultured hepatocytes. ATP7B trafficking was investigated in four different cell lines: BeWo (human placental cells), Cos7 (green monkey kidney cells), HepG2 (human hepatocytes), and Huh7 (human hepatocytes) (Cell staining by Natalie Barnes). Endogenous ATP7B had a perinuclear staining pattern for 200μM BCS treated cells, but when treated with 200μM copper, only ATP7B from hepatocytes trafficked.

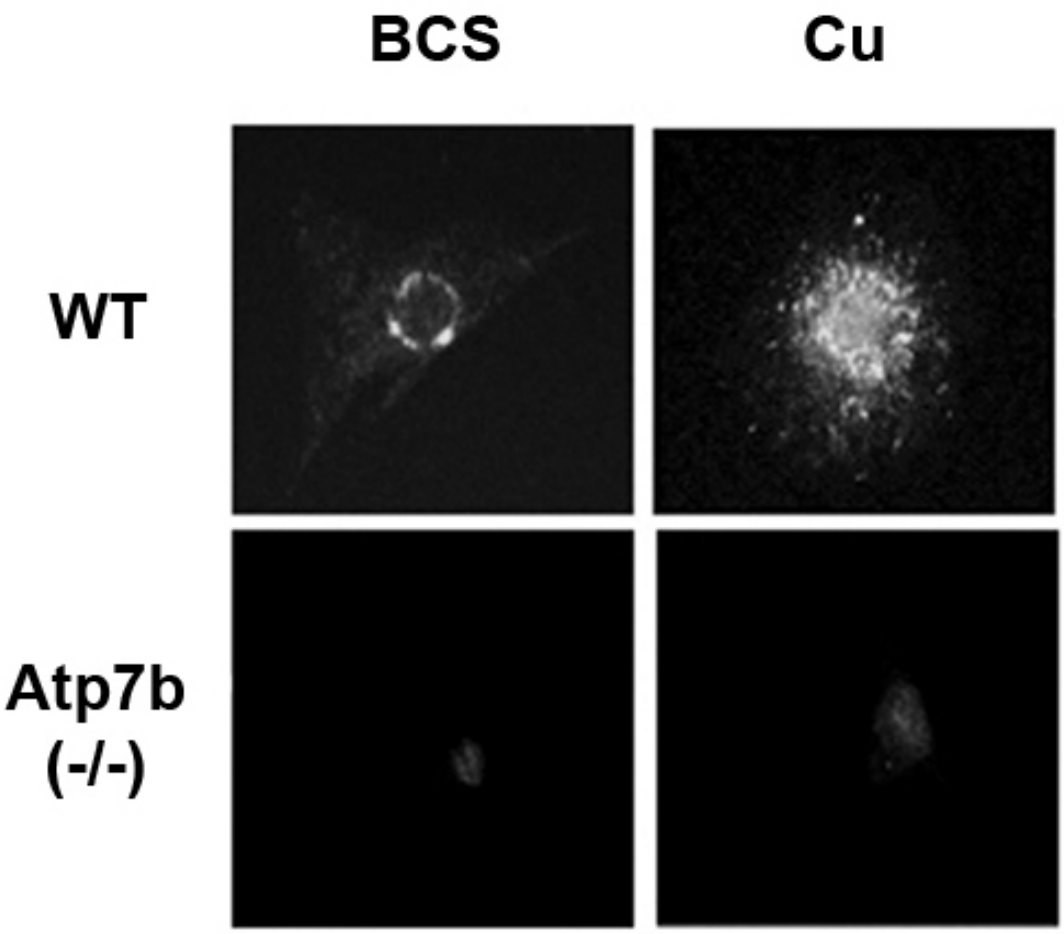

Figure 6: ATP7B traffics in response to copper in primary hepatocytes. Primary hepatocytes were harvested from ATP7B KO and wild type mice. ATP7B was perinuclear for cells treated with 200µM BCS, but 200µM copper treated cells had a vesicular staining pattern (Cell staining by Natalie Barnes). No staining for ATP7B was observed from cells derived from KO mice.

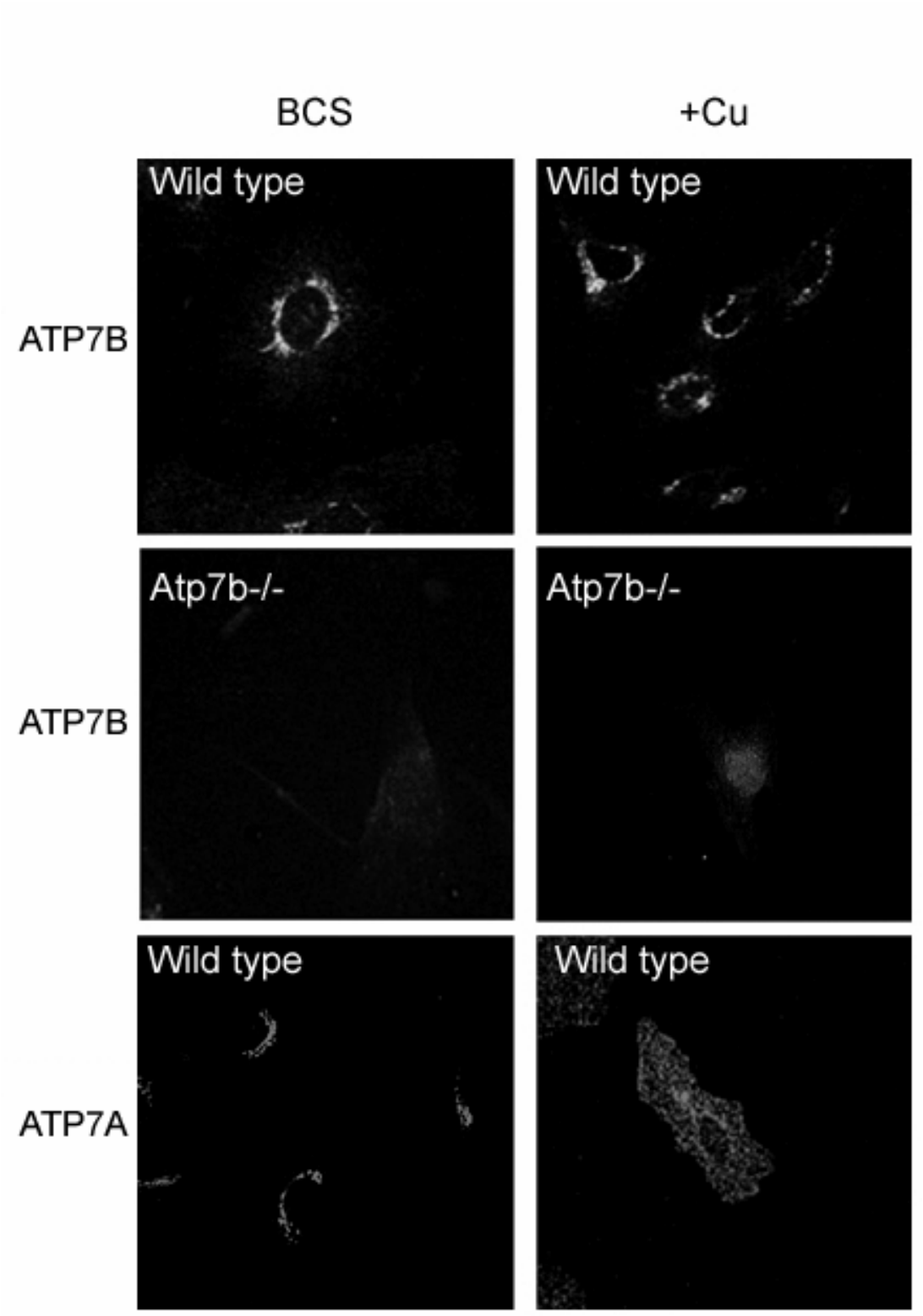
BCS
+Cu
Wild type
Wild type
ATP7B
Atp7b-/-
Atp7b-/-
ATP7B
Wild type
Wild type
ATP7A

Figure 7: ATP7B and ATP7A in primary kidney cells respond differently to elevated copper. Primary kidney cells derived from 2 week-old wild-type and *Atp7b*$^{-/-}$ mice were treated and immuno-stained as in Figure 3 (Cell staining by Natalie Barnes). *Top panel:* in wild-type cells, ATP7B does not relocalize in response to copper; *Middle panel:* no ATP7B is detected in *Atp7b*$^{-/-}$ kidney cells, demonstrating specificity of staining; *Lower panel:* ATP7A displays perinuclear localization in low copper (BCS) and traffics to vesicles and the plasma membrane in response to copper elevation (Cu).

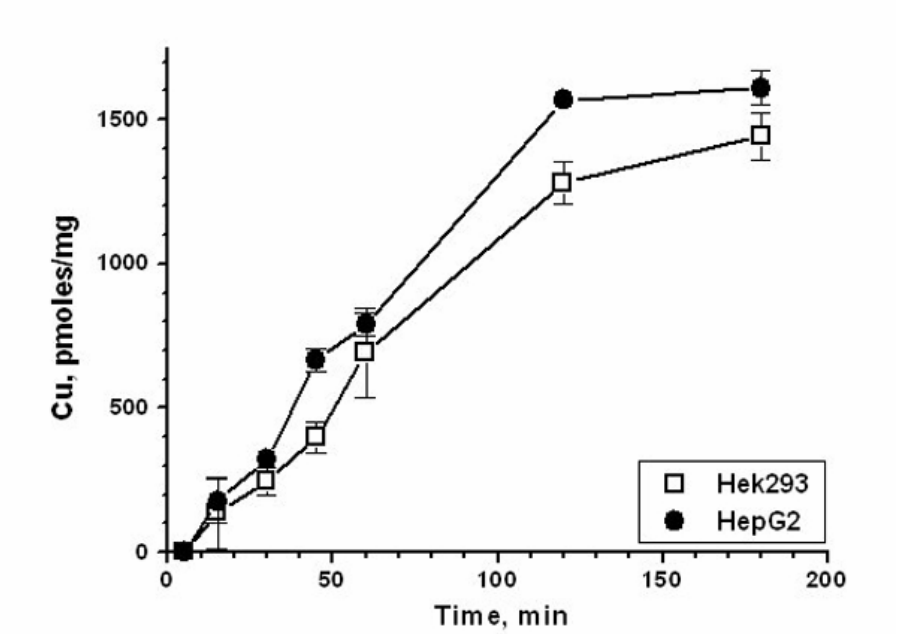

Figure 8: Copper uptake is similar in Hek293 and HepG2 cells. Radioactive copper was added to live cells, and the copper uptake was evaluated by the kinetics of ^{64}Cu accumulation. A representative experiment is shown for 5μM total copper; each point is an average of three independent measurements (Uptake studies by Vladimir Ustiyan). Within the time frame of copper treatment assays, 1-3hrs, the amount of copper accumulated in Hek293 and HepG2 cells are similar.

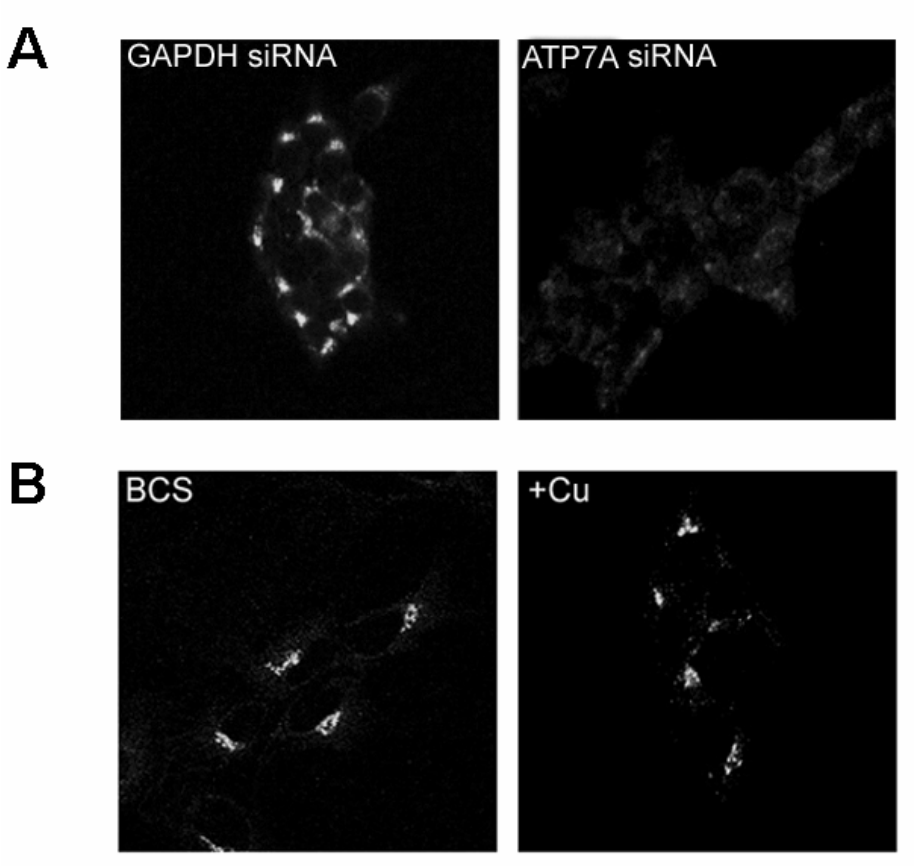

Figure 9: Reduction of cellular ATP7A protein, using siRNA, does not affect localization of ATP7B in Hek293 cells. A) *Left:* Transfection with 800 ng of GAPDH siRNA (used as a negative control) has no effect on ATP7A abundance. *Right:* ATP7A levels are markedly decreased in cells transfected with 800ng of ATP7A specific siRNA. **B**) In cells transfected with ATP7A siRNA (both panels), ATP7B remains at the TGN in BCS (left panel) or elevated copper (right panel), suggesting relative abundance of ATP7A does not affect ATP7B localization (Cell staining by Natalie Barnes).

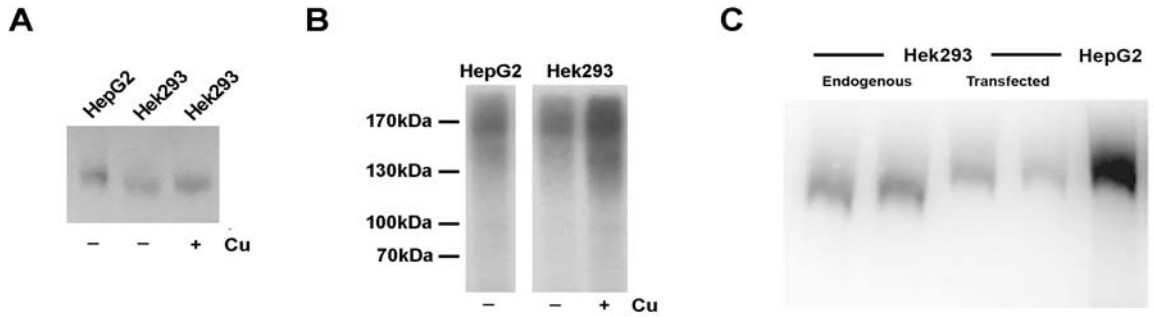

Figure 10: Differences in ATP7B from Hek293 and HepG2 stem from intrinsic differences in the ATP7B protein. A) The mobilities of endogenous ATP7B from HepG2 and Hek293 cells were compared by western blot analysis. Consistently, the electrophoretic mobility of ATP7B from Hek293 cells migrates faster than ATP7B from HepG2 cells. **B**) Autoradiography of ATP7B immunoprecipitated from HepG2 and Hek293 cells, which were metabolically labeled with ^{32}P. **C**) Comparison of electrophoretic mobilities by western blot analysis demonstrates that in renal cells, endogenous ATP7B differs from the liver derived transfected ATP7B. In contrast, endogenous ATP7B in HepG2 cells is very similar to the transfected ATP7B. Endogenous ATP7B is not visible in the transfected lane due to much higher levels of recombinant ATP7B, and hence lower amount of transfected membrane used; the total membrane protein per lane was adjusted with membranes lacking ATP7B and is the same in all lanes.

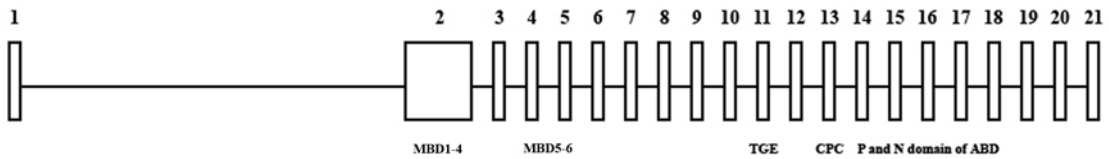

Figure 11: Schematic of ATP7B exon and intron organization. The 21 ATP7B exons are illustrated as rectangles, with the exon number above. Exons coding for key ATP7B regions are indicated.

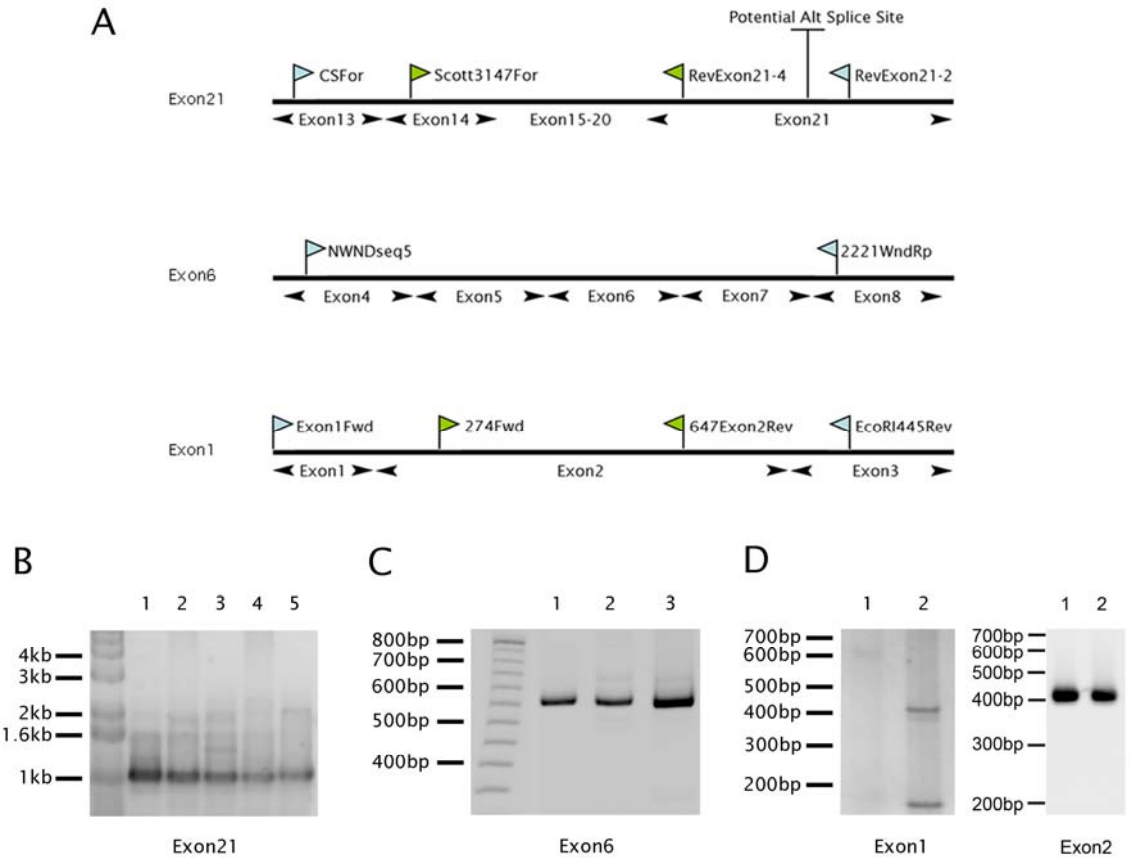
A
Potential Alt Splice Site
Exon21
CSFor
Scott3147For
RevExon21-4
RevExon21-2
Exon13
Exon14
Exon15-20
Exon21
Exon6
NWNDseq5
2221WndRp
Exon4
Exon5
Exon6
Exon7
Exon8
Exon1
Exon1Fwd
274Fwd
647Exon2Rev
EcoRI445Rev
Exon1
Exon2
Exon3
B
1 2 3 4 5
4kb
3kb
2kb
1.6kb
1kb
Exon21
C
1 2 3
800bp
700bp
600bp
500bp
400bp
Exon6
D
1 2
700bp
600bp
500bp
400bp
300bp
200bp
Exon1
1 2
700bp
600bp
500bp
400bp
300bp
200bp
Exon2

Figure 12: PCR products of ATP7B cDNA from Hek293 and HepG2 cells differ in exon 1. **A**) Schematic of primers used for PCR and nested PCR reactions for ATP7B exon 21, 6, and 1. (**B-D**) PCR products generated using exon specific primers. **B**) Nested PCR was performed for exon 21 using cDNA generated from Hek293 using random hexamers (Lane 1) or polyT primer (Lane 2) and from HepG2 cDNA generated using random hexamers (Lane 3) or polyT primer (Lane 4). ATP7B plasmid was used as a positive control (Lane 5). PCR products were run on a 1% agarose gel and stained with ethidium bromide. All cDNA yielded product of the expected size of ~1kb. C) PCR products for exon 6. Lane 1: Hek293 cDNA, lane 2: HepG2 cDNA, lane 3: ATP7B plasmid. Samples were run on an 8% acrylamide gel and stained with SYBR green. All three lanes resulted in similar size products of 530bp. **D**) Nested PCR products for exon 1 (gel on left). Lane 1: Hek293 cDNA and Lane 2: HepG2 cDNA. PCR products were analyzed on 8%acrylamide and stained with SYBR green. Product of the correct size, 396bp was only seen in reactions utilizing the HepG2 template. To test whether the primer pair 274Fwd and 647Exon2Rev could recognize exon2 from Hek293 and HepG2 cDNA (gel on right), first round amplified (216Exon2WndpFwd and EcoRI445Rev) product was used for PCR with the exon2 primers. Lane 1 is Hek293 and Lane 2 is HepG2 cDNA. The primer pair Exon1Fwd and EcoRI445Rev could not be tested together on ATP7B plasmid because the plasmid construct does not encode the region in exon1 that the Exon1Fwd primer binds.

A

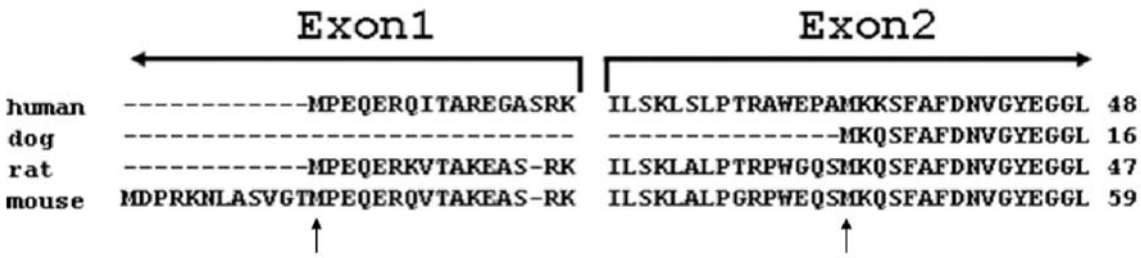

B

```
ATP7B plasmid      ----------------------------------------
ATP7B transcript   tcccaaatgaaggggcggttcccggacccctgtttgcttt

ATP7B plasmid      ----------------------------------------
ATP7B transcript   agagccgagccgcgccgcgccgatgccctcacactctgcg

ATP7B plasmid      ----------------------------------------
ATP7B transcript   cctcctctcccgggactttaacaccacgctctcctccacc

ATP7B plasmid      ----------------------------------------
ATP7B transcript   gaccaggtgacctttgctctgagccagatcagagaagaa

ATP7B plasmid      --------------------atgcctgagcaggagagaca
ATP7B transcript   ttcggtgtccgtgcgggacgatgcctgagcaggagagaca

ATP7B plasmid      gatcacagccagagaaggggccagtcggaaaatcttatct
ATP7B transcript   gatcacagccagagaaggggccagtcggaaaatcttatct

ATP7B plasmid      aagctttctttgcctacccgtgcctgggaaccagcaatga
ATP7B transcript   aagctttctttgcctacccgtgcctgggaaccagcaatga

ATP7B plasmid      agaagagt
ATP7B transcript   agaagagt
```

Figure 13: Sequence alignment of ATP7B. (A) A sequence alignment of ATP7B orthologues was performed using Clustal W (1.83). The boundary between exon 1 and exon 2 (for human ATP7B, used in this study) is indicated. Canine ATP7B (dog) lacks a corresponding exon 1. Arrows point to the methionines in exon 1 and exon 2, which may serve as the initiating Met for hepatic and renal ATP7B, respectively. (B) A sequence alignment of the 5'UTR and exon 1 region of ATP7B compared to ATP7B in liver cDNA derived plasmids. Alignment was created in BioEdit.

Secondary Prediction Structure of WNDP Exon1

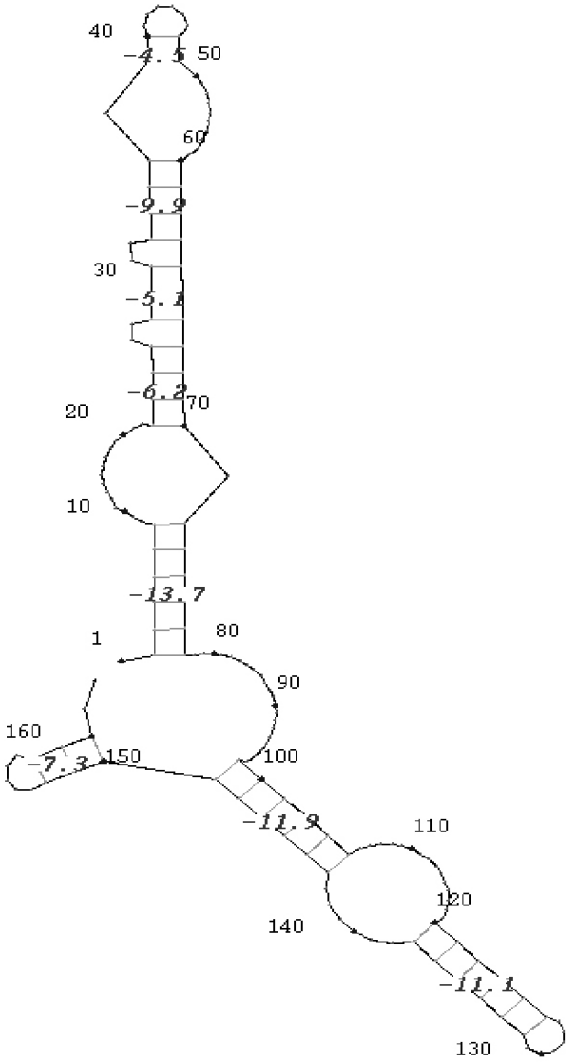

Free Energy of Structure = -31.5kcal/mol

Figure 14: Secondary structure prediction for ATP7B exon1. Generated with the RNA prediction program at http://rna.tbi.univie.ac.at/cgi-bin/RNAfold.cgi

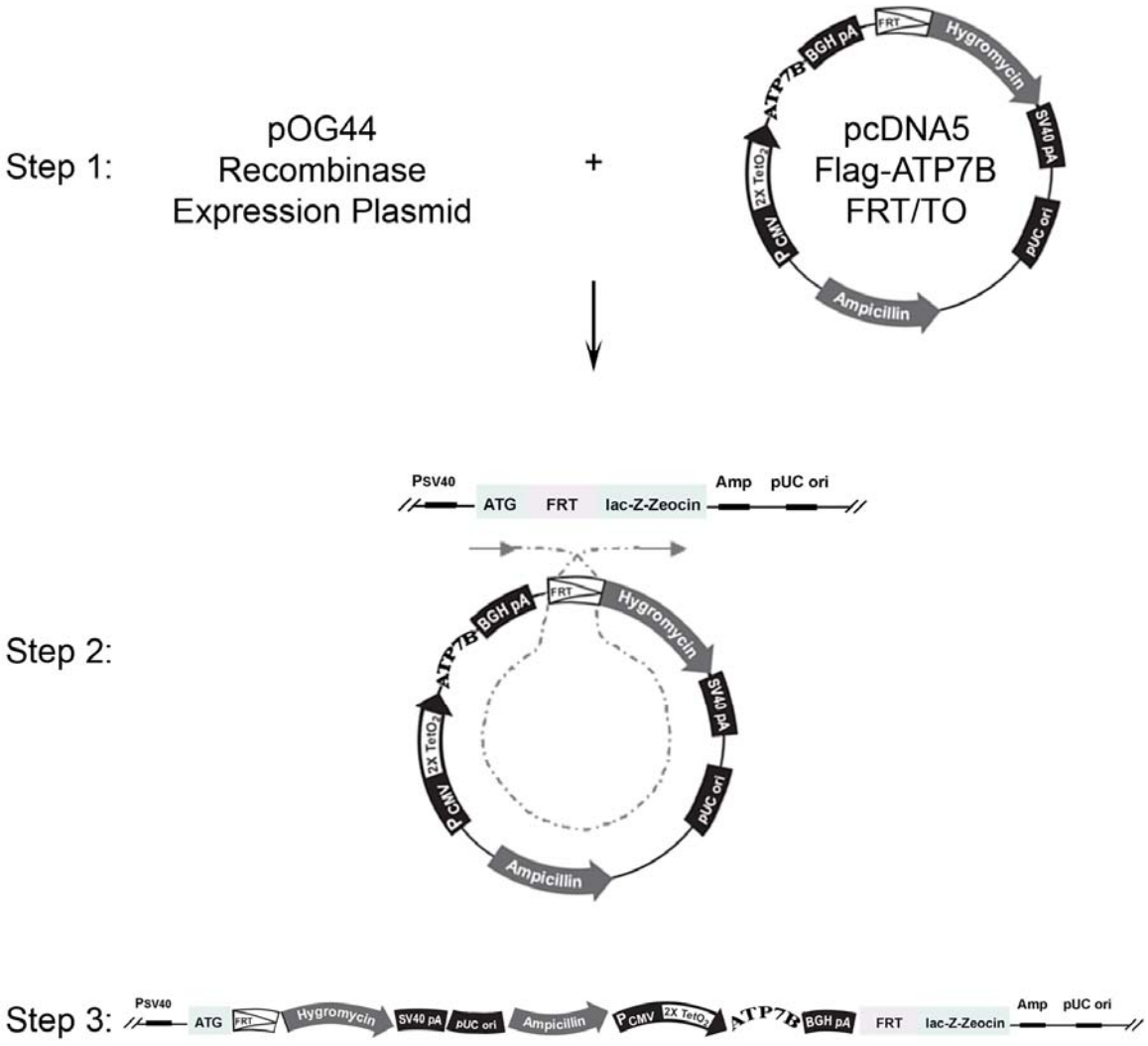

Figure 15: Schematic of chromosomal recombination in FlpIn T-REx Hek293 cells for the generation of tetracycline regulated Flag-ATP7B stable cells. Flag-ATP7B cDNA was cloned into pcDNA5FRT/TO, which contains a tetracycline regulated promoter ($2xTetO_2$). This plasmid also encodes a flp recombinase target (FRT) site. Co-transfection of this construct and pOG44 (which encodes for the flp recombinase) results in the integration of the entire plasmid into a single FRT site in the FlpIn T-REx Hek293 genome. This allows for the selection of stable cells which have flipped in Flag-ATP7B

pcDNA5FRT/TO. Integration of the pcDNA5FRT/TO Flag-ATP7B in between the start Methionine (ATG) and the chromosomal FRT site (pink) results in the displacement of the translational start site for lac-Z-Zeocin. Pre-recombination, the FlpIn T-REx Hek293 cells are resistant to Blasticidin (for the selection of the TetR gene) and Zeocin. Post-transfection and selection, the cells lose Zeocin but gain Hygromycin resistance. Step 1: Co-transfection of pOG44 and pcDNA5 Flag-ATP7B/FRT/TO into FlpIn T-Rex Hek293 cells, Step 2: Integration of Flag-ATP7B into chromosome at the FRT site, Step 3: Selection of cells with the integrated construct. (This figure is derived from the Flp-In system figure in the Invitrogen manual 021042).

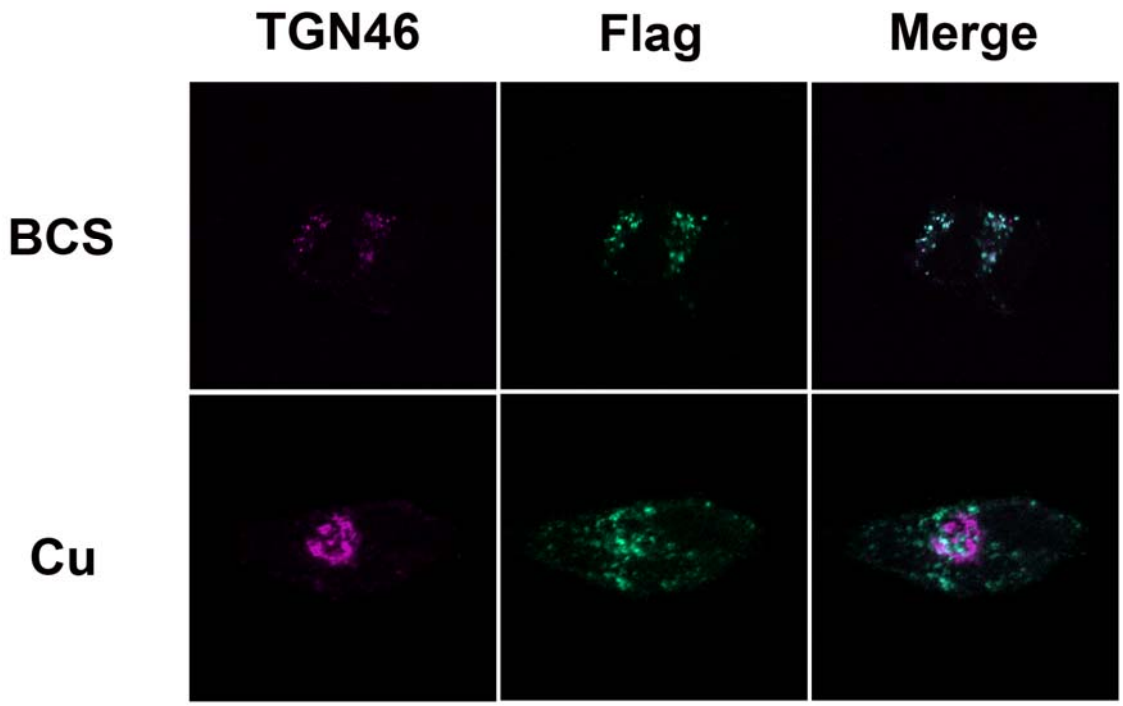

Figure 16: Hepatic Flag-ATP7B expressed in FlpIn T-REx 293 cells traffics in response to copper. Expression of Flag-ATP7B was induced with 40ng/mL of tetracycline for 48hrs; cells were treated with either 50 μM BCS or $CuCl_2$ for 1 hour and stained with anti-Flag (green) and anti-TGN46 (purple). In BCS, Flag-ATP7B co-localizes with the marker TGN46 (top row), but relocalizes to a vesicular compartment when treated with copper (bottom row), as indicated by the loss of co-localization.

Hepatic copper-transporting ATPase ATP7B: function and inactivation at the molecular and cellular level.

Mee Y. Bartee and Svetlana Lutsenko[1]

1 - The correspondence should be addressed to:

Svetlana Lutsenko, Oregon Health & Science University, Department of Biochemistry and Molecular Biology, 3181 SW Sam Jackson Park Rd., Portland, OR 97239-3098, U.S.A.; Tel.: 503-494-6953; E-mail: lutsenko@ohsu.edu

-Figures 20-22 presented in this chapter are published in Biometals 2007; 20(3-4):627-37

-I did all the work and writing for this chapter.

III. Trafficking of ATP7B to the Apical Membrane in Polarized Hepatocytes[191]

3.1 Introduction

The liver is the major organ that regulates copper homeostasis in the body. Very little regulation of dietary copper uptake takes place at the level of absorption, resulting in more absorbed copper if more copper is available in the diet. However, excess copper is promptly exported from the liver into the bile, and copper transporting ATPase ATP7B is essential for this process. Genetic mutations in ATP7B are associated with copper accumulation in the liver and with severe liver pathology known as Wilson's disease. The mechanism of Wilson disease protein (ATP7B) mediated copper export is not well understood.

It has been previously shown ATP7B resides at the TGN under basal and copper limiting conditions [120, 152, 155]. This can be demonstrated by immunoco-localization with such TGN markers as syntaxin 6 and TGN46 (our data). At the TGN, ATP7B transports copper to ceruloplasmin, a secreted copper dependent ferroxidase. In order for ATP7B to export copper from hepatocytes, trafficking to other cellular compartments is necessary. Copper dependent trafficking is indeed an important method of regulation for ATP7B. With exposure to elevated (10-200μM) copper, ATP7B relocalizes from the TGN to a vesicular compartment. This copper dependent movement was demonstrated for ATP7B in primary [152] and cultured hepatocytes [46, 151], as well as in CHO cells expressing recombinant ATP7B[106, 108]. In the vast majority of these experiments, staining of ATP7B in cells treated with elevated copper showed a vesicular pattern. These

results led to the hypothesis that ATP7B cycles between the TGN and intracellular vesicles. After these vesicles are loaded with copper, they move towards the plasma membrane while ATP7B returns to the TGN without ever reaching the plasma membrane. The alternative mechanism suggested by Roelofsen and co-authors involved the movement of ATP7B towards the apical membrane [151].

Most trafficking studies of ATP7B have been performed with recombinant protein expressed in fibroblast cell lines or in non-polarized cells. Since ATP7B is abundantly expressed in the liver and is the only known copper transporter expressed in that organ, we wanted to investigate whether endogenous ATP7B can traffic to the plasma membrane in polarized hepatocytes.

3.2 Materials/Methods

3.2.1 Culturing of HepG2 cells

HepG2 cells were purchased from the ATCC and maintained in MEM + 10%FBS + Non-Essential Amino Acids + PenStrep (InVitrogen) at 37°C + 5% CO_2. They were passaged through a 28 gauge needle (to break up cell clumps) every 3-4 days and maintained at sub-confluent levels.

3.2.2 Co-localization of ATP7B and MRP2 in partially polarized HepG2 cells in low and elevated copper

HepG2 cells were seeded onto glass coverslips at 70% confluency and allowed to partially polarize for 72 hours at 37°C + 5% CO_2 before treatment with 50µM $CuCl_2$ or BCS for 3 hours before fixation with acetone at -20°C for 30 sec. Cells were incubated with blocking buffer (PBS, 1%BSA, 1%gelatin, 0.01%

sodium azide) overnight at 4°C. Incubations with primary antibody anti-N-ATP7B#2, anti-Na,K-ATPase (courtesy of the Kaplan Lab), and anti-MRP2 (Kamiya Biomedical Company) were performed at 1:500 dilution in blocking buffer for 1 hr in a humidifying chamber. Coverslips were washed four times for 10mins with PBS and incubated with secondary antibodies AlexaFluor 555 Donkey anti-Rat (for anti-N-ATP7B#2), AlexaFluor 555 Goat anti-Rabbit (for anti-Na,K-ATPase), and AlexaFluor 488 Donkey anti Mouse (for anti-MRP2) (Molecular Probes) at 1:2,000 in blocking buffer for 1hr in the dark in a humidifying chamber. Coverslips were washed with PBS and mounted with Vectashield + DAPI and sealed with nail polish. Cells were visualized on a Zeiss LSM 5 Pascal confocal microscope with a 100X oil immersion objective lens. Z-sections of HepG2 cells were taken at 0.27-0.38 micron intervals to decrease the possibility of vesicles overlapping in the XY plane due to vertical stacking. For co-staining, images were taken by exciting and scanning the emission separately for each wavelength, to prevent possible emission overlap. LSM software was used to compare regions of overlap between MRP2 and ATP7B.

3.3 Results

3.3.1 Endogenous ATP7B traffics to a vesicular compartment when copper is elevated in non-polarized hepatocytes.

Initially, the localization of endogenous ATP7B in non-polarized HepG2 cells was investigated to verify findings with recombinant ATP7B from other laboratories. Immunostaining for ATP7B was done for HepG2 cells treated with either 50μM BCS or $CuCl_2$ for 1hr. As expected, ATP7B localizes to a

perinuclear region of the cell when treated with BCS and traffics to a vesicular compartment when treated with copper (Figure 17). A similar result was obtained for endogenous ATP7B in Hep3b cells, another hepatocyte cell line (Figure 5).

3.3.2 MRP2 localizes to the canalicular membranes in partially polarized HepG2 cells.

Cell polarization can affect the trafficking of membrane proteins, either inducing change in localization or altering the intracellular trafficking pattern of proteins [206, 207]. Consequently, we investigated whether polarization of hepatocytes affects trafficking of ATP7B.

Hepatocytes are different from most polarized epithelial cell models which have a distinct “top” (apical) and “bottom” (basolateral) membranes when grown on transwell filters. Polarization of hepatocytes involves several cells coming together and forming contacts, creating an apical membrane that is “shared”. This apical membrane is reminiscent of bile canaliculi in the liver. Unlike organized liver tissue, HepG2 cells partially polarize, having no real outlet for clearance of components transported across the apical membrane into the canalicular space. This leads to a larger apical space between cells and distinct canalicular membranes that are easily visible by immunofluorescence.

3.3.3 ATP7B does not traffic to the basolateral membrane.

HepG2 cells were partially polarized by growing on coverslips for 3 days before treatment with BCS or copper. To monitor cell polarization, we used antibody against the multi-drug resistance protein 2 (MRP2). MRP2 is a

membrane protein that relocalizes to the canalicular membrane when hepatic cells polarize[208]. In contrast, Na,K-ATPase is a membrane protein that localizes to the basolateral membrane in polarized cells[209]. A distinct pattern of staining with these markers was taken to indicate that HepG2 cells were polarized, and helped to define the outline of the two different membranes once polarization occurred. In Figure 18, the staining of MRP2 (green) and NaK-ATPase (purple) are shown for polarized HepG2 cells. The staining for the canalicular membrane, represented by the MRP2 staining, is quite distinct and concentrated. This membrane is shared by several cells. The basolateral membrane of the cell is outlined by the NaK-ATPase staining. Treatment of HepG2 cells with BCS or copper does not affect staining of NaK-ATPase or MRP2.

Double staining of ATP7B and NaK-ATPase was also performed to determine if ATP7B can be found at the basolateral membrane (Figure 19). ATP7B staining (green) is contained within the staining of the NaK-ATPase (purple) and shows no overlap with the basolateral marker. This result suggests that the trafficking of ATP7B does not include delivery to the basolateral membrane, i.e. trafficking towards the apical membrane does not involve trans-cytosis. ATP7B could be present at the canalicular membrane, as illustrated in Figure 19, where structures resembling MRP2 (Figure 18) staining in the canalicular membrane can be seen for ATP7B in both BCS and copper treated cells. This staining is quite different from the staining of ATP7B in non polarized HepG2 cells (compare Figure 17 and 19).

3.3.4 Endogenous ATP7B traffics to the canalicular membranes in partially polarized HepG2 cells.

To determine whether ATP7B traffics to the canalicular membrane, co-localization of ATP7B and MRP2 were done for BCS and copper treated cells. Since we observed ATP7B in canaliculi-like structures in both low and high copper conditions (see above), we also quantified whether more ATP7B can be found in this location when copper is elevated (see next paragraph). In Figure 20, ATP7B staining is shown in red and the MRP2 staining in green. For the BCS treated samples, the ATP7B staining is not as tight a perinuclear staining. There is some ATP7B at the canalicular membrane ~30% of the time under BCS conditions. ATP7B containing vesicles are also present surrounding the MRP2 staining, suggestive of sub-apical localization. For the copper treated cells, the majority of the ATP7B is at or near the canalicular membrane (Figure 21).

To determine the degree of overlap between the two markers, the colocalization was determined using LSM software. In Figure 20, 21, the overlap of the pixel density between the emissions of the 488nm and 555nm fluorophore in a 0.27-0.38 micron Z-stack interval is compared. The X-axis represents the MRP2 staining (Quadrant 1), Y-axis ATP7B staining (Quadrant 2), and the overlap is plotted in Quadrant 3. As shown in Figure 20, even for BCS treated samples, there is some overlap in staining, as seen as dots in quadrant 3, although the majority of the protein exists in separate compartments. However, this equilibrium shifts when copper is elevated (Figure 21), as the number of overlapping vesicles increase.

3.4 Discussion

3.4.1 In polarized hepatocytes, ATP7B traffics to the canalicular membrane.

In the literature, ATP7B has been shown to traffic only to vesicles, even when exposed to copper as high as 200μM (Figure 5). However, as shown in Figure 20 and 21, ATP7B traffics to the sub-apical/apical membrane of partially polarized HepG2 cells. This result has been also seen recently from other groups [46, 151, 210]. In terms of ATP7B regulation, this trafficking to the apical membrane is an intriguing observation. The current model of ATP7B trafficking suggests ATP7B traffics from the TGN to vesicles. These vesicles contain copper, either from ATP7B transport into the vesicles or pinching off of vesicles at the TGN in the vicinity of ATP7B where the local concentration of copper is assumed to be high. These copper and ATP7B containing vesicles leave the TGN to some point where the two are sorted. The copper traffics to the plasma membrane and exported out of the cell, and ATP7B is recycled back from the vesicles to the TGN. However, data presented in this chapter suggests a different model of ATP7B trafficking. ATP7B staining at the canalicular membrane suggests that ATP7B and the copper containing vesicles may traffic together to the apical membrane, or even perhaps ATP7B exports copper at the apical membrane, before recycling/endocytosed to the TGN.

It has been previously shown ATP7B can recycle back to the TGN from the vesicles after exposure to copper, so apical membrane staining can not be purely for recycling. So what purpose does apical trafficking serve in ATP7B regulation? In the liver, the canalicular membrane is important for excretion into

the bile. In Wilson's disease patients, copper accumulates in the liver because excess copper can not be cleared into the bile from the canalicular membrane. Perhaps in non polarized cells, the vesicles to which ATP7B traffics can mobilize to the plasma membrane for excretion of copper, in general, without the guide of ATP7B. In polarized cells, ATP7B containing vesicles might direct the copper containing vesicles to the canalicular membrane, as opposed to the basolateral membrane, to ensure the excretion of copper into the bile. This membrane directed regulation would be important to prevent copper release into the blood. It would be interesting to confirm this hypothesis by monitoring radioactive copper accumulation in the canalicular membrane and surrounding media. Access to the canalicular membrane would be difficult, but if ATP7B can be expressed and trafficking assay developed in a different polarized cell model, copper transport studies can be performed.

3.4.2 For copper treated cells, the majority of ATP7B is localized to vesicles.

Only a fraction of ATP7B is found at the canalicular membranes, whereas the majority of ATP7B stains in vesicles. This could suggest a mechanism of fusion of ATP7B and copper containing vesicles to the apical membrane and subsequent rapid recycling (Figure 22). ATP7B contains a tri-leucine motif at the C-terminal tail that when mutated to alanines, results in vesicular localization of ATP7B regardless of the copper levels. ATP7A, a ATP7B homologue, has been shown to display a parallel mechanism of trafficking, where it localizes to sub-basolateral membranes under elevated but physiological levels of copper [29, 188]. Labeling of ATP7B from the canalicular space would be difficult, since it is not

accessible (refer to section 3.3.2). To test whether ATP7B is rapidly recycling/ endocytosed from the canalicular membrane, live cells could be monitored for the trafficking of GFP-ATP7B. The canalicular membrane could be photobleached, and the movement of GFP-ATP7B into and out of the canalicular membrane could be examined. Concurrently, copper containing vesicles could be labeled with Coppersensor-1 (CS1), a membrane permeable and water soluble copper binding fluorescent agent that can be used to monitor copper *in vivo* [211]. Tracking of the CS1:copper complex and GFP-ATP7B would allow differentiation between the vesicles trafficking towards the canalicular membrane and the recycling/ endocytic vesicles. CS1:copper:GFP-ATP7B containing vesicles would fuse with the canalicular membrane, releasing the CS1:copper complex into the bile canalicular space. GFP-ATP7B would then either be endocytosed and traffic back to the TGN or recycled into vesicles. Separately, Brefeldin A, which should minimize forward trafficking from the TGN to the apical membrane without disrupting recycling or endocytosis [212], could be given to cells. GFP-ATP7B containing vesicles near the canalicular membrane could be photobleached, and the trafficking of GFP-ATP7B already at the canalicular membrane would be monitored.

Another possibility could be that in polarized cells, ATP7B directly transports the excess copper across the canalicular membrane. The slightly lower pH of this compartment might increase the efficiency of catalytic turnover of ATP7B, promoting an efficient enzyme which would require only a fraction of ATP7B to exit the TGN for export of copper. If there are differences in the

efficiency of transport, intracellular copper and overall systemic copper would be subtly regulated, just by controlling the localization of a fraction of the total ATP7B.

3.4.3 ATP7B traffics to the canalicular membrane even when copper is limiting.

In copper limiting media, ATP7B stains in a perinuclear region in nonpolarized cells. However, in BCS treated polarized HepG2 cells, a small population of ATP7B is found at the canalicular membrane. The possible purpose of ATP7B canalicular localization is intriguing. This staining may suggest constitutive trafficking of a small pool of ATP7B. Constitutive trafficking of ATP7B would be important for quick response to sudden acute changes in the intracellular copper content in the liver, i.e. food intake. Another possibility would be resident pool of ATP7B localized at the apical membrane that directly transports copper into the bile canalicular space.

In this chapter, I show that ATP7B traffics to the canalicular membrane in response to copper, contrary to the vesicular trafficking model accepted in the field. This apical localization of ATP7B in polarized cells adds an additional layer of regulation in ATP7B trafficking, distinct from fibroblast trafficking systems.

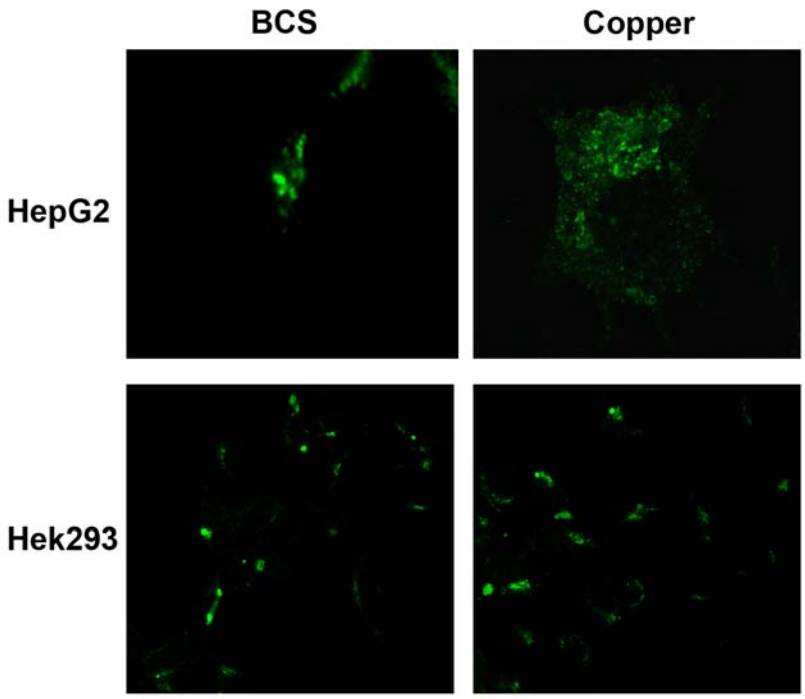

Figure 17: ATP7B staining in HepG2 and Hek293 cells. The staining pattern observed for ATP7B in HepG2 and Hek293 cells in low (BCS) and high copper conditions. The difference in patterns of staining is clearly visible in HepG2 cells, indicating trafficking. No change in the ATP7B pattern is observed in Hek293 cells.

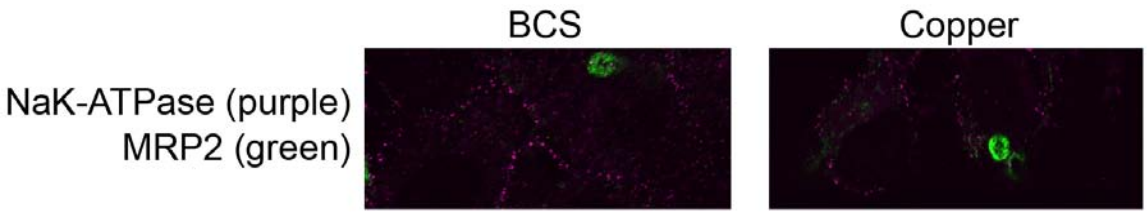

Figure 18: Canalicular and basolateral membrane staining of polarized HepG2 cells. HepG2 cells can be partially polarized to separate the canalicular (apical) membrane and the basolateral membrane. Antibodies to MRP2 (green) stain for the canalicular membrane and NaK-ATPase (purple) stains the basolateral membrane. Treatment of cells with copper does not alter the localization of these markers.

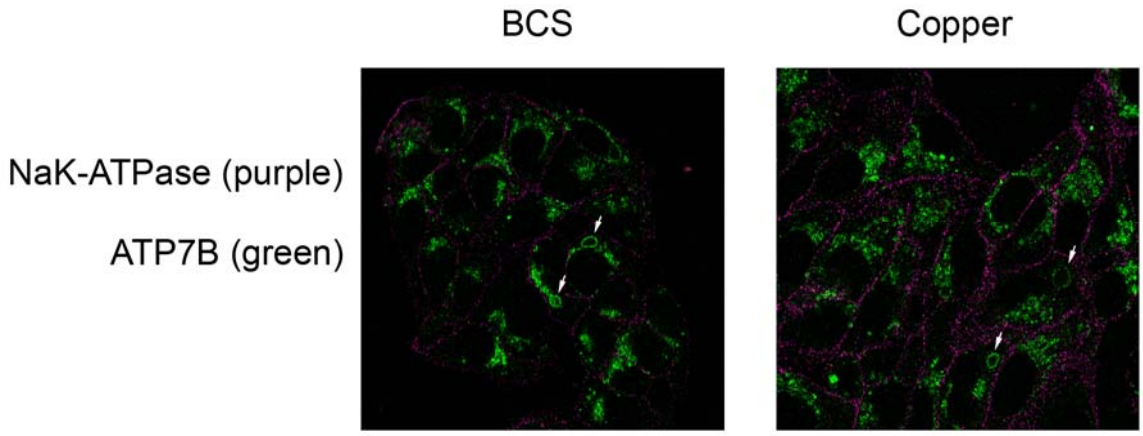

Figure 19: ATP7B and NaK-ATPase staining in polarized HepG2 cells. Polarized HepG2 cells were stained for ATP7B (green) and NaK-ATPase (purple). The NaK-ATPase clearly outlines the cell, indicating the basolateral membrane. ATP7B does not, however, co-localize with NaK-ATPase. Interestingly, for both BCS and copper treated cells, ATP7B localized in a circular structures that look similar to canalicular membranes in some of the cells (indicated by arrows).

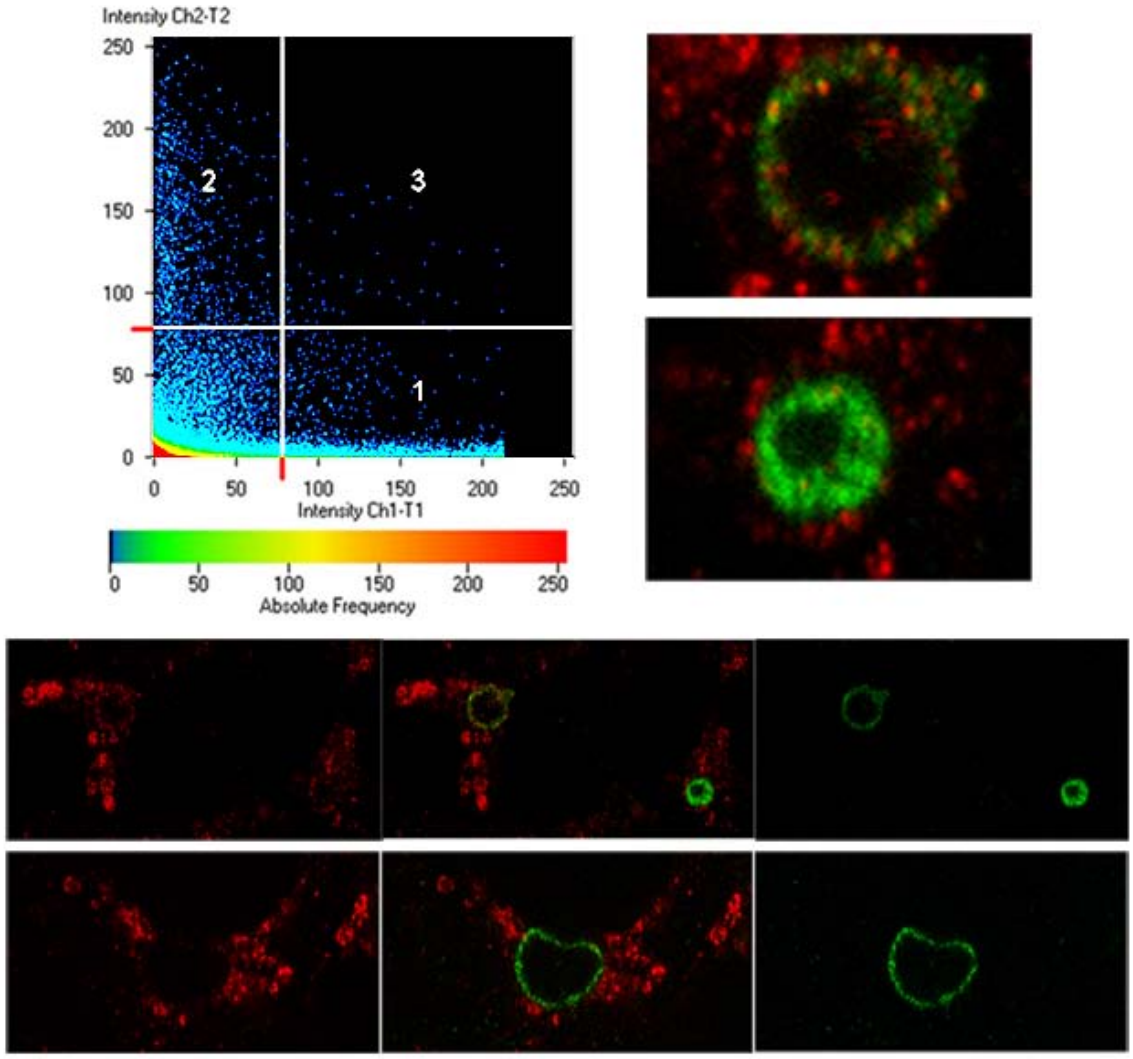

Figure 20: BCS treated ATP7B partially localizes to the canalicular membrane in polarized HepG2 cells. ATP7B (red) and MRP2 (green) co-localize to the canalicular membrane ~30% of the time in BCS treated cells. ATP7B containing vesicles surround the MRP2 staining. In the upper left panel, the X-axis plots the intensity of the MRP2 staining (quadrant 1), the Y-axis ATP7B staining (quadrant 2), and the overlap is plotted in quadrant 3. (The graph in the upper left has been enhanced to better visualize the dots in quadrant 3).

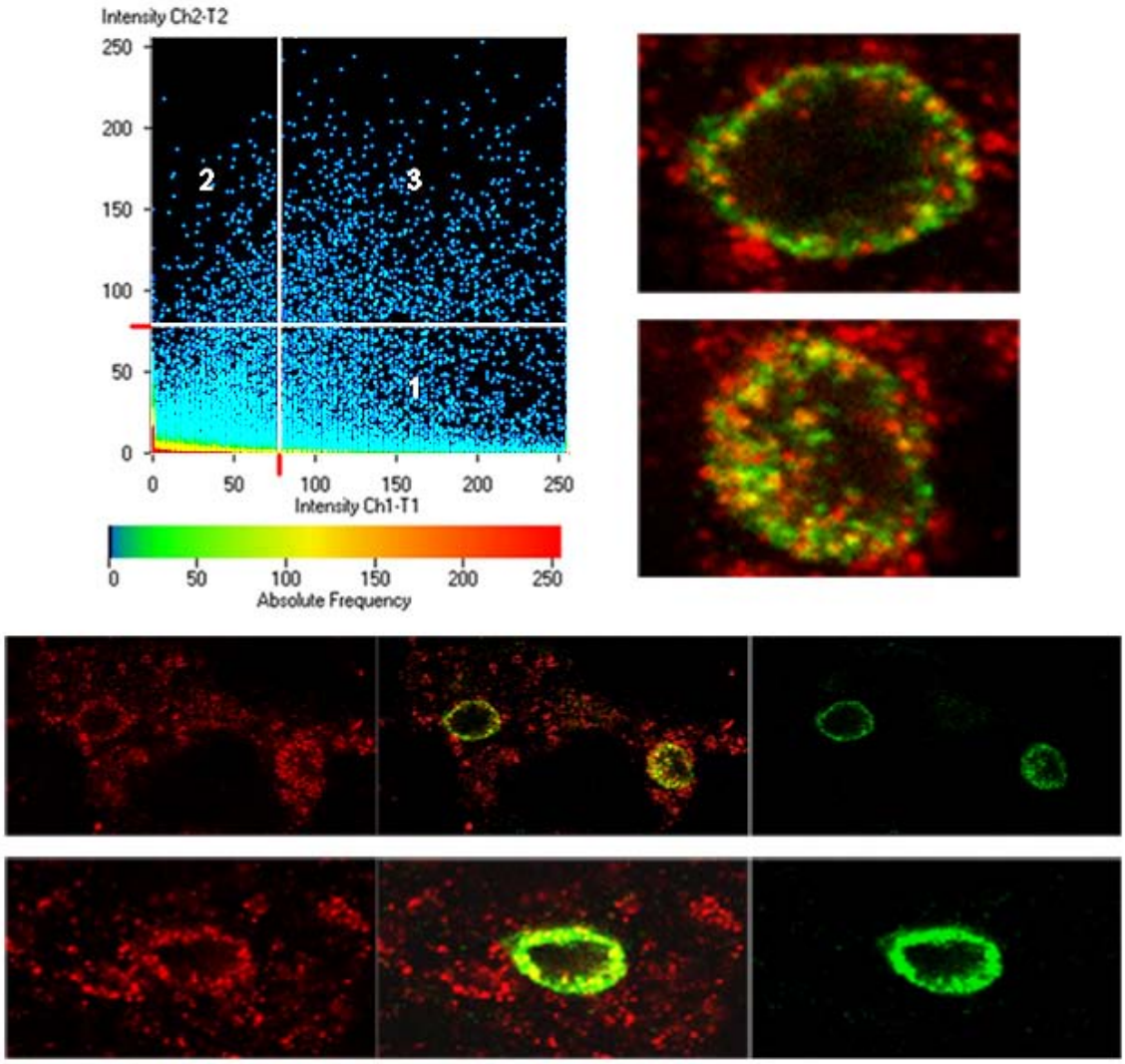

Figure 21: Copper treated ATP7B localizes to the canalicular membrane in polarized HepG2 cells. ATP7B (red) and MRP2 (green) staining was evaluated in copper treated partially polarized HepG2 cells. In the upper left panel, the X-axis plots the intensity of the MRP2 staining (quadrant 1), the Y-axis ATP7B staining (quadrant 2), and the overlap is plotted in quadrant 3.As quantitated by quadrant 3 in the upper left panel, ATP7B and MRP2 co-localize at the canalicular membrane. As highlighted in the images on the lower left panel, the outline of the canalicular membrane can be seen just by ATP7B

staining. (The graph in the upper left has been enhanced to better visualize the dots in quadrant 3).

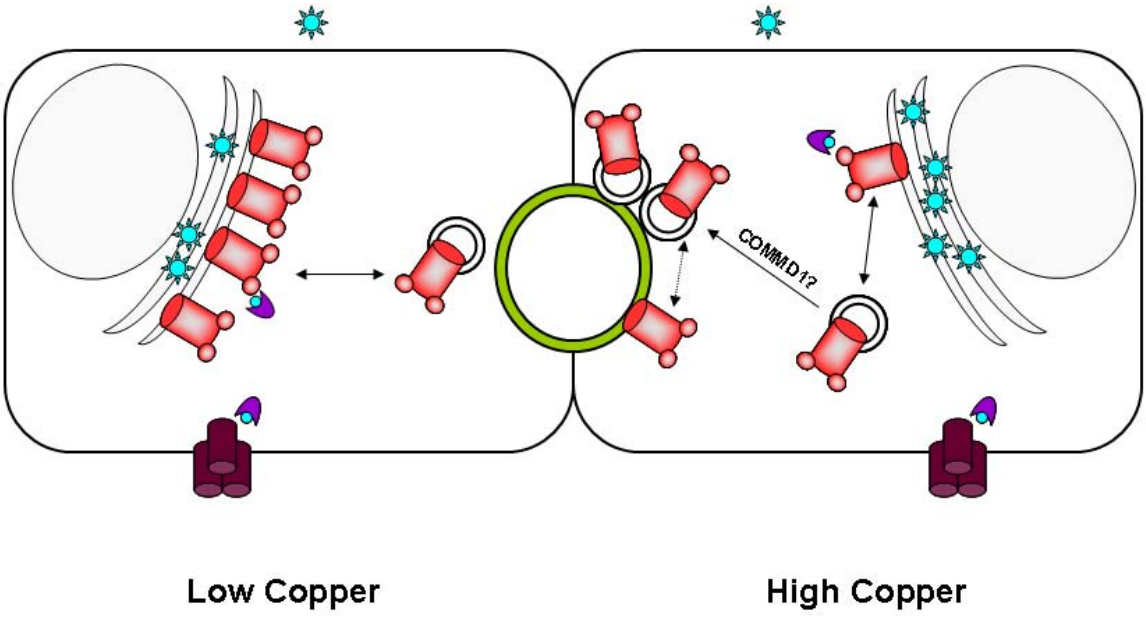

Figure 22: Model of ATP7B trafficking in polarized HepG2 cells. Unlike in other cells, ATP7B traffics to the apical membrane of polarized HepG2 cells. Whether this canalicular membrane localization is part of a recycling mechanism, or has a specific purpose is yet unknown, and requires further testing. Green: canalicular membrane, Red: ATP7B, Blue Stars: ceruloplasmin, Blue circles: copper, Purple: Atox1, Maroon: CTR1.

Identification of the Region of Copper Dependent Phosphorylation in ATP7B

M.Y. Bartee and S. Lutsenko

-This manuscript is in preparation.

-I did all the work and writing for this chapter

IV Identification of Phosphorylation Sites

4.1 Introduction

Copper is a micronutrient essential for the normal function of organisms. In humans, a wide range of proteins require copper for their activity. Enzymes with known function such as superoxide dismutase, cytochrome c oxidase, ceruloplasmin, tyrosinase, and peptidylglycine α-amidating monooxygenase as well as proteins with a less understood role such as prion protein and amyloid precursor protein, all bind copper. It has been shown that copper is important for embryogenesis and development as well as protection against oxidative stress[202, 213]. The importance of copper dependent proteins coupled with the toxicity of excess copper has resulted in the development, in humans, a complex system of copper homeostasis.

Wilson disease protein (Cu-ATPase ATP7B) is an ATP-driven transporter important for the delivery of copper to proteins in the secretory pathway as well as the maintenance of copper homeostasis in cells. ATP7B is a 165 kDa membrane protein with three soluble domains (Figure 1). The large N-terminal domain (N-ATP7B) (~70 kDa) contains six homologous metal binding domains (MBD) that can each bind one Cu(I) molecule. Each MBD contains a conserved metal binding motif of GMT/HCxxC. The six MBDs are connected to each other by loops of varying lengths. These loops are thought to undergo conformational changes upon copper binding, allowing for intramolecular crosstalk as well as intermolecular interactions between the domains [96]. Another cytosolic domain, the ATP binding domain (ABD), is important for the binding and hydrolysis of

ATP, providing energy for the active transport of copper. The ABD has been shown to interact with apo-N-ATP7B; this interaction weakens with the binding of copper to the MBDs [1]. It is not known if the MBDs or the loops connecting MBDs are involved in the copper dependent interaction between N-ATP7B and ABD, but the conformational changes due to copper binding seem to be necessary for the regulation of ATP7B. Deletion of the MBD1-4 speeds up ATP-hydrolysis by ATP7B as evidenced by a faster formation of the catalytic intermediate [107]

ATP7B regulated trafficking is important for the maintenance of copper homeostasis. This is most apparent in patients with Wilsons Disease, where excess copper is not excreted into the bile canaliculi. It has been shown previously that under basal copper conditions, ATP7B transports copper into the lumen of the secretory pathway to be incorporated into copper requiring proteins. As the intracellular copper levels increase, ATP7B traffics to a vesicular compartment to sequester copper for subsequent excretion from the cell. In the liver and in polarized hepatocytes, such as WIF and HepG2, ATP7B traffics further to the canalicular membrane (Figure 20, 21), possibly as part of a recycling mechanism [46, 191]. In parallel to these events, ATP7B undergoes kinase mediated phosphorylation at the basal level under regular conditions (Figure 10B) and the level of phosphorylation increases approximately 2 fold when copper is elevated [75]. The identity of an ATP7B kinase has not yet been established. Similarly, the role of the kinase mediated phosphorylation of ATP7B in the trafficking of this transporter remains unknown. In this chapter, we present data as part of the first step towards understanding the connection between

these two events by identifying the site(s) of phosphorylation in ATP7B and by characterizing the effect of mutations of these sites on trafficking.

ATP7B is a large protein composed of 1,465 amino acids with numerous residues as possible targets for phosphorylation. Originally, phosphorylated material was submitted for mass spectroscopy; however, because of the size of the protein, coverage of the protein was limited to 30-40%. Also, tryptic fragments of ATP7B did not bind/elute from C8/C14 columns very efficiently. So a phosphorylation site was not identifiable through that approach. An alternative method for the identification of the phosphorylation site(s) was developed, as outlined in this chapter. The general plan was to first develop an in vitro phosphorylation assay using radioisotopes to monitor phosphorylated products. Then the target of phosphorylation would be narrowed, starting with the full length construct, to a domain, a region, and then possible residues.

4.2 Materials/Methods

4.2.1 Generation of Flag-ATP7B and Phosphorylation Vector Constructs

PCR fragments were generated for the 5 phosphorylation constructs using the following primer pairs:

WNDPS^{336}>AFwd-[Phos]GGAGCCGAAGGGCTGGGACAGATCACAG

WNDPS^{336}>ARev- [Phos]CTGTGATCTGTCCCAGCCCCTTCGGCTCC

WNDPS$^{342/3}$>AFwd-[Phos]GGGACAGATCACAGGGCTGCCAGTTCTCATTCC

WNDPS$^{342/3}$>ARev- [Phos]GGAATGAGAACTCGCAGCCCTGTGATCTGTCCC

WNDPS$^{344/5}$>AFwd- [Phos]GATCACATCTTCCGCTGCTCATTCCCCTGGC

WNDPS$^{344/5}$>ARev-[Phos]GCCAGGGGAATGAGCAGCGGAAGACCTGTGATC

WNDPS^{347}AFwd- [Phos]TTCCAGTTCTCATGCCCCTGGCTCCCC

WNDPS^{347}ARev- [Phos]GGGGAGCCAGGGGCATGAGAACTGGAA

WNDPS^{350}>AFwd- [Phos]CATTCCCCTGGCGCCCCACCGAGAAAC

WNDPS^{350}>ARev- [Phos]GTTTCTCGGTGGGGCGCCAGGGGAATG

The PCR fragments were TOPO TA cloned (Invitrogen). These fragments were then subcloned into ATP7B pcDNA 3.1 (+). Flag ATP7B was generated by PCR with the following primer:

BamHIKozakFlag-hATP7B-

GGATCCACCATGGACTACAAGGATGACGATGACAAGCCTGAGCAGGAGAG

Flag-ATP7B from pcDNA 3.1 (+) was then subcloned into pcDNA 5 FRT/TO. The Flag phosphorylation mutant constructs were generated by subcloning the mutants from the pcDNA 3.1 (+) constructs into Flag-ATP7B pcDNA 5 FRT/TO using BstEII and NotI as restriction sites.

4.2.2 Generation of intein N-ATP7B deletion constructs

The following primer pairs were used to generate the intein N-ATP7B deletion constructs:

JB-WND-1A- TGCAGGATCCCATATGCCTGAACAGGAGAGACAGAT

JB-WND-1B- CGTGTCGAC TTACACTGCTCTGGTTGATTGTGG

JB-WND-2A- TGCAGGATCCCATATGGCACCGCAGAAGTGCTTC

JB-WND-2B- TGCAGTCGACTTAGGCCAGGGAAGCATG AAAGCC

The coding sequence for the intein deletion N-ATP7B constructs were amplified from recombinant pcDNA 3.1 (+) ATP7B with Pfu DNA polymerase (Invitrogen). Forward primers introduce BamHI and NdeI restriction sites. Reverse primers introduce a SalI restriction site. Amplified fragments were digested with Nde1 and Sal1 restriction endonucleases and ligated into pTYB12 plasmid digested with the same enzymes. (These constructs were created by Jason Burkhead)

4.2.3 Expression of ATP7B in *Sf9* cells

As described previously [130], *Spodoptera frugiperda* (*Sf9*) cells were grown in suspension in Ex-Cell 420 media(JRH Biosciences Inc.) at 27°C with constant spinning for aeration in spinner flasks (BellCo). $1x10^6$ cells were infected with either ATP7B or the D^{1027}>A construct (mutation at the catalytic phosphorylation site) expressing baculovirus for 72hrs before harvesting. Baculovirus constructs were generated by Ruslan Tsivkovskii. Mock infections were also performed as a control with wild type baculovirus. *Sf9* cells were homogenized by douncing with a tight fit dounce (Wheaton) in Homogenization Buffer (HB) (25mM Imidazole, 250mM sucrose, 1mM DTT, 2mM AEBSF, EDTA free Protease Inhibitor Cocktail (Roche)). To clear cell debris, supernatant was centrifuged for 10min at 500 x g, and the supernatant transferred to a fresh tube. Crude membranes were pelleted at 20,000 x g for 30min and resuspended in HB. Subsequently, the crude membrane preparations were quantitated by the Lowry method and expression confirmed by western blot using the N-ATP7B#2 antibody. Samples were stored as small aliquots at -80°C until needed.

4.2.4 Phosphorylation of Sf9 membrane preparations

For kinase mediated phosphorylation (excluding Fig 23B) 50µg of *Sf9* crude membranes were resuspended in 200µl of phosphorylation buffer (PB) (20mM Bis-Tris propane, 200mM KCl, 5mM $MgCl_2$, 1mM DTT, 2mM AEBSF, EDTA free Protease Inhibitor cocktail, 1mM orthovanadate, 100µM ATP pH 7.5) + 5µCi [γ-^{32}P]ATP (Perkin Elmer) and incubated at room temperature for 30min. For experiments in Figure 23A and 23B, catalytic phosphorylation conditions were used (PB at pH 6.0 with 1µM ATP). In the presence of ATP, recombinant ATP7B is also auto-phosphorylated at the catalytic aspartate D^{1027}>A ^{214}. Consequently, regulatory phosphorylation was analyzed at pH 7.5, when the catalytic acyl-phosphate intermediate is unstable. The results were also confirmed using a D^{1027}>A mutant of ATP7B, where the catalytic aspartate residue necessary for formation of the catalytic acyl-phosphate bond is mutated to alanine (Figure 23B). 50µl of 50% TCA in 1mM sodium phosphate was added to stop the reaction.

The precipitated protein was pelleted at 20,000 x g for 30min and rinsed with water before resuspension in sample buffer (SB) (20mM Tris, 2.7M urea, 3.6% SDS, 0.1% β-ME) and loaded onto a 7.5% Laemmli gel. Proteins were transferred onto Immobilon-P PVDF (Millipore) using wet transfer and coomassie stained. Blots were air dried, wrapped in saran wrap, placed under film (Kodak BioMax MS film) in an autoradiography cassette (Fisher) with amplifier screens, wrapped in an electrostatic bag, incubated at -80°C for an average of 16hrs, and lastly, developed. Bands from the coomassie stained PVDF and film were quantitated using a Bio-Rad Molecular Imager & Analyst and normalized per

protein. For calculations of the ratio of phosphate per proteins, the ATP7B band from PVDF were excised, placed into liquid scintillation cocktail and β-emission counted using a liquid scintillation counter. The following formula was used to calculate the efficiency of phosphorylation:

Phosphate/Protein = [(20nmol ATP) (Normalized cpm for sample ÷ 0.95 ÷ 2.2 x 10^6) (half life factor) ÷ 5μCi] ÷ [W pg ÷ 165pg]

4.2.5 Purification of ATP7B-His expressed in *Sf9* cells

Sf9 cells were infected with a baculovirus expressing C-terminal His tag ATP7B cDNA as described above. Crude membranes were solubilized in Phosphorylation buffer (without DTT) containing 1% dodecyl-β-maltoside (Sigma), and centrifuged at 20,000 x g to remove the proteins that did not solubilize. 50μl of Ni-NTA (Qiagen) slurry was rehydrated with PBS and then incubated with 50mM $NiSO_4$ for 1hr before equilibration with HB + 0.01%DDM (with no DTT). Solubilized *Sf9* membranes were added to the Ni-NTA slurry and incubated for 1hr at room temperature by batch method on a rotator. The supernatant was removed, and the resin washed with HB + 0.01%DDM (with no DTT) for 100 slurry volumes. Protein was eluted with PBS + 250mM Imidazole + 2mM AEBSF + EDTA free Protease Inhibitor Cocktail + 0.1%DDM and loaded onto a Laemmli gel.

4.2.6 Phosphorylation mutant subcloning into pMAL vector

The phosphorylation mutants, S^{334}>A, $S^{340}S^{341}$>AA, $S^{342}S^{343}$>AA, S^{345}>A, and S^{348}>A, were subcloned into the wildtype MBP-N-ATP7B pMAL vector using

the AvrII and XhoI restriction sites from their respective pcDNA5 FRT/TO constructs.

4.2.7 Expression of MBP-N-ATP7B and phosphorylation mutants

MBP-N-ATP7B and phosphorylation mutants were co-transformed with a thioredoxin expressing plasmid, pTx, into competent pLys BL21 cells (Invitrogen). pTx improves the solubility of N-ATP7B during expression, presumably by keeping the cysteine residues in the reduced form. Two 5mL overnight cultures were inoculated and added to 1L of LB + 2g/L glucose (Fisher) + 100µg/mL ampicillin the next day. Cells were grown at 37°C until an OD_{600} of 0.5 and then placed at 4°C for 30min. Protein expression was then induced for 3hrs at 16°C with the addition of IPTG to a final concentration of 1mM in the absence or presence of 500µM $CuSO_4$. Cells were spun down and resuspended in PBS + EDTA free protease inhibitors (Roche) + 2mM AEBSF. Cells were lysed by French press and the supernatant centrifuged at 15k for 30min. The cell pellet was discarded and the supernatant was aliquoted into 1ml batches and stored at -20°C until needed.

4.2.8 in vitro Phosphorylation of MBP-N-ATP7B and mutants

Wildtype MBP-N-ATP7B and phosphorylation mutant constructs were bound to equilibrated amylose resin (NEB) by batch method, and washed with PBS + EDTA free protease inhibitors + 2mM AEBSF. To phosphorylate the protein, 150µg of the soluble fraction of Hek293 cells in PB were added to the column and incubated on a rotator for 30min at room temperature. The resin was washed with wash buffer (PBS, 2mM AEBSF, EDTA free Protease Inhibitor

cocktail (Roche)) for a total of 100 slurry volumes and eluted with PBS + 200mM maltose. The eluted protein was resuspended in sample buffer and loaded onto 7.5% Laemmli gels. The gels were subsequently stained with coomassie and dried on a gel drier and placed under film (Kodak BioMax MS film) for 18 hours and developed. Film was then scanned and analyzed using AlphaInnotech, as well as the gels for protein quantitation/normalization.

4.2.9 in vivo Metabolic Labeling of His-N-ATP7B

Hek293 cells were seeded to confluency onto 6 well plates 24hrs before transfection. Cells were transfected with His tagged N-ATP7B pTriEx vector using Lipofectamine 2000 (Invitrogen), as recommended by the manufacturer (4µg DNA with 10µl of reagent). The media was changed 6hrs post-transfection. 24hrs after transfection, cells were washed then incubated for 30min with phosphate free MEM (Gibco) at 37°C. Phosphate free MEM containing 0.1mCi/mL ^{32}P-orthophosphate was added to the cells and incubated for 3hrs. Cells were dounced, centrifuged for 30min at 20,000 x g, and the soluble lysate was incubated with equilibrated chitin resin (to reduce the nonspecific background) for 1hr. The supernatant was then added to charged/equilibrated cobalt resin (Sigma) for 1hr to bind His tag N-ATP7B. After washes with His-Tag Purification Wash Buffer (PBS + 20mM Imidazole + 2mM AEBSF + EDTA free protease inhibitor cocktail + 0.1% DDM), protein was eluted with His-tag Elution Buffer (PBS + 250mM Imidazole + 2mM AEBSF + EDTA free Protease Inhibitor Cocktail + 0.01% DDM) and loaded onto 7.5% Laemmli gels. Gels were

transferred onto PVDF (Immobilon-P, Millipore) and Kodak MS Biomax film was exposed to the gel, and developed.

4.2.10 in vitro phosphorylation of N-terminal domain intein constructs

N-ATP7B, MBD5+6, MBD1-4, and MBD1-4 w/o loop, and chitin binding domain (CBD) were expressed in BL21 cells with pTx. Soluble lysate was bound to chitin resin (NEB) and phosphorylated as described above for MBP-N-ATP7B (Section 4.2.8). Protein was eluted from resin with sample buffer and processed as MBP-N-ATP7B.

4.2.11 Limited proteolysis of MBP-N-ATP7B with trypsin

Phosphorylated MBP-N-ATP7B was incubated with Sequencing Grade Modified trypsin (Promega) at a w/w ratio of 1:2000 for 3hrs at room temperature. The reaction was stopped with the addition of either 2mM AEBSF or sample buffer. These conditions limit the proteolysis to the loop region connecting the metal binding domains so that the individual MBDs remain intact.

4.2.12 2-D polyacrylamide gel electrophoresis

Phosphorylated MBP-N-ATP7B protein fragments proteolyzed with trypsin were processed with PlusOne 2-D Clean-Up kit (Amersham Pharmacia). Protein pellets were resuspended in 250µl Isoelectric Focus Buffer (8M deionized urea, 2% CHAPS, 5µl of IPG (Amersham Pharmacia) for 3-10 nonlinear pH range, and 4.54µl of 1M DTT). Protein was added to an IEF chamber and a 13cm IEF strip pH 3-10 nonlinear strip was placed on top of the protein. 800µl of Dry Strip cover fluid was added on top of the plastic backing of the IEF strip. Samples were run for 20,000-30,000 volt hours (10hrs for rehydration of the IEF strip + ~16-18hrs

for protein focusing). Focused strips were then reduced with 10mg/mL DTT in Laemmli upper buffer (500mM Tris pH 6.8, 0.4%SDS) on a rotator for 20min. The IEF strip was removed and placed into 25mg/mL IAA in Laemmli upper buffer for 20min. The IEF strip was placed on top of a 15% Laemmli gel with a flat stacking gel, leaving a gap of 0.5in at the top. One well for the protein ladder was created and additional stacking gel was poured on top of the IEF strip to seal the top of the Laemmli gel. After running the gels at 20mAmps/gel, protein was transferred onto PVDF, and the phosphorylated spots exposed onto film. Spots were excised and processed by tandem mass spectroscopy.

4.2.13 Mass Spectroscopy

This technique was used to examine ATP7B phosphorylation site(s). In short, samples proteolyzed with trypsin can be analyzed by ionization of peptides and separation of peptides according to the mass to charge ratio. Combined with tandem mass spectroscopy, which cleaves individual amino acids from peptides and records the y and b ions generated, sequence data can be collected concerning modified peptides or identification of peptides. There are several ways a peptide can be cleaved in the mass spectrometer. The resulting y and b ions are the most frequent cleavages and refer to breakage of the peptide bond. If the charge stays with the N-terminal cleavage product, this is the b ion, and if the charge stays with the C-terminal end, this refers to the y ion. Identification of peptides was performed using the SEQUEST program. This program compares the y and b ions from the raw data scan with that of predicted ions from a data bank of sequences. Peptides with the highest ranking correlation scores from a

Fourier transform of the data sets are given and the corresponding protein. This method is useful in that the large amount of data is processed by the SEQUEST program. However, the SEQUEST program does not look for modified peptides, so to identify a phosphorylation site, raw data will have to be processed manually. This will be done by using the Xcalibur program, which allows the user to look at raw data files of the masses in the spectrum and the chromatogram.

4.2.14 Maintenance Media for FlpIn TREx 293 cells

The FlpIn TREx cells were maintained in MEM, PenStrep, nonessential amino acids, 10% FBS, 15µg/mL blasticidin, 100µg/mL zeocin (Invitrogen). Once cells were transfected and under selection, the zeocin was removed and replaced with 200µg/mL hygromycin. For induction of protein expression, the FBS was replaced with tetracycline-tested FBS (Invitrogen) and maintained for several days before tetracycline was added back to a concentration of 40ng/mL into the selection.

4.2.15 Generation of Stable Hek293 Cell Lines in the FlpIn TREx System

A FlpIn T-REx Hek293 cell line was purchased from Invitrogen. This cell line stably expresses the Tet transactivator on a vector conferring resistance to blasticidin. This cell line also contains a single integrated FRT site, which allows integration of a gene of interest into one specific site in the genome. For a schematic, refer to Figure 15. Until the gene of interest is transfected and flipped into the genome, the cells are zeocin resistant. Once integration has occurred, the zeocin cassette loses its promoter, and the hygromycin cassette can utilize the promoter to confer hygromycin resistance.

FlpIn T-REx 293 cells were plated at 70% confluency in duplicates onto 12 well plates two days before transfection. The day before transfection, the media was changed to Opti-MEM (Invitrogen). Cells were co-transfected with the pcDNA FRT/TO vectors and pOG44 (the vector containing the flipin recombinase which contains no selection cassette) at a DNA ratio of 2:6ug pcDNA 5 FRT/TO: pOG44 and 100µl of Lipofectamine 2000 (Invitrogen) for 6hrs at 30°C on a shaker. The media was then changed to MEM, PenStrep, 10% FBS, NEAA and kept at 30°C overnight. The cells were replated the next day and kept at 30°C. 48 hours after transfection, the cells were placed under selection media (MEM + PenStrep + 10% FBS + NEAA + blasticidin and hygromycin) and grown at 37°C. Colonies were pooled and tested for expression.

4.2.16 Trafficking of Flag-ATP7B and Phosphorylation Mutants

To induce expression of Flag-ATP7B and the phosphorylation mutants, cells were grown in the presence of 40ng/mL tetracycline. Cells were seeded onto coverslips in 12 well plates and allowed to grow for 48hrs. Cells were then treated with bathocuproine disulfonate (BCS), a copper chelator, or copper chloride for 1 hr at 37°C in the presence of 40ng/mL of tetracycline. Cells were then washed with cold PBS and fixed in 4% paraformaldehyde for 30min on ice. Cells were then washed/permeabilized with PBS + 0.02% TritonX-100. The cells were blocked overnight in blocking buffer (1% BSA, 1% gelatin, 0.02% TritonX-100, 0.01% Sodium azide) at 4°C. Primary antibody incubation with anti-Flag (Sigma) and anti-TGN46 (GeneTex) were performed at room temperature in blocking buffer at a dilution 1:500 for 1 hour. Secondary antibody incubation was

done with Donkey anti-mouse AlexaFluor488 and Donkey anti-sheep AlexaFluor555 (Molecular Probes) for 1 hr at room temperature in the dark. Cells were mounted in Vectashield + DAPI and sealed with nail polish. Imaging of cells was done on a Zeiss LSM 5 Pascal confocal microscope.

4.3 Results

4.3.1 In vitro phosphorylation of ATP7B from a SF9 expression system.

Identification of phosphorylation sites in large membrane proteins, which are present in human cells in minute quantities, represents a considerable challenge and often requires utilization of recombinant proteins and/or their domains. Previous experiments demonstrated that human ATP7B expressed in insect *Sf9* cells are active [130] and could be kinase phosphorylated *in vivo* [215]. These results indicated that in *Sf9* cells, ATP7B was folded sufficiently well to allow for regulatory phosphorylation to occur. Recombinant expression of ATP7B constitutes 2% of the total membrane protein[130]. Approximately 0.8 µg – 1 µg of ATP7B per 50 µg of crude membrane protein was expressed, and conditions optimized for *in vitro* phosphorylation using cell extracts from human hepatic HepG2 cells.

To exclude the possibility that the observed phosphorylation is not due to any residual catalytic activity, we utilized the D^{1027}>A mutant of ATP7B, which lacks the ability to hydrolyze ATP due to a mutation of the catalytic aspartate [130]. The D^{1027}>A mutant was phosphorylated similarly to the wild-type protein (Figure 23B), indicating that the phosphorylation was unrelated to known catalytic activity of ATP7B and was more likely mediated by a membrane

associated kinase. A similar result was also obtained with ATP7B containing membranes from HepG2 cells (data not shown).

4.3.2 Proteolysis within the N-terminal domain increases phosphorylation of ATP7B.

In addition to the full-length ATP7B (165 kDa protein), a 136kDa protein (that was absent in mock infected controls) was highly phosphorylated (Figure 23). Comparison with the Western blot revealed that the 136 kDa band represents a degradation product of ATP7B (Figure 24B). Attempts to identify the site of proteolytic cleavage by direct amino acid sequencing of the 136 kDa fragment were unsuccessful either due to modification of the N-terminus during sample preparation or due to the presence of several closely spaced cleavage sites (data not shown). Consequently, to determine whether the 136 kDa fragment was generated by proteolysis of the C-terminal or the N-terminal portion, we utilized a C-terminally His tagged variant of ATP7B. Phosphorylation of this construct was similar to the non-tagged ATP7B (data not shown).

Solubilization and purification of Ni-NTA resin yielded both the full-length ATP7B and the 136 kDa fragment (Figure 24A, upper panel). Retention of the C-terminal His-tag indicates that the 136 kDa product was generated by the removal of a N-terminal 29 kDa fragment, which contains approximately 260 residues and includes MBD1, MBD2, and part of MBD3. Based on the densitometry measurements, the 136 kDa product incorporates about 5 fold more phosphate than the full-length ATP7B (Figure 24B,C) (or 4 fold more for the ATP7B D1027A variant). Altogether, these results suggest that the removal of

MBD1-3 increases phosphorylation of ATP7B (at least *in vitro*) either due to the exposure of the remaining MBDs in the N-terminus or due to the unmasking of other domains, such as ABD.

4.3.3 The N-terminal domain of ATP7B (N-ATP7B) is a target of phosphorylation *in vitro* and *in vivo*.

It was previously determined that phosphorylation of ATP7B occurs on a serine residue [215]. The ATP7B sequence contains 126 serines; this excludes site-directed mutagenesis as an efficient strategy for the identification of phosphorylation site(s). To identify such sites, trypsin digestions of purified in vitro phosphorylated ATP7B were performed and mass spectrometry analysis of the resulting peptides. However, very low peptide coverage (only ~30% of the full length ATP7B sequence was recovered for any given experiment, (data not shown)) precluded identification of the phosphopeptides. Consequently, to narrow down the location of the phosphorylation region, three major cytosolic domains of ATP7B were considered: the C-terminal domain, the ATP Binding Domain (ABD), and the N-terminal domain (N-ATP7B). The C-terminal domain, contains signals for the trafficking of ATP7B, however, the deletion of the C-terminal tail does not prevent the phosphorylation of ATP7B in mammalian cells[75]. Both the ABD and the N-ATP7B have a number of potential sites for kinase mediated phosphorylation. From the known data, deletion of the C-terminal tail did not eliminate copper dependent phosphorylation. PINA, an isoform lacking the N-terminal domain as well as part of the A-domain of ATP7B, did not hyper-phosphorylate[75], suggesting the target of phosphorylation is in the

N-terminal domain (Figure 25). To test this theory, soluble domains were expressed and purified and tested for in vitro phosphorylation.

The ABD was phosphorylated minimally above background (data not shown), but MBP-N-ATP7B (Maltose Binding Protein fusion of N-ATP7B) repeatedly showed a significant level of phosphorylation that was dependent on incubation with the lysate (Figure 26A, upper panel). In order to verify that the N-ATP7B is a physiologically relevant target of kinase-mediated phosphorylation, N-ATP7B was tested if it could be phosphorylated *in vivo* in mammalian cells. His-N-ATP7B was expressed in human Hek293 cells, which were subsequently metabolically labeled with orthophosphate (^{32}P). The His-N-ATP7B was then purified and was found, by autoradiography, to be labeled with phosphate (Figure 26B). Thus, His-N-ATP7B is a target for phosphorylation *in vivo* and *in vitro*.

4.3.4 The sites of phosphorylation are located in the loop between MBS 3 and MBS 4.

For further mapping, the purified *in vitro* phosphorylated N-ATP7B was subjected to limited proteolysis with trypsin, as described previously [145]. Under these conditions, proteolysis only occurs in loops between MBDs, leaving the individual MBDs intact. The peptides were then separated by a 2-dimensional gel before analysis of phosphorylated spots by tandem mass spectroscopy (Figure 27). A theoretical map was generated to estimate the location of the tryptic fragments (Figure 28). Although no phosphopeptides were detected, the identity of the phosphorylated region was established, because all peptides recovered from the phosphorylated spots belonged to the protein

segment extending from MBD3 to MBD6 (Figure 29, lower panel), suggesting that the C-terminal half of N-ATP7B was the target of phosphorylation.

Finally, we examined phosphorylation of several deletion variants of N-ATP7B tagged to a chitin-binding domain, CBD (Figure 30A). The N-ATP7B-CBD constructs have the advantage with respect to protein stability, however carrying phosphorylation experiments on a chitin resin produced a higher background (several non-ATP7B bands, originated from the cell lysate, were detected, Figure 30B, Lane 4). Nevertheless, it was apparent that the N-ATP7B variants, including MBD1-4 were phosphorylated, while the fragment including MBD5,6 was not (Figure 30B). No phosphorylation of the chitin binding domain tag was detected (negative control). Altogether, the results of mass-spectrometry of phosphorylated spots (showing peptides from the MBD3-MBD6 region) and limited proteolysis (showing phosphorylation of the MBD1-4 fragment) pointed to the region between MBD3-MBD4 as a target of phosphorylation.

4.3.5 Mutations of $S^{340}S^{341}$>AA and $S^{342}S^{343}$>AA decrease *in vitro* phosphorylation

MBD3 and MBD4 are well-folded domains, connected by a fairly long linker. This linker region includes seven serine residues that are predicted as targets of various kinases (Figure 31 A). To examine if any of these residues are phosphorylated, five constructs were generated mutating Ser to Ala at either single position S^{334}>A, S^{345}>A, and S^{348}>A, or at two consecutive positions at $S^{340}S^{341}$>AA and $S^{342}S^{343}$>AA (Figure 31A). In these experiments, the maltose

binding protein fusions of N-ATP7B were used, since chitin-binding protein fusion showed high background phosphorylation (Figure 30). All mutants showed reduced levels of phosphorylation compared to that of wild-type protein (Figure 31 B, C). The most significant reduction of phosphorylation was for the double mutants, $S^{340}S^{341}$>AA and $S^{342}S^{343}$>AA, which showed 48% and 65% phosphorylation of the wild-type for apo-protein, respectively (Figure 31 B, C). Partial decrease of phosphorylation for all mutants suggested that multiple Ser residues are likely to be targets of phosphorylation, a situation common for tandemly placed serines. It is also possible that the mutations could be disturbing folding of the region.

4.3.6 The trafficking behavior of ATP7B is altered by $S^{340}S^{341}$>AA substitution.

To determine whether the decrease in phosphorylation translates to a functional consequence, we incorporated the $S^{340}S^{341}$>AA and $S^{342}S^{343}$>AA substitutions into the full-length ATP7B and tested the targeting of the mutants and their trafficking in response to elevated copper. Flag-tagged constructs of ATP7B under the control of a tetracycline-regulated promoter were generated to be used in the inducible FlpIn system in FlpIn TREx Hek293 cells. Tet-regulation provides tight control of protein expression and it was essential for these experiments because overexpression induced mislocalization of ATP7B. ATP7B cDNA was cloned into pcDNA 3.1 (+) and a low copy mammalian expression vector from Mick Petris, however, stable selected ATP7B was over-expressed in

the different cell systems tested. Cell systems tested include CHO-K1, Cos7, Hek293, HepG2, and HeLa.

In cells treated with the copper chelator BCS, Flag-ATP7B and $S^{342}S^{343}$>AA were found in the TGN, as evidenced by co-localization with Syntaxin 6, a TGN marker (Figure 32). The addition of copper results in the trafficking of wild-type Flag-ATP7B to a vesicular compartment, similar to what has been previously reported for non-tagged ATP7B (Figure 32, upper panels)[45, 75]. Mutant $S^{342}S^{343}$>AA responds to copper by trafficking to a vesicular compartment (Figure 32, middle panels), similarly to wild-type ATP7B, indicating that residues $S^{342}S^{343}$>AA play no major role in the ability of ATP7B to traffic. In contrast, mutant $S^{340}S^{341}$>AA under both BCS and copper treatment is localized in a vesicular compartment (Figure 32, lower panels). Mutation of $S^{340}S^{341}$>AA resulted in altered localization of this mutant.

4.4 Discussion

ATP7B has dual opposing roles in the cell, supplying proteins in the secretory pathway with copper while maintaining copper homeostasis in the cell by exporting the excess. An appropriate level of intracellular copper is determined by the metabolic needs of individual cells, while the regulation of this level seems to commonly require copper transporters. In hepatocytes, spatial separation of ATP7B from the TGN to a vesicular compartment upon elevated intracellular copper seems to be a very straightforward, but effective, mechanism to redirect excess copper from the biosynthetic towards the secretory pathway. In this study, it was demonstrated that kinase mediated phosphorylation of

ATP7B contributes to regulation of the intracellular targeting of ATP7B, and thus represents an additional way of manipulating copper homeostasis.

4.4.1 Recombinant ATP7B is phosphorylated *in vitro* in *Sf*9 membranes.

Expression of ATP7B in Sf9 insect cells results in ~0.8-1.0 µg of ATP7B per 50 µg of crude membranes. This high level of expression allowed the development of an in vitro phosphorylation assay of ATP7B in *Sf*9 membranes. Phosphorylation was seen for both wildtype and the catalytically inactive D^{1027}>A mutant. Although the *Sf*9 full sequence is not known, Drosophila are known to express an orthologue of ATP7B. It would be interesting to see whether there is phosphorylation of the endogenous copper transporter and how it compares to the recombinant ATP7B, however, the gene in Sf9 is currently unknown. In vitro phosphorylation of ATP7B from an endogenous Sf9 kinase, however, suggests perhaps the targeting region of phosphorylation may be similar. At least in ATP7B mammalian orthologues, the targeted serine rich region is conserved. Also, identification of the ATP7B phosphorylating kinase would be interesting. During purification of ATP7B-His from Sf9 membranes, a 36kDa co-eluting band was seen consistently (data not shown). The identity of this protein was unidentifiable by mass spectroscopy, most likely due to a lack of a *Sf*9 database to compare the MS/MS data.

4.4.2 N-ATP7B is the target for copper dependent phosphorylation.

We demonstrate that N-ATP7B is the target for kinase dependent phosphorylation *in vitro* and *in vivo*. The MBDs of the N-terminal domain bind copper, and binding of copper elicits conformational changes within the domain.

This leads to the disruption of protein-protein interaction of N-ATP7B with the ATP binding domain, making the N-terminal domain an excellent target for a multi-faceted point of regulation [1, 96]. Our data shows the lack of MBDs 1-2 in the 136kDa degradation product of ATP7B results in elevated phosphorylation per protein (Figure 24). Perhaps the loop between MBD3 and MBD4 is more protected in the full length protein under apo conditions. With increased copper binding, the entire protein undergoes conformational changes resulting in decreased interaction of N-ATP7B with the ABD, leading to exposure of loop 3.

N-ATP7B has been previously shown to be important for copper dependent trafficking. We show in chapter 2 that one of the exons that encode for the N-terminal domain is also a targeted for alternative splicing. N-ATP7B also has been shown to regulate copper entry into the intramembrane site. Atox1 mediated copper transfer to MBD2 also regulates copper delivery to the N-terminal domain. It is not surprising then that the N-terminal domain is also the target of kinase mediated phosphorylation. The importance of MBD 1-4 as regulatory domains is further reinforced, as well as the complexity of copper regulation.

4.4.3 Phosphorylation is dependent on accessibility to target sites.

As shown in Figure 24 and 25, ATP7B expressed in Sf9 cells has a degradation band that has an apparent molecular mass of 136 kDa. The 136 kDa degradation product is calculated to have lost the N-terminal region including MBD 1, 2 and loop 2. This loss of MBDs 1 and 2 results in a protein that is more efficiently phosphorylated (Figure 25C). In the full length protein, access of the

kinase to the phosphorylation site(s) may be limited unless the protein is copper bound, and the intermolecular interactions between N-ATP7B and ABD decrease. However, the 136 kDa product would allow better access of loop 3 to the kinase. Comparison of phosphorylation between the degradation product from wildtype and the catalytic mutant further support this idea. The wildtype 136 kDa product is better phosphorylated than the 136 kDa product from the D^{1027}>A mutant, which is still better phosphorylated than the full length wildtype and D^{1027}>A mutant. This suggests catalytically active protein is better phosphorylated. ATP7B undergoes conformational changes as part of its catalytic cycle for copper export (Figure 2B). Stabilization of specific conformations may alter the efficiency of kinase mediated phosphorylation because certain loops may be better exposed. The D^{1027}>A construct, which in wildtype protein would form an acyl phosphate bond from ATP hydrolysis, can not undergo conformational changes from E1 to E1-Pi-Cu and the completion of the catalytic cycle, unlike the wildtype. This suggests the D^{1027}>A construct would be in a more E1 like conformation with interaction between the N-terminal domain and ABD, making the phosphorylation sites more inaccessible. The wildtype construct, on the other hand, would be under different equilibrium conditions, since some fraction of ATP7B could be participating in any step of the catalytic cycle and thus more likely to be in a conformation that would allow the kinase to phosphorylate ATP7B.

4.4.4 $S^{340}S^{341}$ are targets for phosphorylation.

The region of phosphorylation was identified, and serine residues mutated to alanines. In vitro phosphorylation of the mutants were investigated to determine which residue(s) were responsible for copper dependent phosphorylation, and trafficking studies performed to determine the effect of the lack of phosphorylation. The in vitro phosphorylation of $S^{340}S^{341}$>AA was only partially inhibited.

$S^{340}S^{341}$ may not be the only targets for phosphorylation. They were the only residues mutated that showed both a decrease in phosphorylation and unresponsiveness to exogenous copper. It is possible that $S^{342}S^{343}$ may still play a role in phosphorylation. To test if these residues could still be theoretical targets for phosphorylation, synthetic peptides containing different combinations of serine mutants from this region could be generated and spotted onto PVDF. In vitro phosphorylation with lysate can then be performed on the membrane to see which serine residues are phosphorylated. Since the stoichiometry of phosphorylation is not known, this may provide a clue to how many of the serine residues can be phosphorylated.

It would be important to test if phosphorylation could be cooperative. In the case of phosphorylation, if S^{341} and S^{342} were the actual targets of phosphorylation with S^{342} facilitating phosphorylation of S^{341}, the functional serine, then it is possible to see phosphorylation for both $S^{340}S^{341}$>AA and $S^{342}S^{343}$>AA (Figure 31). Another possibility for seeing only a partial loss of phosphorylation is that the structure of loop 3 is slightly altered such that the ATP7B kinase phosphorylates one of the surrounding serines, such as $S^{342}S^{343}$.

In the in vitro phosphorylation assay, it is assumed that there are phosphatase in the lysate along with the kinase. If the mutations in the mutant constructs alter the phosphatase binding site instead of the phosphorylation site, instead of inhibition of phosphorylation, there would be an inhibition of dephosphorylation. There would also have to be an effect on the phosphorylation, because there is less phosphorylation of the mutants compared to wildtype. To address this issue, samples could be treated with the casein kinase phosphatase, which previously has been used to dephosphorylate full length ATP7B in vitro. If $S^{340}S^{341}$>AA can be dephosphorylated, that would suggest that the mutation does not affect the phosphatase binding site. If it remains phosphorylated, in vivo metabolic labeling with orthophosphate or gel mobility shifts would show whether the constructs are constitutively phosphorylated. Under those circumstances, phosphorylation would not be a retrieval signal, but may promote forward trafficking.

4.4.5 Phosphorylation may play a role in the retrieval of ATP7B

Mutation of $S^{340}S^{341}$>AA resulted in the partial loss of phosphorylation of the protein, as well as constitutive vesicular localization of the construct. This vesicular staining was unaffected by the addition of BCS or copper, similar to the C-terminal LLL>AAA mutation in Cater et al [210]. These data were contrary to what we hypothesized was the function of copper dependent phosphorylation. We expected no trafficking from the TGN in either low or elevated copper for $S^{340}S^{341}$>AA. If the mutant was localized in the TGN, one would assume

phosphorylation relieves an inhibition signal, which would allow forward trafficking.

In contrast, $S^{340}S^{341}$>AA localized at the vesicles which might suggest phosphorylation could be a retrieval signal. ATP7A contains a di-leucine motif important for the retrieval of the protein from the plasma membrane. Mutation of these leucines results in plasma membrane localization of ATP7A, independent of copper levels. ATP7B also has a similar tri-leucine motif, which leads to vesicular localization of ATP7B. Mutation of the serine residues and the tri-leucine motif lead to similar vesicular localization that does not respond to changes in copper. This may suggest phosphorylation is required for the retrieval of ATP7B from the vesicles. Perhaps phosphorylation is a signal for recruitment of trafficking machinery to interact with the C-terminal tail, leading to ATP7B return to the TGN.

If we assume ion transport by ATP7B is not dependent on its cellular localization, but the availability of copper, ATP7B should be able to transport copper whether it is localized at the TGN or vesicles. However, an increased length of time spent in vesicles might lead to less intracellular copper, and more exported copper. Phosphorylation might moderate that length of time, returning ATP7B to the TGN when copper homeostasis has returned.

In the case of the $S^{340}S^{341}$>AA mutant, which has partial loss of phosphorylation, ATP7B is localized to vesicles under copper limiting and excess conditions. This is expected for elevated copper conditions if phosphorylation is a retrieval signal, since ATP7B has been shown to traffic in response to copper.

Vesicular localization for the BCS treated cells is expected if some fraction of ATP7B constitutively traffics. In experiments with endogenous ATP7B protein in HepG2 cells, ATP7B has been shown to traffic to the canalicular membrane under basal and BCS conditions, albeit only a fraction of the total protein that traffics under elevated copper. ATP7A, a ATP7B homologue, is also known to traffic constitutively[195]. It would be interesting to compare the intracellular copper levels in the $S^{340}S^{341}$>AA cells to see if there is less copper in these cells where ATP7B spends more time in vesicles. The localization pattern of the $S^{340}S^{341}$>AA mutant might also change in polarized cells. Mutant $S^{340}S^{341}$>AA might remain at the plasma membrane as opposed to vesicles. Regulation of ATP7B through phosphorylation leads to many interesting questions in the mechanism of regulation of copper homeostasis.

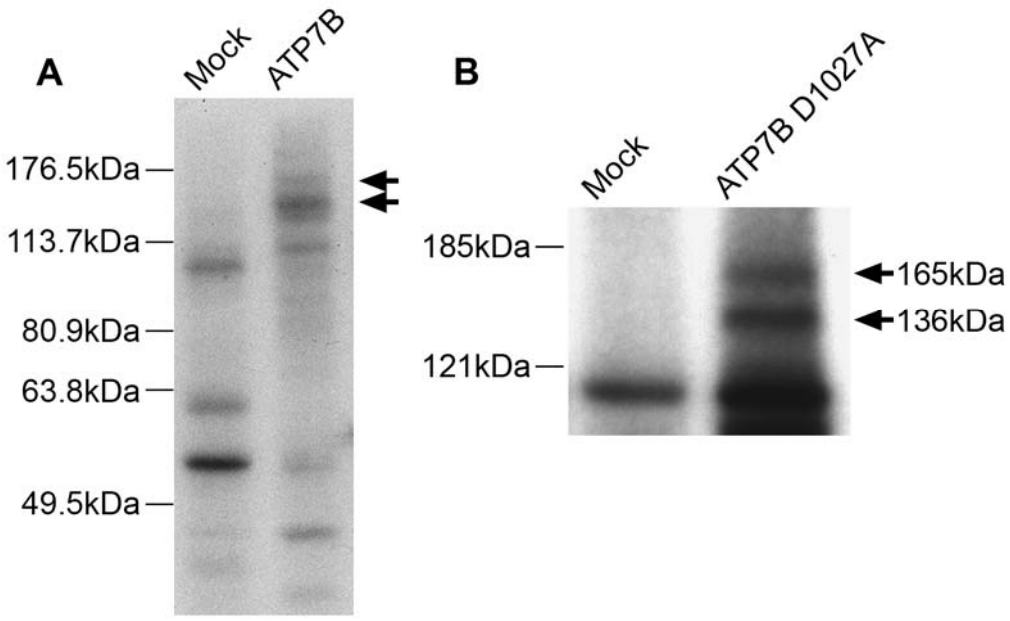

Figure 23: *in vitro* phosphorylation of ATP7B expressed in *Sf9* cells. *Sf9* cells were infected with baculovirus that express either the empty vector, ATP7B, or ATP7B D^{1027}>A. Microsomal membrane fractions were prepared and *in vitro* phosphorylated with γ-^{32}P-ATP. Protein concentrations were determined by Lowry method, and equal amounts of membrane protein from mock transfected cells and from cells expressing ATP7B (**A**) or ATP7B D^{1027}>A mutants (**B**) were separated by Laemmli gel, dried, and analyzed by autoradiography. The arrows indicate the position of full-length (165 kDa) and a degradation product of (136 kDa) ATP7B.

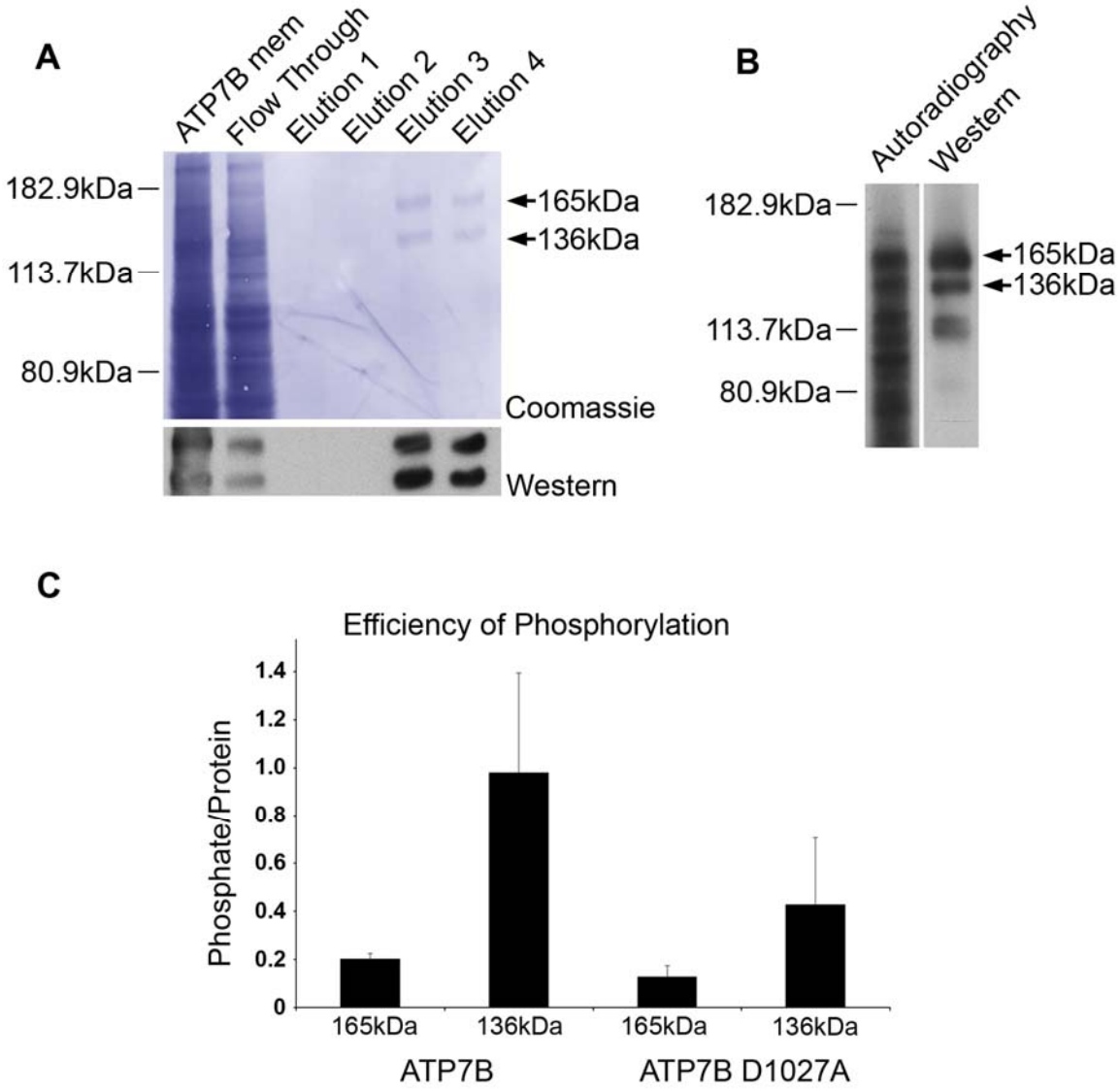
A
ATP7B mem
Flow Through
Elution 1
Elution 2
Elution 3
Elution 4
182.9kDa
113.7kDa
80.9kDa
165kDa
136kDa
Coomassie
Western
B
Autoradiography
Western
182.9kDa
113.7kDa
80.9kDa
165kDa
136kDa
C
Efficiency of Phosphorylation
Phosphate/Protein
1.4
1.2
1.0
0.8
0.6
0.4
0.2
0
165kDa
136kDa
165kDa
136kDa
ATP7B
ATP7B D1027A

Figure 24: Proteolysis of the N-terminal domain of ATP7B increase the efficiency of phosphorylation. A C-terminal His-tagged ATP7B was expressed in *Sf9* cells as above. (**A**) Solubilized ATP7B-His and the 136kDa degradation product can be purified with Ni-NTA and coomassie stained PVDF (upper panel). The western blot shows both the 165kDa and 136kDa product are ATP7B (lower panel). (**B**) Autoradiography and western of a blot of phosphorylated ATP7B-His indicating the phosphorylation of both the 165kDa and 136kDa protein product. (**C**) A graph summarizing the efficiency of phosphorylation for 165kDa/136kDa ATP7B and ATP7B D^{1027}>A. (The maximum incorporation of phosphate in these conditions was ~1 phosphate per 136 kDa protein; this number could be due to complete phosphorylation of one site or partial phosphorylation of multiple sites).

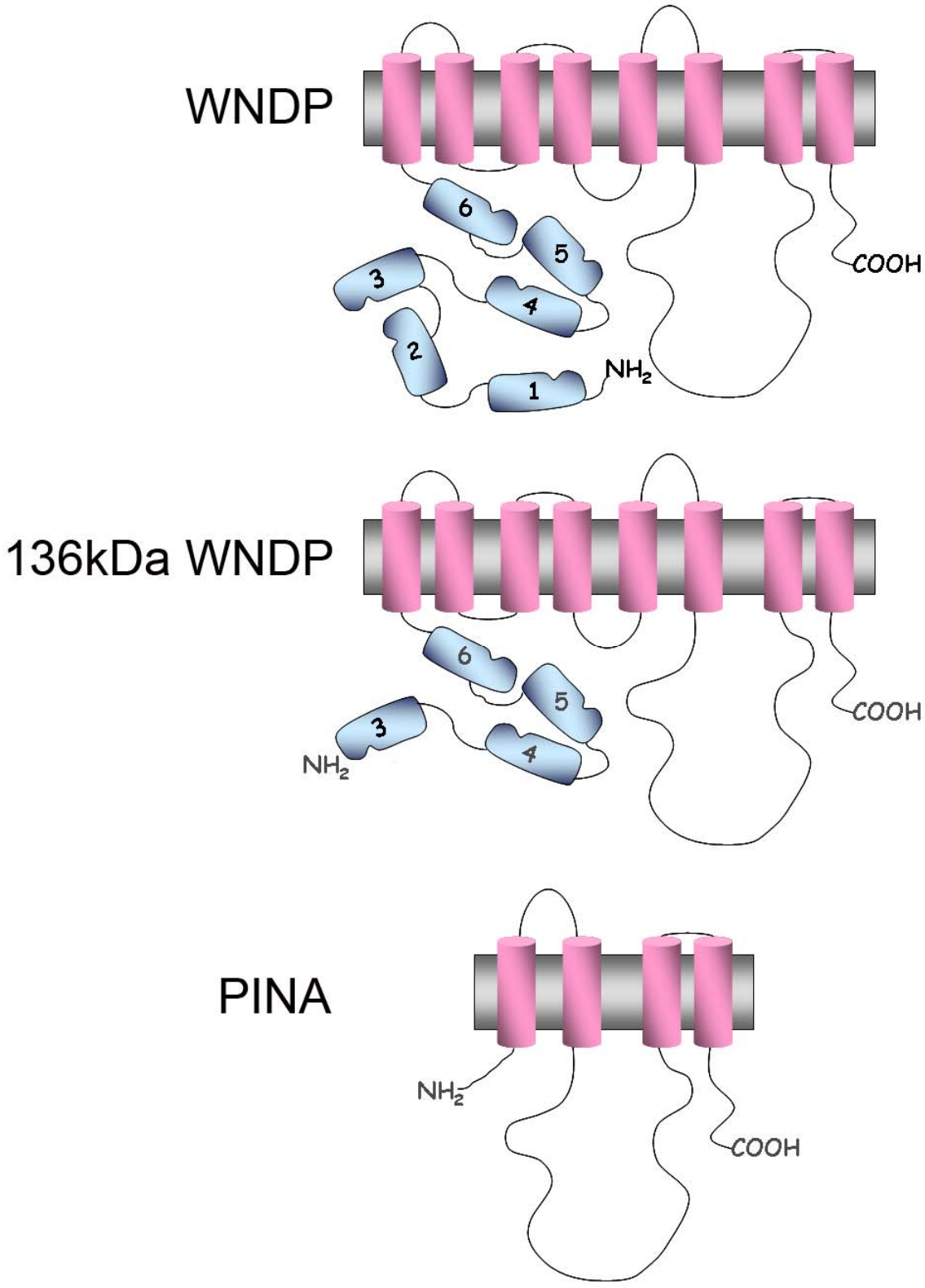
WNDP
6
5
3
4
2
1
NH2
COOH
136kDa WNDP
6
5
3
4
NH2
COOH
PINA
NH2
COOH

Figure 25: Cartoon of possible targets of ATP7B phosphorylation. ATP7B has three soluble regions that can be targeted for phosphorylation, the N-terminal copper binding domain, the ATP Binding domain, and the C-terminal tail. Previous work showed deletion of the C-terminal tail still results in phosphorylation. The PINA construct, where the first half of ATP7B is absent, does not undergo copper dependent phosphorylation. This leaves N-ATP7B as a good candidate for phosphorylation. If N-ATP7B is the target for phosphorylation, the region of phosphorylation is most likely between MBD3 and the first transmembrane. This is based on the phosphorylation of the 136kDa ATP7B degradation product, which is missing part of the N-terminal region by western blot of the C-terminal His tag construct (data not shown). Also, per protein, the 136 kDa product is better phosphorylated (1.0 phosphate/ protein as opposed to 0.2 phosphate/ protein (data not shown)) suggesting N-ATP7B is a target for phosphorylation.

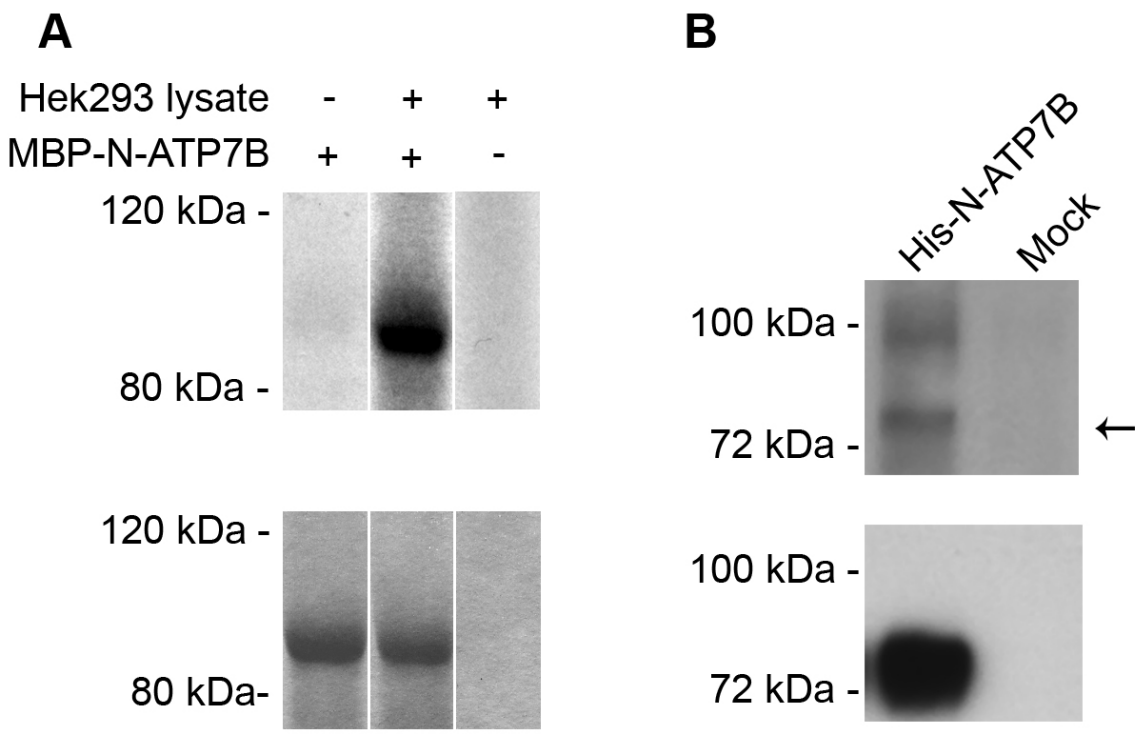

Figure 26: The N-terminal domain of ATP7B is a target for kinase mediated phosphorylation *in vitro* and *in vivo*. **A**) MBP-N-ATP7B (~100 kDa) was expressed in E.coli and phosphorylated on amylose resin with Hek293 cell lysate (upper panel: autoradiography, lower panel: coomassie staining). **B**) To confirm the kinase mediated phosphorylation of N-ATP7B also occurs *in vivo*, Hek293 cells were transfected with His-N-ATP7B (~70 kDa) and metabolically labeled with orthophosphate (^{32}P) (upper panel: radiography, lower panel : western blot).

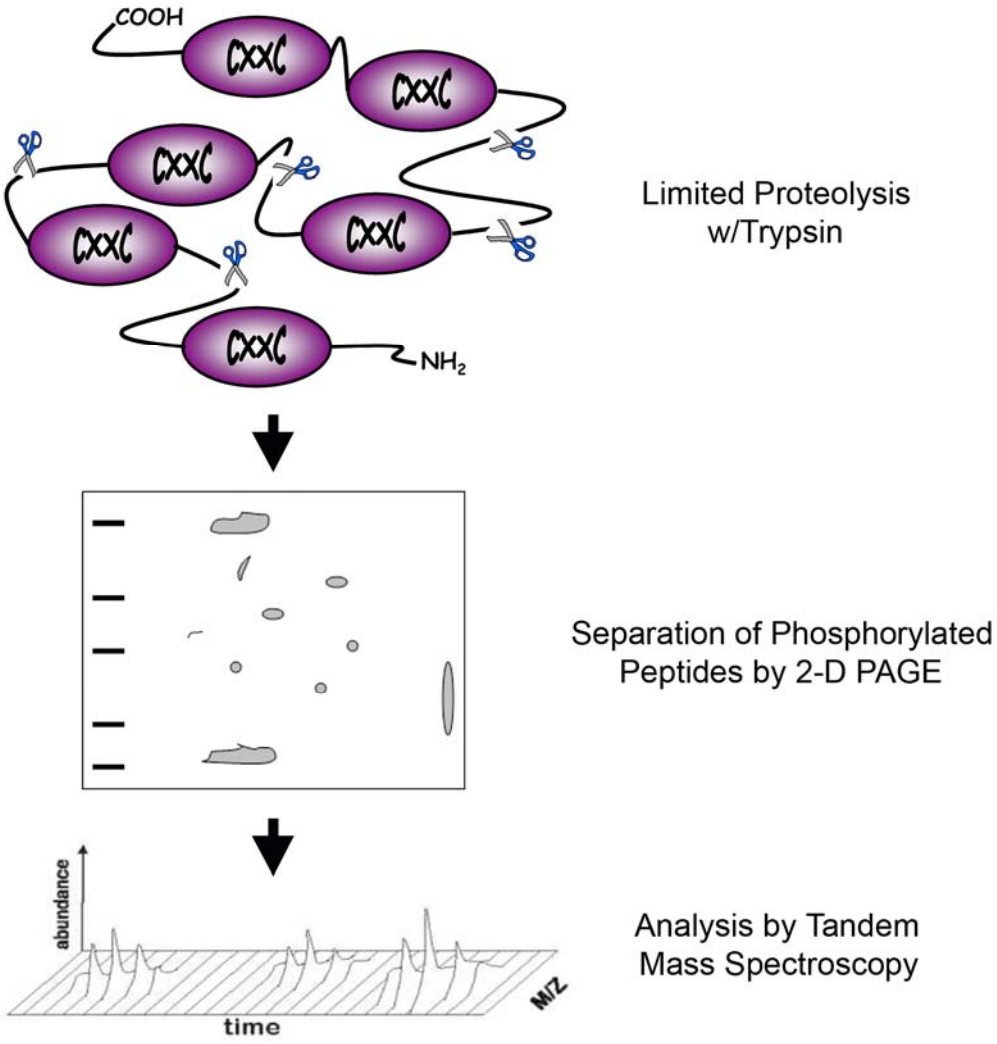

Figure 27: Schematic of Separating phosphorylated N-ATP7B peptides by 2-D PAGE. To narrow the region of phosphorylation in N-ATP7B, phosphorylated N-ATP7B underwent limited proteolysis with trypsin. As a result, primarily the loop regions connecting the individual MBDs are cut. Phosphorylated peptides are run on a 2-D gel to separate the MBDs. Phosphorylated spots, visualized by autoradiography, are further proteolyzed and analyzed by tandem mass spectroscopy.

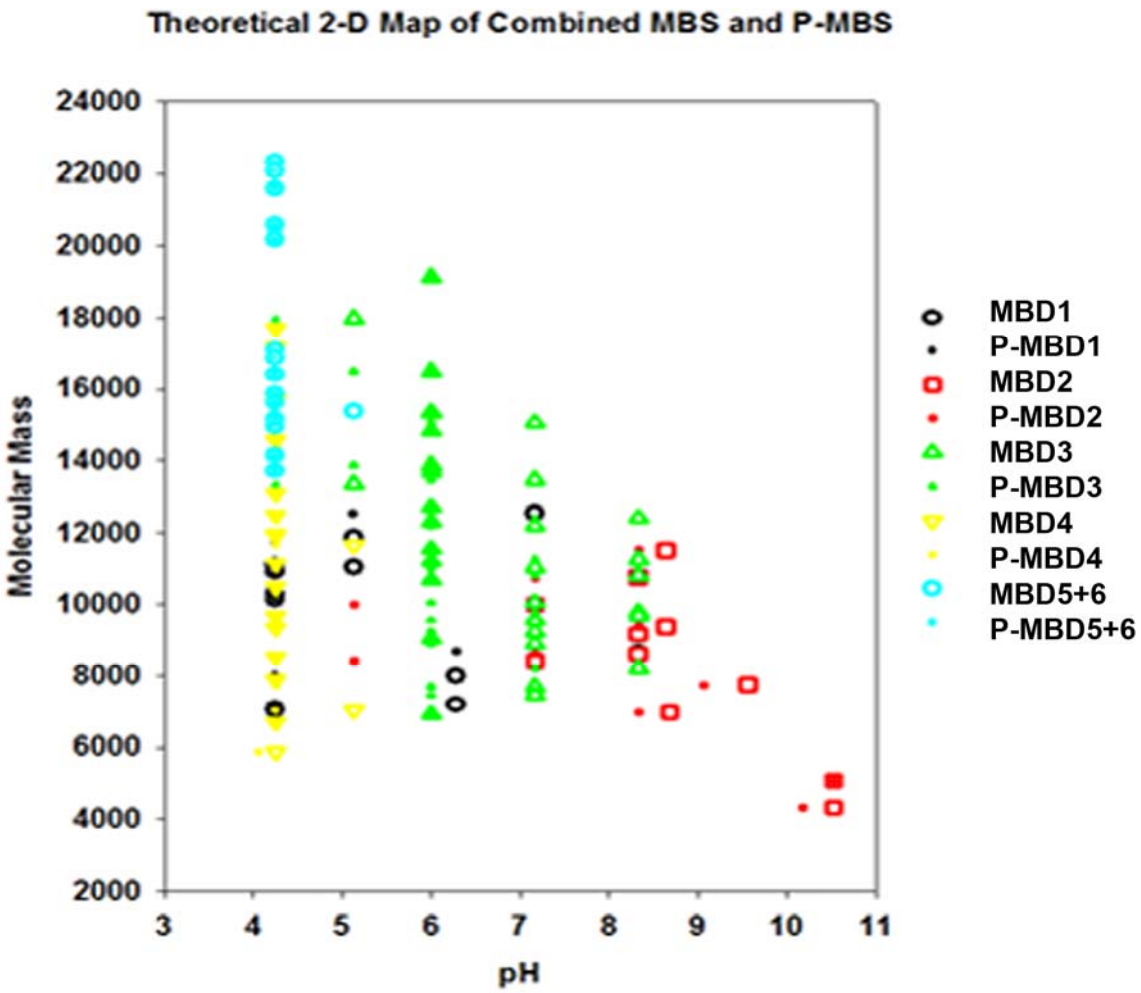

Figure 28: Theoretical 2-D PAGE map of trypsinized N-ATP7B and phosphorylated N-ATP7B peptides. Molecular masses for the theoretical proteolysis of N-ATP7B by trypsin were calculated with SEQUEST, and the resulting pI was calculated for both phosphorylated and un-phosphorylated peptide. The resulting information was plotted using SigmaPlot.

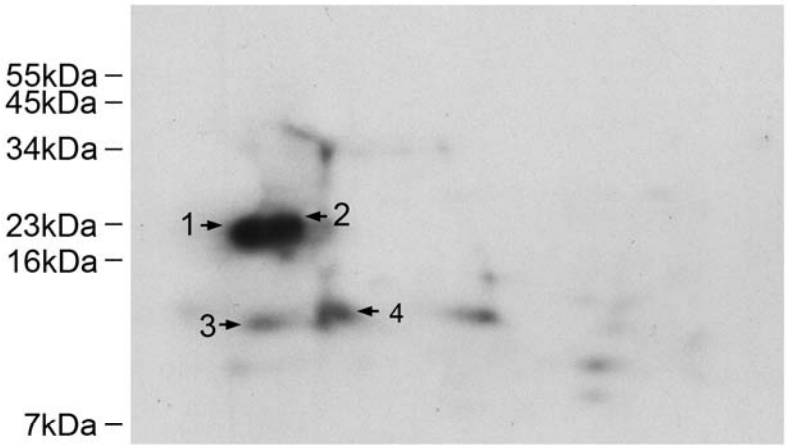

SPOT 1:

407 VISPEELR
439 HSAGNSMVQTTDGTPTSVQEVAPHTGR
466 LPANHAPDILAK
589 TNGITYASVALATSK

SPOT 2:

352 NQVQGTCSTTL
340 SSSSHSPGSPPR
415 AAIEDMGFEASVVSESCSTNPLGNHSAGN
444 SMVQTTDGTPTSVQEVAPHTGR
466 LPANHAPDILAK
496 GMTCASCVSNIER
512 EAGVLSVLVALMAGK
595 ASVALATSK
608 FDPEIIGPR

SPOT 3:

512 EAGVLSVLVALMAGK
589 TNGITYASVALATSK
608 FDPEIIGPR

SPOT 4:

314 AIEALPPGNFK
270 SCVLNIEENIGQLLGVQSIQVSLENK

Figure 29: Autoradiograph of phosphorylated N-ATP7B peptides and list of peptides retrieved by tandem mass spectroscopy. As described in Figure 28, phosphorylated N-ATP7B was proteolyzed and separated by pI using a nonlinear 3-10 pI range strip. The peptides were further separated by mass on a 7.5% Laemmli gel. The arrows indicate the spot analyzed, and the corresponding peptides retrieved are listed below the gel.

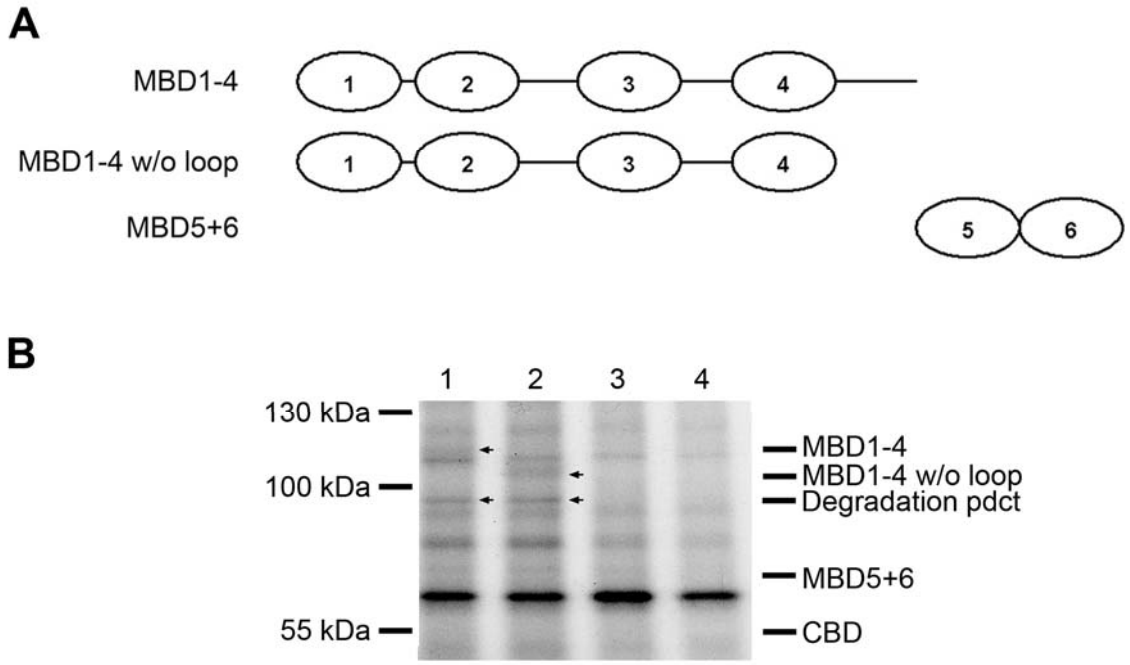

Figure 30: The region of phosphorylation is located in loop 3, between MBD3 and 4. **A**) Deletion constructs of intein N-ATP7B were generated. **B**) Protein was expressed and phosphorylated on chitin resin with Hek293 cell lysate and γ-^{32}P–ATP. (Lane1:MBD1-4, 2:MBD1-4 w/o loop, 3:MBD5+6, 4:Chitin Binding Domain).

A

Wildtype	LPDGAEGSGTDHRSSSSHSPGSPPRNQVQG
S334A	LPDGAEG**A**GTDHRSSSSHSPGSPPRNQVQG
S340/1A	LPDGAEGSGTDHR**AA**SSHSPGSPPRNQVQG
S342/3A	LPDGAEGSGTDHRSS**AA**HSPGSPPRNQVQG
S345A	LPDGAEGSGTDHRSSSSH**A**PGSPPRNQVQG
S348A	LPDGAEGSGTDHRSSSSHSPG**A**PPRNQVQG

B

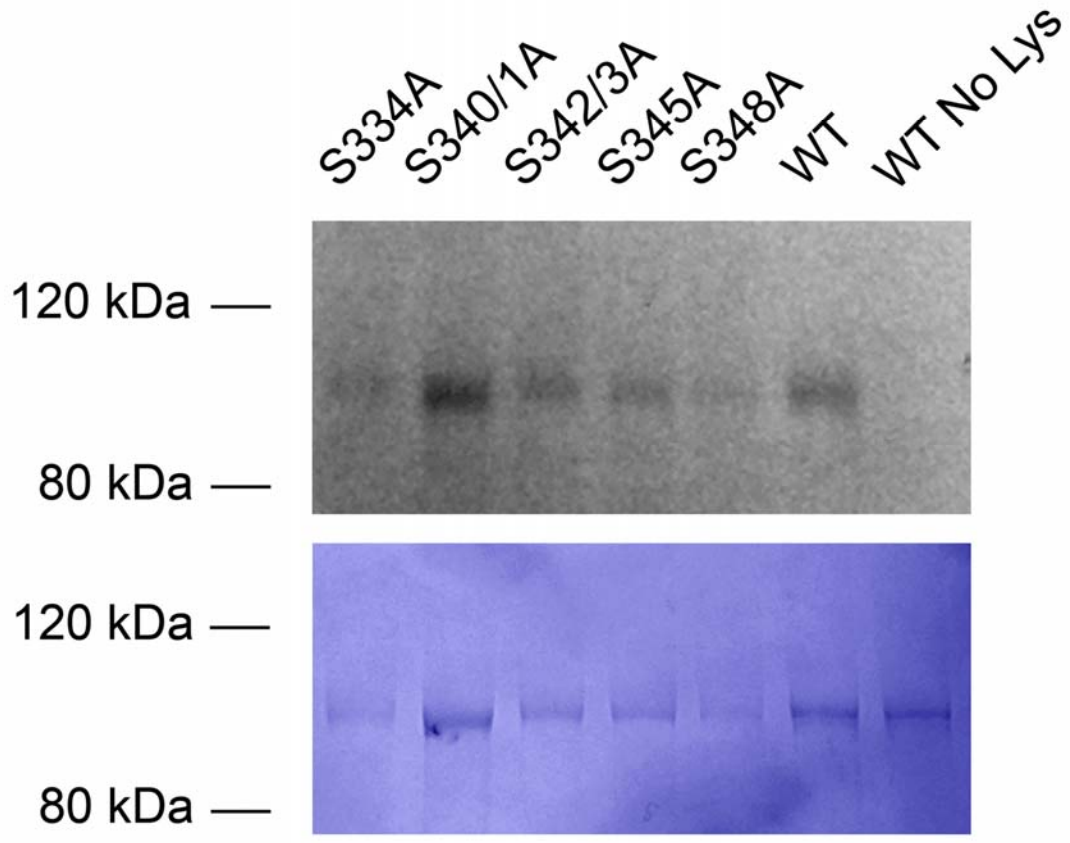

C

Construct	334	340/1	342/3	345	348	WT
Apo	0.73±0.21	0.48±0.05	0.65±0.02	0.73±0.22	0.81±0.06	1.0
Copper	0.58±0.12	0.55±0.07	0.68±0.13	0.68±0.11	0.62±0.02	1.0

Figure 31: Mutation of $S^{340}S^{341}$>AA and $S^{342}S^{343}$>AA in N-ATP7B decreases in vitro phosphorylation. **A**) Cartoon indicating the serine mutation sites. **B**) MBP-N-ATP7B constructs were phosphorylated with Hek293 cell lysates on amylose resin (upper panel: autoradiography, lower panel: coomassie staining). **C**) Phosphorylation for the mutants was normalized for loading and relative phosphorylation compared to the wildtype which is set at 100%.

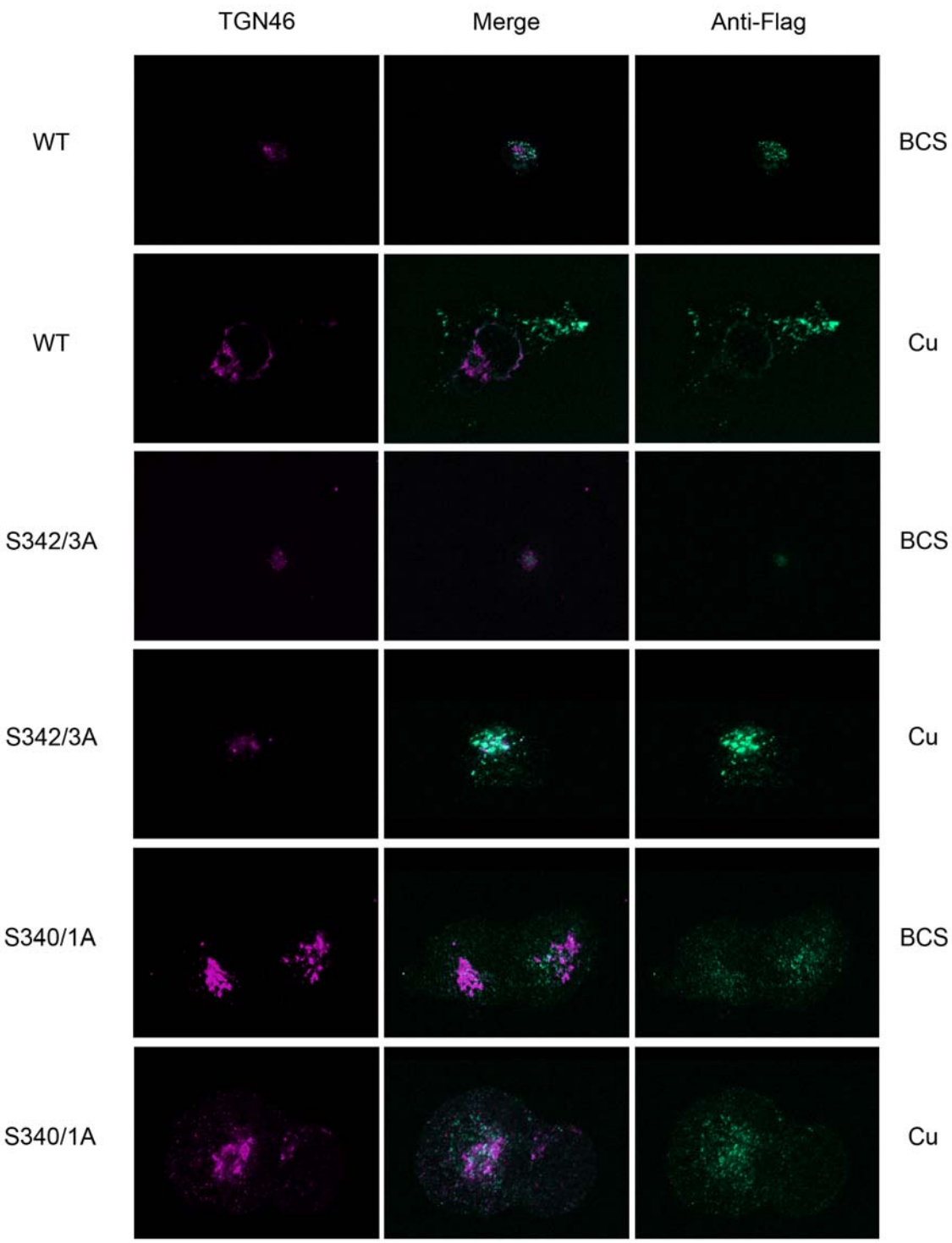
TGN46
Merge
Anti-Flag
WT
BCS
WT
Cu
S342/3A
BCS
S342/3A
Cu
S340/1A
BCS
S340/1A
Cu

Figure 32: Mutation of $S^{340}S^{341}$>AA localizes ATP7B to vesicles. FlpIn T-REx Hek293 cells were stably transfected with Flag-ATP7B and mutant constructs expressed in pcDNA5FRT/TO. Cells were treated with 50μM BCS (copper chelator) or $CuCl_2$ for 1hr, and stained with antibodies for Flag (Green) and TGN46 (Purple) with secondary antibodies Donkey anti-mouse Alexa488 and Donkey anti-sheep Alexa555, respectively. Wildtype Flag-ATP7B (upper panels) and $S^{342}S^{343}$>AA ATP7B (center panels) co-localizes with the TGN46 marker when treated with BCS, but are in vesicles when treated with $CuCl_2$. Mutant $S^{340}S^{341}$>AA (lower panels) is localized in vesicles under both conditions.

THE N-TERMINAL DOMAIN OF ATP7B IS A TARGET OF A KINASE-MEDIATED PHOSPHORYLATION

Mee Y. Bartee and Svetlana Lutsenko[1]

Key words: ATP7B, P-type ATPase, copper, kinase, phosphorylation

Running title: Kinase-mediated phosphorylation of ATP7B

1 - The correspondence should be addressed to:
Svetlana Lutsenko, Oregon Health & Science University, Department of Biochemistry and Molecular Biology, 3181 SW Sam Jackson Park Rd., Portland, OR 97239-3098, U.S.A.; Tel.: 503-494-6953; E-mail: lutsenko@ohsu.edu

This work was supported by the National Institute of Health Grant P01 GM067166 to SL . Mee Y Bartee (Min) was a recipient of NRSA fellowship 1-F31-NS047963-01

-This manuscript is under preparation.

-Chapter 5 is taken from this paper.

-I did all the work and writing for this chapter

V Characterization of ATP7B kinase

5.1 Introduction

As mentioned previously, ATP7B localization in hepatocytes is dependent on the intracellular copper levels in the cell. In parallel, it has been shown by the Lutsenko lab, ATP7B undergoes a kinase-mediated phosphorylation[75]. The phosphorylation by a kinase can also be observed for the recombinant ATP7B expressed in insect (*Sf*9) cells. The ATP7B homologue, ATP7A, also has been shown to be phosphorylated by a kinase in insect cells (*Sf9*)[216]. Currently, the kinase that mediates the copper dependent phosphorylation of either transporter is unknown. To provide initial characterization of the ATP7B kinase, we utilized recombinant ATP7B expressed in *Sf9* cells. There are two major advantages for using the *Sf*9 system. Recombinant ATP7B in this system constitutes 2% of the total membrane protein, a level that is significantly higher than levels of endogenous or transfected ATP7B in hepatocytes. The consistent expression level also allowed the development of a simple and reproducible *in vitro* assay for the kinase mediated phosphorylation of ATP7B. Our laboratory has developed a functional assay for analysis of catalytic activity of ATP7B in *Sf*9 membranes. Consequently, for future applications, the effect of the kinase mediated phosphorylation on catalytic activity of ATP7B can also be explored using stepwise reactions.

5.2 Materials/Methods

5.2.1 Culturing *Sf9* cells

Sf9 cells were cultured in Ex-Cell 420 media (JRH Biosciences Inc.) in spinner flasks (BellCo) on magnetic stir plates with constant aeration. The cells were kept at 27°C in ambient air. For expression of ATP7B, $1x10^6$cells/mL was infected with ATP7B expressing baculovirus for 72 hrs before harvesting of protein. *Sf9* cells were homogenized by douncing with a tight fit dounce (Wheaton) in Homogenization Buffer (HB) (25mM Imidazole pH 7.4, 250mM sucrose, 1mM DTT, 2mM AEBSF, and EDTA free Protease Inhibitor Cocktail tablet per manufacturer instructions (Roche)). To clear cell debris, homogenate was centrifuged for 10min at 500 x g, supernatant was collected, and microsomal membranes were then pelleted at 20,000 x g for 30min. The protein concentration in membrane preparations was quantitated by the Lowry method [217] and the ATP7B expression was confirmed by western blot using the N-ATP7B #2 antibody. Small aliquots of membrane protein were stored at -80°C until needed.

5.2.2 *In vitro* phosphorylation of recombinant ATP7B expressed in *Sf9* membranes.

For kinase mediated phosphorylation, 50µg of *Sf9* membrane protein isolated as described above, were resuspended in 200µl of phosphorylation buffer (PB) (20mM Bis-Tris propane, 200mM KCl, 5mM $MgCl_2$, 1mM DTT, 2mM AEBSF, EDTA free Protease Inhibitor cocktail, 1mM sodium orthovanadate, 100µM ATP, pH 7.5) + 5µCi [γ-^{32}P]ATP (Perkin Elmer) and incubated at room temperature for 30min. 50µl of 50% TCA in 1mM sodium phosphate was added to stop the reaction. In the initial experiments before conditions were optimized,

(experiments conducted for Figures 33 to 36) the phosphorylation buffer was pH 6.0 with 1µM cold ATP. For Figure 41, ATP7B containing membranes were incubated with increasing BCS (0-100µM), for 30min on ice. Prior to phosphorylation, the BCS is removed by pelleting the membranes by centrifugation, and resuspending in phosphorylation buffer. The autoradiograph was normalized to the coomassie staining, and graphed using SigmaPlot.

5.2.3 Optimization of *in vitro* phosphorylation conditions for ATP7B membranes

To optimize the *in vitro* kinase assay, the effect of various metals on the levels of *in vitro* phosphorylation of ATP7B expressed in *Sf9* membranes was examined. 50 µg of membrane protein resuspended in buffer (20mM Bis-Tris propane, 200mM KCl, 1mM DTT, 2mM AEBSF, EDTA free Protease Inhibitor cocktail, 1mM sodium orthovanadate, 1µM ATP) was mixed with one of the following: 5mM EDTA, 5mM $MgCl_2$, no metal, 5mM $MnCl_2$, or 5 mM $CoCl_2$. Radioactive ATP was added and the reaction was carried out as described above

To calculate the apparent Km of the kinase for ATP, the ATP7B containing membranes were treated with a wide range of ATP concentrations, from 50nM to 700µM ATP; the apparent Km was calculated to be ~50µM ATP. For subsequent experiments, a concentration of 100µM was used to *in vitro* phosphorylate ATP7B.

5.2.4 Size exclusion chromatography of Hek293 cell lysate

In order to obtain mammalian cell lysates, twenty confluent 10cm plates of Hek293 cells were used. These cells are not very adherent on tissue culture plates, and therefore were dislodged by pipetting with PBS and pelleted. They were washed with PBS, and pelleted again. Cells were then resuspended in 700µl of phosphorylation buffer and lysed by homogenization in a dounce on ice. The homogenate was centrifuged for 30min at 20,000xg, 4°C. The pellet was discarded and the soluble lysate transferred into a fresh tube and passed through a 0.22 micron filter. Some sample was lost during the filtration step. Purified chromatography standards (Sigma), ranging from 13.7kDa to 2,000kDa, were separated with phosphorylation buffer at a flow rate of 0.5mL/min on a Superose 12 size exclusion column (Amersham Pharmacia) to indicate approximate molecular mass of protein separated. 500 µl of Hek293 soluble lysate was loaded onto the Superose 12 column equilibrated with phosphorylation buffer. The proteins were separated at a flow rate of 0.5mL/min and 1mL fractions were collected and stored at -20°C until needed.

5.2.5 *In vitro* phosphorylation of His-N-ATP7B on 96 well Nickel-NTA plates

His-N-ATP7B was expressed from the pTriEx plasmid in BL21 cells + pTx (Thioredoxin expressing plasmid). In short, BL21 (DE3) cells were grown in LB to an OD_{600} of ~0.5 at 37°C, shaking at 250rpm. The culture was then cooled by transfer into the cold room for 30min. The flasks were transferred to a room temperature platform orbital shaker, and expression induced with 1mM IPTG for 3hrs. Cultures were pelleted, resuspended (50mM Tris pH 7.4, 20mM Imidazole,

150mM NaCl, EDTA free protease inhibitor tablets (Roche)), French pressed, centrifuged for 30min at 15,000 rpm, and the supernatant transferred into fresh tubes, and stored at -20°C until required. His-N-ATP7B was purified on 96 well Nickel-NTA coated plates (Sigma). The bound N-ATP7B was incubated with 200µl of each fraction collected from size exclusion chromatography (see above) and 5µCi [γ-^{32}P]ATP (Perkin Elmer) for 30min at room temperature. Reactions were stopped by removing the supernatant and the addition of Laemmli sample buffer. Samples were run on 7.5% Laemmli gels, dried, and placed under Kodak BioMax MS film in autoradiography cassettes with amplifier screens (Fisher) and placed in a static bag in the -80°C for 48 hrs, and the film was developed.

5.2.6 *in vitro* phosphorylation of MBP-N-ATP7B

MBP-N-ATP7B was expressed, purified, and phosphorylated as described in sections 4.2.7 and 4.2.8. Hek293 cells were treated with or without 50µM copper chloride, and the soluble fraction collected by centrifugation. His-ABD was purified as described previously [1]. In short, His-ABD was expressed in BL21(DE3) cells in the presence of 1mM IPTG and purified on Ni-NTA in the presence of 50mM imidazole. Protein was eluted with 200mM imidazole, dialyzed with phosphorylation buffer and concentrated.

5.3 Results

5.3.1 ATP7B containing membranes expressed in *Sf9* cells are phosphorylated in vitro.

To determine conditions under which recombinant ATP7B can be phosphorylated *in vitro* using mammalian cell lysate, conditions were optimized.

First, 50µg of ATP7B containing membranes were phosphorylated with soluble lysate from HepG2 cells. As shown in Figure 33, recombinant ATP7B is phosphorylated in vitro. Further analysis showed ATP7B containing membranes alone are sufficient for the phosphorylation of ATP7B (Figure 33).

5.3.2 The ATP7B phosphorylating kinase is associated with the membrane.

This phosphorylation is not due to autophosphorylation of the catalytic phosphorylation residue, D^{1027}, because the inactive mutant, D^{1027}>A, is still phosphorylated in this in vitro assay (Figure 23B). The catalytic acyl-phosphate in wildtype ATP7B is not stable under more basic conditions of a Laemmli gel compared to acidic gels (data not shown). Although a possibility, whether an endogenous Sf9 copper transporter is autophosphorylating ATP7B at the kinase targeted phosphorylation site is unlikely. In P-type ATPases, there is one ATP binding domain, and the ATP binds in the ATP binding pocket of the nucleotide binding domain (N-domain). ATP binding leads to large overall structural changes in the protein [218], although not that many in the nucleotide binding domain [113]. This brings the P-domain closer to the N-domain for phosphorylation of the invariant aspartate residue in the P-domain [218]. Inspection of the solution structure reveals hydrogen bonding networks co-coordinating/ aligning the AMPPCP such that the gamma phosphate is 3.4 Å away from the target aspartate residue, with possible hydrogen bonding [218]. There would be proximity issues as well as problems with steric hindrance and accessibility in trying to transfer the phosphate from the ATP binding pocket in the N-domain of a Sf9

copper transporter to the serine residues in loop 3 of recombinant ATP7B. Also, purified ATP7B-His (data not shown) and MBP-N-ATP7B (Figure 26A) does not undergo phosphorylation in the presence of [γ-^{32}P] ATP alone, suggesting a kinase is required.

It was hypothesized a kinase could be in proximity to ATP7B in the membranes. To determine whether this kinase is membrane bound or membrane associated with the ATP7B at the membrane, a variation of salt concentrations were tested to disrupt the interaction. If the kinase is membrane associated, the salt treatment could disrupt the interactions. ATP7B containing membranes were incubated with 0, 0.1, 0.5, and 1.0 NaCl before phosphorylation of the membranes. Incubation with high salt disrupts weak hydrogen bonding and ionic interactions between proteins. Incubation of ATP7B membranes with NaCl did not result in a significant change in the degree of phosphorylation (Figure 34), suggesting the kinase is membrane bound or in tight association with ATP7B and/or the membrane.

5.3.3 ATP7B kinase phosphorylation requires various metals.

Kinases have different metal preferences. The majority of kinases utilize magnesium, but other kinases have been shown to use cobalt as a cofactor for phosphorylation. The metals act to stabilize ATP and/or create hydrogen bonding contacts in the ATP binding pocket. From previous work, casein kinase was shown to be a possible candidate as the ATP7B kinase, and this kinase can utilize cobalt as a substrate. To investigate the metal characteristics of the ATP7B kinase in *Sf*9 cells, the magnesium chloride in the phosphorylation buffer

was substituted with manganese chloride, cobalt chloride, EDTA (non specific metal chelator), or no additional metal was added. As shown in Figure 35, magnesium and manganese were interchangeable. The no metal and EDTA samples showed the phosphorylation is metal dependent, and the phosphorylation is not autophosphorylation (catalytic phosphorylation is magnesium dependent). Cobalt chloride also phosphorylated ATP7B, but not to the same efficiency of magnesium or manganese (Figure 35).

5.3.4 Determining the apparent Km for ATP and GTP for the ATP7B kinase

Previous *in vitro* phosphorylation experimental conditions required the addition of 1μM ATP to the phosphorylation buffer. These conditions were obtained for catalytic phosphorylation of ATPases, which generally have affinities in the nM range for ATP. To optimize the conditions for ATP7B kinase mediated phosphorylation, a range of ATP concentrations from 50nM to 700μM were utilized. It was determined that the apparent Km of the ATP7B kinase for ATP is ~50μM (Figure 36). GTP is also another substrate that can substitute for ATP, in some kinases. To determine if GTP can substitute for ATP, ATP7B was incubated with 1.3pmol [γ-^{32}P] ATP, with and without 50μM GTP. As seen in Figure 37 lane 1, the two bands corresponding to ATP7B are phosphorylated when the samples are labeled with [γ-^{32}P] ATP, but no cold ATP. This signal sets the maximum level of [γ-^{32}P] ATP incorporation into ATP7B. However, since the Km for ATP is 50 μM, the [γ-^{32}P] ATP is limiting. In lane 3, addition of 50μM GTP and the same amount of [γ-^{32}P] ATP does not decrease the signal, suggesting GTP is not being used for ATP7B phosphorylation. To more

dramatically emphasize the difference, the specific activity (ratio of hot to cold) was kept the same, but the overall total radioactivity and cold ATP/GTP was increased to 13.3pmol [γ-^{32}P] ATP with 500μM ATP/GTP. In lane 4, ATP7B was treated with 500 μM cold ATP with 13.3pmol [γ-^{32}P] ATP. This amount of ATP is above the Km for ATP. The signal for ATP7B in this lane is lower because cold ATP is in excess, therefore less total [γ-^{32}P] ATP is being used for ATP7B phosphorylation. In lane 2, 500 μM cold GTP was used with 13.3pmol [γ-^{32}P] ATP. The ATP7B signal is higher than lane 3 or 4, suggesting GTP is not a substrate for the ATP7B kinase. If the GTP had been used for phosphorylation, there would have been a decrease in the signal, as in lane 4, where cold ATP was added in excess. However, since the signal is higher, more [γ-^{32}P] ATP was used to phosphorylate ATP7B even though there was 500 μM cold GTP present. The signal is also higher than in lane 3 because the total amount of [γ-^{32}P] ATP is higher, although the specific activity is the same.

5.3.5 The ATP7B kinase phosphorylates ATP7B in plasma membrane, ER, and Golgi enriched fractions from *Sf9* cells.

In previous experiments, crude membrane preparations were used to phosphorylate ATP7B. However, to determine if ATP7B contained in the different membrane compartments are equally well phosphorylated, sucrose fractionation was performed in ATP7B expressed *Sf9* membranes [130]. Plasma, ER, and Golgi enriched membranes were phosphorylated in vitro. ATP7B from the plasma membrane enriched preparation had the highest level of phosphorylation (Figure 38). Whether ATP7B is better phosphorylated in this

compartment because of the availability of the kinase or if the protein is better folded or more enriched per protein is not known.

5.3.6 Partially purified kinase from Hek293 cell lysates phosphorylates N-ATP7B in vitro.

In Figure 33, we show that HepG2 lysate can be used to phosphorylate ATP7B. However, as shown in Figure 26, a kinase present in Hek293 cell lysate can phosphorylate N-ATP7B both *in vitro* and *in vivo*. Since culturing Hek293 cells is simpler and the cells grow faster, Hek293 lysate was used for phosphorylation of N-ATP7B unless otherwise indicated. To further purify this kinase, Hek293 soluble lysate was subjected to size exclusion chromatography, and fractions collected (Figure 39). Due to the number of fractions collected, a large scale phosphorylation schematic was developed. His-tag N-ATP7B was expressed in BL21(DE3) cells, and bound to nickel coated plates. His-N-ATP7B was phosphorylated in 96 well plates with fractions collected from Hek293 lysate. As shown by the autoradiography of phosphorylated His-N-ATP7B, fractions 8-11 were able to phosphorylate His-N-ATP7B (Figure 40, upper panel). The elution profile indicates the fractions were eluted from a small shoulder, and the mass of the kinase in the range of albumin. Arrows on the chromatogram indicate where the fractions that phosphorylated His-N-ATP7B were eluted from the column (Figure 39). These fractions were combined, and further purified on an anion exchange column. One sample, fraction 10, had the highest level of phosphorylation (Figure 40, lower panel).

5.3.7 Removal of copper from ATP7B decreases the level of *in vitro* phosphorylation of ATP7B in *Sf9* membranes.

In vivo, the regulation of ATP7B is dependent on the copper status of the cell. It has been shown with increased copper binding of the N-ATP7B, ATP7B undergoes conformation changes [96]. These changes are not just limited to the N-terminal copper binding domains, but affect the protein as a whole. It was shown in vitro, less ABD co-eluted with copper bound N-ATP7B than with apo-N-ATP7B. Conversely, no detectible N-ATP7B was co-eluted with ABD when N-ATP7B was copper bound [1]. These data suggest that the interaction of N-ATP7B and ABD is dependent on the copper binding status of the protein. Copper binding to the MBDs induces conformational changes that disrupt the interaction between N-ATP7B and ABD. ATP7B phosphorylation occurs when cells are exposed to copper, but eventually the phosphorylation returns to basal levels, when the copper containing medium is removed and replaced with basal media containing cyclohexamide for 5hrs [75]. Presumably, the intracellular copper levels return to steady state levels. Under similar conditions, ATP7B was shown to be re-localized back to the TGN [46]. For longer copper exposure, 24hrs, steady state is reached, with a subpopulation of hyperphosphorylated protein as well as basally phosphorylated protein.

To test whether hyperphosphorylation is directly dependent on the copper bound status of ATP7B, BCS treated ATP7B was *in vitro* phosphorylated. ATP7B containing *Sf9* membranes were treated with increasing concentrations of BCS, to strip bound copper, and subsequently tested for phosphorylation (Figure

41). It is not known how many coppers are bound to ATP7B expressed in Sf9 cells; however, there is sufficiently bound copper for monitoring catalytic phosphorylation.

At lower levels of BCS, 5 and 10 μM, the level of kinase mediated in vitro phosphorylation did not decrease, but slightly increased. More replicates may render the variation of phosphorylation negligible. At the same concentrations of BCS, 5 and 10 μM, it has been shown BCS only slightly decreases the level of catalytic phosphorylation [130]. With 100 μM, the level of kinase mediated phosphorylation decreased down to ~60% of the untreated sample. Similar to this result, at 100 μM BCS, catalytic phosphorylation was shown to be reduced to less than 60% of untreated samples [130]. In this in vitro system, both catalytic and kinase mediated phosphorylation can be observed. Results obtained testing the effect of BCS on the two different phosphorylations are consistent with idea that copper binding affects the regulatory and catalytic activity of ATP7B, suggesting the *Sf*9 membrane phosphorylation system used is a applicable model for studying the role of phosphorylation, either kinase mediated or catalytic, of ATP7B.

However, the effect of copper on the kinase can not be excluded. If the kinase is also regulated by copper or is dependent on copper for activity, copper chelation would also decrease the activity of the kinase resulting in less AT7B phosphorylation.

5.3.8 Phosphorylation of N-ATP7B is determined by the copper bound status.

From the in vitro phosphorylation of ATP7B, chelation of copper from ATP7B containing membranes was sufficient to decrease the level of phosphorylation. In the previous sections (sections 5.3.1 and 5.3.2), it was demonstrated ATP7B containing membranes are sufficient for kinase mediated phosphorylation, suggesting the kinase is associated with ATP7B at the membranes. It was important to determine whether BCS altered ATP7B such that the phosphorylation sites are not accessible or the activity of the ATP7B kinase is affected by BCS. To differentiate between these two cases, phosphorylation was performed on purified apo or copper bound MBP-N-ATP7B. Hek293 lysates were used to phosphorylate MBP-N-ATP7B. Before obtaining the soluble lysate, Hek293 cells were treated with 50 μM copper chloride for 1 hr before cell lysis. If the kinase needed to be activated directly by copper or some other factor, then the lysate from the copper treated cells should phosphorylate MBP-N-ATP7B more efficiently, unless the kinase phosphorylation is associated with a specific membrane compartment in vivo or copper changes the localization of the kinase. However, if the copper bound status of the N-terminal domain is important, then there should be a difference between the apo and copper bound protein. In Figure 42, apo-MBP-N-ATP7B (red) phosphorylation is reduced compared to that of copper bound MBP-N-ATP7B (green).

Interestingly, in vitro phosphorylation of apo protein was not inhibited. Phosphorylation with lysate from copper treated cells did not increase the level of phosphorylation, compared to that of basal lysate. This data suggests the copper bound status of N-ATP7B has an effect in the level of in vitro

phosphorylation, consistent with the idea that copper binding to the N-ATP7B induces conformational changes that expose the target of phosphorylation. However, the copper bound status is not the only decisive factor for phosphorylation because apo protein is also phosphorylated, albeit not as well. The effect of lysate from copper treated cells compared to basal lysate is not definitive. There is no further increase in the level of phosphorylation when MBP-N-ATP7B is treated with lysate from copper treated cells. If the ATP7B kinase is activated in the membranes, or the trafficking is altered by copper, then a change is not expected. In vivo, copper may have a greater effect on the kinase due to spatial and temporal control of the phosphorylation.

If the copper bound status of the isolated N-ATP7B is important for phosphorylation, it was not clear how ABD would affect the phosphorylation of apo-N-ATP7B. Since the ABD interacts with apo-N-ATP7B, it might interfere with the phosphorylation of apo-N-ATP7B. Apo-MBP-N-ATP7B and copper bound MBP-N-ATP7B was phosphorylated in the presence of purified ABD. As seen in Figure 43, phosphorylation in the presence of ABD greatly reduced the level of phosphorylation of MBP-N-ATP7B. Phosphorylation of apo-MBP-N-ATP7B was reduced from 60% to 40% of the maximal phosphorylation. This might not appear to be much of a reduction, but the copper bound MBP-N-ATP7B phosphorylation decreased to a similar level, from 100% to 40%. The ATP Binding domain decreased the level of phosphorylation of both apo and copper bound MBP-N-ATP7B.

5.4 Discussion

5.4.1 An endogenous kinase in *Sf*9 cells phosphorylates ATP7B

In *Sf*9 cells, we observe phosphorylation of ATP7B, which we conclude is a result of kinase mediated phosphorylation, since the D^{1027}>A mutant is also phosphorylated in this assay. The gene for the ATP7B orthologue is known in *Drosophila*, however not in *Spodoptera frugiperda*. Phosphorylation of ATP7B in Sf9 cells suggests perhaps there is regulation of the endogenous copper ATP-ase by phosphorylation. To characterize the ATP7B phosphorylating kinase, several experiments were conducted. Various phosphorylation conditions were used to try to see if the ATP7B kinase had special characteristics that would distinguish it from most kinases, and therefore make identification simpler. From previous work, copper dependent phosphorylation was reduced by a casein kinase inhibitor. However, from the metal dependence experiment, cobalt was not a good substitute for magnesium, suggesting that casein kinase was not the kinase. Also, this kinase is ATP dependent with an apparent Km of ~50μM for ATP, and does not utilize GTP for phosphorylation.

5.4.2 The ATP7B kinase is associated at the membrane.

From Figure 33, it was concluded that just the membrane fraction was sufficient for the phosphorylation of ATP7B in the membrane. This is also true for ATP7B containing HepG2 membranes (data not shown). Comparing lane 4 (Sf9 membrane with soluble lysate) and lane 6 (Sf9 membrane alone) of Figure 33, the intensity of the phosphorylated ATP7B is greater in the sample without the soluble lysate. Just by incubating with soluble lysate, the total number of proteins exposed to ATP has increased, decreasing the total available ATP for

ATP7B phosphorylation. Also, the lysate may contain phosphatases, which would decrease the overall phosphorylation compared to the membrane alone.

Phosphorylation of ATP7B in membranes suggests the ATP7B kinase can localize to the membranes. At the plasma membrane, there are peripherally associated proteins that interact noncovalently with either the membrane or the lipid bilayer. Treatment of ATP7B membranes with high salt did not abolish phosphorylation, which we concluded to mean the kinase was not completely stripped from the membrane, although the level of phosphorylation decreased (Figure 34). This may indicate the kinase is associated at the membrane with ATP7B or in close proximity. However, considering the ATP7B kinase is also found in the soluble fraction, the kinase may be modified by addition of a myristoyl fatty acid, glycosyl-phophatidylinositol, or farnesyl or geranylgeranyl groups which would allow the kinase to be soluble and localize to membranes.

ATP7B normally localizes to the TGN or vesicles, in most mammalian systems. However, in polarized HepG2 cells, ATP7B can traffic to the apical membrane (Figure 20, 21). It was therefore interesting to see that ATP7B was in the plasma membrane fraction of *Sf9* cells. Plasma membrane localization of ATP7B has also been previously seen in *Xenopus* oocytes, but whether there is a functional relevance in *Sf9* cells or in oocytes is unclear. The level of phosphorylation was highest in the plasma membrane enriched fraction (Figure 38), although there is less ATP7B at the plasma membrane [130]. This may suggest ATP7B is better phosphorylated at the plasma membrane because the ATP7B kinase is enriched there. If this is also the case in mammalian cells,

ATP7B would become phosphorylated at the canalicular membrane in polarized cells.

On the other hand, it is not known what percentage of recombinant ATP7B expressed in Sf9 is catalytically active, which would be indicative of a properly folded protein. Catalytically inactive protein is not as well phosphorylated by the kinase, although ATP7B from all the membrane fractions can be catalytically phosphorylated (Ruslan Tsivkovskii, unpublished data from Lutsenko lab). It is possible that the plasma membrane localized ATP7B is retained at the plasma membrane by phosphorylation and therefore could have a higher fraction of phosphorylated protein. Equal amount of membrane protein was used for the in vitro phosphorylation assay, but ATP7B per µg of membrane protein is not equal for each type of membrane [130].

5.4.3 The ATP7B kinase purifies from the soluble fraction of Hek293 cells

Fractions 8-11 eluted from size exclusion chromatography phosphorylated His-N-ATP7B in vitro, which we concluded to mean the kinase is contained in those fractions. This suggests the ATP7B kinase has an apparent molecular mass of ~40-70kDa. A similarly sized ~36 kDa protein was found to co-elute with ATP7B from Sf9 membranes (data not shown). Whether this protein is a kinase would need to be tested.

Although the ATP7B kinase fractionated from the size exclusion column phosphorylates His-N-ATP7B efficiently, the level of phosphorylation from the anion exchange fractionated samples is not as strong. The kinase should be more concentrated, however, although fraction 10 phosphorylates His-N-ATP7B

better than the other fractions, the signal is not as strong as the gel filtration samples, and there is a low background signal from fractions 11-14. It is possible that exposure to salt partially denatures the protein, thereby decreasing the efficiency of phosphorylation. However, as shown in Figure 34, salt does not dramatically alter the efficiency of kinase mediated phosphorylation in full length ATP7B, although this could be due to species differences, insect versus human. Also, the increase of the NaCl concentration could have been too shallow, causing the elution of the kinase from the anion exchange column to distribute to too many fractions. Another possibility is the kinase could be composed of more than one subunit, and separation by anion exchange causes the dissociation of the subunits, resulting in decreased phosphorylation. In spite of these possibilities, the ATP7B kinase was partially purified, and a protocol developed for the future isolation and identification of the ATP7B kinase.

5.4.4 Copper binding to the N-terminal domain influences phosphorylation.

There is limited data available regarding the effects of copper dependent phosphorylation of ATP7B. What is known is in regards to the trafficking of ATP7B. The data presented in this section suggest there is a correlation between copper binding, phosphorylation, and conformational changes in the ATP7B structure. Copper binding alters the secondary and tertiary structure of N-ATP7B [96]. The accessibility of specific copper binding domains are also altered [145]. The loops connecting the copper binding domains are rearranged, resulting in a decrease in disordered loops [96]. In parallel, interdomain interactions are disrupted, resulting in the dissociation of N-ATP7B and the ABD

[1]. Catalytic phosphorylation also has its own set of conformational changes [130] [219] [113], yet copper dependent phosphorylation causes further conformational changes. Copper binding affects phosphorylation, and phosphorylation affects the overall conformation of ATP7B.

Copper binding to the MBDs alters the connecting loop region of ATP7B, which may lead to greater exposure and accessibility of the site of phosphorylation or improve binding of the kinase, resulting in a higher probability of phosphorylation. Walker et al showed apo and copper bound N-ATP7B results in a different proteolysis pattern [145]. The resulting conformational change alters the inter domain interaction with the ABD. The data from Figure 45, however, are puzzling. A decrease in the amount of phosphorylation was not unexpected, since the ABD could bind to N-ATP7B, inhibiting access to the site of phosphorylation. However, the dramatic decrease in the copper bound protein was surprising. Copper bound N-ATP7B has a weaker interaction with ABD than apo protein. Nevertheless, the level of phosphorylation of copper bound N-ATP7B dropped to that of the ABD treated apo N-ATP7B. These experiments were performed with soluble protein. The copper bound status does alter the conformation of N-ATP7B, but perhaps the fold change in interaction of the ABD and N-ATP7B is not as dramatic in vitro to alter phosphorylation. In the full length protein, the two domains are constrained by the transmembrane domains. Changes in N-ATP7B could be amplified in the full length protein. The proximity/orientation of the ABD and N-ATP7B to each other could be changed

as the conformational changes are amplified throughout the entire length of the protein.

Copper binding of the MBDs in the N-terminal domain seems to have the greatest effect on phosphorylation. BCS treatment of ATP7B containing membranes decreased the level of phosphorylation, suggesting the chelation of copper from the MBDs causes a decrease in phosphorylation. This decrease is most likely due to loss of copper from the MBDs and not the activity of the kinase, although that can not be excluded. The experiments with purified soluble MBP-N-ATP7B showed that copper bound protein is better phosphorylated than apo protein, suggesting it is the conformational changes associated with copper binding that is important for phosphorylation. These structural changes cause rearrangements in the loops between MBDs, which may expose the phosphorylation site/ make the phosphorylation site(s) a better binding site for the kinase/ increase the possible target sites/ decrease the affinity for a phosphatase.

These experiments do not exclude the possible role of copper on the kinase activity. Copper treated lysate did not affect the phosphorylation of MBP-N-ATP7B. If the localization of the kinase changes with copper, then a copper effect would not be seen with this assay. Since ATP7B is an integral membrane protein that changes localization with copper, the localization of the kinase would also need to be changed. In vitro phosphorylation of plasma membrane enriched fractions resulted in a higher level of phosphorylation in ATP7B, which may suggest *in vivo*, this would also be the case. Increased copper may result in the

enrichment of the ATP7B kinase at the membranes that ATP7B is phosphorylated.

In this chapter we present data that indicate the kinase that phosphorylates ATP7B is a soluble protein that is also membrane associated and has specific metal and nucleotide requirements. This kinase is also present in Hek293 cells, and can be partially purified to phosphorylate His-N-ATP7B in vitro. Copper binding of the N-terminal domain of ATP7B is important for phosphorylation.

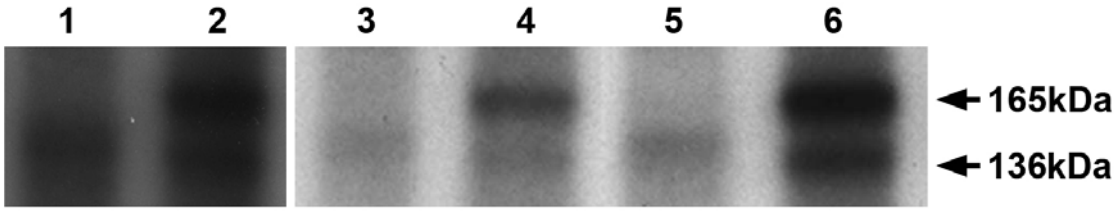

Figure 33: Phosphorylation of recombinant ATP7B expressed in Sf9 membranes. To optimize the kinase dependent phosphorylation of ATP7B in *Sf*9 membranes, protein was phosphorylated in the presence or absence of soluble lysate. Lane 1: Mock membrane + HepG2 soluble lysate, Lane 2: ATP7B membrane + HepG2 soluble lysate, Lane 3: Mock membrane + Sf9 soluble lysate, Lane 4: ATP7B membrane + Sf9 soluble lysate, Lane 5: Mock membrane, Lane 6: ATP7B membrane. ATP7B containing membranes are sufficient for the phosphorylation of ATP7B. Arrows indicate full length ATP7B and the degradation product.

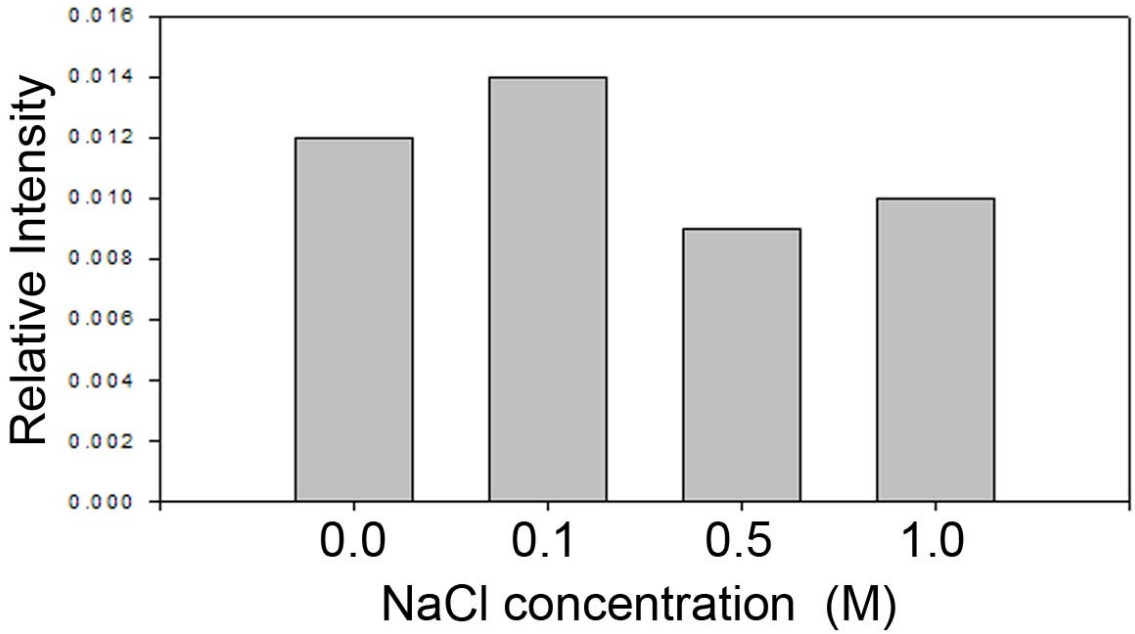

Figure 34: The ATP7B kinase in *Sf*9 membranes is tightly associated with the membrane. To investigate the degree of association of the ATP7B kinase and the Sf9 membrane, ATP7B containing membranes were incubated with a range of NaCl concentrations, 0-1.0M, and in vitro phosphorylation was evaluated by autoradiography. As shown here, incubation of ATP7B membranes with high salt does not completely inhibit phosphorylation of ATP7B, suggesting the ATP7B kinase is tightly associated with the membrane (n=1).

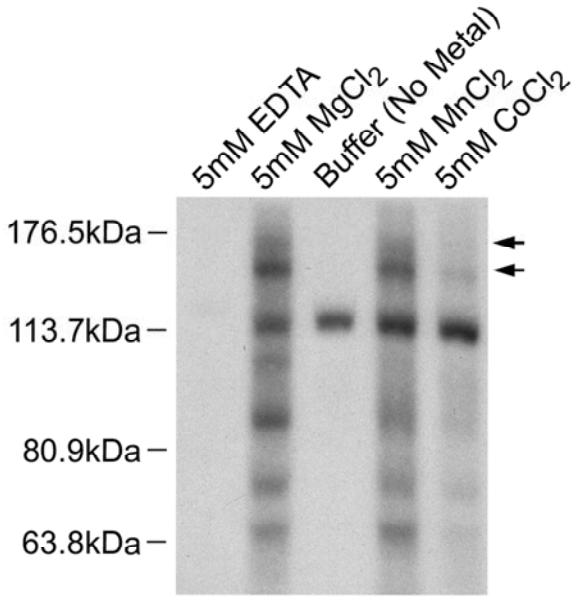

Figure 35: Metal dependence of the ATP7B kinase. To test which metals the ATP7B kinase has preference, different metals were substituted in the phosphorylation buffer for $MgCl_2$. Arrows indicate where ATP7B migrates in the autoradiograph. In the absence of metal or presence of EDTA, a nonspecific metal chelator, there is no phosphorylation of ATP7B. $MnCl_2$ is a good substitute; however $CoCl_2$ does not completely substitute for $MgCl_2$.

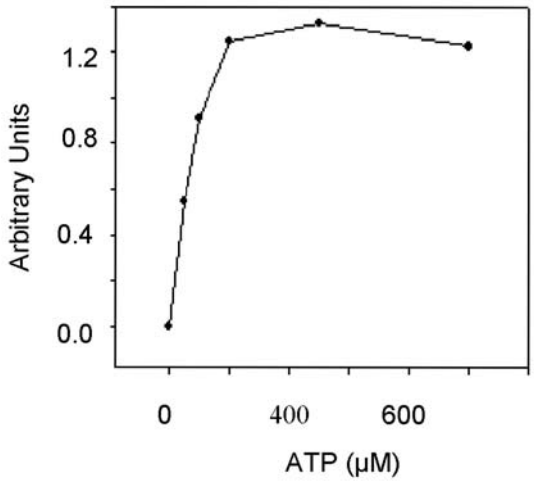

Figure 36: Apparent Km of the ATP7B kinase. To determine the amount of ATP to use for the in vitro phosphorylation assay, the apparent Km of the ATP7B kinase was tested. A range of ATP concentrations were used, from 0.05 to 700μM ATP. The apparent Km was calculated to be ~50μM ATP, and 100μM ATP was used in subsequent experiments.

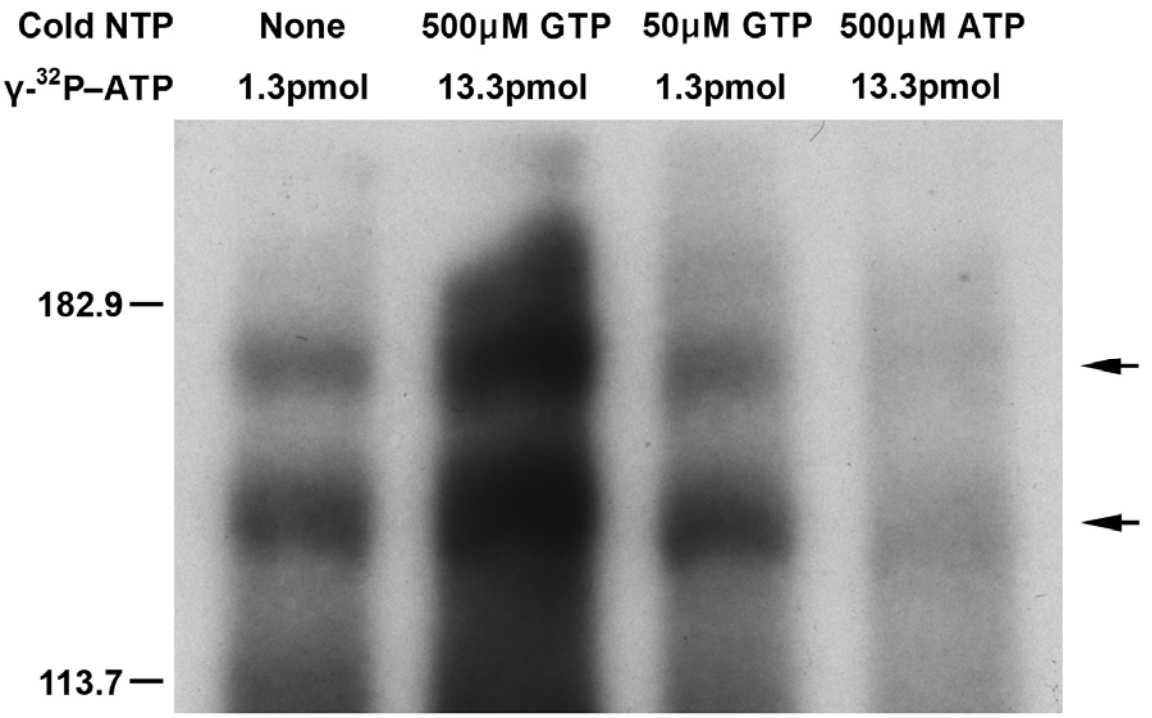

Figure 37: The ATP7B kinase utilizes ATP, but not GTP for phosphorylation. To further characterize the ATP7B kinase, the nucleotide specificity was investigated. In the above autoradiograph, the specific activity remained the same, but the total amount of cold ATP or GTP was varied as well as radioactive ATP. In the absence of cold ATP, only the radioactive ATP is used (lane 1). If the total amount of cold nucleotide is increased, the signal should decrease if that nucleotide is utilized because there is more cold nucleotide. If the signal increases, that means only the radioactive ATP is being used, and the cold nucleotide is not. Comparison of lane 2 to 4 indicates GTP is not utilized by the ATP7B kinase. Also, there is no difference between lane 1 and 3.

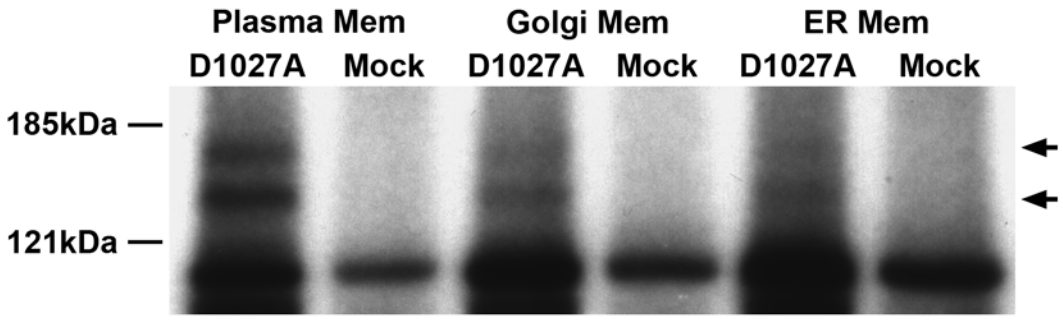

Figure 38: ATP7B is phosphorylated in Plasma membrane, Golgi membrane, and ER membrane enriched fractions. By sucrose fractionation, ATP7B was found in all three enriched membrane fractions of the plasma, Golgi, and ER membrane. To determine if there is a specificity of the ATP7B kinase for a particular membrane, the membrane compartments of Sf9 cells were enriched by sucrose fractionation and phosphorylated. ATP7B was phosphorylated in all three membrane fractions, but had the highest degree of phosphorylation in the plasma membrane enriched fraction. Arrows indicate the ATP7B bands in the autoradiograph.

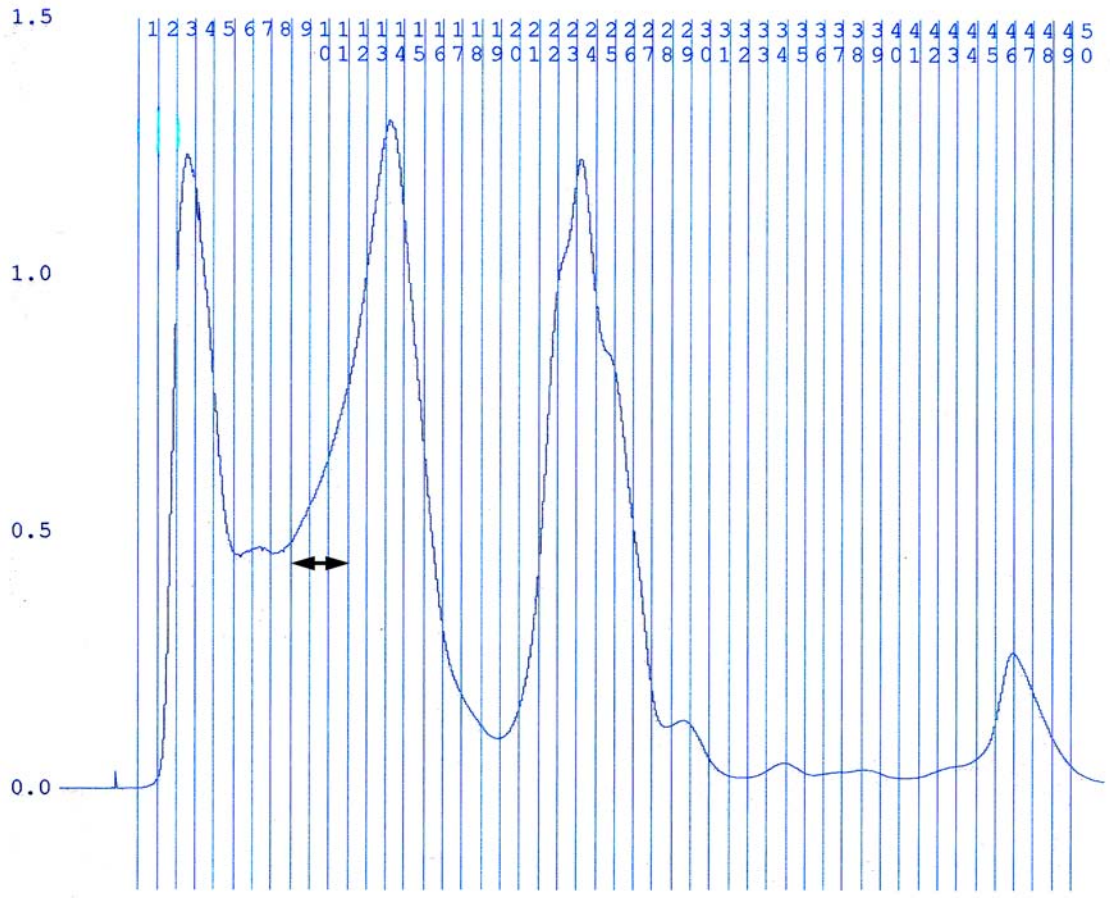

Elution Fraction	Gel Filtration Marker	
1	Blue Dextran	2000kDa
9	Albumin	67kDa
13	Ovalbumin	43kDa
15	Chymotrypsin	25kDa
17	RNase A	13.7kDa

Figure 39: Elution profile of Hek293 soluble lysate from a Superose 12 size exclusion column. Soluble lysate from Hek293 cells was separated on a Superose 12 size exclusion column using a Shimadzu FPLC system. The Y-axis is the 280nm, and the X-axis is the fraction collected.

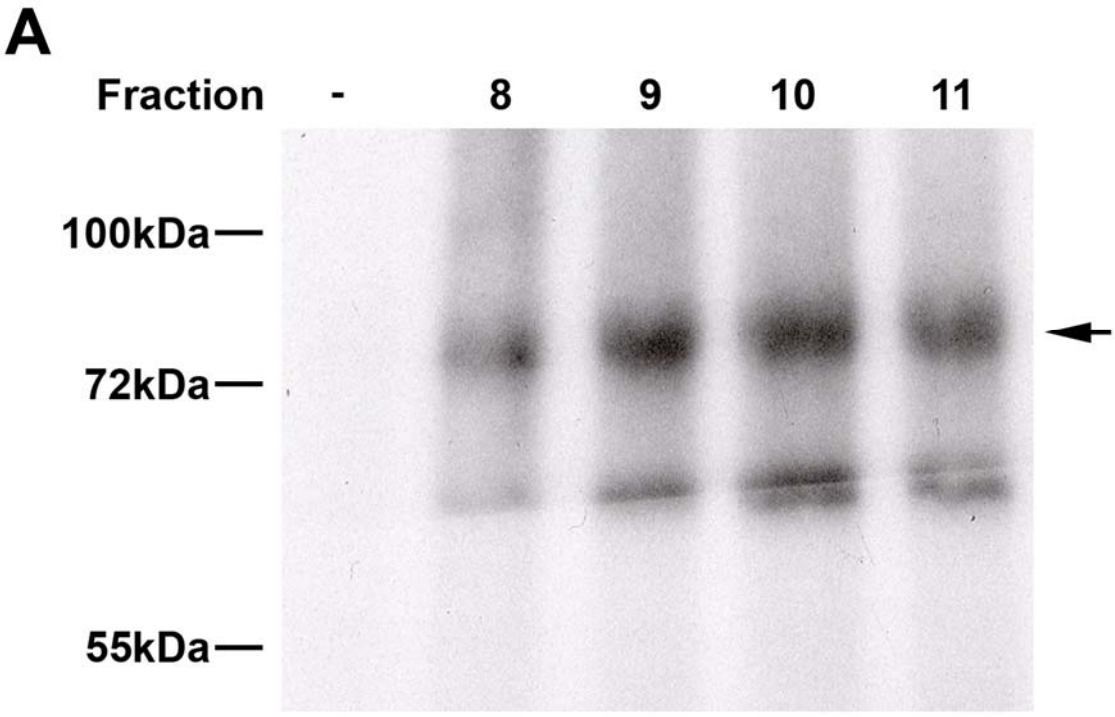
A
Fraction
-
8
9
10
11
100kDa
72kDa
55kDa

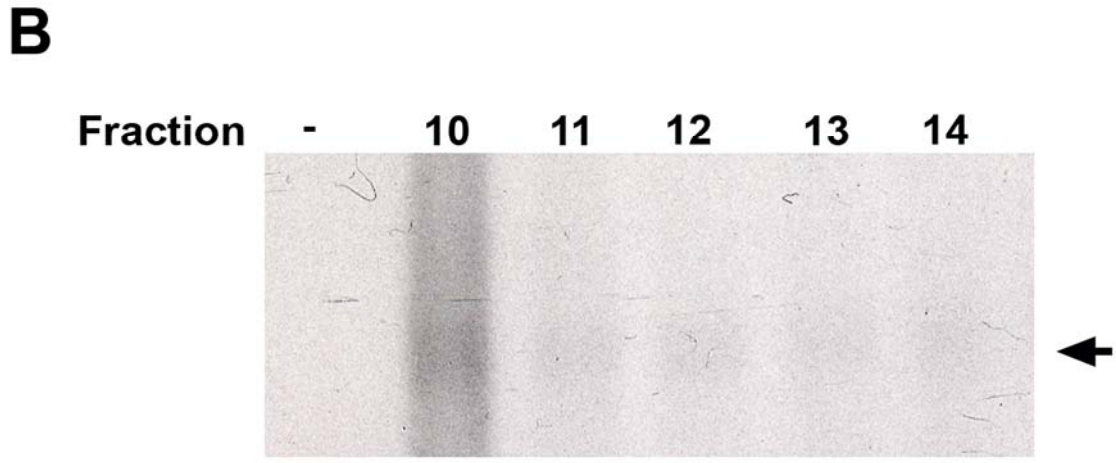
B
Fraction
-
10
11
12
13
14

Figure 40: Phosphorylation of His-N-ATP7B with fractionated Hek293 soluble lysate. His-N-ATP7B was bound on Nickel coated 96 well plates, and phosphorylated with fractionated Hek293 soluble lysate. (A) In the upper panel, fractions 8-11 from the size exclusion column successfully phosphorylated His-N-ATP7B. (B) These fractions were combined and further separated on a Shimadzu anion exchange column. Fraction 10 (lower panel) phosphorylated His-N-ATP7B with good efficiency.

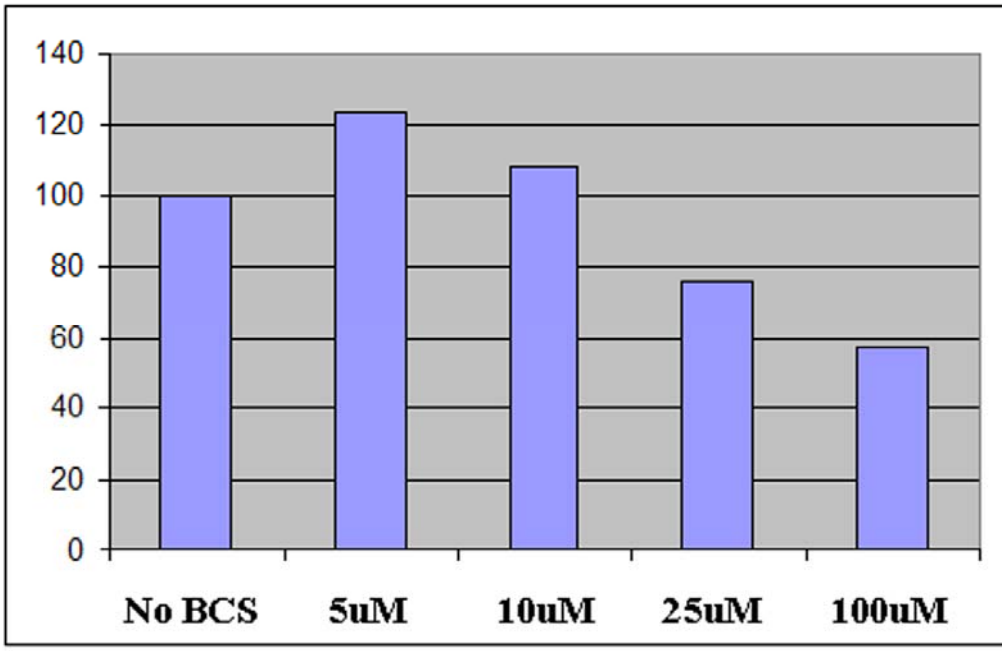

Figure 41: Treatment of ATP7B containing membranes with BCS decreases the kinase dependent phosphorylation. ATP7B containing membranes were incubated with a range of 0 to 100µM BCS to test whether copper bound protein is necessary for the kinase dependent phosphorylation. As shown in the graph, as the concentration of BCS increases, the level of phosphorylation decreases (n=1).

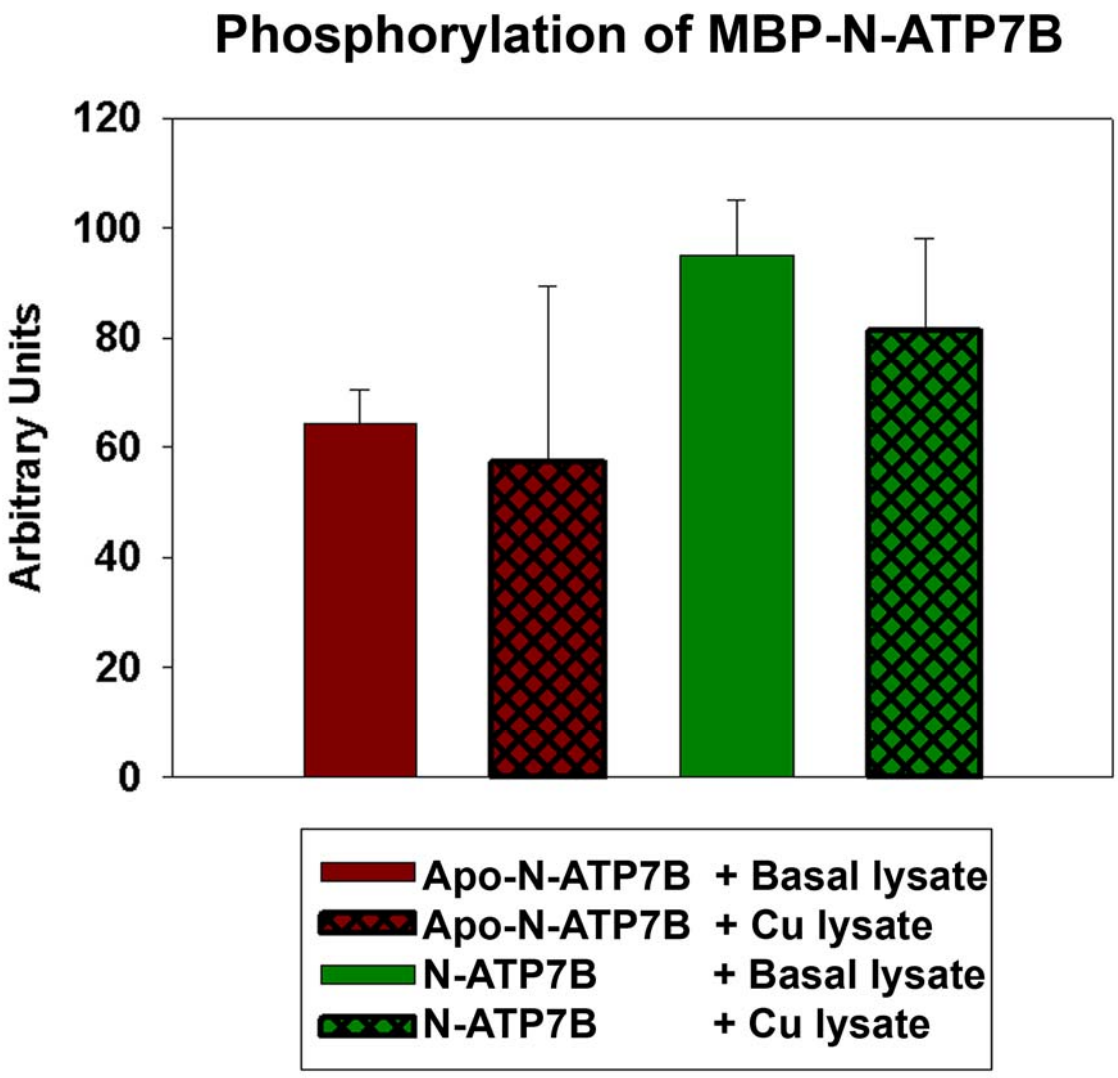

Figure 42: Phosphorylation of MBP-N-ATP7B increases with copper bound protein, but not copper treated cell lysate. In full length ATP7B, the in vitro phosphorylation was affected by treatment with BCS. To determine whether it was the kinase or ATP7B that was affected by the level of copper, apo and copper bound MBP-N-ATP7B was phosphorylated with basal Hek293 cell lysate or copper treated. As seen in the above graph, the copper bound status of MBP-N-ATP7B is the most important aspect of MBP-N-ATP7B phosphorylation.

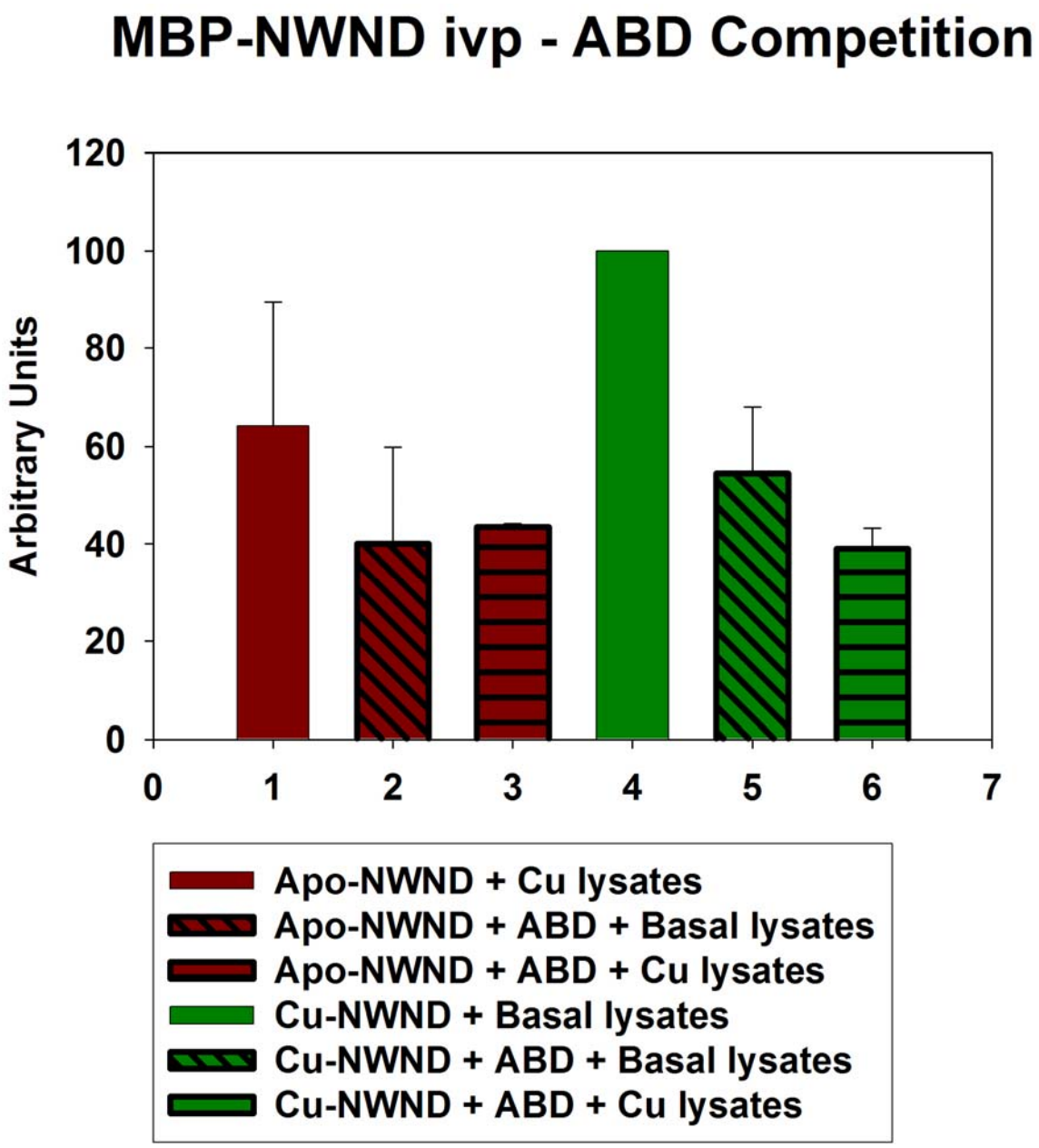

Figure 43: The presence of the ATP Binding Domain inhibits in vitro phosphorylation of MBP-N-ATP7B. To test whether the ABD affects the phosphorylation of MBP-N-NWDP in vitro, phosphorylation was performed in the presence of ABD. Surprisingly, in vitro phosphorylation of both apo and copper bound MBP-N-ATP7B was decreased.

AI Characterization of phosphorylation induced changes in ATP7B

A1.1 Introduction

ATP7B is a membrane protein composed of several domains that must work in concert to transport copper. As expected, copper binding to the metal binding domains of the N-terminus results in changes of the intramolecular interactions between the individual metal binding domains and the loops as well as the intermolecular interactions with the ATP binding domain and perhaps the transmembrane segments and the C-terminal tail. Kinase mediated phosphorylation of ATP7B is also thought to elicit conformational change. Accessibility to the site of phosphorylation is already dependent on the dissociation of the N-terminal domain from the ATP binding domain as well as rearrangement in the loops interconnecting the MBDs. Phosphorylation of ATP7B is expected to result in some form of change in ATP7B, most likely its structure or interaction with other proteins. In this study we wanted to address the question of whether there is an effect of copper dependent phosphorylation on ATP7B structure.

A1.2 Materials/Methods

A1.2.1 Phosphorylation of ATP7B containing *Sf9* membranes

The protocol is similar to that in section 4.2.4. In brief, 50 µg of ATP7B containing *Sf*9 membranes in phosphorylation buffer (20mM Bis-Tris propane, 200mM KCl, 5mM $MgCl_2$, 1mM DTT, 2mM AEBSF, EDTA free Protease Inhibitor

cocktail, 1mM orthovanadate, 100µM ATP pH 7.5) + 5µCi [γ-^{32}P]ATP (Perkin Elmer) is incubated for 30 minutes at RT.

A1.2.2 Precipitation of ATP7B in *Sf9* membranes

ATP7B containing membranes were treated with 100µM ATP and solubilized with 25% immunoprecipitation buffer (20mM Tris pH 7.5, 1mM EDTA, 0.1%SDS, 1%TritonX-100, 0.5%Deoxycholate, 1M NaCl) in water. These samples were then precipitated with 50% TCA for a final concentration of 10%. The precipitated protein was loaded onto a 7.5% Laemmli gel and western blotted with N-ATP7B#2 antibody (refer to section 2.2.1: Generation of the N-ATP7B antibody).

A1.2.3 Purification of ATP7B-His on Ni-NTA

ATP7B-His was originally phosphorylated as described in section 4.2.4. Phosphorylated ATP7B-His was centrifuged at 20,000xg and resuspended in His –tag purification buffer (PBS + 20 mM Imidazole + 2 mM AEBSF + EDTA free Protease Inhibitor Cocktail + 1% DDM). The solubilized protein was added to Ni-NTA charged with 50 mM $NiSO_4$, and equilibrated with His-tag wash buffer (PBS + 20 mM Imidazole + 2 mM AEBSF + EDTA free Protease Inhibitor Cocktail + 0.1% DDM). After incubation with lysate for 1 hour at room temperature, resin bound protein was washed then eluted with sample buffer, or just eluted from the resin without washes. Protein was run on 7.5% Laemmli gels, incubated with film, and the autoradiograph evaluated.

A1.3 Results

A1.3.1 Phosphorylation alters the solubility of ATP7B.

ATP7B is a P-type ATPase, and as such, undergoes conformational changes as part of the changes associated with ATP binding, catalysis, and release. From data concerning the ABD and N-ATP7B, these domains interact and the interaction should affect the conformation and catalysis of ATP7B. The data from Figure 41-43 suggests the phosphorylation of ATP7B depends on copper induced conformational changes. It is not clear if phosphorylation induces further changes in ATP7B, and whether these changes result in the trafficking of ATP7B.

One of the observations made when immunoprecipitating ATP7B from *Sf9* membranes is that the N-ATP7B#2 antibody efficiently binds to ATP7B. This antibody was used to clearly immunoprecipitate 5ng of ATP7B expressed in *Sf9* membranes, the main limitation due to detection by western blot with the ATP Binding Domain antibody (data not shown). Two nanogram amounts of protein have been used for detection by western blot analysis (data not shown). This facile immunoprecipitation of native ATP7B, however, disappears when immunoprecipitating native phosphorylated ATP7B. What was once detectable for nonphosphorylated protein is undetectable once ATP7B is phosphorylated, whether the N-ATP7B#2 antibody or ABD antibody was used (data not shown). To understand what the effect phosphorylation has on ATP7B, protein was treated with 100μM ATP and then resuspended in immunoprecipitation buffer. The samples were then precipitated with TCA, washed, and resuspended into sample buffer. After running on a 7.5% Laemmli gel and transferred onto PVDF, the samples were western blotted with the N-ATP7B#2 antibody. As seen in

Figure 44, WDNP is detectable in the sample not treated with ATP, but the sample incubated with ATP, there is no detectable ATP7B. It is not clear whether ATP treated ATP7B did not precipitate when treated with TCA, resuspend in sample buffer, or enter the separating layer of the Laemmli gel,, but no ATP7B was detected on the western blot. This is not an effect of N-ATP7B#2 antibody not recognizing phosphorylated protein. N-ATP7B#2 is able to recognize denatured phosphorylated protein (Figure 24B and 26B) by western blot analysis. Also, N-ATP7B#2 recognizes copper bound native ATP7B from Sf9 membranes (data not shown), which are already pre-loaded with copper [130]. The effect of free copper has not been tested on the antibody, however, no additional free copper other than trace amounts normally found in salts were used with the antibody.

A1.3.2 Phosphorylation obscures the C-terminal tail of ATP7B

In parallel, phosphorylation affects the binding of ATP7B-His onto Ni-NTA. As shown in Figure 24, ATP7B-His is highly expressed in Sf9 membranes, and purification of unphosphorylated His tagged protein facile. However, when phosphorylated ATP7B-His is added to Ni-NTA, the protein does not bind to the resin as tightly (Figure 45). After incubation with the resin, samples were washed with buffer and eluted from the resin with sample buffer. In parallel, protein was eluted from the resin after binding without washing the resin. In the autoradiography in Figure 45, there is no detectable phosphorylated protein that remained on the resin after the resin was washed (left lane). Some protein had loosely bound to the resin, because when the resin was not washed, protein

could be eluted from the resin. This curious behavior of ATP7B suggests that phosphorylation perhaps alters the conformation such that the C-terminal His-tag is partly obscured. In subsequent experiments, 2M-6M urea was added to the binding buffer, to partly unfold ATP7B to better expose the His tag (data not shown). Addition of urea to the binding buffer did improve the binding percentage of ATP7B that was eluted with sample buffer, but still only for those samples not washed. Histidine phosphorylation is another possibility for altered binding to Ni-NTA, however, phosphorylated histidines are acid labile [220]. ATP7B-His remained phosphorylated after TCA precipitation, treatment with urea, or when the protein was run on an acidic gel (data not shown) suggesting ATP7B-His may not be phosphorylated at histidines or at the His tag. The results from these experiments suggested phosphorylation alters the accessibility of the C-terminal His tag.

A1.4 Discussion

Phosphorylation of ATP7B elicits a conformational change within ATP7B. How phosphorylation changes ATP7B structure is uncertain. Precipitation of proteins with TCA in the presence of detergents such as 0.1% or higher SDS is inhibited [221]. The final detergent concentration in the IP buffer is 0.025% SDS, 0.0125% Deoxycholate and 0.25% Triton X-100. The reaction had 0.125% Deoxycholate which facilitates protein precipitation, and as can be seen in Lane 1 of Figure 44, the precipitation of ATP7B not incubated with ATP was not inhibited, suggesting the presence of 0.025% SDS did not significantly inhibit protein precipitation. Recognition of ATP7B by N-ATP7B#2 and ABD antibodies

by immunoprecipitation is also lost when ATP7B is phosphorylated (data not shown). Phosphorylated proteins are recognized by these antibodies on western blots, which are under denaturing conditions, as opposed to the more native conditions for immunoprecipitation. The antibodies are anti-sera that are polyclonal, generated against the N-ATP7B and ABD domains. So, loss of recognition by the antibodies suggests changes in the accessibility of epitopes in two separate domains of ATP7B that are otherwise exposed under denaturing conditions.

From the TCA precipitation experiment, precipitation of phosphorylated ATP7B is inhibited, suggesting ATP7B did not localize to the TCA insoluble fraction that can be resolubilized with sample buffer (20mM Tris pH 6.8, 2.7M urea, 3.6% SDS, 0.1% β-ME). Phosphorylated ATP7B could have remained in the soluble fraction after the addition of TCA, although SDS precipitates at the temperature used (4ºC), and Deoxycholate and Triton X-100 does not interfere with TCA precipitation. Alternatively, phosphorylation of ATP7B could lead to the aggregation of ATP7B, preventing re-solubilization of phosphorylated ATP7B. Also, if phosphorylation leads to oligomerization of ATP7B, this complex may not enter the separating gel efficiently due to the size of the complex and percentage of acrylamide in the Laemmli gel, since as a monomer, ATP7B is 165 kDa. It is not unheard of in vivo for proteins to form higher ordered structures, from dimers to large oligomers for efficient trafficking and signaling[222 223]. This would explain why the antibody might not recognize protein or why His-tagged protein would not bind to resin, because the epitopes are not available.

Alternatively, this might suggest the C-terminal loop of ATP7B is not readily accessible upon phosphorylation of ATP7B. If there are proteins that bind to the C-terminal tail after the protein is phosphorylated, such as the trafficking machinery, the His tag could be obscured and prevent binding to resin.

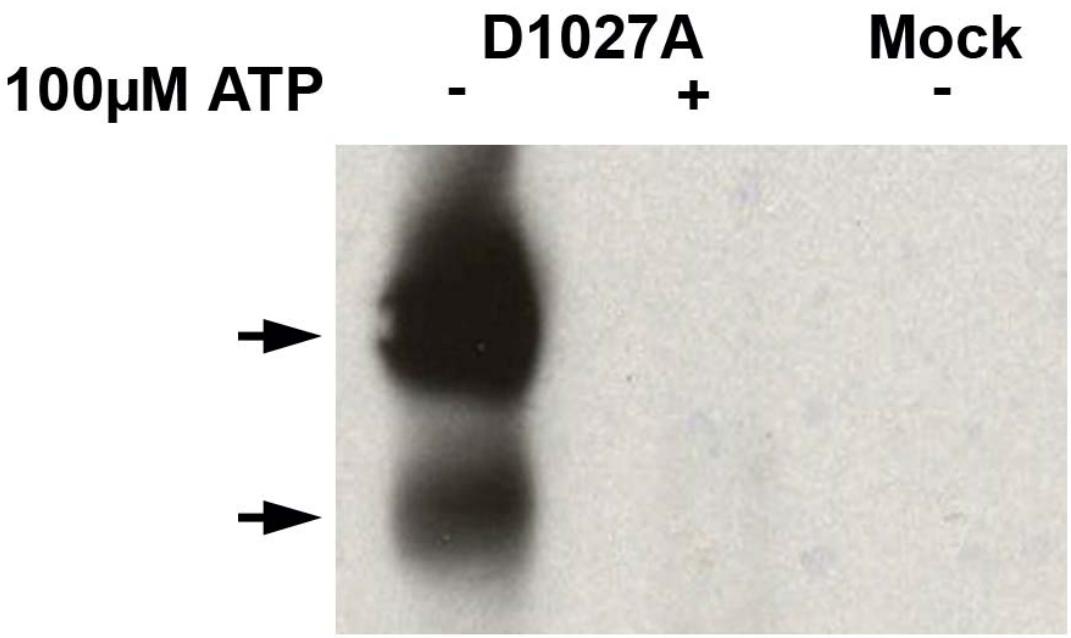

Figure 44: Phosphorylation decreases the solubility of ATP7B. ATP7B from *Sf9* membranes were treated with ATP and solubilized in immunoprecipitation buffer. Samples were precipitated with TCA (trichloroacetic acid) and run on a 7.5% Laemmli gel. Western blots were performed with the N-ATP7B#2 antibody. As shown in the figure, ATP7B not treated with ATP was detected by western blot. However, when treated with ATP, the protein was no longer detected by western blot analysis. This data suggests phosphorylation affects the structure of ATP7B.

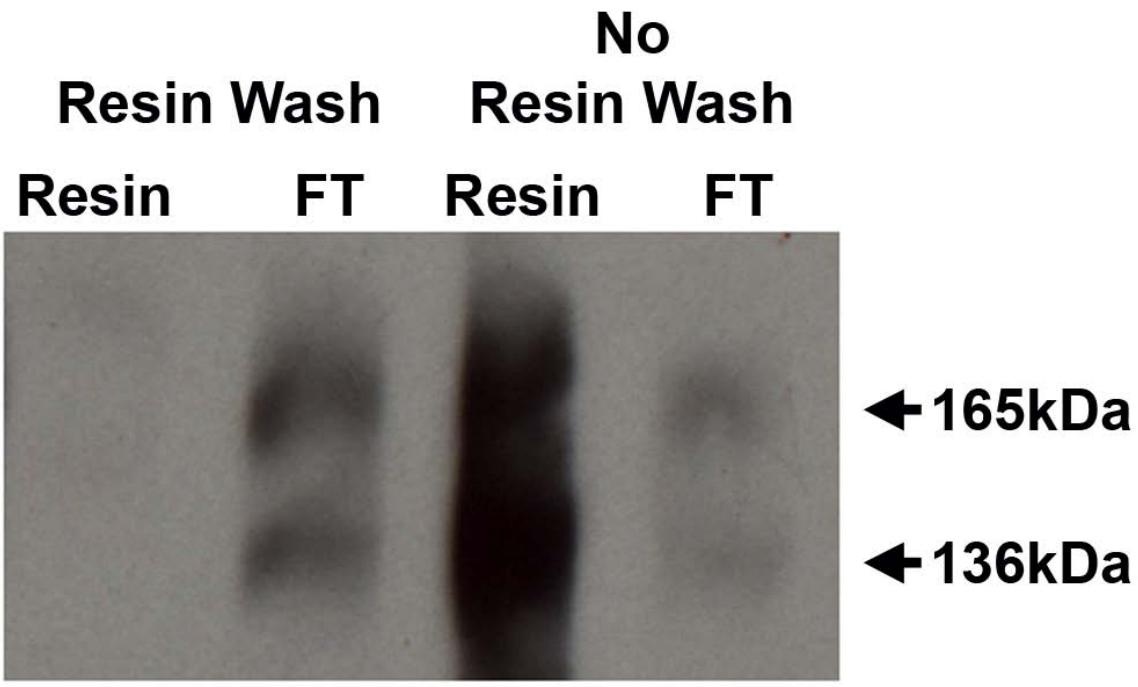

Figure 45: Phosphorylation of ATP7B-His disrupts binding to Ni-NTA. ATP7B-His was phosphorylated 20mM Bis-Tris propane, 200mM KCl, 5mM $MgCl_2$, 1mM DTT, 2mM AEBSF, EDTA free Protease Inhibitor cocktail, 1mM orthovanadate, 100µM ATP pH 7.5 + 5µCi [γ-^{32}P]ATP (Perkin Elmer) at room temperature for 30min, pelleted, solubilized in PBS + 20mM Imidazole + 2mM AEBSF + EDTA free Protease Inhibitor Cocktail + 1%DDM and incubated with Ni-NTA. The resin was either washed or not washed with wash buffer (PBS + 20mM Imidazole + 2mM AEBSF + EDTA free Protease Inhibitor Cocktail + 0.1%DDM), and protein was eluted with sample buffer. The autoradiograph of the samples suggest phosphorylation affects the structure of ATP7B-His such that it can no longer bind efficiently from Ni-NTA since mild washes result in the elution of the protein from the resin. In comparison, unphosphorylated ATP7B-

His can be purified on Ni-NTA using the same (data not shown) and similar (Figure 24A) buffer conditions.

AII Hepatocytes Contain Two Forms of Ceruloplasmin with Distinct Cellular Localization

A2.1 Introduction

The majority of serum copper, 60-70%, is bound to ceruloplasmin. Holo-ceruloplasmin is secreted into the blood, where it functions as a copper dependent oxidase. Ceruloplasmin oxidizes Fe^{+2} to Fe^{+3}, allowing iron binding to transferrin and subsequent uptake into cells. Through ceruloplasmin, copper metabolism and that of iron are connected. Copper is biosynthetically incorporated into ceruloplasmin in the trans-Golgi network [49, 224] in a poorly understood process that requires the functional activity of ATP7B. Inactivation of ATP7B disrupts copper delivery to the Golgi and results in apo-ceruloplasmin secretion into the blood. Apo-ceruloplasmin lacks catalytic activity and (in humans) is unstable. Low holo-ceruloplasmin (copper bound) levels in the blood [225] is one of the diagnostic symptoms of Wilson disease.

Serum ceruloplasmin is a 132kDa glycoprotein. The protein is composed of three homologous domains comprising a three fold axis of symmetry [226 227], resulting from the internal triplication of an ancestral gene [228]. This trimeric architecture is further verified by the crystal structure [226 227]. The exact amount of copper bound per protein is unclear and the stoichiometries reported in the literature vary. The crystal structure predicts three type I copper sites (one in each domain), the tri-nuclear copper cluster composed of one type II copper and a type III copper pair, for a total of six copper atoms[229, 230]. However, binding of a total 7 copper atoms per protein was also reported [231]. The seventh copper is

labile, and bound to a surface residue, His[426], which has pro-oxidant activity. This copper may not be required for enzymatic activity and could be exchangeable. Iron bound to ceruloplasmin is oxidized by the electron transfer from the type I copper atoms to the oxygen bound at the tri-nuclear cluster, for the reduction of O_2 to H_2O. *In vitro*, ceruloplasmin has been shown to also have cuprooxidase activity, but at a log affinity lower than for iron. Whether this has any biological consequence is unknown.

The secreted form of ceruloplasmin is produced primarily by hepatocytes in the liver, and a small fraction by monocytes/macrophages. There is also a GPI-linked C-terminal alternatively spliced form of the protein expressed in astrocytes[232]. Recently, hephaestin, a homologue of ceruloplasmin was identified, which has ferroxidase activity and is bound to the membrane by a single transmembrane domain. In tissues, ceruloplasmin is important for the mobilization of iron stores, while hephaestin plays a central role in dietary iron absorption in the intestine. The role of ceruloplasmin is evident from the phenotypic manifestation of aceruloplasminemia, a genetic disorder resulting from varied mutations in ceruloplasmin. In aceruloplasminemic patients, the very little to no active ceruloplasmin is associated with iron build up in tissues such as the liver and central nervous system [233].

Ceruloplasmin is well established in its importance in iron metabolism. Through ceruloplasmin, it is evident that copper has an important role in iron metabolism. However, whether ceruloplasmin plays a role in copper metabolism is not clear. As mentioned previously, cells maintain their copper homeostasis by

regulating the localization of ATP7B. Under low/basal intracellular copper, ATP7B resides at the TGN, delivering copper to proteins in the secretory pathway, such as ceruloplasmin. However, when the intracellular copper is elevated beyond the point of which is required by the cell, ATP7B traffics to a vesicular compartment, and in the liver, to the canalicular membrane to export the excess copper. It is not clear whether or not ATP7B transports copper into the vesicular compartment/canalicular membrane, or if vesicles are formed from a copper concentrated region of the TGN where ATP7B is localized. If ATP7B does transport copper in vesicles, the presence of a cofactor that will remove the copper as it accumulates in the vesicle would prevent inhibition of transport. ATP7A contains a longer extracellular loop in between TMS 1 and 2 which is rich in methionines and histidines. It is thought this loop is important for the removal of copper from the intramembrane site, and a possible reason for the increased turnover rate of ATP7A. ATP7B lacks this extracellular loop, and compared to ATP7A, ATP7B is not as efficient at transporting copper [81]. In vitro, transport of copper in ATP7B containing vesicles requires a chelator (Ruslan Tsivkovskii, unpublished data from Lutsenko lab). Although ATP7B utilizes ATP to transport copper against a gradient, removal of copper from the extracellular side when ATP7B releases it into the vesicle, similar to the release of copper to copper binding proteins in the TGN, may be important for efficient transport. We hypothesized since ceruloplasmin can bind up to 7 copper atoms per protein and is a known recipient of copper from ATP7B, ceruloplasmin would be a good

candidate to receive copper from ATP7B in the vesicles or at the apical membrane.

A2.2 Materials/Methods

A2.2.1 Cell Culture

Hek293 and HepG2 cells were purchased from ATCC. The cells were cultured in Minimal Essential Media, 10% Fetal Bovine Serum, and Penicillin/Streptomycin and incubated at 37°C with 5% CO_2.

A2.2.2 Western Blot Analysis

Hek293 and HepG2 cells were homogenized in a 1mL dounce (Wheaton) in Lysis Buffer (PBS, 2mM AEBSF, EDTA-free Protease Inhibitor Tablet (Roche), 1mM DTT). The sample was then diluted with Sample Buffer (20mM Tris, 2.7M urea, 3.6% SDS, 1% β-ME), and 50µg of the lysate was run on a 7.5% Laemmli gel. Protein was transferred onto Immobilon-P PVDF (Millipore) and blocked in 5% nonfat dry milk (Safeway) in PBS-T (PBS, 0.1% Tween20) at RT overnight. Antibody incubations were performed at RT for 1hr diluted in PBS-T. The goat anti-human ceruloplasmin anti-sera (cat# C0911) and secondary HRP-conjugated anti-Goat antibodies were purchased from Sigma. The chemiluminescence reaction was performed with SuperSignal West Pico (Pierce). Western blots were developed using Kodak BioMax MS film.

A2.2.3 Immunofluorescence

HepG2 cells were seeded to 25% confluency onto glass coverslips 48 hrs prior to treatment. For experiments with polarized HepG2 cells, cells were seeded at 50% density 72hrs before treatment. Cells were washed with PBS,

and incubated with media containing either 50μM BCS or copper for 3hrs. Before fixation with acetone (-20°C), cells were washed with PBS to remove traces of the media. Fixed cells were blocked overnight in Blocking Buffer (PBS, 1%BSA, 1%gelatin, 0.01% sodium azide) at 4°C. The next day, the Blocking Buffer was melted by incubation for 30min at 37°C. Cells were then stained with one or more of the following primary antibodies for 1hr at RT: anti-ceruloplasmin (Sigma, Bethyl Labs), anti-NATP7B#2, and anti-MRP2 (Kamiya Biomedical Company). The following secondary antibodies were used at RT for 1hr: AlexaFluor 488 Donkey anti-Rat, AlexaFluor 555 Donkey anti-Goat, AlexaFluor 488 Donkey anti-Mouse (Molecular Probes). Coverslips were mounted onto glass slides with Vectashield with DAPI (Vector Laboratories). Cells were imaged on a Zeiss LSM 5 Pascal confocal microscope and analyzed using the Zeiss LSM Imager.

A2.2.4 Partial Purification of ceruloplasmin

HepG2 cells constitutively secrete ceruloplasmin into tissue culture medium. Culture media incubated with HepG2 cells were taken and centrifuged in a Centricon 100 (Millipore). The two most abundant components in the media are BSA and ceruloplasmin (data not shown). All the components smaller than 100kDa were filtered through, including BSA. Ceruloplasmin, which is 130kDa, is remained in the Centricon 100, and was used for subsequent experiments requiring the addition of exogenous ceruloplasmin.

A2.2.5 Cell Surface Labeling

For labeling just the plasma membrane of HepG2 and Hek293 cells, cells are seeded as described above. The 12 well plate was placed on ice and the cells were washed with cold PBS. Cells were fixed with cold 4% Paraformaldehyde in PBS for 30min on ice. Paraformaldehyde (PFA) was used for fixation instead of acetone because under these conditions, cells are fixed but not permeabilized, whereas acetone permeabilizes the cells while fixing by dissolving lipids. Cells were further washed in cold PBS, and then blocked in Blocking Buffer II (PBS, 1%BSA, 0.25%gelatin) for 30min at 4°C. Next, ceruloplasmin antibody incubation was performed in Blocking Buffer II for 1 hr on ice. Cells are then processed as described above except Blocking Buffer II with 0.02% TritonX-100 (for membrane solubilization) is substituted for Blocking Buffer.

A2.2.6 Cell Stripping

Cells were grown on 10cm plates until confluent. Media was removed and the cells were washed twice with PBS, once with 100mM glycine pH 2.0, twice with PBS, and incubated in media with either 50µM BCS or copper chloride for 1hr at 37°C in 5%CO_2. Cells were then used for cell sorting.

A2.2.7 Flow Cytometry

Cells were grown on 10cm tissue culture plates until confluent. To detach the cells from the plate, cells were washed in PBS and trypsinized. 3mLs of 10% FBS in PBS was added to stop the trypsin reaction and cells were transferred into FACS tubes. Cells were further washed 2x with PBS and centrifuged for 5min at 4°C at 1500rpm. Cells were resuspended in 1mL of cold PBS.

Ceruloplasmin antibody (Bethyl Labs, cat# A80-124) was diluted in 500µl of 10% FBS in PBS and added to the cells for 30min at 4°C. Cells were washed,3 times with PBS and the incubation with the secondary antibody, AlexaFluor 488 Donkey anti-Goat (Molecular Probes), was performed as with the primary antibody, but in the dark. Cells were washed again 3 times in PBS and resuspended in 500µl of 1% PFA in PBS. Fluorescent labeling with antibodies were analyzed by flow cytometry on a FACSCalibur (BD Biosciences). Cells were gated by size and granularity to exclude debris and cell clumps (by measuring the forward and side scatter) and the intensity of fluorescence was measured. Generated data was then analyzed with a freeware program, WinMDI2.8.

As negative controls, the following conditions were used: 1)No antibody, 2)No primary antibody, 3)No secondary antibody, 4)Golgin97 staining (an intracellular cell marker) for extracellular flow cytometry (data not shown). Only single antibody staining was performed, to minimize the additional controls needed. Secondary antibody only negative controls were performed for every experiment.

A2.3 Results

In the liver, ceruloplasmin is the primary recipient of copper from ATP7B. As an integral partner of copper homeostasis to ATP7B, we wanted to investigate the interaction of ceruloplasmin with ATP7B by looking at the localization of the two proteins in copper limiting and excess conditions.

A2.3.1Western blot analysis of ceruloplasmin

To test the specificity of the ceruloplasmin antibody, western blots were performed on HepG2 and Hek293 cell lysates using ceruloplasmin antibodies from two different companies. Lysate from HepG2 cells showed a band at ~132kDa, but there was no corresponding band in Hek293 cells (Figure 46). Hek293 cell lysate was therefore used as a negative control for ceruloplasmin expression in further experiments.

A2.3.2 ATP7B and ceruloplasmin have different cellular localization in non-polarized HepG2.

To investigate the possibility that ceruloplasmin might play a role in copper export by accepting copper from ATP7B in vesicles, we compared the localization of ceruloplasmin and ATP7B by immunofluorescence upon the treatment with either 50μM BCS (a copper chelator) or copper chloride for 3 hours.

In the top panel of Figure 47, under copper limiting conditions, ATP7B has a perinuclear staining, whereas in cells treated with copper, ATP7B staining is more vesicular. HepG2 cells are relatively small cells compared to fibroblasts; the cells do not grow flat and therefore the cytoplasm appears small which makes imaging of vesicles difficult. Hence, three different panels are shown for the copper treated cells to provide a sampling of the ATP7B and ceruloplasmin staining in HepG2 cells. Ceruloplasmin has a vesicular staining pattern, consistent with it being in secretory vesicles. However, the ATP7B containing vesicles do not overlap with the ceruloplasmin containing vesicles. If ceruloplasmin is required for efficient ATP7B activity, this might suggest ATP7B

does not function in vesicles. However, it is more likely ceruloplasmin is not the copper sink for ATP7B in vesicles. These cells are also not polarized, which might affect the trafficking properties of ceruloplasmin.

There also appears to be staining that outlines the cell, for both BCS and copper treated cells. Since these cells were fixed with acetone, to determine cell surface staining, further experiments need to be done on unfixed cells. In the liver, ceruloplasmin is a known secreted protein. The staining of ceruloplasmin that we see could be ceruloplasmin fixed to the cell surface during acetone treatment. However, it has been reported that in the brain, astrocytes express an alternatively spliced transcript of ceruloplasmin that is GPI-linked. Although the predominant transcript for ceruloplasmin is for the secreted version in liver, an alternative transcript has been observed by Northern blot analysis in longer exposures[232, 234]. The possibility of a previously unreported observation of ceruloplasmin staining at the cell surface in hepatocytes was further investigated.

A2.3.3In addition to intracellular staining, ceruloplasmin localizes to the plasma membrane.

In previous experiments, by indirect immunofluorescence, the ceruloplasmin staining appeared to be at/near the plasma membrane. To further investigate whether this staining of ceruloplasmin was at the plasma membrane, cell surface labeling was performed on HepG2 cells. Staining for ceruloplasmin was performed on PFA fixed but non permeabilized cells. As seen in Figure 48, ceruloplasmin staining was seen at the cell surface.

Since this was a novel finding, it was important to verify ceruloplasmin localization to the plasma membrane by other techniques. Cell surface biotinylation was performed on HepG2 cells. If ceruloplasmin localizes to the plasma membrane, plasma membrane localized protein should be labeled with biotin, and bind/elute from a neutravidin column. Labeling of cells at 4˚C should prevent secretion of ceruloplasmin, and multiple washes of the cells should clear secreted ceruloplasmin. As seen by the western blot in Figure 49, ceruloplasmin was purified from a neutravidin column, indicating ceruloplasmin was labeled with biotin at the cell surface.

A2.3.4Ceruloplasmin is tightly associated to the plasma membrane of HepG2 cells.

As discovered above, a subpopulation of ceruloplasmin was found to localize to the plasma membrane. To examine changes in ceruloplasmin binding at the plasma membrane, extracellular flow cytometry was performed on HepG2 and Hek293 cells, the latter serving as a negative control. Extracellular flow cytometry measures the fluorescent intensity of cell surface labeling of a defined (gated) population of cells. Figure 50B illustrates the results for a negative signal, when cells are not labeled.

In the experiments for flow cytometry, cells are incubated with the ceruloplasmin antibody and subsequently, a fluorescently labeled secondary antibody. The presence of ceruloplasmin at the cell surface results in labeling of that particular cell, which can be measured. As seen in Figure 51, incubation with only the secondary antibody results in no cell labeling, results similar to

Figure 50B, where no antibody was used. Ceruloplasmin staining of HepG2 cells shifted the number of labeled cells to the right, where 84.4% of the cells are labeled for ceruloplasmin at the cell surface. There was no labeling of the plasma membrane for ceruloplasmin in Hek293 cells, consistent with the lack of staining in the Western blot (Figure 46)

An experiment was done to test if ceruloplasmin was non-covalently associated with the cell surface. The antibody for ceruloplasmin is not fixed to the protein until just before analysis by flow cytometry. In the normal course of the procedure, there are also numerous washes, so secreted protein is expected to be washed away. Nevertheless more stringent washes were done on HepG2 cells with 50mM glycine pH 2.0, to attempt to strip protein from the cell surface. As seen in Figure 51, the glycine wash did decrease the percentage of cells with bound ceruloplasmin at the cell surface from 84.4% to 25.1%. However, a significant number of cells remained that had ceruloplasmin bound at the cell surface, suggesting ceruloplasmin binding at the plasma membrane is very tight and is unlikely to be a result of non-specific interaction between secreted ceruloplasmin and the plasma membrane.

A2.3.5 Exogenous ceruloplasmin does not restore cell surface binding.

Binding to the plasma membrane of ceruloplasmin appeared to be specific, but it was unclear if the ceruloplasmin at the cell surface originates from secreted ceruloplasmin bound to a specific protein at the plasma membrane or whether there is a distinct membrane-anchored form of ceruloplasmin. Treatment of HepG2 cells with copper results in 93.3% (Figure 52B) of the cells

staining for ceruloplasmin, decreasing to 52.5% after treatment with 50mM glycine (Figure 52C). These two controls set the maximum and minimum percentage of cells stained. To monitor the reappearance of ceruloplasmin at the plasma membrane, HepG2 cells were treated with 50mM glycine to remove cell surface ceruloplasmin, and then incubated with copper for 30min, 1hr, and 3hrs (Figure 52, middle panel). The percentage of cells stained for ceruloplasmin increases over time, 66% after 30 min, 84.8% after 1hr, and 75.1% after 3hrs. These percentages are higher than cells treated with glycine (Figure 52C), but less than cells that were not treated with glycine (Figure 52B). The increase in the percentage of cells with cell surface ceruloplasmin after the glycine washes suggest the cells are still viable. Western blots were performed on the media from these cells, and after the 30mins, HepG2 cells do begin to secrete some ceruloplasmin (Figure 52H). However, the levels of secreted ceruloplasmin remain low and similar for the 30min, 1hr, and 3hr time points.

To test whether the addition of exogenous ceruloplasmin increases the number of cells with bound ceruloplasmin, glycine treated HepG2 cells were incubated with media containing 50mM copper chloride and partially purified ceruloplasmin. Incubating HepG2 cells with ceruloplasmin did not significantly alter the level of ceruloplasmin labeled cells, 73.9% (Figure 52G). This data suggests exogenous ceruloplasmin is not the source of the plasma membrane localization, since the percentage of labeled cells incubated with ceruloplasmin do not increase compared to cells allowed to recover in the presence of copper (Figure 52 D-F).

It would have been better if I had monitored cell surface biotinylation compared to the overall number of cells labeled with ceruloplasmin. With this method, I would have had a control for the ceruloplasmin present before stripping the cell surface that could be compared to the newly synthesized ceruloplasmin and the added exogenous ceruloplasmin.

In parallel to the glycine stripping experiments, we tested if exogenous ceruloplasmin can bind to the plasma membrane of Hek293 cells. As seen in Figure 53, there is no labeling for ceruloplasmin at the plasma membrane, either for the BCS or copper treated sample. As a control, the cells were treated with media containing 10%FBS (Figure 53, middle panel). Hek293 cells were also treated with media taken from HepG2 cells that contain secreted ceruloplasmin. Figure 53, lower panel, shows that incubation with exogenous ceruloplasmin had no impact on the cellular membrane staining for ceruloplasmin in Hek293 cells. These experiments reinforced the conclusion from the HepG2 experiments that exogenous ceruloplasmin may not be the source of ceruloplasmin at the plasma membrane.

A2.3.6 Ceruloplasmin traffics to the canalicular membrane in polarized HepG2 cells.

We observed that ATP7B and ceruloplasmin did not co-localize in ATP7B containing vesicles in un-polarized HepG2 cells (Figure 47). However, in polarized cells, ATP7B traffics to the canalicular membrane. Since ceruloplasmin localizes to the plasma membrane, it was interesting to investigate whether ceruloplasmin could also localize to the canalicular membrane. HepG2 cells

were polarized on glass coverslips, and stained for ceruloplasmin and MRP2, a canalicular membrane marker. As seen in Figure 54, in polarized HepG2 cells, ceruloplasmin stains in a vesicular compartment. There is also concentrated ceruloplasmin staining in ring like structures. This staining overlaps with the MRP2 staining suggesting that some ceruloplasmin could be localized at the canalicular membrane. Some ceruloplasmin is seen at the basolateral membrane, suggesting perhaps ceruloplasmin needs to transcytose before reaching the canalicular membrane. Preliminary triple staining with ATP7B, MRP2, and ceruloplasmin have been done in polarized HepG2 cells, however, there was significant background resulting from the secondary antibodies; it was difficult to determine if there was any co-localization (data not shown).

A2.4 Discussion

Ceruloplasmin is primarily associated with iron metabolism, since it is the major circulating ferroxidase. Its loading with copper in the TGN is dependent on ATP7B. Although loss of ceruloplasmin primarily affects iron metabolism, recent findings suggest ceruloplasmin might have a more active role in copper regulation. Ceruloplasmin has been shown to be expressed in the brain as a GPI–linked form [232], novel from the secreted ceruloplasmin expressed in the liver. In mice, this protein is expressed in mature Purkinje neurons with ATP7B, but not in Bergmann glia cells that express ATP7A. However, in ATP7B KO mice, the localization of ceruloplasmin-GPI alters to Bergman glia cells from the Purkinje neurons, which no longer express ATP7B [81].

A2.4.1ATP7B and ceruloplasmin do not co-localize in vesicles

ATP7B lacks a methionine and histidine rich extracellular loop between TMS 1 and 2 that is present in ATP7A which is thought to help with the release of copper from the transport channel. Once copper is released, ATP7B can complete the catalytic cycle, and reset to transport the next copper molecule (Figure 2B). Originally, we hypothesized ceruloplasmin may oxidize copper that have been transported by ATP7B into the vesicles, to increase the efficiency of ATP7B turnover, substituting for the lack of this metal binding extracellular loop. This turnover would be important for when copper is elevated to quickly export excess copper. However, ATP7B and ceruloplasmin did not colocalize in ATP7B vesicles when copper was elevated. The lack of colocalization may suggest ATP7B does not require a copper sink or that ATP7B does not transport copper into the vesicles. Work presented in this thesis suggests the vesicular localization may be part of ATP7B recycling; however, this does not exclude ATP7B transport into vesicles. To address this issue, ATP7B transport into these vesicles first needs to be measured. If Atox1 can be stained delivering copper to ATP7B and correlated with increased copper accumulation in vesicles in vivo, this would suggest ATP7B transports copper into vesicles. Ceruloplasmin staining was seen at the canalicular membrane, which means it can not be excluded as a copper oxidase participating in copper transport.

A2.4.2 Ceruloplasmin traffics to the canalicular membranes in polarized HepG2 cells.

From the immunofluorescence data, staining of ceruloplasmin to the plasma membrane for both polarized and unpolarized cells can be seen.

Ceruloplasmin is primarily a secreted protein. The purpose of this second class of ceruloplasmin is not clear. Localization of ceruloplasmin seems to be specific, and not a result of exogenous binding to the plasma membrane (Figure 52, 53). Membrane staining is reproducible by microscopy, cell surface biotinylation, and flow cytometry. One would argue the plasma membrane staining could be an artifact of staining. Ceruloplasmin is secreted into the blood through the basolateral membrane, but in polarized HepG2 cells, the majority of the membrane staining is at the apical membrane suggesting this is more than secreted ceruloplasmin rebinding to the cell surface.

In partially polarized HepG2 cells, ceruloplasmin staining at the canalicular membrane suggests the protein traffics to the apical membrane. Whether ceruloplasmin has a role at the apical membrane is not known. In the case of apical membrane staining, ceruloplasmin might facilitate export. In ceruloplasmin KO mice, copper accumulates in the liver even though ATP7B is present. There are several possibilities that might contribute to this accumulation. The liver is one of the primary recipients of copper, and therefore the intracellular copper might be slightly higher. Copper that would have been incorporated into ceruloplasmin and exported from the cell might result in the accumulation of the excess copper in the absence of ceruloplasmin. Compared to ATP7A, ATP7B is a slower copper transporter, with a lower turnover rate. It is possible that direct export of copper from the liver is not as efficient as copper incorporated ceruloplasmin.

Alternatively, ATP7B and ceruloplasmin might be working in concert for efficient export of copper. Ceruloplasmin and ATP7B both localize at the canalicular membrane. If copper transported by ATP7B either into subcanalicular vesicles or at the canalicular membrane was oxidized by ceruloplasmin, the turnover efficiency of ATP7B might increase. Whether these two proteins co-localize at the canalicular membrane still needs to be determined. It is thought ATP7B transports copper into the lumen of the TGN where ceruloplasmin acquires copper. No direct binding has been shown for ceruloplasmin and ATP7B, but it could be possible. However, direct binding may not be necessary at the canalicular membrane. Oxidation of the released copper in itself may be sufficient for increased turnover of ATP7B, since ATP7B binds Cu^{+1}, not Cu^{+2}.

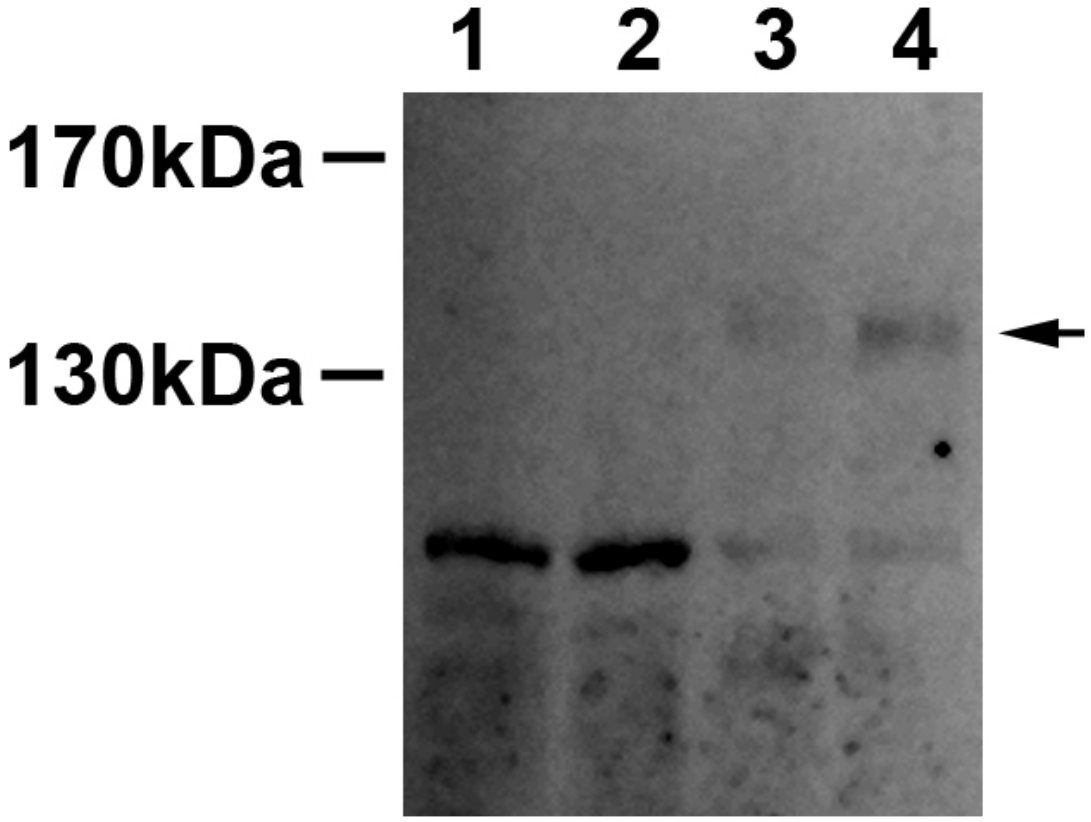

Figure 46: Protein expression profile of ceruloplasmin in Hek293 and HepG2 cells. To determine if ceruloplasmin was expressed in both Hek293 and HepG2 cells, Western blots were performed on total cell lysate. 50µg of lysate from 50µM BCS and 50µM copper treated Hek293 (Lane 1 and 2 respectively) and HepG2 (Lane 3 and 4 respectively) were run on 7.5% Laemmli gels, and transferred onto PVDF. A Western blot using anti-ceruloplasmin antibody (Sigma) was utilized for detection of protein. Only protein of the correct size was detected in HepG2 cells (arrow).

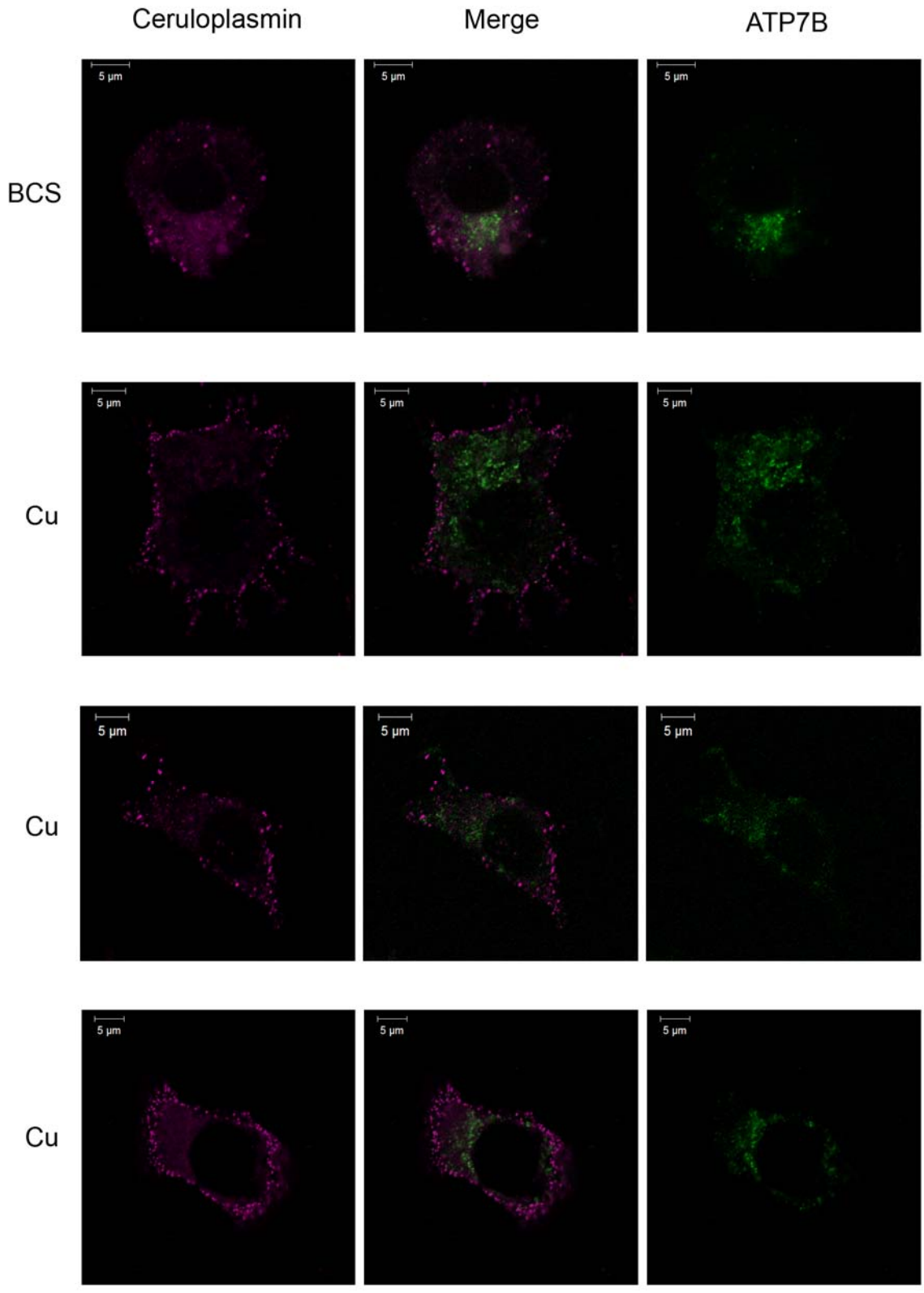
Ceruloplasmin
Merge
ATP7B
BCS
Cu
Cu
Cu
5 µm

Figure 47: Immunofluorescence staining of ceruloplasmin and ATP7B. For 50μM BCS treated cells, ATP7B is located in a perinuclear compartment. When treated with 50μM copper, ATP7B traffics to vesicles in HepG2 cells. Ceruloplasmin is known to localize to secretory vesicles, where it can then be released into the extracellular milieu. To determine if there is any overlap between the ceruloplasmin and ATP7B containing vesicles, immunostaining using antibodies against ceruloplasmin and ATP7B, co-localization studies were done. Cells were treated with 50μM BCS or copper chloride for 3hrs before fixation with acetone. In the top panel, there is small overlap between ceruloplasmin (purple) and ATP7B (green) in the TGN for BCS treated cells. In copper treated cells, the ATP7B (green) containing vesicles do not overlap with the ceruloplasmin (purple) containing vesicles. The copper treated samples are shown in triplicate.

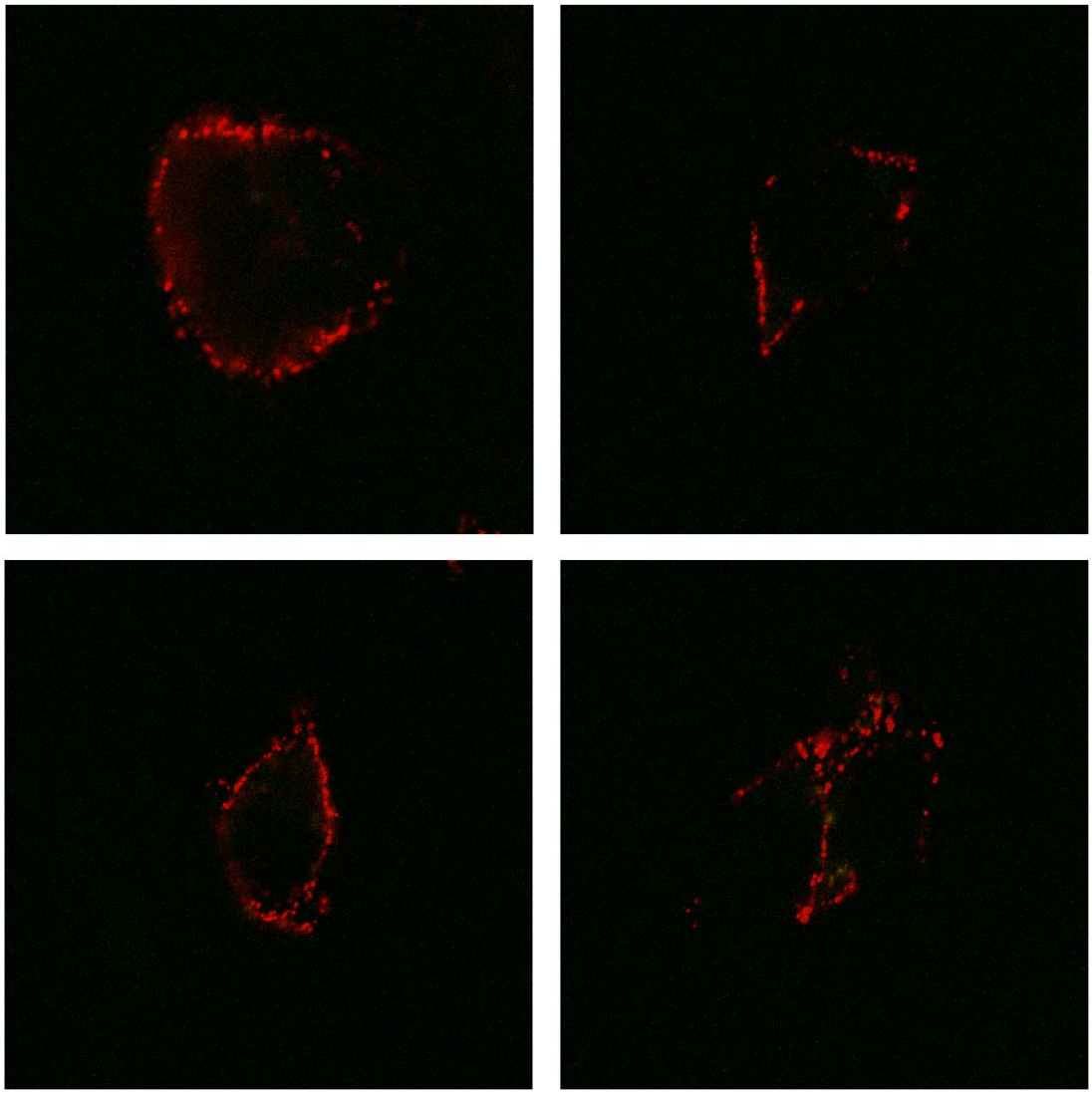

Figure 48: Cell surface staining of ceruloplasmin in HepG2 cells. Since ceruloplasmin is a secreted protein, cell surface staining was done in order to confirm ceruloplasmin (red) localized at the plasma membrane. HepG2 cells were immunostained with a ceruloplasmin antibody (Bethyl) on ice before fixation with acetone to stain for extracellular ceruloplasmin. Ceruloplasmin had a punctate staining that out lined the plasma membrane of HepG2 cells.

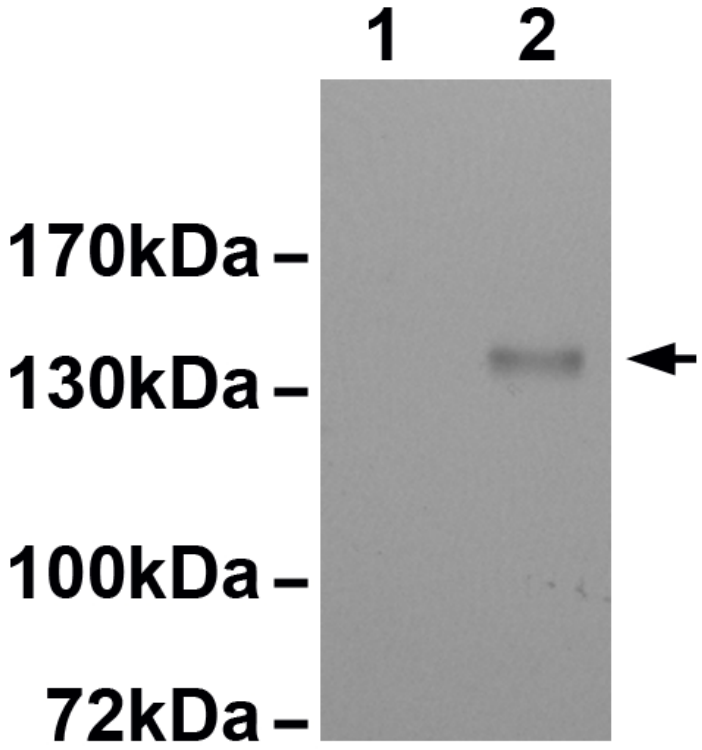

Figure 49: Ceruloplasmin is cell surface biotinylated. Protein was cell surfaced biotinylated, and purified on a NeutrAvidin column (Pierce). Eluted protein was run on a 7.5% Laemmli gel, and western blotted for ceruloplasmin. Lane 1: Hek293, Lane 2: HepG2. As shown above, cell surface biotinylated ceruloplasmin was purified from HepG2 cells only.

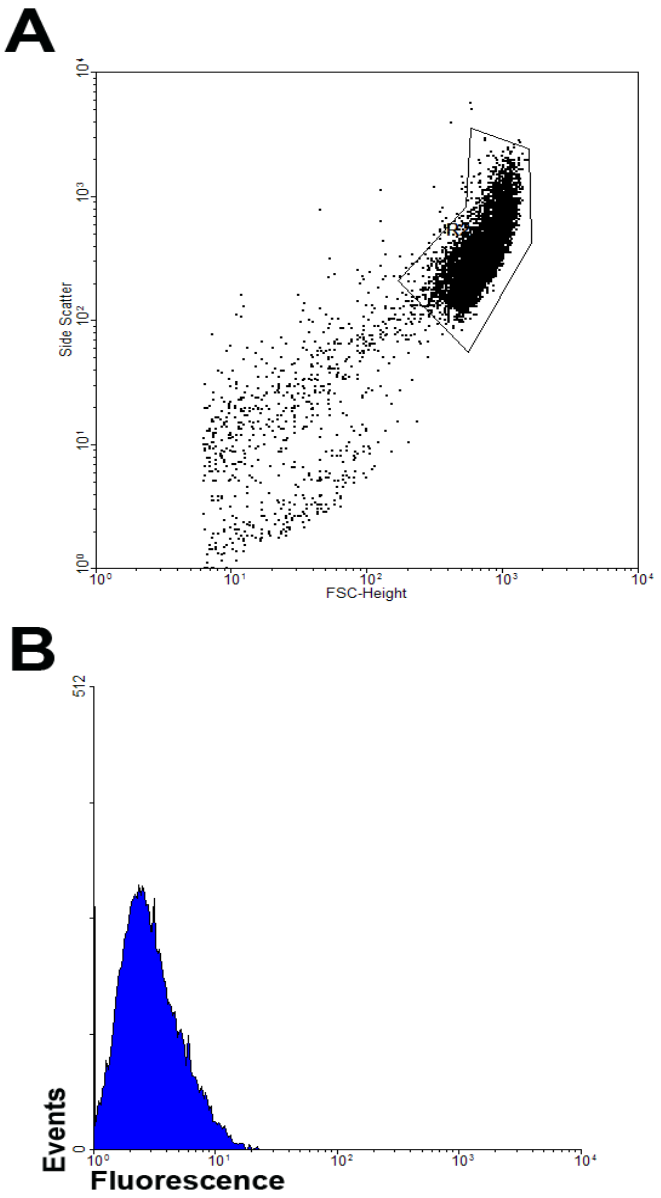

Figure 50: Gating of Hek293 and HepG2 cells for Flow cytometry. A) For all the Flow cytometry experiments, gating was done for size only. Forward and side scatter of cells were measured to determine intact, non clumpy cells. The outlined area indicates the population of intact cells, and those are the cells that were selected for analysis. B) Unstained HepG2 cells were tested for background fluorescence emission at 530nm, as a baseline control.

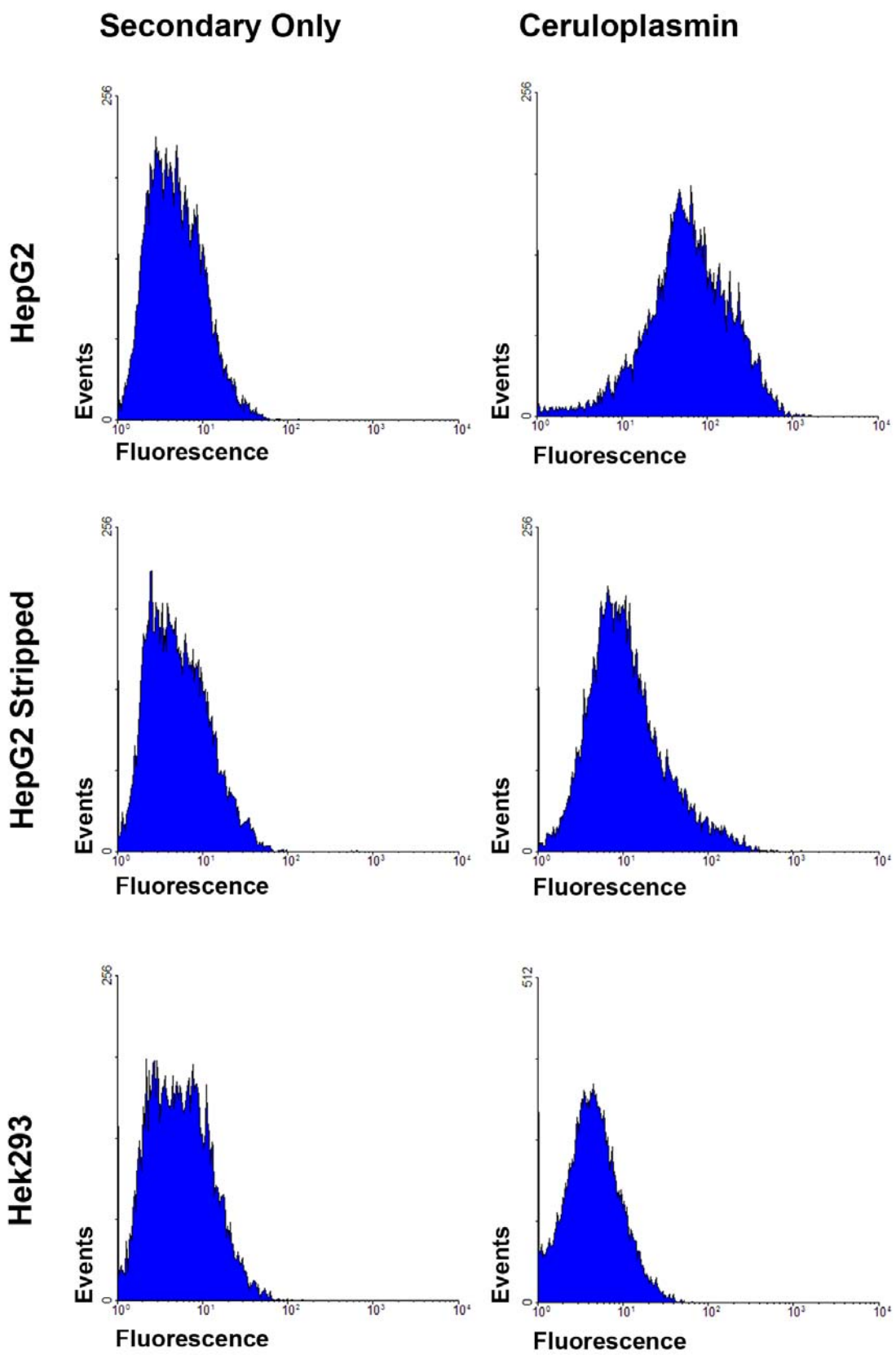
Secondary Only
Ceruloplasmin
HepG2
HepG2 Stripped
Hek293
Events
Fluorescence
256
512
0
10^0
10^1
10^2
10^3
10^4

Figure 51: Ceruloplasmin is tightly associated with the plasma membrane of HepG2 cells. To quantitate changes in the cell surface staining of ceruloplasmin on the cell surface, flow cytometry was used. Cells were stained with the ceruloplasmin antibody (Bethyl) and AlexaFluor488 Donkey anti-Goat secondary antibody (Molecular Probes), or just the secondary antibody as a control. The bottom panel illustrates no binding of ceruloplasmin in Hek293 cells. In the top panel, 84.4% of HepG2 cells were labeled for ceruloplasmin. To determine the degree of ceruloplasmin binding at the plasma membrane, HepG2 cells were treated with 100mM glycine pH 2.0 to strip peripheral membrane proteins. This harsh treatment decreased the population of cells that stain for ceruloplasmin, but a significant number of cells still stained for ceruloplasmin, suggesting ceruloplasmin is tightly associated to the plasma membrane.

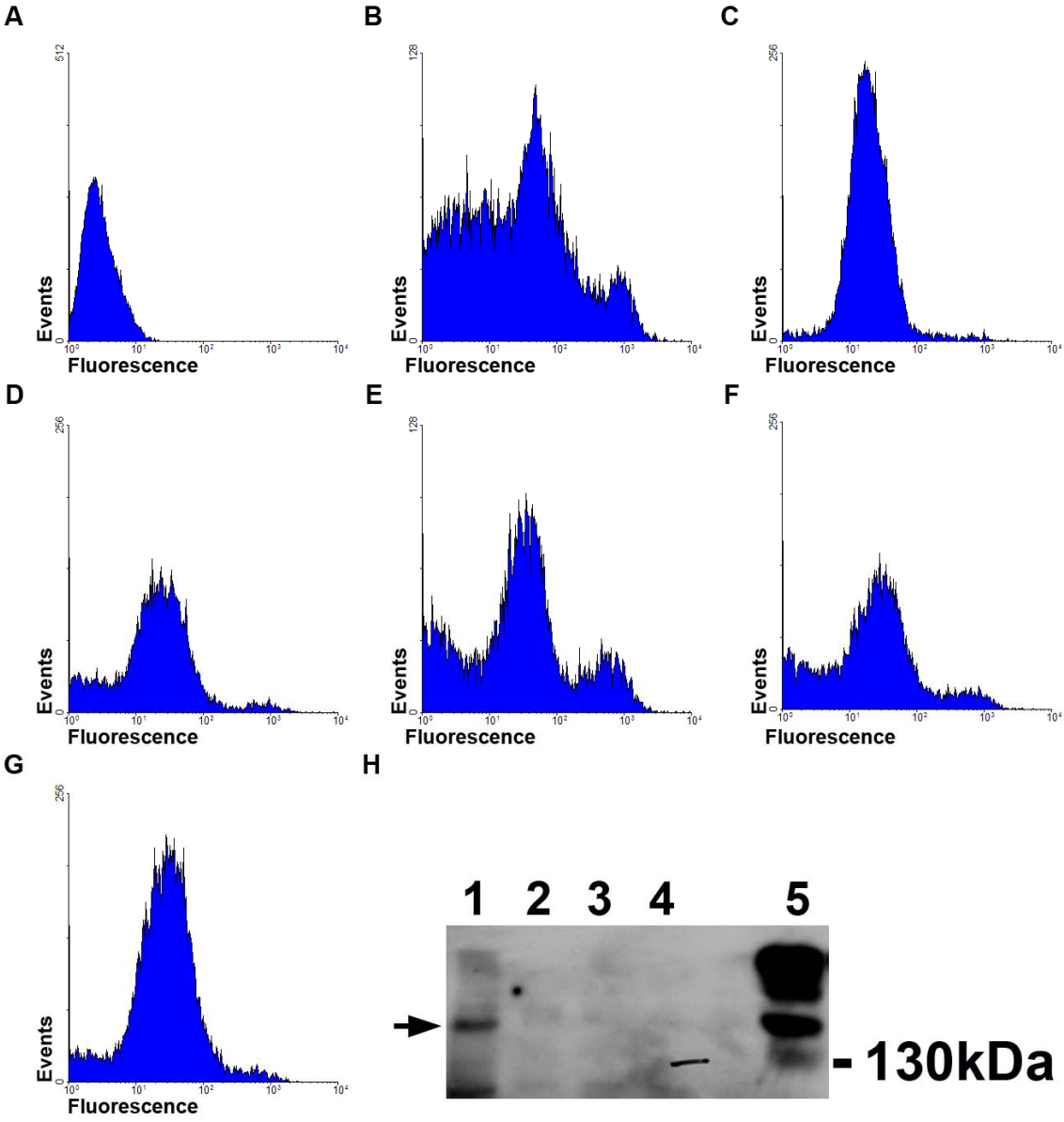
A
B
C
D
E
F
G
H
Events
Fluorescence
1 2 3 4 5
- 130kDa

Figure 52: Addition of exogenous ceruloplasmin to HepG2 cells does not promote binding of ceruloplasmin to the plasma membrane. To test whether the ceruloplasmin found at the plasma membrane is a result of binding to another plasma membrane protein, soluble ceruloplasmin was added to HepG2 cells stripped with 100mM glycine. Cells were stained for ceruloplasmin. A: No antibody, B: 50µM $CuCl_2$ for 1hr, C: 50µM $CuCl_2$ for 1hr → Strip, D: Strip → 30min 50µM $CuCl_2$, E: Strip → 1hr 50µM $CuCl_2$, F: Strip → 3hr 50µM $CuCl_2$, G: Strip → 1hr 50µM $CuCl_2$ + ceruloplasmin, H: Western blot of ceruloplasmin secreted into the extracellular milieu after copper treatment. Lane 1: total cell lysate from HepG2, Lane 2: Media collected from cells in part (D), Lane 3: Media collected from cells in part (E), Lane 4: Media collected from cells in part (F), Lane 5: Media used to incubate part (G). Post stripping, cells secrete very little ceruloplasmin (Lanes 2-4) into the media. There is very little change in the cells in (C) and (G), suggesting the ceruloplasmin at the plasma membrane is not coming from ceruloplasmin secreted into the media.

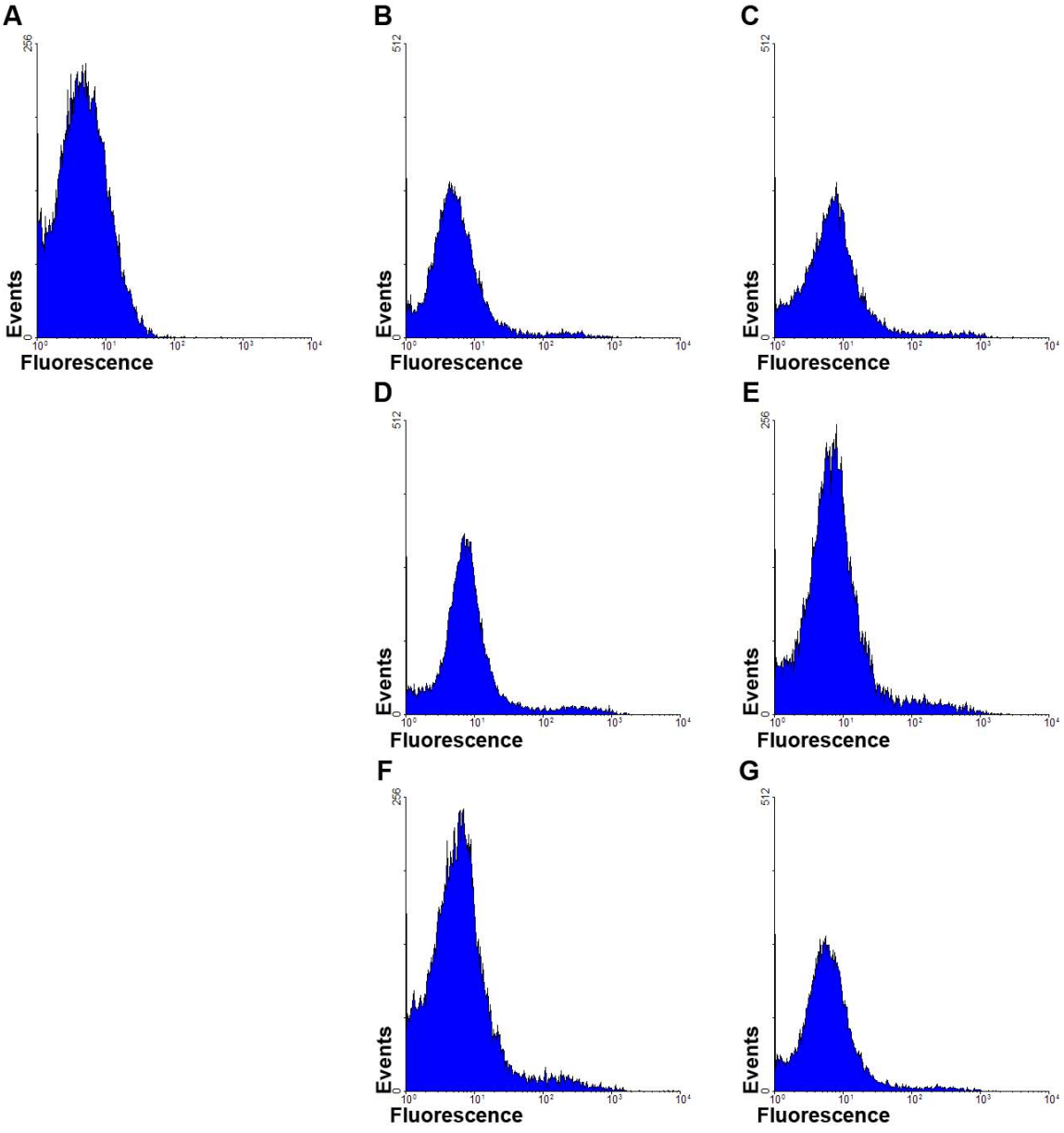
A
B
C
D
E
F
G
Events
Fluorescence

Figure 53: Ceruloplasmin does not bind to the plasma membrane of Hek293 cells. Hek293 cells were tested for cell surface binding of exogenous ceruloplasmin. A: Secondary Antibody only, B: Cells treated with 50µM BCS, C: Cells treated with 50µM copper, D: Cells treated with BCS and FBS, E: Cells treated with 50µM copper and FBS, F: Cells treated with BCS and ceruloplasmin, G: Cells treated with 50µM copper and ceruloplasmin. Addition of exogenous ceruloplasmin did not result in binding of ceruloplasmin to the cell surface of Hek293 cells. Interestingly, in this particular experiment, a small population of the cells had cell surface expression of ceruloplasmin.

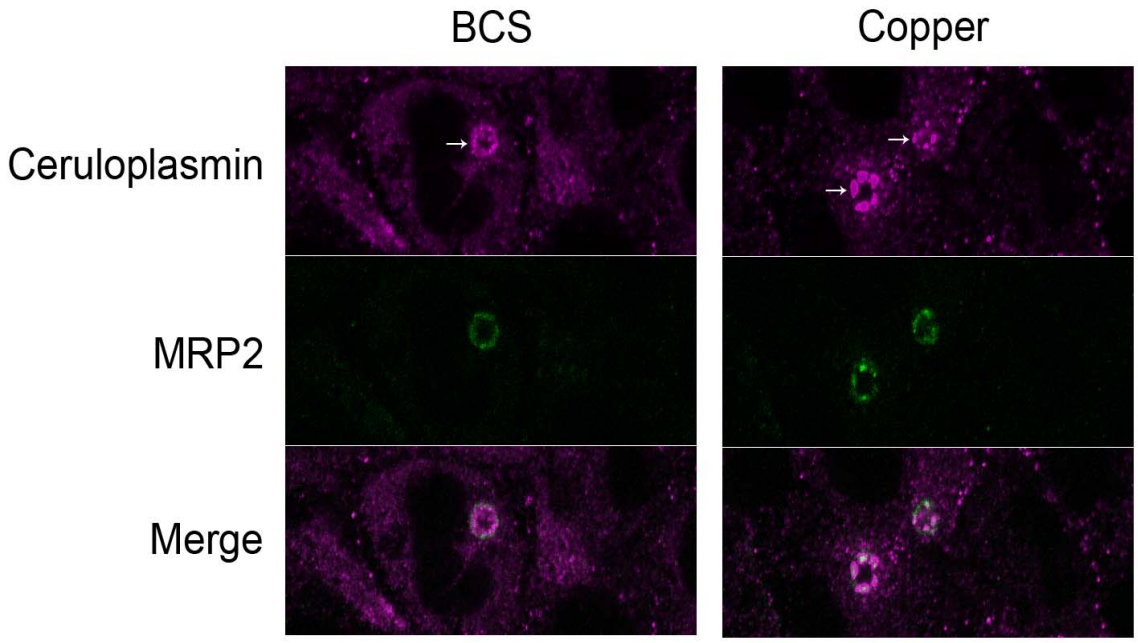

Figure 54: Ceruloplasmin localizes to the canalicular membrane in polarized HepG2 cells. In previous experiments with non-polarized cell, ceruloplasmin was detected at the plasma membrane. Whether ceruloplasmin is sorted unequally to the basolateral and apical membranes was investigated in polarized HepG2 cells. Polarized HepG2 cells were treated with 50µM BCS or copper and stained for ceruloplasmin (Bethyl) (purple) and MRP2 (Kamiya Biomedical Company) (green). MRP2 is a marker for the canalicular membrane, the liver equivalent of the apical membrane. Ceruloplasmin co-localized with the canalicular marker, but there was also staining surrounding and within the canalicular membrane, suggesting in polarized HepG2 cells, ceruloplasmin traffics to the canalicular membrane. Interestingly, there is some ceruloplasmin staining at the basolateral membrane (outline of cell in copper treated cells), perhaps due to incomplete polarization of HepG2 cells.

AIII Development of Yeast Two Hybrid Reagents

A3.1 Introduction

Since the cloning of ATP7B in 1996, other proteins involved in maintenance of copper homeostasis have since been discovered, such as CTR1, hephaestin, and COMMD1. However, there are still many unaccounted players in ATP7B regulation. The kinase(s) that regulate(s) ATP7B copper dependent phosphorylation as well as the phosphatase, the trafficking machinery that promotes relocalization to the vesicles and canalicular membrane, and proteins that regulate the hormonal response. To identify ATP7B interacting partners, a yeast two hybrid system was generated for screening a liver cDNA library.

A3.2 Materials/Methods

A3.2.1 Generation of N-ATP7B yeast constructs

N-ATP7B was cloned by PCR using pMC3 as a template, ligated into TOPO vector, and subcloned into pGBKT7 by digestion with NdeI and EcoRI. The primer set is:

NWND/NdeIFwd: CATATGCCAGAGCAAGAG

NWND/EcoRIRev: GGATCCTAACTAGTCGCTTGTGGTCGAGGT

Two constructs were generated, a full length N-ATP7B and ΔN-ATP7B lacking MBS 5 & 6. The ΔN-ATP7B was generated by complete digestion with EcoRI. DNA was transformed into DH5α (TOP10 cells from Invitrogen). Plasmid was purified by Qiagen plasmid preparation kit. Clones were sequenced for correct orientation with primers to the vector backbone.

A3.2.2 Constructs

The vectors and controls used were from Clontech. N-ATP7B and ΔN-ATP7B were cloned into pGBKT7, generating a DNA Binding Domain (DNA-BD) fusion construct, and serving as the bait. The bait will be used for screening with a liver cDNA library fused to an Activation Domain (AD), pACT2. A positive control pair used in this assay is pGADT7-T (encodes the T-antigen fused to the AD) and pGBKT7-53 (encodes for a DNA-BD fused p53 construct). Another positive control used is pCL1, which encodes for the full length GAL4.

A3.2.3 Transformation of AH109 yeast

The yeast two hybrid system and protocol used were from Clontech. AH109 cells were plated onto YPDA plates and the next day, colonies were inoculated into 1mL of YPDA (10g yeast extract, 20g peptone, and 0.10g adenine in 900mL + 100mL 20%glucose) and resuspended by vortexing and then transferred into 50mL of YPDA. Cell were then grown overnight at 30°C at 250 rpm. The next day, cells were transferred into 300mLs of YPDA to an OD_{600} = 0.2. The cells were grown for 3hrs at 30°C until OD_{600} = 0.5. The cells are pelleted and resuspended in 2mL of 0.1M LiAc in TE (100mM Tris, 50mM EDTA pH 7.4) and incubated for 10min at RT. 1µg of each plasmid and 100µg of freshly denatured sheared salmon sperm DNA were added to the 100µl of yeast, and mixed. Additionally, 600µl of 100mM LiAc + 40% PEG 3350 in TE were added, mixed, and incubated at 30°C for 30min. Cells were heat shocked by adding 70µl of DMSO, then mixed by inversion, and incubated for 15min at 42°C. The cells were then placed on ice for 2min, centrifuged, and the supernatant

removed. The pellets were washed and resuspended in 0.5mL TE. 100µl of the transformed cells were plated onto various plates, DO-His-Trp-Leu, Do-Trp-Leu, DO-His-Trp, DO-His, DO-Trp, and YPDA.

A3.2.4 Optimization of Colony growth

To eliminate growth of colonies on plates due to autoactivation, combinations of various constructs were grown in the presence of 3-AT (3-amino-1,2,4-triazole), ranging from 1µM to 5µM 3-AT in the different DO media. Plates were observed for colony growth everyday, up to eight days.

A3.2.5 Protein Expression of N-ATP7B

The N-ATP7B and ΔN-ATP7B were transformed and grown in AH109 cells as described above. Yeast were pelleted and resuspended in complete cracking buffer (8M urea, 5% w/v SDS, 40mM Tris pH 6.8, 0.1mM EDTA, 0.4mg/mL bromophenol blue, 0.1% β-mercaptoethanol, complete protease inhibitors (Roche), 1mM AEBSF). ~100µl of ~0.45 micron silica glass beads were added to the samples, and vortexed. The lysate was loaded onto 7.5% Laemmli gels, and western blotted with N-ATP7B #2 antibody at 1:10,000 and Donkey anti-Rat HRP at 1:10,000.

A3.3 Results

A3.3.1 Generation of N-ATP7B and ΔN-ATP7B pGBKT7 constructs.

N-ATP7B and ΔN-ATP7B were cloned into pGBKT7, the yeast two hybrid DNA Binding Protein fusion vector. To check for expression, AH109 transformed cells were lysed with 0.45 micron silica glass beads, and run on a Laemmli gel.

The sample was western blotted with N-ATP7B#2 for detection of protein. As shown in Figure 55, both constructs express in yeast.

A3.3.2 Optimization of N-ATP7B and ΔN-ATP7B growth on plates.

Empty pGBKT7, N-ATP7B and ΔN-ATP7B transformed AH109 cells were grown on YPDA and DO-Trp-His plates. Colony growth on the medium stringency plates, DO-Trp-His, was not expected. However, due to autonomous activation, the lack of histidine did not inhibit growth (Figure 57). The same was true for pACT2 co-transformed cells on DO-Leu-Trp-His plates (Figure 57B, left two columns). In order to reduce the false negative background from autonomous activation, DO plates were made with 3-AT. MSK1, a positive control for activation of the GAL4 promoter, was used to determine the concentration of 3-AT to inhibit autonomous activation without inhibiting positive signal. A range from 1μM to 5μM 3-AT was used to screen for reduction in the number of colonies. As seen in Figure 56, 1μM 3-AT was enough inhibitor to not prevent a reduction of colonies, whereas in higher concentrations, colony growth was inhibited. Subsequently, this concentration was used in the DO plates. As seen in Figure 59 (A & B right column), 1μM was sufficient for the inhibition of autonomous activation.

A3.4 Future Directions

The yeast two hybrid system was developed to screen for possible interacting partners with the N-ATP7B. In the future, the N-ATP7B and ΔN-ATP7B can be used with a liver, brain, or kidney cDNA library to identify novel interacting partners.

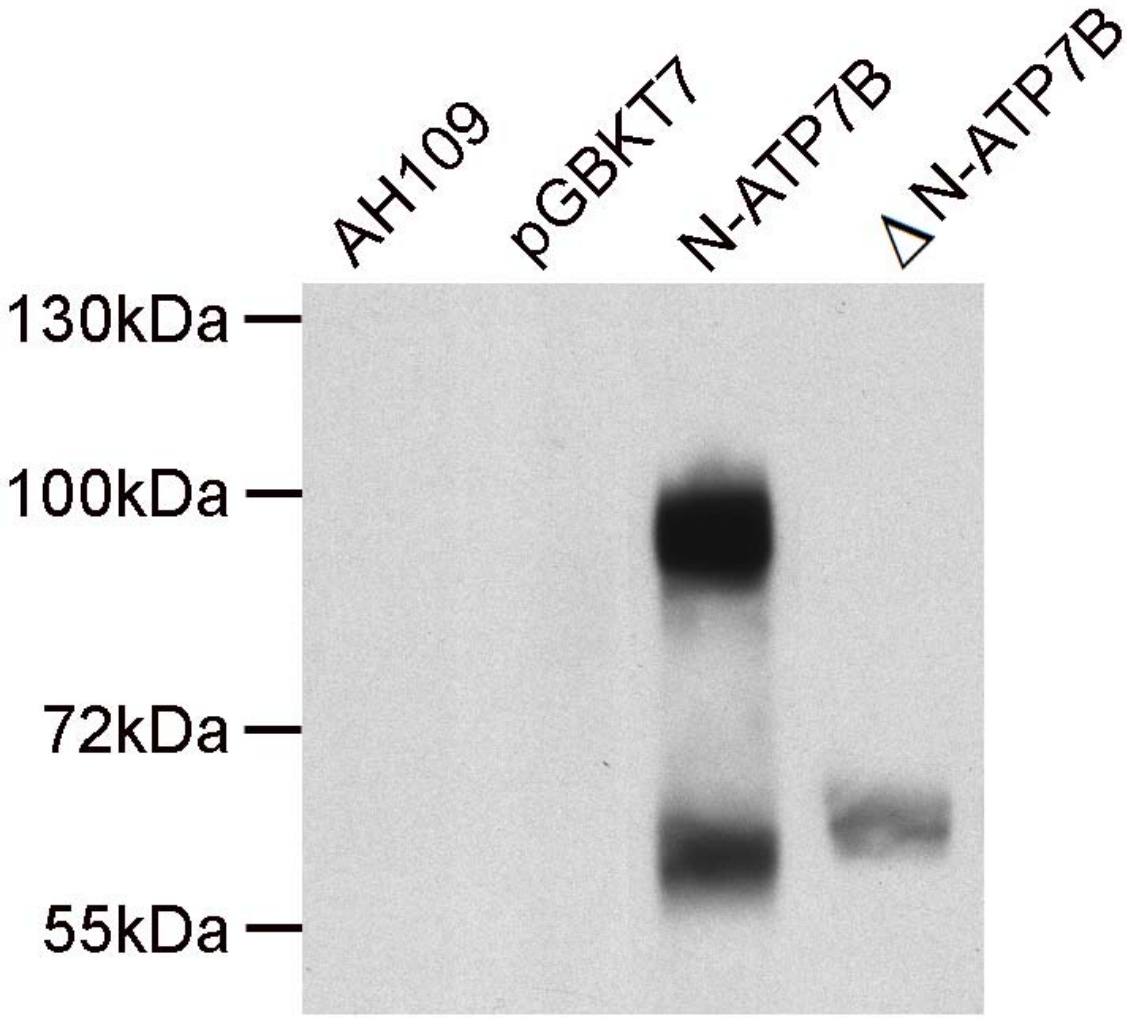

Figure 55: Detection of N-ATP7B and ΔN-ATP7B expression in AH109 cells. N-ATP7B and ΔN-ATP7B were transformed into competent AH109 yeast, and expressed. Western blot analysis was performed on the lysate with N-ATP7B#2 antibody. Lane 1: untransformed AH109 lysate, Lane 2: empty vector control, Lane 3: N-ATP7B, and Lane 4: ΔN-ATP7B.

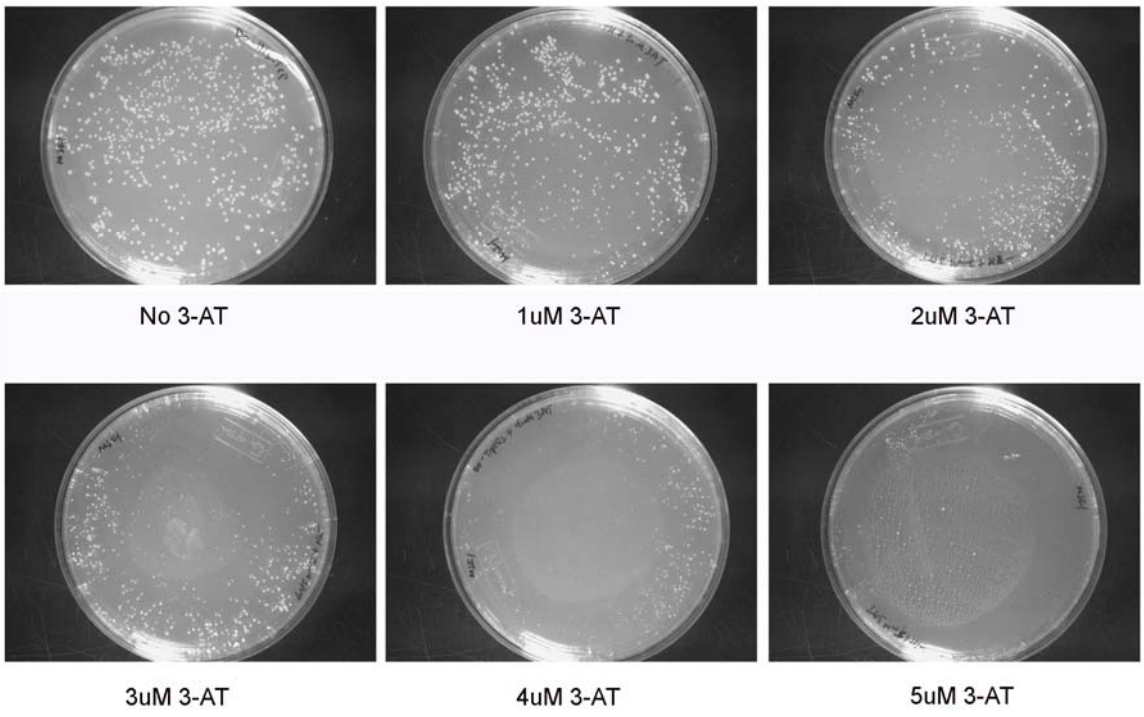

Figure 56: Optimization of 3-AT concentration for inhibition of autonomous activation. MSK1, a constitutively expressed construct, was transformed into AH109 cells and grown on DO-His-Trp plates containing 1-5µM 3-AT. 1µM 3-AT did not significantly inhibit cell growth, whereas 2-5µM decreased cell growth. 1µM 3-AT was used subsequently for elimination of autonomous activation.

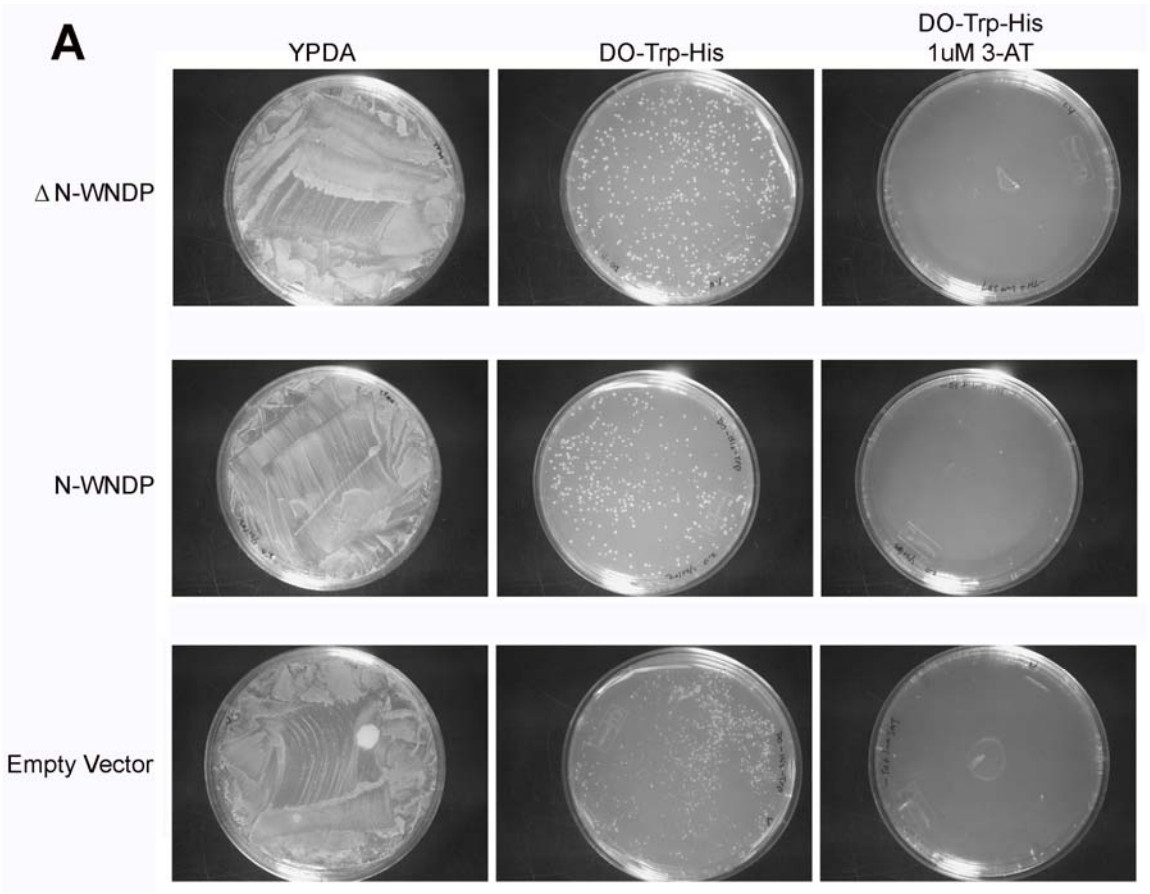
A
YPDA
DO-Trp-His
DO-Trp-His
1uM 3-AT
ΔN-WNDP
N-WNDP
Empty Vector

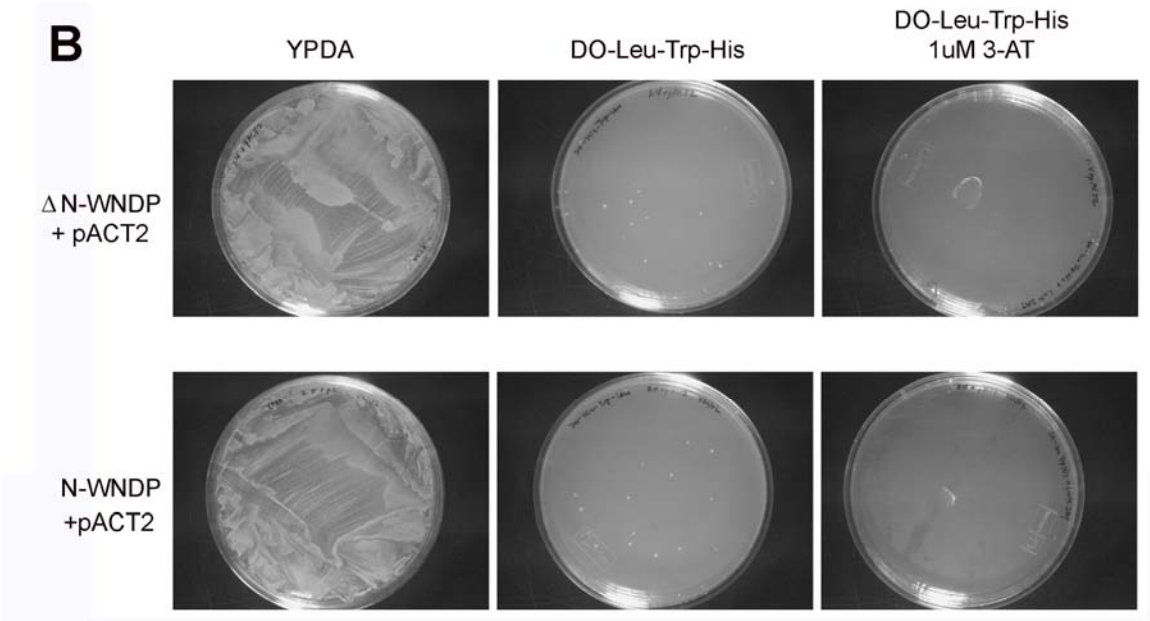
B
YPDA
DO-Leu-Trp-His
DO-Leu-Trp-His
1uM 3-AT
ΔN-WNDP
+ pACT2
N-WNDP
+pACT2

Figure 57: Optimization of yeast growth in drop out media. A) N-ATP7B, ΔN-ATP7B, and empty pGBKT7 were transformed in AH109 cells and plated onto YPDA, DO-Trp-His, and DO-Trp-His+1μM 3-AT plates. Addition of 3-AT in the plates inhibited autonomous activation. **B)** N-ATP7B and ΔN-ATP7B were co-transformed with empty pACT2 and grown on selection plates, YPDA, DO-Leu-Trp-His, and DO-Leu-Trp-His+ 1μM 3-AT. 3-AT eliminated the non-specific growth.

Hepatic copper-transporting ATPase ATP7B: function and inactivation at the molecular and cellular level.

Mee Y. Bartee and Svetlana Lutsenko[1]

1 - The correspondence should be addressed to:

Svetlana Lutsenko, Oregon Health & Science University, Department of Biochemistry and Molecular Biology, 3181 SW Sam Jackson Park Rd., Portland, OR 97239-3098, U.S.A.; Tel.: 503-494-6953; E-mail: lutsenko@ohsu.edu

-Published in Biometals 2007; 20(3-4):627-37

-Some of the sections in chapter 6 are taken from this paper.

-I did all the writing for this chapter.

VI Conclusions

Maintenance of copper homeostasis is important in organisms because it is required for function yet can be toxic to cells. ATP7B is crucial to copper homeostasis since copper is regulated on the level of export. Regulation of copper homeostasis through ATP7B is controlled on the level of trafficking. Work presented in this thesis suggests ATP7B trafficking can subtly be regulated by cell type dependent alternative translational products, cell polarization, and phosphorylation controlled conformational changes. The many varied modes of ATP7B regulation are different than the simple copper induced trafficking model and establish the importance of ATP7B in copper homeostasis.

ATP7B regulation was studied in cells from the two organs that process the most copper, the liver and the kidney. My work shows there is tissue specific regulation of ATP7B. In the kidney where both ATP7B and ATP7A are present, ATP7B does not traffic, implying ATP7B plays primarily a biosynthetic role. Regulation of ATP7B is quite different in the liver where ATP7B has not just a biosynthetic role but is important for export. The tissue specific regulation observed is useful for understanding the effects of copper accumulation in Wilsons disease. Liver and brain function are the most noticeably affected in Wilsons disease. As stated previously, ATP7B is the only transporter expressed in the liver. Since it is the primary exporter of copper and is responsible for a higher capacity of copper, the ramifications of its malfunction would be larger. In the brain, some cell types express only ATP7B, such as Purkinje neurons. The effects of mutations in ATP7B are not as poignant except in regions of the brain

such as the cerebellum, due to the compensatory mechanism of ATP7A. Understanding ATP7B function and regulation provides a better understanding in the systemic control of copper.

6.1 Previous model of ATP7B trafficking

The dual biosynthetic and homeostatic role of ATP7B in the liver is performed in distinct cell compartments. My data and current data in the literature indicate that several factors including copper concentration, catalytic activity, post-translational modification, transcription, and interactions with other proteins affect the intracellular localization of ATP7B [75, 152, 189]. It is also clear that certain structural elements may profoundly affect copper dependent localization of ATP7B [46, 106, 235]. Studies from several laboratories provided convincing evidence that under basal copper conditions ATP7B is present in the Golgi, particularly the TGN [45, 46, 151, 152]. In this compartment ATP7B delivers copper to ceruloplasmin, which is also found in vesicles in the secretory pathway, presumably in the copper bound form. When copper is elevated, ATP7B leaves the TGN and traffics to a vesicular compartment [46, 151, 152]. This re-localization serves to remove excess copper from the cell.

The previous trafficking model in the field was based primarily on work with recombinant ATP7B, mouse and human, in CHO-K1 cells, where ATP7B always traffics. As shown in Figure 58A, ATP7B resides at the TGN normally, serving a biosynthetic role. As copper becomes elevated, ATP7B traffics to vesicles that contain copper, either as a result of ATP7B transport activity at the vesicles or from activity at the TGN. For copper to be exported from the cell,

ATP7B and the copper are sorted into different vesicles, ATP7B returning to the TGN whereas the copper laden vesicles traffic to the plasma membrane where it is excreted from the cell.

6.2 Proposed models of ATP7B trafficking

Data presented in this thesis suggest that regulation of copper dependent trafficking is more complicated than the previous model. The model does not explain the lack of trafficking in some of the endogenous ATP7B tested nor apical trafficking in polarized hepatocytes. To address these issues, I am proposing two new models of ATP7B trafficking.

6.2.1 Trafficking in non-hepatocytes

As shown in chapter 2, contrary to the previously accepted model of ATP7B trafficking, ATP7B does not relocalize from the TGN in response to copper in some cell types, both in cultured and primary cells. The lack of ATP7B trafficking can be explained in cells that co-express ATP7A by specialization of function. Instead of both transporters performing the same task, ATP7B can be dedicated to biosynthetic function and ATP7A to export. siRNA knockdown of ATP7A did not result in trafficking of ATP7B, which is supportive of this model.

This does however, raise a few questions. Does ATP7B traffic in all cell types where it is the only expressed copper transporter? This is the case in hepatocytes, however, in other cell types, ATP7B and ATP7A may be co-expressed. As seen in WD patients, ATP7B is required for copper excretion. What would be the mechanism of copper excretion if ATP7B does not traffic? Interestingly, mATP7B was shown to efflux copper in Menkes patient fibroblasts

without trafficking to vesicles [160] (although mATP7B has been shown to traffic to vesicles in response to copper in CHO-K1 cells [161]) suggesting ATP7B can export copper from the cell without trafficking. It may be possible that as the copper concentration increases in the TGN, copper may be non-specifically incorporated into the lumen of vesicles, ultimately being released into the extracellular space. This mechanism would not work in the diseased state, as in mutants of ATP7B because a functional transporter would still be required. Also, in cells that must respond to sudden large changes in the copper load, as in the liver after a meal, this mechanism may be too slow, so would be limited to cells that do not handle a significant amount of copper.

In the experiments conducted for this thesis, we studied copper induced trafficking of ATP7B. Recent publications indicate, however, ATP7B can traffic in Jeg-3 cells (polarized placental cells) in response to hormonal cues. The lack of trafficking that we see in some cell types may be due to copper not being the inducer. It would be important to identify all the different signals that induce trafficking of ATP7B. This may lead to new insight into the regulation of ATP7B or discovery of pathways affected by copper.

6.2.2 Trafficking in liver

In the liver, export across the basolateral membrane results in the release of compounds into the blood whereas export from the apical membrane would lead to excretion into the canalicular space and then expulsion into the feces. Hence the directionality of exported compounds is more important in tissues, and thus the need to study trafficking in polarized cells. The final destination of

ATP7B during copper induced trafficking has been a matter of debate. In the human liver, immunoreactivity for hepatic ATP7B was observed close to the plasma membrane [153]. However, the results from several laboratories [152, 210] show that ATP7B does not traffic preferentially to the plasma membrane, as most of the localization of ATP7B in high copper is intracellular (vesicular) in primary and cultured hepatocytes, as well as transfected fibroblasts [106, 152], supporting the model in Figure 58A and section 6.1. These experiments were not done in polarized cell lines. As my data shows, ATP7B does traffic to the canalicular membrane.

I propose a slightly different model of ATP7B trafficking in polarized hepatocytes that incorporates the findings of this thesis. As shown in Figure 58C, ATP7B resides in the TGN, and when copper is elevated, traffics in vesicles to the canalicular membrane. Whether ATP7B transports copper into the vesicles and/or at the canalicular membrane is something that would need to be tested. Copper is released into canalicular space. At the canalicular membrane, ATP7B might export copper. In doing so, ATP7B may interact with ceruloplasmin for oxidation of transported copper, helping the release of copper from the intramembrane space of ATP7B. To control the amount of ATP7B at the apical membrane, ATP7B would undergo phosphorylation by a kinase, which would remove ATP7B from the canalicular membrane and into vesicles. Phosphorylated ATP7B may stay in these vesicles in close proximity to the canalicular membrane for recycling with the membrane, for quick mobilization.

As the copper levels decrease, the amount of ATP7B required decreases, resulting in the dephosphorylation of ATP7B and trafficking back to the TGN.

This trafficking model of ATP7B in polarized hepatocytes raises many questions. Is this model of ATP7B trafficking unique to just polarized hepatocytes? Initial experiments with polarized OK and MDCK cells suggest ATP7B does not traffic in those cell lines, with the caveat being ATP7A is expressed in those cells.

Aside from the TGN, what compartment does ATP7B transport copper, vesicles or the canalicular membrane? ATP7B staining was also seen at the canalicular membrane when copper is low, which we concluded to mean a small fraction of ATP7B is at the membranes constitutively for quick responsiveness to sudden influxes of copper. If this is true, this would suggest ATP7B transports copper at the apical membrane. However, in nonpolarized cells, vesicular localization is sufficient for ATP7B mediated copper export. Whether ATP7B transports in either or both compartments still needs to be determined. Interestingly, in hepatocytes, not all of the ATP7B leaves the TGN, even at high copper (our observation). Some protein remains behind, presumably for biosynthetic purposes. The molecular basis for this apparent heterogeneity in ATP7B is currently unknown.

We proposed ATP7B is phosphorylated at the apical membrane, based on the efficient phosphorylation of ATP7B from plasma membrane enriched Sf9 fractions. However, since ATP7B undergoes copper dependent phosphorylation in both polarized and non-polarized cells, it would be important to answer in what

compartment does ATP7B get phosphorylated? Also, the identities of the ATP7B kinase and phosphatase will need to be identified.

Although our data shows trafficking of ATP7B to the canalicular membrane, some of the trafficking studies done by other groups employing the same hepatic cell types, methods, and similar reagents, did not see or conclude the same outcome, localization of ATP7B at the canalicular membrane. For example, in contrast to Roloefson et al, Cater and colleagues detected very little ATP7B in the canalicular membrane of partially polarized HepG2 cells, while vesicles surrounding the canalicular membrane were very apparent [151, 210].

There are a few possible reasons for the apparent discrepancy in the results. The staining of bile canaliculi markers are typically intense, since the local concentration of proteins in this very small region is relatively high. Thus, the signal from the marker protein can easily mask the overlapping staining of ATP7B, which is not very abundant and distributed between several membrane compartments. Secondly, for continuously cycled vesicles/protein only a certain percent of ATP7B-containing vesicles fuses with the membranes at every given time and thus, by definition, more intense staining is observed in the sub-canalicular vesicles and not at the membrane. Consequently, the detection of ATP7B at the plasma membrane may depend significantly on the sensitivity of anti-ATP7B antibodies. Also, HepG2 cells are only partially polarized, and the degree of polarization of the cells contributing to form the canalicular membrane may differ within the same cell population. The extent to which degree of polarization affects ATP7B trafficking is unknown.

6.3 The molecular architecture of ATP7B contributes to its regulation

The copper transporting ATPase ATP7B is a large membrane transporter with distinct functional properties that are reflected in the architecture of the protein (Figure 2). ATP7B binds and hydrolyzes ATP; copper binding to the transporter stimulates this reaction [1]. The energy released during ATP hydrolysis is utilized to bring about conformational changes within the ATP7B structure and release bound copper at the extracellular membrane. Five functional domains can be identified in the structure of ATP7B (Figure 2). The transmembrane domain consists of 8 transmembrane segments (TMS) and forms the copper translocation pathway. Recent studies identified several residues in this portion of the protein which are critical for the function of ATP7B or other copper transporting ATPases [86, 139, 189], however the detailed structure of the copper-permeation pathway remains to be determined. TMS 6 contains the characteristic CysProCys motif, in which Cys residues are thought to be involved in copper coordination during metal translocation (Figure 2). By analogy with bacterial copper transporting ATPases, other copper coordinating residues could be provided by TMSs 7, 8 [87, 129, 189]

It is not known how the conformational changes required for ATP hydrolysis in ATP7B directly affects the copper trafficking and regulation of ATP7B. It is assumed based on some of the mutational analysis of ATP7A, that a catalytically functional transporter is necessary for the proper trafficking of ATP7B. Whether this is true in ATP7B has not been definitively determined. However, comparison of the wildtype and catalytically inactive protein

degradation product suggests that active protein is better phosphorylated, suggesting that copper induced phosphorylation requires a functional protein.

The cytosolic N-terminal domain (N-ATP7B) has 6 metal binding domains (MBD) and accepts copper from the copper chaperone Atox1 [37, 149]. The N-terminal MBD are similar in sequence and structure [236], and each binds one copper in the conserved sequence GMT/HCxxC via cysteines [93, 96]. Binding of copper to MBD is ordered [145] and although structural changes within individual MBD are small [237], the entire N-ATP7B undergoes conformational transitions as evidenced by circular dichroism and proteolysis [96, 145]. Large body of mutagenesis work indicates that the MBDs closest to the membrane (MBD 5 and MBD 6) are required for the transport function while more distal MBDs play a regulatory role [46, 106, 107, 146]. Binding of copper to MBD 5 and 6 appears to alter the affinity of the intramembrane site(s) for copper [107] and thus control the catalytic activity of ATP7B [130]. MBD1-4, which are separated from MBD 5,6 by a long linker, interact with the ATP-binding domain in the apo form and down-regulate catalytic activity; binding of copper or deletion of these domains relieve the interaction and accelerates catalysis [107, 130].

Exon 2 encodes for MBD1-4 (Figure 11) whereas the exons encoding for the catalytically important MBD 5 and 6 are encoded in exon 4 and 5. This is an intriguing genomic organization, considering other organisms have either 1 or 2 MBDs. Experiments by the Lutsenko lab has previously shown that deletion of MBD1-5 results in a faster transporter, suggesting the first couple MBDs are more for regulation of transport. MBD 2, the preferential MBD that receives

copper from Atox1, is encoded in exon2. The molecular architecture of ATP7B is such that the regulatory components of ATP7B are encoded primarily in the first two exons of the gene. It would be interesting to explore the evolution of this region into regulatory components.

The N-terminal domain is also involved in directing ATP7B to the appropriate intracellular compartments during copper induced relocalization [46] (see below) and is the site of interaction with various proteins, implicated in regulation of protein activity and trafficking. These include copper-chaperone Atox1 [37], Murr1/Commd1 [177], dynactin subunit p62 [238] and glutaredoxin [239]. Although the functional consequences for most of these interactions remain to be characterized, the diversity of interacting proteins emphasizes the complexity of regulatory processes mediated by the N-terminal domain. It is important to note that the ATP7B kinase is still unknown, as well as the phosphatase. Hopefully the in vitro phosphorylation plate assay and purification scheme set up will be useful for identification of these unknown proteins (Figure 39, 40).

The ATP-binding domain (ABD) is central for the activity of ATP7B. It is the harnessing of the energy of ATP hydrolysis by this domain that fuels the transport of copper across the membrane by ATP7B. ATP7B functions as a P-type ATPase, i.e. it forms a transient acyl-phosphorylated intermediate during ATP hydrolysis [130] (Figure 2B). The phosphorylated residue D^{1027} belongs to a DKTG motif that is a signature sequence of the P-type ATPase family and is located within the ABD. The ABD is divided into two parts: the phosphorylation domain (P-domain), which houses D^{1027} and is structurally similar in all P-type

ATPases, including copper-transporting ATPases [218, 240] and the nucleotide-binding domain (N-domain). The high-resolution structure of the N-domain of ATP7B in the presence of ATP has been recently solved by multidimensional NMR [113]. The structure revealed unique a nucleotide binding environment of ATP7B and other copper-ATPases compared to other P-type ATPases and provided structural framework for the analysis of various disease causing mutations located in this domain.

No direct structural information is available for the other two cytosolic domains of ATP7B. The A-domain is located between TMS5 and TMS6 and contains the invariant sequence TGE. Recent structure of the A-domain of bacterial thermophilic copper-transporting ATPase CopA suggests that this domain is very similar in its structure to the A-domain of Ca^{2+}-ATPase [240]. In Ca^{2+}-ATPase and other P-type ATPases, the A-domain is essential for dephosphorylation of the catalytic intermediate, with the invariant TGE motif playing a central role in this process [241]. The A-domain undergoes significant movements during catalysis coordinating conformational changes in the cytosolic and transmembrane portion of the pump [117, 218]. It seems likely that in ATP7B the A-domain can be involved in a cross-talk between the N-terminal MBD5 and MBD6 and the transmembrane portion via copper-dependent protein-protein interactions. In this scenario, MBD5 and/or MBD6 may interact with the A-domain (see Figure 2A), as previously suggested [242], and copper binding to MBD5 and/or MBD6 would alter the interaction resulting in the A-domain movement and coupled conformational changes in the transmembrane portion of

the transporter. This hypothesis is supported by the observation that the Cys>Ala mutations within MBD6 or MBD1-5 of ATP7B affect the apparent affinity of the intra-membrane sites for copper [107]. The binding of copper to the MBDs results in the conformational changes that expose the copper dependent phosphorylation site. Phosphorylation may lead to further dissociation of the ABD and the N-terminal domain, shifting the equilibrium of the transporter such that it stays in the E2 conformation for an extended period, resulting in the recycling of the protein.

The C-terminal tail of ATP7B is not required for catalytic function but is important for protein stability [42, 119] and for regulation of the intracellular localization of ATP7B [210]. Recent studies from Cater and colleagues demonstrated that the C-terminal leucine based sequence $L^{1454}LL^{1456}$ is necessary for the TGN localization of ATP7B in basal medium and therefore may have a role in the recycling of trafficked ATP7B molecules back to the TGN [210] and/or TGN retention.

The coordination of all the domains contributes to the transport function and regulation of ATP7B and thus copper homeostasis. With the binding of copper to the N-terminal domain, protein-protein interaction between is disrupted between MBD 1-4 of N-ATP7B and ABD. Copper binding also results in secondary and tertiary structural changes that most likely expose the sites of phosphorylation. The ATP7B kinase would be able to have access because of domain dissociation and loop exposure. ATP7B would traffic to a vesicular compartment, where it could be targeted for phosphorylation. Phosphorylation of

the full length ATP7B (Figure 44) and N-ATP7B (data not shown) alters the solubility of the protein. Solubility of ATP7B containing Sf9 membranes in detergent decreases if the membranes are solubilized after phosphorylation as opposed to before (data not shown). Exposure of the N-terminal His_6 tag is also obscured with phosphorylation (Figure 45). This phosphorylation leads to further conformational changes, where ATP7B might form oligomers, sequestering all the ATP7B molecules in vesicles for either 1) more efficient transport of copper, 2) creating a larger target for Atox1 copper delivery, 3) segregation of ATP7B from other molecules for separation into different compartments, 4) creation of an efficient signaling pathway.

6.4 The N-terminal domain is a major target for regulation of ATP7B trafficking

As presented in this thesis, the N-terminal domain is a major target for regulation. Work done by others show that the MBDs are important for the copper induced trafficking of ATP7B. I show that trafficking is regulated by more than elevated copper in the cell, and try to derive a mechanism of control.

6.4.1 Copper binding

Copper binding to the MBDs has been shown previously to result in conformational changes in the loops that connect them. I show that copper bound protein facilitates phosphorylation compared to apo protein *in vitro*. This further supports the idea that the copper bound status of ATP7B determines its regulation. Although copper binding increases the percentage of phosphorylated protein, what the significance of copper binding *in vivo* is more difficult to predict.

While at the TGN, ATP7B presumably is transporting copper into the biosynthetic pathway to copper dependent enzymes. That would require Atox1 to deliver copper to the N-terminal domain. Yet under these basal conditions, ATP7B is primarily at the TGN. Perhaps *in vivo*, the N-terminal domain has to be saturated or surpass a certain threshold of copper binding before trafficking can occur. After delivery of copper to MBD 2, copper can re-distribute to the other MBDs for delivery to the intramembrane site from MBD 5 or 6. However when copper is elevated, the amount of copper available may exceed the rate at which copper can be transported. If this is the case, copper would stay bound to the MBDs a longer length of time. The N-terminal domain will remain in the "copper bound" conformation which would increase the chance trafficking machinery could interact with the N-terminal domain and cause ATP7B to traffic.

This would also suggest that trafficking may not be limited to just copper bound protein, but that trafficking could occur as long as target sites are accessible. Canalicular localization of ATP7B when copper is limiting may be suggestive of this mechanism. Stringent trafficking conditions may not be conducive in hepatocytes that have to respond to sudden fluctuations in copper. ATP7B and ATP7A co-expression in the kidneys, on the other hand, may reflect finer control of copper homeostasis.

6.4.2 Transcriptional control

Alternative spliced products of ATP7B are known to exist in tissues such as the brain. Western blot analysis of protein from murine brain leads to the detection of many bands that may be alternative splice products of ATP7B

(Natalie Barnes unpublished data from the Lutsenko lab). Aside from PINA, the pineal isoform of ATP7B, these alternative transcripts have not been well studied.

What function some of these spliced products could have is intriguing. The central core of ATP7B is required for transport activity. The N-terminal domain is important for regulation of transport and trafficking. The C-terminal tail regulates trafficking and required for protein stability.

We show that in the kidney derived Hek293 cells, endogenous ATP7B may be alternatively spliced in exon 1, which leads to TGN localization of ATP7B even in the presence of elevated copper. Alternative splicing would result in the loss of the first 32 amino acids of the N-terminal domain. This region may be important for interaction with the trafficking machinery allowing forward trafficking of ATP7B. Transfection of the full length cDNA resulted in copper dependent trafficking of ATP7B implying the loss of this region in kidney ATP7B is responsible for the lack of trafficking.

Another possible role for exon 1 is directional trafficking in polarized cells, which is not necessary in fibroblasts. Apical trafficking of ATP7B results in the export of copper from the body whereas basolateral trafficking would lead to copper secretion into the blood. Deletion of the first 62 amino acids of the N-terminus of ATP7B leads to basolateral trafficking of ATP7B in WIF-B cells [46]. This suggests membrane targeting signals are located in the N-terminal domain. Examination of the N-terminal exon and intron sequences shows intron 1 is ~32kb. Compared to intron 1, all the other introns are quite small. Exon 1 and 2 encode for the first four regulatory MBDs, so it is no coincidence intron 1 is

flanked by these two exons. Intron 1 is likely important for regulation of transcription or control of alternative spliced sites. By controlling the sequence of the very N-terminal region before MBD 1, ATP7B trafficking can be controlled to suit the cell type or metabolic needs of the cell.

Preliminary results in OK (possum derived proximal kidney cells) and MDCK (Mavin Darby Canine Kidney derived distal kidney cells) indicate that in polarized kidney cells, endogenous ATP7B does not relocalize from the TGN after treatment with copper in either cell type. It would be interesting to compare the three constructs, wildtype, exon 1 deletion, and 62 amino deletion of ATP7B in unpolarized and polarized cells. If exon 1 is important for the trafficking of ATP7B in polarized cells, the deletion of exon 1 should lead to no trafficking of ATP7B in nonpolarized cells. However, in polarized cells, deletion of exon 1 could result in no copper dependent trafficking or basolateral localization. This would establish splicing of exon1 as an important tissue specific control of trafficking of ATP7B, reflective of the role of ATP7B in different cells.

6.4.3 Phosphorylation

Copper dependent phosphorylation of ATP7B adds another layer of complexity to ATP7B regulation. In vivo metabolic labeling and gel mobility shift data suggest ATP7B in kidney and liver cells undergoes copper dependent phosphorylation (Figure 10). Yet, ATP7B in HepG2 cells traffic and ATP7B in Hek293 cells do not. What primary role does phosphorylation have on ATP7B regulation? The region of ATP7B trafficking was identified to the serine rich loop3. Mutation of $S^{342}S^{343}$>AA resulted in normal trafficking of ATP7B, although

the in vitro phosphorylation of the mutant N-ATP7B resulted in a reduction in the level of phosphorylation (Figure 31). The $S^{340}S^{341}$>AA mutant however localized to vesicles (Figure 32) for both BCS and copper treated cells. Although the trafficking of $S^{342}S^{343}$>AA mutant had reduced phosphorylation, this protein trafficked normally, suggesting the reduction in phosphorylation is due to alteration in the folding of the loop3 region, which is more magnified in the N-ATP7B construct as opposed to the full length construct.

Mutation of the serine residues targeted for phosphorylation resulted in vesicular localization of ATP7B; suggesting phosphorylation does not play a role in the forward trafficking of ATP7B, but perhaps the recycling. The tri-leucine cytoplasmic tail is important for signaling the return of ATP7B to the TGN. Conceivably, lack of phosphorylation has the opposite effect, retaining proteins at the vesicles. If Atox1 can deliver copper to ATP7B regardless of the cellular localization, then it is possible to shift the ratio of excreted copper to the copper sent to the biosynthetic pathway. Localization of ATP7B in the vesicles for extended periods of time would increase the amount of copper transported in to the vesicles for export. Extended localization of ATP7B in vesicles may alter copper homeostasis in cells, particularly cells that express many proteins requiring copper as a cofactor. It would be interesting to test copper accumulation in cells expressing the $S^{340}S^{341}$>AA mutant. Vesicular localization may lead to copper depletion in these cells. In polarized cells, perhaps this phosphorylation mutant will localize primarily at the canalicular membrane, irrespective of the exogenous copper. Alternatively, it would be important to

study the effects of copper delivery into the biosynthetic pathway. Monitoring of the ratio of apo vs. holoprotein for proteins such as ceruloplasmin, dopamine-ß-hydroxylase, and peptidyl-α-monooxygenase would be intriguing.

6.5 Interacting proteins that may regulate trafficking

ATP7B regulation is dependent on the localization of ATP7B. For this trafficking to occur, there is the involvement of many proteins, including the trafficking machinery and the specific proteins that control ATP7B trafficking, such as the ATP7B kinase and phosphatase. The identification of these interacting proteins is important for the future study of ATP7B trafficking.

6.5.1 Kinase

Mutation of the serines in the phosphorylation site alters the localization of ATP7B. The ATP7B kinase may phosphorylate ATP7B in any of the compartments it localizes, and that may differ between polarized and unpolarized cells. Exactly where in the trafficking the step this occurs is unknown. The appearance of phosphorylated ATP7B occurs at ~45min after treatment with copper (Svetlana Lutsenko's observations), at which point ATP7B is already in vesicles. This suggests copper dependent phosphorylation does not occur at the TGN. The vesicular localization of the $S^{340}S^{341}$>AA mutant points to kinase mediated phosphorylation at the vesicles in nonpolarized cells. However, in polarized HepG2 cells, phosphorylation may occur at the canalicular membrane.

Where the kinase phosphorylates ATP7B may help answer why ATP7B is phosphorylated. In polarized cells, phosphorylation may remove ATP7B from the canalicular membrane and into vesicles. This retention in the vesicles would be

a sort of limbo as the cell waits for signals as to exactly how much copper the body needs and how much it needs to export. Instead of a continuous uptake of copper into the body, copper is taken up into the body whenever food is ingested. Therefore the body must store and recycle cellular stores of copper between meals. If ATP7B exported all the excess cellular copper from the liver, that might lead to deficiencies in copper in other tissues. By trapping the majority of ATP7B in vesicles, hepatocytes can control how much copper is released and how quickly. After the initial elevation of copper the copper levels still remains high, then the phosphorylated ATP7B trapped in vesicles can quickly return to the canalicular membrane with the eventual release of excess copper.

Alternatively, the kinase may phosphorylate ATP7B, inactivating the transport activity of the protein. This may occur in any of the compartments ATP7B traffics except the TGN, regulating export of copper as opposed to the biosynthetic function. Inactivation of ATP7B transport by phosphorylation may necessitate in the return of ATP7B to the TGN. At the TGN, ATP7B would then be de-phosphorylated by a phosphatase, reactivating the protein.

Identification of the kinase and phosphatase would help answer some of the questions of how phosphorylation regulates ATP7B. If phosphorylation inhibits transport activity, this could be tested in vitro with the Sf9 expression system. The $S^{340}S^{341}$>AA mutant should have a higher level of catalytic activity compared to wildtype protein if kinase mediated phosphorylation inactivates transport.

The in vitro phosphorylation experiments presented in Figure 44 and 45 suggest phosphorylation results in more than intra-domain modifications in N-ATP7B. Phosphorylation *in vivo* may lead to changes in the interaction between monomers of ATP7B. It is not known if there is crosstalk between ATP7B, and how the interaction would change the activity. Oligomerization would allow clustering of ATP7B so that the kinase could efficiently phosphorylate the protein. This alteration in protein-protein interaction could be a mechanism to quickly respond to changes in copper. Trafficking, inactivation of activity, or other changes to ATP7B can be acted on more swiftly.

6.5.2 Ceruloplasmin

Ceruloplasmin is important for the maintenance of iron homeostasis as well as the major copper load in the serum. Ceruloplasmin is not embryonic lethal, and although knockout mice do accumulate some copper in the liver, copper transport and export is not interrupted[38]. Although ceruloplasmin does not play an essential role in copper homeostasis, it may still play a role in fine tune regulation of copper. Ceruloplasmin has been shown to have copper oxidase activity in vitro, albeit at 10 fold lower efficiency as that for iron. It could be possible that membrane associated ceruloplasmin could have some role in the conversion of Cu^{+1} to Cu^{+2}, to increase the efficiency of export of copper. Addition of copper to HepG2 cells increases the expression of ceruloplasmin, both secreted and expression at the plasma membrane (data not shown). Ceruloplasmin could possibly play both roles of increasing copper export and decreasing copper uptake, dependent on the cellular localization. The additional

copper accumulation of ceruloplasmin in KO mice could be a result of a slight decrease in the efficiency of copper export at the canalicular membrane.

Ceruloplasmin may play a more active role in copper homeostasis in the liver. In Figure 54, ceruloplasmin localized to structures resembling the bile canaliculi in partially polarized HepG2 cells. This apical membrane localization of a protein that is normally secreted into the blood is quite intriguing, considering ATP7B also traffics to the same membrane compartment. Transport of wastes to the canalicular membrane leads to export from the body. Ceruloplasmin perhaps assists ATP7B transport by converting transported Cu(I) to Cu(II) or by receiving copper from the intramembrane copper binding site of ATP7B to facilitate efficient turnover of the protein.

Another possible role of ceruloplasmin could be as a copper sensor. Ceruloplasmin is a blood circulating oxidase. There has always been controversy about the amount of copper per molecule detected compared to the number of copper binding sites from the crystal structure. A labile seventh copper binding histidine was discovered. If in vivo, ceruloplasmin could bind excess copper at this histidine residue, perhaps monitoring of copper can be done on a systemic level.

Copper transport by ATP7B is a complex process, fine tuned in the different cells that express ATP7B to reflect the role of copper in that tissue and the needs of the entire body. Beginning to understand the regulation of ATP7B on a cellular level provides insight to copper homeostasis on a systemic level. Simplistically, intracellular copper is controlled by the regulation of the spatial and

temporal localization of ATP7B. The variety of complex mechanisms of that control exemplifies the importance of copper regulation.

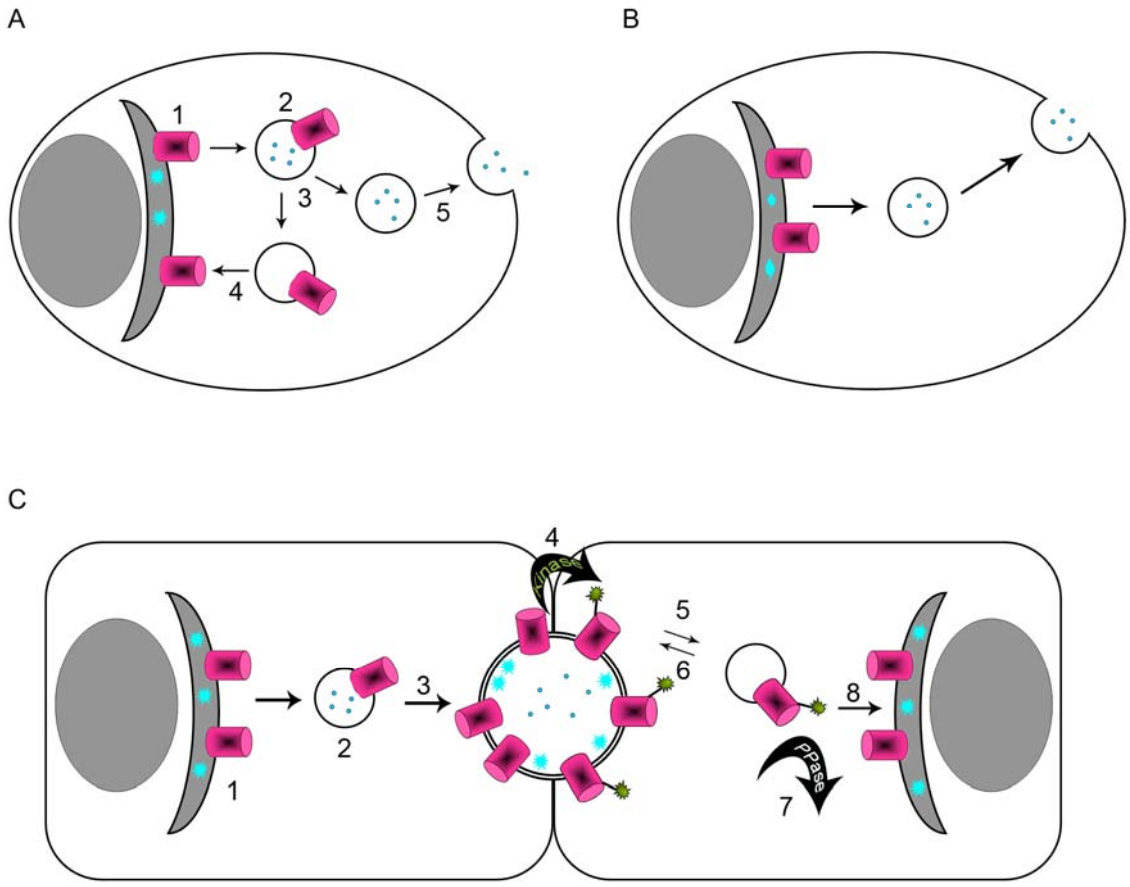

Figure 58 Comparison of ATP7B trafficking models. Based on the findings of my thesis work, I propose two possible models of ATP7B trafficking. A) The previous model of ATP7B trafficking. 1. ATP7B resides at the TGN. 2. ATP7B traffics to vesicles, and these vesicles contain copper. 3. ATP7B and the copper are sorted into different vesicles. 4. ATP7B returns to the TGN. 5. Copper containing vesicles traffic to the plasma membrane where the copper is released. B) Model of copper excretion in cell types ATP7B does not traffic. ATP7B transport copper into the lumen of the TGN. Vesicles containing copper traffic to the plasma membrane where it is released. C) Model of ATP7B trafficking in polarized hepatocytes. 1. ATP7B resides in the TGN. 2. ATP7B traffics to

vesicles; the vesicles contain copper either through ATP7B transport activity or excess copper from the TGN lumen. 3. ATP7B vesicles traffic further to the apical membrane where it might interact with ceruloplasmin and/or transport copper. 4. ATP7B may be phosphorylated by a kinase. 5. Phosphorylated ATP7B traffics to a sub-canalicular compartment. 6. Depending on cellular cues, ATP7B may traffic back to the canalicular membrane. 7. ATP7B is de-phosphorylated by a phosphatase. 8. ATP7B traffics back to the TGN.

Abbreviations

ABD	ATP binding domain
AEBSF	Aminoethylbenzesulfonylflouride hydrochloride
Ala, A	Alanine
Asp,D	Aspartate
Atox1	ATX1 antioxidant protein homologue 1
ATP	Adenine triphosphate
ATP7B	Wilson's disease protein
$Atp7b^{-/-}$	Wilson's disease protein knockout mice
ATP7A	Menkes disease protein
BCS	Bathocuproine disulfonate
BeWo	Human placental choriocarcinoma cells
BL21	E.coli used for protein expression
β-Me	Beta Mercapto ethanol
cDNA	Complementary DNA
CHAPS	3-(3-Cholamidopropyl)dimethylammonio-1-propanesulfonate
CHO-K1	Chinese hamster ovary cells
$CoCl_2$	Cobalt chloride
CO_2	Carbon dioxide
Cos7	Green monkey kidney cells
Cp	Ceruloplasmin
cpm	counts per minute
CTR1	Copper transporter receptor 1

$CuCl_2$	Copper chloride
$CuSO_4$	Copper sulfate
Cys, C	Cysteine
D^{1027}>A	Aspartate 1027 mutated to Alanine
DAPI	4',6-diamidino-2-phenylindole
DDM	n-Dodecyl-β-D-maltopyranoside
DH5α	E.coli cloning bacterial cell line
DMEM	Dulbecco's Modified Eagle's Medium
DNA	Deoxyribonucleic acid
DTT	Dithiothreitol
E.coli	Escherichia coli
EDTA	Ethylenediaminetetraacetic acid
ER	Endoplasmic reticulum
FBS	Fetal bovine serum
FlpIn TREx	Flp recombinase tetracylcine regulated system
FPLC	Fine pressure liquid chromatography
FT	Flow through
[γ-^{32}P]ATP	radiolabeled gamma phosphate ATP
GTP	Guanosine triphosphate
HB	Homogenation buffer
HeLa	Henrietta Lacks cervical cancer cells
His, H	Histidine
His-ABD	N-terminal His tagged ATP Binding Domain

His-N-ATP7B	N-terminal His tagged N-terminal ATP7B
Hek293	Human embryonic kidney cells
Hep3b	Human hepatoma cells
HepG2	Human hepatoma cells
Huh7	Human hepatic cells
IAA	Iodoacetamide
IEF	isoelectric focusing
IPG	Immobilized pH gradient
IPTG	isopropyl-beta-D-thiogalactopyranoside
ivp	in vitro phosphorylation
Jeg-3	Human placental choriocarcinoma cells
KCl	Potassium chloride
kDa	kilodalton
Km	Michaelis constant
KO	Knockout
LB	Luria Bertani broth
MBD	Metal binding domain
MBP-N-ATP7B	Maltose binding protein N-terminal domain of ATP7B
MDCK	Madin Darby canine kidney cells
mem	membrane
MEM	Minimum Essential Media
mg	milligram
$MgCl_2$	Magnesium chloride

$MnCl_2$	Manganese chloride
mRNA	messenger RNA
MRP2	Multi-Drug Resistant Protein 2
Na,K-ATPase	Sodium Potassium ATPase
N-ATP7B	N-terminal domain of ATP7B
N-ATP7B#2	Second N-terminal ATP7B antibody
N-domain	Nucleotide binding domain
NaCl	Sodium chloride
Ni-NTA	Nickel-nitrilotriacetic acid
$NiSO_4$	Nickel Sulfate
OD	Optical density
OK	Opossum kidney epithelial cells
^{32}P	Orthophosphate
PCR	Polymerase chain reaction
P-domain	Phosphorylation domain
PB	Phosphorylation buffer
PBS	Phosphate buffered solution
PFA	Paraformaldehyde
pH	*Potentia hydrogenii*
pI	Isoelectric point
PINA	Pineal Night-specific ATPase
pcDNA3.1	Plasmid cDNA vector
pTx	Plasmid thioredoxin vector

pTriEx1	Plasmid tri-expression vector
PVDF	Polyvinylidene fluoride
RACE	Rapid Amplification of cDNA Ends
RNA	Ribonucleic acid
SDS	sodium dodecyl sulfate
Ser, S	Serine
Sf9	*Spodoptera fugiperda*
siRNA	small interfering RNA
TAE	Tris acetic acid EDTA
TBE	Tris boric acid EDTA
TCA	Trichloroacetic acid
TGN	Trans Golgi Network
TGN46	Trans Golgi Network 46kDa
TMS	Trans membrane segments
µCi	microCurie
µg	microgram
µM	microMolar
WIF-B	Human rat hybrid hepatic cells
WD	Wilson’s disease
ATP7B	Wilson’s disease protein

References

1. Tsivkovskii R, MacArthur BC, Lutsenko S. The Lys1010-Lys1325 fragment of the Wilson's disease protein binds nucleotides and interacts with the N-terminal domain of this protein in a copper-dependent manner. J Biol Chem 2001;276(3):2234-42.
2. Lutsenko S, Barnes NL, Bartee MY, Dmitriev OY. Function and regulation of human copper-transporting ATPases. Physiol Rev 2007;87(3):1011-46.
3. Gerbasi V, Lutsenko S, Lewis EJ. A mutation in the ATP7B copper transporter causes reduced dopamine beta-hydroxylase and norepinephrine in mouse adrenal. Neurochem Res 2003;28(6):867-73.
4. Petris MJ, Strausak D, Mercer JF. The Menkes copper transporter is required for the activation of tyrosinase. Hum Mol Genet 2000;9(19):2845-51.
5. Steveson TC, Ciccotosto GD, Ma XM, Mueller GP, Mains RE, Eipper BA. Menkes protein contributes to the function of peptidylglycine alpha-amidating monooxygenase. Endocrinology 2003;144(1):188-200.
6. Terada K, Nakako T, Yang XL, Iida M, Aiba N, Minamiya Y, et al. Restoration of holoceruloplasmin synthesis in LEC rat after infusion of recombinant adenovirus bearing WND cDNA. J Biol Chem 1998;273(3):1815-20.
7. Kaler SG. Diagnosis and therapy of Menkes syndrome, a genetic form of copper deficiency. Am J Clin Nutr 1998;67:1029S-34S.

8. Kodama H, Murata Y. Molecular genetics and pathophysiology of Menkes disease. Pediatr Int 1999;41(4):430-5.

9. Kodama H, Murata Y, Kobayashi M. Clinical manifestations and treatment of Menkes disease and its variants. Pediatr-Int 1999;41(4):423-9.

10. Strausak D, Mercer JF, Dieter HH, Stremmel W, Multhaup G. Copper in disorders with neurological symptoms: Alzheimer's, Menkes, and Wilson diseases. Brain Res Bull 2001;55(2):175-85.

11. Vulpe C, Levinson B, Whitney S, Packman S, Gitschier J. Isolation of a candidate gene for Menkes disease and evidence that it encodes a copper-transporting ATPase. Nat Genet 1993;3(1):7-13.

12. Harada M. Wilson disease. Med Electron Microsc 2002;35(2):61-6.

13. Ferenci P. Review article: diagnosis and current therapy of Wilson's disease. Aliment Pharmacol Ther 2004;19(2):157-65.

14. Gitlin JD. Wilson disease. Gastroenterology 2003;125(6):1868-77.

15. Shimizu N, Yamaguchi Y, Aoki T. Treatment and management of Wilson's disease. Pediatr Int 1999;41(4):419-22.

16. Jablonska-Kaszewska I, Dabrowska E, Drobinska Jurowiecka A, Falkiewicz B. Treatment of Wilson's disease. Med Sci Monit 2003;9 Suppl 3:5-8.

17. Pandit A, Bavdekar A, Bhave S. Wilson's disease. Indian J Pediatr 2002;69(9):785-91.

18. Guthrie R, Susi A. A Simple Phenylalanine Method for Detecting Phenylketonuria in Large Populations of Newborn Infants. Pediatrics 1963;32:338-43.

19. Fox PL. The copper-iron chronicles: the story of an intimate relationship. Biometals 2003;16(1):9-40.

20. Loudon I. The diseases called chlorosis. Psychol Med 1984;14(1):27-36.

21. Gubler CJ, Lahey ME, Ashenbrucker H, Cartwright GE, Wintrobe MM. Studies on copper metabolism I. A method for the determination of copper in whole blood, red blood cells, and plasma. J Biol Chem 1952;196(1):209-20.

22. Lahey ME, Gubler CJ, Chase MS, Cartwright GE, Wintrobe MM. Studies on copper metabolism. II. Hematologic manifestations of copper deficiency in swine. Blood 1952;7(11):1053-74.

23. Gubler CJ, Lahey ME, Chase MS, Cartwright GE, Wintrobe MM. Studies on copper metabolism. III. The metabolism of iron in copper deficient swine. Blood 1952;7(11):1075-92.

24. Chase MS, Gubler CJ, Cartwright GE, Wintrobe MM. Studies on copper metabolism. IV. The influence of copper on the absorption of iron. J Biol Chem 1952;199(2):757-63.

25. Chase MS, Gubler CJ, Cartwright GE, Wintrobe MM. Studies on copper metabolism. V. Storage of iron in liver of copper-deficient rats. Proc Soc Exp Biol Med 1952;80(4):749-51.

26. Ravia JJ, Stephen RM, Ghishan FK, Collins JF. Menkes Copper ATPase (Atp7a) is a novel metal-responsive gene in rat duodenum, and immunoreactive protein is present on brush-border and basolateral membrane domains. J Biol Chem 2005;280(43):36221-7.

27. Hardman B, Manuelpillai U, Wallace EM, Monty JF, Kramer DR, Kuo YM, et al. Expression, localisation and hormone regulation of the human copper transporter hCTR1 in placenta and choriocarcinoma Jeg-3 cells. Placenta 2006;27(9-10):968-77.

28. Knopfel M, Smith C, Solioz M. ATP-driven copper transport across the intestinal brush border membrane. Biochem Biophys Res Commun 2005;330(3):645-52.

29. Monty JF, Llanos RM, Mercer JF, Kramer DR. Copper exposure induces trafficking of the menkes protein in intestinal epithelium of ATP7A transgenic mice. J Nutr 2005;135(12):2762-6.

30. Knopfel M, Solioz M. Characterization of a cytochrome b(558) ferric/cupric reductase from rabbit duodenal brush border membranes. Biochem Biophys Res Commun 2002;291(2):220-5.

31. Linder MC, Wooten L, Cerveza P, Cotton S, Shulze R, Lomeli N. Copper transport. Am J Clin Nutr 1998;67(5 Suppl):965S-71S.

32. Punter FA, Glerum DM. Mutagenesis reveals a specific role for Cox17p in copper transport to cytochrome oxidase. J Biol Chem 2003;278(33):30875-80.

33. Horng YC, Cobine PA, Maxfield AB, Carr HS, Winge DR. Specific copper transfer from the Cox17 metallochaperone to both Sco1 and Cox11 in the assembly of yeast cytochrome c oxidase. J Biol Chem 2004.

34. Prohaska JR, Gybina AA. Intracellular copper transport in mammals. J Nutr 2004;134(5):1003-6.

35. Hamza I, Faisst A, Prohaska J, Chen J, Gruss P, Gitlin JD. The metallochaperone Atox1 plays a critical role in perinatal copper homeostasis. Proc Natl Acad Sci U S A 2001;98(12):6848-52.

36. Hamza I, Prohaska J, Gitlin JD. Essential role for Atox1 in the copper-mediated intracellular trafficking of the Menkes ATPase. Proc Natl Acad Sci U S A 2003;100(3):1215-20.

37. Walker JM, Tsivkovskii R, Lutsenko S. Metallochaperone Atox1 transfers copper to the NH2-terminal domain of the Wilson's disease protein and regulates its catalytic activity. J Biol Chem 2002;277(31):27953-9.

38. Meyer LA, Durley AP, Prohaska JR, Harris ZL. Copper transport and metabolism are normal in aceruloplasminemic mice. J. Biol. Chem. 2001;276:36857–61.

39. Langner C, Denk H. Wilson disease. Virchows Arch 2004;445(2):111-8.

40. Tanzi RE, Petrukhin K, Chernov I, Pellequer JL, Wasco W, Ross B, et al. The Wilson disease gene is a copper transporting ATPase with homology to the Menkes disease gene. Nat Genet 1993;5(4):344-50.

41. Yuan DS, Stearman R, Dancis A, Dunn T, Beeler T, Klausner RD. The Menkes/Wilson disease gene homologue in yeast provides copper to a

ceruloplasmin-like oxidase required for iron uptake. Proc Natl Acad Sci U S A 1995;92(7):2632-6.

42. Hsi G, Cullen LM, Moira Glerum D, Cox DW. Functional assessment of the carboxy-terminus of the Wilson disease copper-transporting ATPase, ATP7B. Genomics 2004;83(3):473-81.

43. Iida M, Terada K, Sambongi Y, Wakabayashi T, Miura N, Koyama K, et al. Analysis of functional domains of Wilson disease protein (ATP7B) in Saccharomyces cerevisiae. FEBS Lett 1998;428(3):281-5.

44. El Meskini R, Culotta VC, Mains RE, Eipper BA. Supplying copper to the cuproenzyme peptidylglycine alpha-amidating monooxygenase. J Biol Chem 2003;278(14):12278-84.

45. Hung IH, Suzuki M, Yamaguchi Y, Yuan DS, Klausner RD, Gitlin JD. Biochemical characterization of the Wilson disease protein and functional expression in the yeast Saccharomyces cerevisiae. J Biol Chem 1997;272(34):21461-6.

46. Guo Y, Nyasae L, Braiterman LT, Hubbard AL. NH2-terminal signals in ATP7B Cu-ATPase mediate its Cu-dependent anterograde traffic in polarized hepatic cells. Am J Physiol Gastrointest Liver Physiol 2005;289(5):G904-16.

47. Tchaparian EH, Uriu-Adams JY, Keen CL, Mitchell AE, Rucker RB. Lysyl oxidase and P-ATPase-7A expression during embryonic development in the rat. Arch Biochem Biophys 2000;379(1):71-7.

48. Dagenais SL, Adam AN, Innis JW, Glover TW. A novel frameshift mutation in exon 23 of ATP7A (MNK) results in occipital horn syndrome and not in Menkes disease. Am J Hum Genet 2001;69(2):420-7.

49. Sato M, Gitlin JD. Mechanisms of copper incorporation during the biosynthesis of human ceruloplasmin. J. Biol. Chem. 1991;266:5128-34.

50. Petrukhin K, Lutsenko S, Chernov I, Ross BM, Kaplan JH, Gilliam TC. Characterization of the Wilson disease gene encoding a P-type copper transporting ATPase: genomic organization, alternative splicing, and structure/function predictions. Hum Mol Genet 1994;3(9):1647-56.

51. Paynter JA, Grimes A, Lockhart P, Mercer JF. Expression of the Menkes gene homologue in mouse tissues lack of effect of copper on the mRNA levels. FEBS Lett 1994;351(2):186-90.

52. Elmore BO, Bollinger JA, Dooley DM. Human kidney diamine oxidase: heterologous expression, purification, and characterization. J Biol Inorg Chem 2002;7(6):565-79.

53. Kirby BJ, Danks DM, Legge GJ, Mercer JF. Analysis of the distribution of Cu, Fe and Zn and other elements in brindled mouse kidney using a scanning proton microprobe. J Inorg Biochem 1998;71(3-4):189-97.

54. Kodama H. Recent developments in Menkes disease. J. Inher. Metab. Disease 1993;16:791-99.

55. Theophilos MB, Cox DW, Mercer JF. The toxic milk mouse is a murine model of Wilson disease. Hum.Mol.Genet. 1996;5(10):1619-24.

56. Wu J, Forbes JR, Chen HS, Cox DW. The LEC rat has a deletion in the copper transporting ATPase gene homologous to the Wilson disease gene. Nat Genet 1994;7(4):541-5.

57. Kelly EJ, Palmiter RD. A murine model of Menkes disease reveals a physiological function of metallothionein. Nat-Genet 1996;13(2):219-22.

58. Mori M, Nishimura M. A serine to proline mutation in the copper-transporting ATPase gene of the macular mouse. Mamm. Genome 1997;8:407-10.

59. Yoshimura N, Kida K, Usutani S, Nishimura M. Histochemical localization of copper in various organs of brindled mice after copper therapy. Pathol Int 1995;45(1):10-8.

60. Kurasaki M, Okabe I, Saito K, Suzuki-Kurasaki M. Copper metobolism in the kidney of rats administered copper and copper-metallothionein. American Journal of physiology 1998;274(F783-F790).

61. Grimes A, Hearn CJ, Lockhart P, Newgreen DF, Mercer JF. Molecular basis of the brindled mouse mutant (Mo(br)): a murine model of Menkes disease. Hum Mol Genet 1997;6(7):1037-42.

62. Grimes A, Hearn C, Lockhart P, Newgreen D, Mercer JFB. Molecular basis of the brindled mouse mutant (*Mo*^{br}): a murine model of Menkes disease. Hum. Mol. Genet. 1997;6:1032-42.

63. Murata Y, Kodama H, Mori Y, Kobayashi M, Abe T. Mottled gene expression and copper distribution in the macular mouse, an animal model for Menkes disease. J Inher. Metab. Dis. 1998;21:199-202.

64. Moore SD, Cox DW. Expression in mouse kidney of membrane copper transporters Atp7a and Atp7b. Nephron 2002;92(3):629-34.

65. Elsas LJ, Hayslett JP, Spargo BH, Durant JL, Rosenberg LE. Wilson's disease with reversible renal tubular dysfunction. Correlation with proximal tubular ultrastructure. Ann Intern Med 1971;75(3):427-33.

66. Danks DM, Campbell PE, Stevens BJ, Mayne V, Cartwright E. Menkes's kinky hair syndrome:an inherited defect in copper absorption with wide-spread effects. Pediatrics 1972;50:188-201.

67. Oga M, Matsui N, Anai T, Yoshimatsu J, Inoue I, Miyakawa I. Copper disposition of the fetus and placenta in a patient with untreated Wilson's disease. Am. J. Obster. Gynecol. 1993;169:196-98.

68. LaBadie GU, Beratis NG, Price PM, Hirschhorn K. Studies of the copper-binding proteins in Menkes and normal skin fibroblast lysates. J. Cell Physiol. 1981;106:173-78.

69. Hardman B, Manuelpillai U, Wallace EM, van de Waasenburg S, Cater M, Mercer JF, et al. Expression and localization of menkes and Wilson copper transporting ATPases in human placenta. Placenta 2004;25(6):512-7.

70. Ackland LM, Cornish J, Paynter JA, Grimes A, Michalczyk A, Mercer JFB. Expression of Menkes (ATP7a) and Wilson (ATP7b) disease genes in mammary carcinoma cells. Biochem. J. 1997;328(1):237-43.

71. Ackland ML, Anikijenko P, Michalczyk A, Mercer JF. Expression of menkes copper-transporting ATPase, MNK, in the lactating human breast:

possible role in copper transport into milk. J Histochem Cytochem 1999;47(12):1553-62.

72. Kelleher SL, Lonnerdal B. Marginal maternal Zn intake in rats alters mammary gland Cu transporter levels and milk Cu concentration and affects neonatal Cu metabolism. J Nutr 2003;133(7):2141-8.

73. Michalczyk AA, Rieger J, Allen KJ, Mercer JF, Ackland ML. Defective localization of the Wilson disease protein (ATP7B) in the mammary gland of the toxic milk mouse and the effects of copper supplementation. Biochem-J 2000;352:2565-71.

74. Jaeger JL, Shimizu N, Gitlin JD. Tissue-specific ceruloplasmin gene expression in the mammary gland. Biochem J 1991;282:835-39.

75. Vanderwerf SM, Cooper MJ, Stetsenko IV, Lutsenko S. Copper specifically regulates intracellular phosphorylation of the Wilson's disease protein, a human copper-transporting ATPase. J Biol Chem 2001;276(39):36289-94.

76. Takahashi S, Ishii K, Matsumoto K, Higano S, Ishibashi T, Zuguchi M, et al. Cranial MRI and MR angiography in Menkes' syndrome. Neuroradiology 1993;35(7):556-8.

77. Bekiesinska-Figatowska M, Rokicki D, Walecki J, Gremida M. Menkes' disease with a Dandy-Walker variant: case report. Neuroradiology 2001;43(11):948-50.

78. Sener RN. Diffusion MR imaging changes associated with Wilson disease. AJNR Am J Neuroradiol 2003;24(5):965-7.

79. Verma A, Singh NN, Misra S. Early white matter changes in Wilson disease. J Assoc Physicians India 2004;52:578-9.

80. Saito T, Okabe M, Hosokawa T, Kurasaki M, Hata A, Endo F, et al. Immunohistochemical determination of the Wilson Copper-transporting P-type ATPase in the brain tissues of the rat. Neurosci Lett 1999;266(1):13-6.

81. Barnes N, Tsivkovskii R, Tsivkovskaia N, Lutsenko S. The copper-transporting ATPases, menkes and wilson disease proteins, have distinct roles in adult and developing cerebellum. J Biol Chem 2005;280(10):9640-5.

82. Iwase T, Nishimura M, Sugimura H, Igarashi H, Ozawa F, Shinmura K, et al. Localization of Menkes gene expression in the mouse brain; its association with neurological manifestations in Menkes model mice. Acta Neuropathol (Berl) 1996;91(5):482-8.

83. Reichenbach A, Siegel A, Rickmann M, Wolff JR, Noone D, Robinson SR. Distribution of Bergmann glial somata and processes: implications for function. J. Hirnforsch. 1995;36(4):509-17.

84. Furuya S, Tabata T, Mitoma J, Yamada K, Yamasaki M, Makino A, et al. L-serine and glycine serve as major astroglia-derived trophic factors for cerebellar Purkinje neurons. Proc Natl Acad Sci U S A 2000;97(21):11528-33.

85. Kuo YM, Gitschier J, Packman S. Developmental expression of the mouse mottled and toxic milk genes suggests distinct functions for the Menkes

and Wilson disease copper transporters. Hum Mol Genet 1997;6(7):1043-9.

86. Mana-Capelli S, Mandal AK, Arguello JM. Archaeoglobus fulgidus CopB is a thermophilic Cu2+-ATPase: functional role of its histidine-rich-N-terminal metal binding domain. J Biol Chem 2003;278(42):40534-41.

87. Mandal AK, Yang Y, Kertesz TM, Arguello JM. Identification of the transmembrane metal binding site in Cu+-transporting PIB-type ATPases. J Biol Chem 2004;279(52):54802-7.

88. Wernimont AK, Yatsunyk LA, Rosenzweig AC. Binding of copper(I) by the Wilson disease protein and its copper chaperone. J Biol Chem 2004;279(13):12269-76.

89. Jensen PY, Bonander N, Moller LB, Farver O. Cooperative binding of copper(I) to the metal binding domains in Menkes disease protein. Biochim-Biophys-Acta 1999;1434(1):103-13.

90. Lutsenko S, Petrukhin K, Cooper MJ, Gilliam CT, Kaplan JH. N-terminal domains of human copper-transporting adenosine triphosphatases (the Wilson's and Menkes disease proteins) bind copper selectively in vivo and in vitro with stoichiometry of one copper per metal-binding repeat. J Biol Chem 1997;272(30):18939-44.

91. DiDonato M, Narindrasorasak S, Forbes JR, Cox DW, Sarkar B. Expression, purification, and metal binding properties of the N-terminal domain from the wilson disease putative copper-transporting ATPase (ATP7B). J Biol Chem 1997;272(52):33279-82.

92. Cobine PA, George GN, Winzor DJ, Harrison MD, Mogahaddas S, Dameron CT. Stoichiometry of complex formation between Copper(I) and the N-terminal domain of the Menkes protein. Biochemistry 2000;39(23):6857-63.

93. Ralle M, Lutsenko S, Blackburn NJ. Copper transfer to the N-terminal domain of the Wilson disease protein (ATP7B): X-ray absorption spectroscopy of reconstituted and chaperone-loaded metal binding domains and their interaction with exogenous ligands. J Inorg Biochem 2004;98(5):765-74.

94. Ralle M, Cooper MJ, Lutsenko S, Blackburn NJ. X-ray absorption studies on the soluble N-terminal domain of the Menkes disease protein (N-MNK-P) with multiple copper site occupancy. Evidence for a two-coordinate copper-cysteinate coordination environment. J. Am. Chem. Soc. 1998;120:13525-26.

95. Ralle M, Cooper MJ, Lutsenko S, Blackburn NJ. The Menkes Disease Protein Binds Copper via Novel 2-Coordinate Cu(I)-Cysteinates in the N-Terminal Domain. J Am Chem Soc 1998;120(51):13525-26.

96. DiDonato M, Hsu HF, Narindrasorasak S, Que L, Jr., Sarkar B. Copper-induced conformational changes in the N-terminal domain of the Wilson disease copper-transporting ATPase. Biochemistry 2000;39(7):1890-6.

97. DiDonato M, Zhang J, Que L, Jr., Sarkar B. Zinc binding to the NH2-terminal domain of the Wilson disease copper-transporting ATPase:

implications for in vivo metal ion-mediated regulation of ATPase activity. J Biol Chem 2002;277(16):13409-14.

98. Qian Y, Zheng Y, Abraham L, Ramos KS, Tiffany-Castiglioni E. Differential profiles of copper-induced ROS generation in human neuroblastoma and astrocytoma cells. Brain Res Mol Brain Res 2005;134(2):323-32.

99. Banci L, Bertini I, Cantini F, Chasapis CT, Hadjiliadis N, Rosato A. A NMR study of the interaction of a three-domain construct of ATP7A with copper(I) and copper(I)-HAH1: the interplay of domains. J Biol Chem 2005;280(46):38259-63.

100. Banci L, Bertini I, Del Conte R, D'Onofrio M, Rosato A. Solution structure and backbone dynamics of the Cu(I) and apo forms of the second metal-binding domain of the Menkes protein ATP7A. Biochemistry 2004;43(12):3396-403.

101. Gitschier J, Moffat B, Reilly D, Wood WI, Fairbrother WJ. Solution structure of the fourth metal-binding domain from the Menkes copper-transporting ATPase. Nat Struct Biol 1998;5(1):47-54.

102. DeSilva TM, Veglia G, Opella SJ. Solution structures of the reduced and Cu(I) bound forms of the first metal binding sequence of ATP7A associated with Menkes disease. Proteins 2005;61(4):1038-49.

103. Jones CE, Daly NL, Cobine PA, Craik DJ, Dameron CT. Structure and metal binding studies of the second copper binding domain of the Menkes ATPase. J Struct Biol 2003;143(3):209-18.

104. Arnesano F, Banci L, Bertini I, Bonvin AM. A docking approach to the study of copper trafficking proteins; interaction between metallochaperones and soluble domains of copper ATPases. Structure (Camb) 2004;12(4):669-76.

105. Wernimont AK, Huffman DL, Lamb AL, O'Halloran TV, Rosenzweig AC. Structural basis for copper transfer by the metallochaperone for the Menkes/Wilson disease proteins. Nat Struct Biol 2000;7(9):766-71.

106. Cater MA, Forbes J, La Fontaine S, Cox D, Mercer JF. Intracellular trafficking of the human Wilson protein: the role of the six N-terminal metal-binding sites. Biochem J 2004;380(Pt 3):805-13.

107. Huster D, Lutsenko S. The distinct roles of the N-terminal copper-binding sites in regulation of catalytic activity of the Wilson's disease protein. J Biol Chem 2003;278(34):32212-8.

108. Mercer JF, Barnes N, Stevenson J, Strausak D, Llanos RM. Copper-induced trafficking of the cU-ATPases: a key mechanism for copper homeostasis. Biometals 2003;16(1):175-84.

109. Strausak D, La Fontaine S, Hill J, Firth SD, Lockhart PJ, Mercer JF. The role of GMXCXXC metal binding sites in the copper-induced redistribution of the Menkes protein. J Biol Chem 1999;274(16):11170-7.

110. Voskoboinik I, Strausak D, Greenough M, Brooks H, Petris M, Smith S, et al. Functional analysis of the N-terminal CXXC metal-binding motifs in the human menkes copper-transporting P-type ATPase expressed in cultured mammalian cells. J Biol Chem 1999;274(31):22008-12.

111. Forbes JR, Hsi G, Cox DW. Role of the copper-binding domain in the copper transport function of ATP7B, the P-type ATPase defective in Wilson disease. J Biol Chem 1999;274(18):12408-13.

112. Efremov RG, Kosinsky YA, Nolde DE, Tsivkovskii R, Arseniev AS, Lutsenko S. Molecular modelling of the nucleotide-binding domain of Wilson's disease protein: location of the ATP-binding site, domain dynamics and potential effects of the major disease mutations. Biochem J 2004;382(Pt 1):293-305.

113. Dmitriev O, Tsivkovskii R, Abildgaard F, Morgan CT, Markley JL, Lutsenko S. Solution structure of the N-domain of Wilson disease protein: distinct nucleotide-binding environment and effects of disease mutations. Proc Natl Acad Sci U S A 2006;103(14):5302-7.

114. Haupt M, Bramkamp M, Coles M, Altendorf K, Kessler H. Inter-domain motions of the N-domain of the KdpFABC complex, a P-type ATPase, are not driven by ATP-induced conformational changes. J Mol Biol 2004;342(5):1547-58.

115. Clausen JD, McIntosh DB, Woolley DG, Anthonisen AN, Vilsen B, Andersen JP. Asparagine 706 and glutamate 183 at the catalytic site of sarcoplasmic reticulum Ca2+-ATPase play critical but distinct roles in E2 states. J Biol Chem 2006;281(14):9471-81.

116. Petris MJ, Voskoboinik I, Cater M, Smith K, Kim BE, Llanos RM, et al. Copper-regulated trafficking of the Menkes disease copper ATPase is

associated with formation of a phosphorylated catalytic intermediate. J Biol Chem 2002;277(48):46736-42.

117. Moller JV, Olesen C, Jensen AM, Nissen P. The structural basis for coupling of Ca2+ transport to ATP hydrolysis by the sarcoplasmic reticulum Ca2+-ATPase. J Bioenerg Biomembr 2005;37(6):359-64.

118. Petris MJ, Camakaris J, Greenough M, LaFontaine S, Mercer JF. A C-terminal di-leucine is required for localization of the Menkes protein in the trans-Golgi network. Hum Mol Genet 1998;7(13):2063-71.

119. Majumdar R, Al Jumah M, Al Rajeh S, Fraser M, Al Zaben A, Awada A, et al. A novel deletion mutation within the carboxyl terminus of the copper-transporting ATPase gene causes Wilson disease. J Neurol Sci 2000;179(S 1-2):140-3.

120. Yang XL, Miura N, Kawarada Y, Terada K, Petrukhin K, Gilliam T, et al. Two forms of Wilson disease protein produced by alternative splicing are localized in distinct cellular compartments. Biochem J 1997;326 (Pt 3):897-902.

121. Borjigin J, Payne AS, Deng J, Li X, Wang MM, Ovodenko B, et al. A novel pineal night-specific ATPase encoded by the Wilson disease gene. J Neurosci 1999;19(3):1018-26.

122. Li X, Chen S, Wang Q, Zack DJ, Snyder SH, Borjigin J. A pineal regulatory element (PIRE) mediates transactivation by the pineal/retina-specific transcription factor CRX. Proc-Natl-Acad-Sci-U-S-A 1998;95(4):1876-81.

123. Ahmed S, Deng J, Borjigin J. A new strain of rat for functional analysis of PINA. Brain Res Mol Brain Res 2005;137(1-2):63-9.

124. Oh WJ, Kim EK, Park KD, Hahn SH, Yoo OJ. Cloning and characterization of the promoter region of the Wilson disease gene. Biochem. Biophys. Res. Commun. 1999;259:206-11.

125. Oh WJ, Kim EK, Ko JH, Yoo SH, Hahn SH, Yoo OJ. Nuclear proteins that bind to metal response element a (MREa) in the Wilson disease gene promoter are Ku autoantigens and the Ku-80 subunit is necessary for basal transcription of the WD gene. Eur J Biochem 2002;269(8):2151-61.

126. Harris ED, Reddy MC, Majumdar S, Cantera M. Pretranslational control of Menkes disease gene expression. Biometals 2003;16(1):55-61.

127. Levinson B, Packman S, Gitschier J. Deletion of the promoter region in the Atp7a gene of the *mottled dappled* mouse. Nature Genet. 1997;16:224-25.

128. Loudianos G, Dessi V, Lovicu M, Angius A, Figus A, Lilliu F, et al. Molecular characterization of wilson disease in the Sardinian population--evidence of a founder effect. Hum-Mutat 1999;14(4):294-303.

129. Voskoboinik I, Mar J, Strausak D, Camakaris J. The regulation of catalytic activity of the menkes copper-translocating P-type ATPase. Role of high affinity copper-binding sites. J Biol Chem 2001;276(30):28620-7.

130. Tsivkovskii R, Eisses JF, Kaplan JH, Lutsenko S. Functional properties of the copper-transporting ATPase ATP7B (the Wilson's disease protein) expressed in insect cells. J Biol Chem 2002;277(2):976-83.

131. Katano K, Safaei R, Samimi G, Holzer A, Rochdi M, Howell SB. The copper export pump ATP7B modulates the cellular pharmacology of carboplatin in ovarian carcinoma cells. Mol Pharmacol 2003;64(2):466-73.

132. Komatsu M, Sumizawa T, Mutoh M, Chen ZS, Terada K, Furukawa T, et al. Copper-transporting P-type adenosine triphosphatase (ATP7B) is associated with cisplatin resistance. Cancer Res 2000;60(5):1312-6.

133. Nakayama K, Kanzaki A, Ogawa K, Miyazaki K, Neamati N, Takebayashi Y. Copper-transporting P-type adenosine triphosphatase (ATP7B) as a cisplatin based chemoresistance marker in ovarian carcinoma: comparative analysis with expression of MDR1, MRP1, MRP2, LRP and BCRP. Int J Cancer 2002;101(5):488-95.

134. Samimi G, Varki NM, Wilczynski S, Safaei R, Alberts DS, Howell SB. Increase in expression of the copper transporter ATP7A during platinum drug-based treatment is associated with poor survival in ovarian cancer patients. Clin Cancer Res 2003;9(16 Pt 1):5853-9.

135. Samimi G, Safaei R, Katano K, Holzer AK, Rochdi M, Tomioka M, et al. Increased expression of the copper efflux transporter ATP7A mediates resistance to cisplatin, carboplatin, and oxaliplatin in ovarian cancer cells. Clin Cancer Res 2004;10(14):4661-9.

136. Voskoboinik I, Brooks H, Smith S, Shen P, Camakaris J. ATP-dependent copper transport by the Menkes protein in membrane vesicles isolated from cultured Chinese hamster ovary cells. FEBS Lett 1998;435(2-3):178-82.

137. Voskoboinik I, Greenough M, La Fontaine S, Mercer JF, Camakaris J. Functional studies on the Wilson copper P-type ATPase and toxic milk mouse mutant. Biochem Biophys Res Commun 2001;281(4):966-70.

138. Voskoboinik I, Mar J, Camakaris J. Mutational analysis of the Menkes copper P-type ATPase (ATP7A). Biochem Biophys Res Commun 2003;301(2):488-94.

139. Bissig KD, La Fontaine S, Mercer JF, Solioz M. Expression of the human Menkes ATPase in Xenopus laevis oocytes. Biol Chem 2001;382(4):711-4.

140. Davis-Kaplan SR, Askwith CC, Bengtzen AC, Radisky D, Kaplan J. Chloride is an allosteric effector of copper assembly for the yeast multicopper oxidase Fet3p: an unexpected role for intracellular chloride channels. Proc Natl Acad Sci U S A 1998;95(23):13641-5.

141. Wang T, Weinman SA. Involvement of chloride channels in hepatic copper metabolism: ClC-4 promotes copper incorporation into ceruloplasmin. Gastroenterology 2004;126(4):1157-66.

142. Stoj C, Kosman DJ. Cuprous oxidase activity of yeast Fet3p and human ceruloplasmin: implication for function. FEBS Lett 2003;554(3):422-6.

143. Hung IH, Casareno RL, Labesse G, Mathews FS, Gitlin JD. HAH1 is a copper-binding protein with distinct amino acid residues mediating copper homeostasis and antioxidant defense. J Biol Chem 1998;273(3):1749-54.

144. Ralle M, Lutsenko S, Blackburn NJ. X-ray absorption spectroscopy of the copper chaperone HAH1 reveals a linear two-coordinate Cu(I) center

capable of adduct formation with exogenous thiols and phosphines. J Biol Chem 2003;278(25):23163-70.

145. Walker JM, Huster D, Ralle M, Morgan CT, Blackburn NJ, Lutsenko S. The N-terminal metal-binding site 2 of the Wilson's Disease Protein plays a key role in the transfer of copper from Atox1. J Biol Chem 2004;279(15):15376-84.

146. Achila D, Banci L, Bertini I, Bunce J, Ciofi-Baffoni S, Huffman DL. Structure of human Wilson protein domains 5 and 6 and their interplay with domain 4 and the copper chaperone HAH1 in copper uptake. Proc Natl Acad Sci U S A 2006;103(15):5729-34.

147. Anastassopoulou I, Banci L, Bertini I, Cantini F, Katsari E, Rosato A. Solution structure of the apo and copper(I)-loaded human metallochaperone HAH1. Biochemistry 2004;43(41):13046-53.

148. Strausak D, Howie MK, Firth SD, Schlicksupp A, Pipkorn R, Multhaup G, et al. Kinetic analysis of the interaction of the copper chaperone Atox1 with the metal binding sites of the Menkes protein. J Biol Chem 2003;278(23):20821-7.

149. Larin D, Mekios C, Das K, Ross B, Yang AS, Gilliam TC. Characterization of the interaction between the Wilson and Menkes disease proteins and the cytoplasmic copper chaperone, HAH1p. J Biol Chem 1999;274(40):28497-504.

150. Petris MJ, Mercer JF, Culvenor JG, Lockhart P, Gleeson PA, Camakaris J. Ligand-regulated transport of the Menkes copper P-type ATPase efflux

pump from the Golgi apparatus to the plasma membrane: a novel mechanism of regulated trafficking. Embo J 1996;15(22):6084-95.

151. Roelofsen H, Wolters H, Van Luyn MJ, Miura N, Kuipers F, Vonk RJ. Copper-induced apical trafficking of ATP7B in polarized hepatoma cells provides a mechanism for biliary copper excretion. Gastroenterology 2000;119(3):782-93.

152. Schaefer M, Hopkins RG, Failla ML, Gitlin JD. Hepatocyte-specific localization and copper-dependent trafficking of the Wilson's disease protein in the liver. Am J Physiol 1999;276(3 Pt 1):G639-46.

153. Fanni D, Pilloni L, Orru S, Coni P, Liguori C, Serra S, et al. Expression of ATP7B in normal human liver. Eur J Histochem 2005;49(4):371-8.

154. Forbes JR, Cox DW. Copper-dependent trafficking of Wilson disease mutant ATP7B proteins. Hum Mol Genet 2000;9(13):1927-35.

155. Payne AS, Kelly EJ, Gitlin JD. Functional expression of the Wilson disease protein reveals mislocalization and impaired copper-dependent trafficking of the common H1069Q mutation. Proc Natl Acad Sci U S A 1998;95(18):10854-9.

156. Katano K, Safaei R, Samimi G, Holzer A, Tomioka M, Goodman M, et al. Confocal microscopic analysis of the interaction between cisplatin and the copper transporter ATP7B in human ovarian carcinoma cells. Clin Cancer Res 2004;10(13):4578-88.

157. Harada M, Sakisaka S, Kawaguchi T, Kimura R, Taniguchi E, Koga H, et al. Copper does not alter the intracellular distribution of ATP7B, a copper-transporting ATPase. Biochem-Biophys-Res-Commun 2000;275(3):871-6.

158. Harada M, Kumemura H, Sakisaka S, Shishido S, Taniguchi E, Kawaguchi T, et al. Wilson disease protein ATP7B is localized in the late endosomes in a polarized human hepatocyte cell line. Int J Mol Med 2003;11(3):293-8.

159. Harada M, Kawaguchi T, Kumemura H, Terada K, Ninomiya H, Taniguchi E, et al. The Wilson disease protein ATP7B resides in the late endosomes with Rab7 and the Niemann-Pick C1 protein. Am J Pathol 2005;166(2):499-510.

160. La Fontaine SL, Firth SD, Camakaris J, Englezou A, Theophilos MB, Petris MJ, et al. Correction of the copper transport defect of Menkes patient fibroblasts by expression of the Menkes and Wilson ATPases. J Biol Chem 1998;273(47):31375-80.

161. La Fontaine S, Theophilos MB, Firth SD, Gould R, Parton RG, Mercer JF. Effect of the toxic milk mutation (tx) on the function and intracellular localization of Wnd, the murine homologue of the Wilson copper ATPase. Hum Mol Genet 2001;10(4):361-70.

162. Britt DP, Yeoman GH. Susceptibility of North Ronaldsay sheep to copper from cupric oxide needles. Vet Res Commun 1985;9(1):57-65.

163. Haywood S, Muller T, Mackenzie AM, Muller W, Tanner MS, Heinz-Erian P, et al. Copper-induced hepatotoxicosis with hepatic stellate cell

activation and severe fibrosis in North Ronaldsay lambs: a model for non-Wilsonian hepatic copper toxicosis of infants. J Comp Pathol 2004;130(4):266-77.

164. Haywood S, Simpson DM, Ross G, Beynon RJ. The greater susceptibility of North Ronaldsay sheep compared with Cambridge sheep to copper-induced oxidative stress, mitochondrial damage and hepatic stellate cell activation. J Comp Pathol 2005;133(2-3):114-27.

165. Fuentealba IC, Aburto EM. Animal models of copper-associated liver disease. Comp Hepatol 2003;2(1):5.

166. Lockhart PJ, Wilcox SA, Dahl HM, Mercer JF. Cloning, mapping and expression analysis of the sheep Wilson disease gene homologue. Biochim-Biophys-Acta 2000;1491(1-3):229-39.

167. Lockhart PJ, La Fontaine S, Firth SD, Greenough M, Camakaris J, Mercer JF. Correction of the copper transport defect of Menkes patient fibroblasts by expression of two forms of the sheep Wilson ATPase. Biochim Biophys Acta 2002;1588(2):189-94.

168. Lockhart PJ, Mercer JF. Functional analysis of the sheep Wilson disease protein (sATP7B) in CHO cells. Eur J Cell Biol 2001;80(5):349-57.

169. Tsay MJ, Fatemi N, Narindrasorasak S, Forbes JR, Sarkar B. Identification of the "missing domain" of the rat copper-transporting ATPase, atp7b: insight into the structural and metal binding characteristics of its N-terminal copper-binding domain. Biochim Biophys Acta 2004;1688(1):78-85.

170. Goodyer ID, Jones EE, Monaco AP, Francis MJ. Characterization of the Menkes protein copper-binding domains and their role in copper-induced protein relocalization. Hum Mol Genet 1999;8(8):1473-8.

171. Hantos MB, Szalay F, Lakatos PL, Hegedus D, Firneisz G, Reiczigel J, et al. Elevated plasma nociceptin level in patients with Wilson disease. Brain Res Bull 2002;58(3):311-3.

172. Ferenci P, Caca K, Loudianos G, Mieli-Vergani G, Tanner S, Sternlieb I, et al. Diagnosis and phenotypic classification of Wilson disease. Liver Int 2003;23(3):139-42.

173. Cauza E, Ulrich-Pur H, Polli C, Gangl A, Ferenci P. Distribution of patients with Wilson disease carrying the H1069Q mutation in Austria. Wien-Klin-Wochenschr 2000;112(13):576-9.

174. Kim BE, Smith K, Petris MJ. A copper treatable Menkes disease mutation associated with defective trafficking of a functional Menkes copper ATPase. J Med Genet 2003;40(4):290-5.

175. van De Sluis B, Rothuizen J, Pearson PL, van Oost BA, Wijmenga C. Identification of a new copper metabolism gene by positional cloning in a purebred dog population. Hum Mol Genet 2002;11(2):165-73.

176. Klomp AE, van de Sluis B, Klomp LW, Wijmenga C. The ubiquitously expressed MURR1 protein is absent in canine copper toxicosis. J Hepatol 2003;39(5):703-9.

177. Tao TY, Liu F, Klomp L, Wijmenga C, Gitlin JD. The copper toxicosis gene product Murr1 directly interacts with the Wilson disease protein. J Biol Chem 2003;278(43):41593-6.

178. Frieden E. Perspectives on copper biochemistry. Clin Physiol Biochem. 1986;4(1):11-9.

179. Bocharova OV, Breydo L, Salnikov VV, Baskakov IV. Copper(II) inhibits in vitro conversion of prion protein into amyloid fibrils. Biochemistry 2005;44(18):6776-87.

180. Simons A, Ruppert T, Schmidt C, Schlicksupp A, Pipkorn R, Reed J, et al. Evidence for a copper-binding superfamily of the amyloid precursor protein. Biochemistry 2002;41(30):9310-20.

181. Bull PC, Cox DW. Long range restriction mapping of 13q14.3 focused on the Wilson disease region. Genomics 1993;16(3):593-8.

182. Yamaguchi Y, Heiny ME, Gitlin JD. Isolation and characterization of a human liver cDNA as a candidate gene for Wilson disease. Biochem Biophys Res Commun 1993;197(1):271-7.

183. Mercer JF, Livingston J, Hall B, Paynter JA, Begy C, Chandrasekharappa S, et al. Isolation of a partial candidate gene for Menkes disease by positional cloning. Nat Genet 1993;3(1):20-5.

184. Chelly J, Tumer Z, Tonnesen T, Petterson A, Ishikawa-Brush Y, Tommerup N, et al. Isolation of a candidate gene for Menkes disease that encodes a potential heavy metal binding protein. Nat Genet 1993;3(1):14-9.

185. La Fontaine S, Firth SD, Lockhart P, Brooks H, Camakaris J, Mercer JFB. Activity and intracellular localization of Mnk, the murine homologue of the Menkes protein in cells from blotchy (Moblo) and brindled (Mobr) mouse mutants. Hum. Mol. Genet 1999;8:1069-75.

186. La Fontaine S, Firth SD, Lockhart PJ, Brooks H, Parton RG, Camakaris J, et al. Functional analysis and intracellular localization of the human menkes protein (MNK) stably expressed from a cDNA construct in Chinese hamster ovary cells (CHO-K1). Hum Mol Genet 1998;7(8):1293-300.

187. Petris MJ, Mercer JF. The Menkes protein (ATP7A; MNK) cycles via the plasma membrane both in basal and elevated extracellular copper using a C-terminal di-leucine endocytic signal. Hum Mol Genet 1999;8(11):2107-15.

188. Nyasae L, Bustos R, Braiterman L, Eipper B, Hubbard A. Dynamics of endogenous ATP7A (Menkes protein) in intestinal epithelial cells: copper-dependent redistribution between two intracellular sites. Am J Physiol Gastrointest Liver Physiol 2007;292(4):G1181-94.

189. Forbes JR, Cox DW. Functional characterization of missense mutations in ATP7B: Wilson disease mutation or normal variant? Am. J. Hum. Genet. 1998;63:1663-74.

190. Huster D, Hoppert M, Lutsenko S, Zinke J, Lehmann C, Mossner J, et al. Defective cellular localization of mutant ATP7B in Wilson's disease patients and hepatoma cell lines. Gastroenterology 2003;124(2):335-45.

191. Bartee MY, Lutsenko S. Hepatic copper-transporting ATPase ATP7B: function and inactivation at the molecular and cellular level. Biometals 2007;20(3-4):627-37.

192. La Fontaine S, Firth SD, Lockhart PJ, Brooks H, Camakaris J, Mercer JF. Intracellular localization and loss of copper responsiveness of Mnk, the murine homologue of the Menkes protein, in cells from blotchy (Mo blo) and brindled (Mo br) mouse mutants. Hum. Mol. Genet 1999;8(6):1069-75.

193. Buiakova OI, Xu J, Lutsenko S, Zeitlin S, Das K, Das S, et al. Null mutation of the murine ATP7B (Wilson disease) gene results in intracellular copper accumulation and late-onset hepatic nodular transformation. Hum.Mol.Genet. 1999;8(9):1665-71.

194. Eisses JF, Kaplan JH. Molecular characterization of hCTR1, the human copper uptake protein. J Biol Chem 2002;277(32):29162-71.

195. Greenough M, Pase L, Voskoboinik I, Petris MJ, O'Brien AW, Camakaris J. Signals regulating trafficking of Menkes (MNK; ATP7A) copper-translocating P-type ATPase in polarized MDCK cells. Am J Physiol Cell Physiol 2004;287(5):C1463-71.

196. Thomas GR, Forbes JR, Roberts EA, Walshe JM, Cox DW. The Wilson disease gene: spectrum of mutations and their consequences. Nature Genetics 1995;9:210-16.

197. Lorinczi E, Tsivkovskii R, Haase W, Bamberg E, Lutsenko S, Friedrich T. Delivery of the Cu-transporting ATPase ATP7B to the plasma membrane in Xenopus oocytes. Biochim Biophys Acta 2008;1778(4):896-906.

198. Mercer JF. The molecular basis of copper-transport diseases. Trends Mol Med 2001;7(2):64-9.

199. Linz R, Barnes NL, Zimnicka AM, Kaplan JH, Eipper B, Lutsenko S. The Intracellular Targeting of Copper-Transporting Atpase Atp7a in a Normal and Atp7b-/- Kidney. Am J Physiol Renal Physiol 2007.

200. Pase L, Voskoboinik I, Greenough M, Camakaris J. Copper stimulates trafficking of a distinct pool of the Menkes copper ATPase (ATP7A) to the plasma membrane and diverts it into a rapid recycling pool. Biochem J 2004;378(Pt 3):1031-7.

201. Hardman B, Michalczyk A, Greenough M, Camakaris J, Mercer JF, Ackland ML. Hormonal regulation of the Menkes and Wilson copper-transporting ATPases in human placental Jeg-3 cells. Biochem J 2007;402(2):241-50.

202. Schlief ML, West T, Craig AM, Holtzman DM, Gitlin JD. Role of the Menkes copper-transporting ATPase in NMDA receptor-mediated neuronal toxicity. Proc Natl Acad Sci U S A 2006;103(40):14919-24.

203. Kelleher SL, Lonnerdal B. Mammary gland copper transport is stimulated by prolactin through alterations in Ctr1 and Atp7A localization. Am J Physiol Regul Integr Comp Physiol 2006;291(4):R1181-91.

204. Barnes N, Tsivkovskii R., Tsivkovskaia N., Lutsenko S. 2004.

205. Konig H, Matter N, Bader R, Thiele W, Muller F. Splicing segregation: the minor spliceosome acts outside the nucleus and controls cell proliferation. Cell 2007;131(4):718-29.

206. Zegers MM, Hoekstra D. Mechanisms and functional features of polarized membrane traffic in epithelial and hepatic cells. Biochem J 1998;336 (Pt 2):257-69.

207. Slimane TA, Trugnan G, Van ISC, Hoekstra D. Raft-mediated trafficking of apical resident proteins occurs in both direct and transcytotic pathways in polarized hepatic cells: role of distinct lipid microdomains. Mol Biol Cell 2003;14(2):611-24.

208. Cui Y, Konig J, Buchholz JK, Spring H, Leier I, Keppler D. Drug resistance and ATP-dependent conjugate transport mediated by the apical multidrug resistance protein, MRP2, permanently expressed in human and canine cells. Mol Pharmacol 1999;55(5):929-37.

209. Dunbar LA, Caplan MJ. Ion pumps in polarized cells: sorting and regulation of the Na+, K+- and H+, K+-ATPases. J Biol Chem 2001;276(32):29617-20.

210. Cater MA, La Fontaine S, Shield K, Deal Y, Mercer JF. ATP7B mediates vesicular sequestration of copper: insight into biliary copper excretion. Gastroenterology 2006;130(2):493-506.

211. Zeng L, Miller EW, Pralle A, Isacoff EY, Chang CJ. A selective turn-on fluorescent sensor for imaging copper in living cells. J Am Chem Soc 2006;128(1):10-1.

212. Miller SG, Carnell L, Moore HH. Post-Golgi membrane traffic: brefeldin A inhibits export from distal Golgi compartments to the cell surface but not recycling. J Cell Biol 1992;118(2):267-83.

213. El Meskini R, Crabtree KL, Cline LB, Mains RE, Eipper BA, Ronnett GV. ATP7A (Menkes protein) functions in axonal targeting and synaptogenesis. Mol Cell Neurosci 2007;34(3):409-21.

214. Vanderwerf SMaLS. Wilson's disease protein expressed in Sf9 cells is phosphorylated. Paper presented at: Biochemical Society Transactions for Biometals 2002: 3rd International Biometals Symposium, 2002; King's College London, UK,.

215. Vanderwerf SM, Lutsenko S. The Wilson's disease protein expressed in Sf9 cells is phosphorylated. Biochem Soc Trans 2002;30(4):739-41.

216. Voskoboinik I, Fernando R, Veldhuis N, Hannan KM, Marmy-Conus N, Pearson RB, et al. Protein kinase-dependent phosphorylation of the Menkes copper P-type ATPase. Biochem Biophys Res Commun 2003;303(1):337-42.

217. Lowry OH, Rosebrough NJ, Farr AL, Randall RJ. Protein measurement with the Folin phenol reagent. J Biol Chem 1951;193(1):265-75.

218. Toyoshima C, Mizutani T. Crystal structure of the calcium pump with a bound ATP analogue. Nature 2004;430(6999):529-35.

219. Tsivkovskii R, Efremov RG, Lutsenko S. The role of the invariant His-1069 in folding and function of the Wilson's disease protein, the human copper-transporting ATPase ATP7B. J Biol Chem 2003;278(15):13302-8.

220. Steeg PS, Palmieri D, Ouatas T, Salerno M. Histidine kinases and histidine phosphorylated proteins in mammalian cell biology, signal transduction and cancer. Cancer Lett 2003;190(1):1-12.

221. Yeang HY, Yusof F, Abdullah L. Protein purification for the Lowry assay: acid precipitation of proteins in the presence of sodium dodecyl sulfate and other biological detergents. Anal Biochem 1998;265(2):381-4.

222. Cao TT, Brelot A, von Zastrow M. The composition of the beta-2 adrenergic receptor oligomer affects its membrane trafficking after ligand-induced endocytosis. Mol Pharmacol 2005;67(1):288-97.

223. Chen X, Molino C, Liu L, Gumbiner BM. Structural elements necessary for oligomerization, trafficking, and cell sorting function of paraxial protocadherin. J Biol Chem 2007;282(44):32128-37.

224. Hellman NE, Kono S, Mancini GM, Hoogeboom AJ, De Jong GJ, Gitlin JD. Mechanisms of copper incorporation into human ceruloplasmin. J Biol Chem 2002;277(48):46632-8.

225. Scheinberg H, Gitlin J. Deficiency of ceruloplasmin in patients with hepatolenticular degeneration (Wilson's disease). Science 1952;116:484-85.

226. Messerschmidt A, Rossi A, Ladenstein R, Huber R, Bolognesi M, Gatti G, et al. X-ray crystal structure of the blue oxidase ascorbate oxidase from zucchini. Analysis of the polypeptide fold and a model of the copper sites and ligands. J Mol Biol 1989;206(3):513-29.

227. Zaitseva I, Zaitsev V, Card G, Moshkov K, Bax B, Ralph A, et al. The X-ray structure of human serum ceruloplasmin at 3.1 Å: nature of the copper centres. Journal of Biological Inorganic Chemistry; 1996. p. 15-23.

228. Takahashi N, Bauman RA, Ortel TL, Dwulet FE, Wang CC, Putnam FW. Internal triplication in the structure of human ceruloplasmin. Proc Natl Acad Sci U S A 1983;80(1):115-9.

229. Magdoff-Fairchild B, Lovell FM, Low BW. An x-ray crystallographic study of ceruloplasmin. Determination of molecular weight. J Biol Chem 1969;244(13):3497-9.

230. Irina Zaitseva VZ, Graeme Card, Kirill Moshkov, Benjamin Bax, Adam Ralph and Peter Lindley The X-ray structure of human serum ceruloplasmin at 3.1 Å: nature of the copper centres. Journal of Biological Inorganic Chemistry 1996;1(1):15-23.

231. Mukhopadhyay CK, Mazumder B, Lindley PF, Fox PL. Identification of the prooxidant site of human ceruloplasmin: a model for oxidative damage by copper bound to protein surfaces. Proc Natl Acad Sci U S A 1997;94(21):11546-51.

232. Patel BN, David S. A novel glycosylphosphatidylinositol-anchored form of ceruloplasmin is expressed by mammalian astrocytes. J Biol Chem 1997;272(32):20185-90.

233. Harris ZL, Takahashi Y, Miyajima H, Serizawa M, MacGillivray RT, Gitlin JD. Aceruloplasminemia: molecular characterization of this disorder of iron metabolism. Proc. Natl. Acad. Sci. U.S.A. 1995;92:2539-43.

234. Patel BN, Dunn RJ, David S. Alternative RNA Splicing Generates a Glycosylphosphatidylinositol-anchored Form of Ceruloplasmin in Mammalian Brain. J. Biol. Chem. 2000;275(6):4305-10.

235. Cater MA, La Fontaine S, Mercer JF. Copper binding to the N-terminal metal binding sites or the CPC motif is not essential for copper-induced Trafficking of the Human Wilson Protein (ATP7B). Biochem J 2006.

236. Arnesano F, Banci L, Bertini I, Ciofi-Baffoni S, Molteni E, Huffman DL, et al. Metallochaperones and metal-transporting ATPases: a comparative analysis of sequences and structures. Genome Res 2002;12(2):255-71.

237. Bunce J, Achila D, Hetrick E, Lesley L, Huffman DL. Copper transfer studies between the N-terminal copper binding domains one and four of human Wilson protein. Biochim Biophys Acta 2006;1760(6):907-12.

238. Lim CM, Cater MA, Mercer JF, La Fontaine S. Copper-dependent interaction of dynactin subunit p62 with the N terminus of ATP7B but not ATP7A. J Biol Chem 2006;281(20):14006-14.

239. Lim CM, Cater MA, Mercer JF, La Fontaine S. Copper-dependent interaction of glutaredoxin with the N termini of the copper-ATPases (ATP7A and ATP7B) defective in Menkes and Wilson diseases. Biochem Biophys Res Commun 2006;348(2):428-36.

240. Sazinsky MH, Mandal AK, Arguello JM, Rosenzweig AC. Structure of the ATP binding domain from the Archaeoglobus fulgidus Cu+-ATPase. J Biol Chem 2006;281(16):11161-6.

241. Anthonisen AN, Clausen JD, Andersen JP. Mutational analysis of the conserved TGES loop of sarcoplasmic reticulum Ca2+-ATPase. J Biol Chem 2006;281(42):31572-82.

242. Paulsen M, Lund C, Akram Z, Winther JR, Horn N, Moller LB. Evidence that translation reinitiation leads to a partially functional menkes protein containing two copper-binding sites. Am J Hum Genet 2006;79(2):214-29.